Identification and characterisation of the familial partial lipodystrophy gene

Thesis submitted for the degree of Doctor of Philosophy
At the University of Leicester

by

David John Lloyd BSc. (Birmingham)

Department of Genetics

University of Leicester

October 2001

ProQuest LLC
789 East Eisenhower Parkway
P.O. Box 1346
Ann Arbor, MI 48106-1346

CONTENTS

LIST OF FIGURES

LIST OF TABLES

LIST OF APPENDICES

ABBREVIATIONS

°C	degrees centrigrade
×*g*	times gravity
3-AT	3 amino triazole
5-FOA	5 fluoro-orotic acid
Å	angstrom
ABI	Applied Biosystems
ACC	acetyl-CoA carboxylase
AD	autosomal dominant
ADD1	adipocyte differentiation determinant
ADE2	adenine gene
ADH1	alcohol dehydrogenase
AGL	acquired generalised lipodystrophy
aP2	adipocyte fatty-acid binding protein
APLD	acquired partial lipodystrophy
APP	amyloid precursor protein
APS	ammonium persulphate
AR	autosomal recessive
ATP	adenosine triphosphate
BAC	bacterial artificial chromosome
BAT	brown adipose tissue
BDH	British Drug Houses
bHLH	basic-helix-loop-helix
BLAST	basic local alignment search tool
bp	base pair
BSA	bovine serum albumin
C/EBP	CCAAT/enhancer binding protein
cAMP	cyclic adenosine monophosphate
cdc2	cyclin dependent kinase 2
cDNA	cloned DNA
cf.	*confer* (compared to)
c-fos	p55-cellular proto-oncogene
CGL	congenital lipodystrophy
CHLC	Co-operative Human Linkage Centre
CHOP	C/EBP homologous protein
cm	centimetre
cM	centiMorgan
CMD1A	cardiomyopathy dilated type 1A
CoA	co-enzyme A
Co-IP	co-immunoprecipitation
cR	centiRay
CRABP2	cellular retinoic acid binding protein 2
CT	computed tomography
C-terminal	carboxy-terminal
CUP	C/EBP undifferentiated proetin
DAP3	death associated protein gene
dATG	dATP/dTTP/dGTP
dATP	deoxy-adenosine triphosphate
DBD	DNA binding domain

dCTP	deoxy-cytidine triphosphate
ddATP	di-dATP
ddNTP	di-dNTP
del	deletion
DGAT	diacylglycerol transferase
Dgat	diacylglycerol transferase gene
dGTP	deoxy-guanadine triphosphate
dH_2O	distilled water
DHPLC	denaturing high performance liquid chromatography
DMSO	dimethyl sulphoxide
DNA	deoxyribonucleic acid
dNTP	deoxy-nucleoside triphosphate
dTTP	deoxy-thymidine triphosphate
E-box	enhancer box
E. coli	*Escherichia coli*
EDMD	Emery Dreifuss muscular dystrophy
EDTA	ethylenediamine tetra-acetic acid
e.g.	*exempli gratia*
ER	endoplasmic reticulum
EST	expressed sequence tag
et al	*et alia* (and others)
FABP4	fatty-acid binding protein 4
Fam	family
FAS	fatty acid synthase
FCHL	familial combined hyperlipidaemia
FISH	fluorescence *in situ* hybridisation
FPC	fingerprinting contigs software
FPLD	familial partial lipodystropy
FS	frameshift
g	gram
GAL4	*S. cerevisiae* β-galactosidase gene
GLUT4	glucose transporter 4
Gng3lg	gamma-3-linked gene
GMP-PNP	guanylyl-5'-imidophosphate
GST	glutathione-S-transferase
GTP	guanosine triphosphate
HCl	hydrochloric acid
HD	Huntingtons disease
HDL	high density lipoprotein
HIS3	histidine gene
HIV	human-immunodeficiency virus
HMG-CoA	3-hydroxy-3-methylglutaryl-coenzyme A
HP1	heterochromatin protein 1
hr	hour
HSL	hormone sensitive lipase
HTGS	high throughput genome sequence
IBMX	isobutylmethylxanthine
IF	intermediate filaments
IL-6	interleukin-6
IMAGE	integrated molecular analysis of gene expression

Inc	Incorporated
INM	inner nuclear membrane
INSRR	insulin receptor-related-receptor
IPF-1	insulin promoter factor 1
IPTG	isopropyl-β-D-thiogalactosidase
IVT	*in vitro* translation
jun-B	JUN proto-oncogene
kb	kilobase
KCl	potassium chloride
kDa	kiloDalton
KH_2PO_4	potassium hydrogen phosphate
kJ	kiloJoule
KOAc	potassium phosphate
LAP	lamina associated polypeptide
LB	Luria Bertani
LBR	lamin B receptor
LDL	low density lipoprotein
LEM	LAP/emerin/MAN1
LEU2	leucine gene
LGMD1B	limb-girdle muscular dystrophy type 1B
LiOAc	lithium acetate
LIPA	lamin interacting protein from adipocytes
Lipa	lamin interacting protein from adipocytes gene
LMNA	human lamin A/C gene
Lmna	mouse lamin A/C gene
LOD	Logarithm of the odds
LPL	lipoprotein lipase
Ltd	limited company
M	molar
MAR	matrix associated region
Mb	megabase
mg	milligram
$MgCl_2$	magnesium chloride
$MgSO_4$	magnesium sulphate
min	minutes
ml	millilitre
mm	millimetre
mM	millimolar
$MnCl_2$	manganese chloride
MRI	magnetic resonance imaging
mRNA	messenger RNA
Na_2CO_3	sodium carbonate
Na_2HPO_4	disodium hydrogen phosphate
NaCl	sodium chloride
NaH_2PO_4	sodium dihydrogen phosphate
NaOAc	sodium acetate
NaOH	sodium hydroxide
Narf	nuclear lamin A associated factor
NCBI	National Centre for Biotechnology Information
NEFA	non-esterified fatty acid

Nek2	never in mitosis gene A-related kinase 2
NETN	nonidet P-40/EDTA/Tris-HCl/NaCl
ng	nanogram
$(NH_4)_2SO_4$	ammonium sulphate
NL	Netherlands
NLS	nuclear localisation signal
nm	nanometre
NPC	nuclear pore complex
NPR1	natriuretic peptide receptor A
nSREBP	nuclear SREBP
N-terminal	amino terminal
Nup	nucleoporin
nurim	nuclear rim protein
ob	obese
OD	optical density
OMIM	online Mendelian inheritance in man
ONPG	*o*-nitrophenyl pyranogalactosidase
ORF	open reading frame
p	petite
PAC	P1 artificial chromosomes
PAGE	polyacrylamide
PBS	phosphate buffered saline
PCR	polymerase chain reaction
PEG	polyethylene glycol
PEPCK	phosphoenolpyruvate carboxykinase
pers comm	personal communication
Pfu	*Pyrococcus furiosus* DNA polymerase
pH	potential of hydrogen
PI	protease inhibitor
PIPES	piperazine-1,4 bis-2-ethane sulfonic acid
PKA	protein kinase A
PPARγ	peroxisome proliferator-activated receptor γ
Pref-1	preadipocyte repressor factor 1
PS	presenilin
q	que
Ran	Ras related nuclear protein.
RanBPM	Ran binding protein at microtubule organising centre
RFLP	restriction fragment length polymorphism
RH	radiation hybrid
RNA	ribonucleic acid
RP	retinitis pigmentosa
RPCI	Roswell Park Cancer Institute
rpm	revolutions per minute
RT	room temperature
RXR	retinoid X receptor
S. pombe	*Schizosaccharomyces pombe*
S1P	site-1 protease
S2P	site-2 protease
Sad1	spindle pole associated protein
SAR	scaffold attachment region

SCAP	SREBP cleavage activation protein
SDS	sodium dodecyl sulphate
sec	seconds
SNP	single nucleotide polymorphism
SRE	sterol response element
SREBP	SRE binding protein
ss	single-stranded
SSC	standard saline citrate
SSCP	single-stranded conformational polymorphism
STS	sequence tagged site
SUN	Sad1-UNC-84 related protein
T_a	annealing temerature
TBE	tris/borate/EDTA
TE	tris/EDTA
TEA	triethylammonium
TEM	transmission electron microscopy
TEMED	tetramethyl-ethylenediamine
Temp	temperature
TFIIIA	transcription factor IIIA
Tg	transgenic
TIGR	The Institute for Genome Research
TM	transmembrane
TMpred	TM prediction
TNF-α	tumour necrosis factor α
TNT®	transcription and translation
Tris	tris[hydroxmethyl]aminomethane
TZD	thiazolidinediones
µl	microlitre
µm	micrometre
µM	micromolar
U	units
UK	United Kingdom
UNC-84	uncoordinated 84 protein
URA3	uracil gene
USA	United States of America
UTR	untranslated region
UV	ultra-violet
v	version
V	Volts
v/v	volume to volume
VLDL	very low density lipoprotein
w/v	weight to volume
WAT	white adipose tissue
WT	wild-type
X-Gal	5-Bromo-4-chloro-3-indoxyl-beta-D-galactopyranoside
Y2H	yeast two-hybrid
YAC	yeast artificial chromosome
YNB	yeast nitrogenous base
YPD	yeast extract/peptone/dextrose
Zip	leucine zipper

CONTRIBUTORS

Sue Shackleton shared an equal amount of duty performing the initial mutation screening of the original nine UK FPLD families **(Section 4.2)**. Additionally, the co-immunoprecipitation of lamin A and SREBP1a was carried out by Sue **(Section 5.1.2)**.

Steve Jackson initiated this project and ascertained the FPLD patient DNAs either directly or indirectly through other clinicians from the UK, the Netherlands and Germany **(Section 3.1.3)**.

Richard Evans performed the fluorescent fingerprinting of the 1q21 BAC clones **(Section 3.2.5)** and continued the completion of the 1q21 physical map after we identified mutations in the *LMNA* gene **(Section 3.2.9)**.

ACKNOWLEDGEMENTS

I would like to use this opportunity to express my gratitude and thanks to those who have supported me towards this achievement. Diabetes UK is gratefully acknowledged for providing financial support, so is Prof. Richard Trembath whom firstly, gave me this opportunity and furthermore allowed and advocated my independent study. Several others have also significantly contributed to this project and to all I am appreciative.

This project has been interesting and enjoyable, however the day to day lab-life has been made all the more fun by my friends and colleagues. Of those who have lasted the same term as myself I want to express my thanks to Sue Shackleton, Julie Taylor and Colin Veal. Furthermore, Steve Jackson and Rajiv Machado have shown their true friendship and support over this period of time. Without all of these guys I would only be leaving with a qualification and not the memories. I suppose I should also thank these individuals for providing, but more so listening to my (in their mind 'terrible') jokes over the past three years. I promise you will hear some better ones in the future.

I would like to thank those close to me including my father, mother and grandmother who have endured the trials of a perennial student. I would like to assure them that I will now find employment!

Lastly, I thank my partner, Nancy Livesey. Nancy has been a constant friend and companion, and whilst at times, some aspects of my study have been negative, her presence has provided the necessary support that has enabled my relentless devotion to this project. Not only has Nancy been emotionally supportive but also has proven to be a limitless source of amusement which has enabled me to keep my studies in perspective.

ABSTRACT

Identification and characterisation of the familial partial lipodystrophy gene

David J. Lloyd

The lipodystrophies are a heterogeneous group of disorders characterised by a reduction or absence of subcutaneous fat. Familial partial lipodystrophy (FPLD) is an inherited condition in which regional fat loss occurs at onset of puberty. Additionally, endocrine dysfunctions manifest as insulin resistance and hyperlipidaemia. FPLD is an autosomal dominant disorder and a disease locus has been identified on chromosome 1q21. Through a positional-candidate cloning approach we identified the causative gene. Haplotype analyses were used to refine the disease critical interval to 3.8 cM, between the microsatellite markers *D1S2346* and *D1S2624*. A physical map of the region was constructed and used to position candidate genes. Missense mutations were detected in the *LMNA* gene in independent FPLD families; all localised to codons 482 and 486, within exon 8. Interestingly, heterozygous mutations have been reported in *LMNA* in kindreds exhibiting myocyte and cardiomyocyte abnormalities.

The *LMNA* gene encodes the lamin A/C proteins, components of the nuclear lamina – a meshwork-like structure within the inner nuclear membrane. We speculated that an adipocyte specific interaction exists with lamin A and is perturbed in FPLD subjects. We therefore performed a yeast two-hybrid screen with lamin A as bait to identify adipocyte protein interactions. The most interesting interacting proteins were a group of sterol-regulatory element binding proteins (SREBPs) and a group of novel transcripts, hereafter referenced as LIPA. *In vitro* and *in vivo* analyses have confirmed these interactions. SREBP is known to be associated with cholesterol and triglyceride biosynthesis and is recognised as an adipogenic transcription factor. Furthermore, transgenic studies leading to overexpression of the nuclear form of SREBP1c resulted in the production of a murine model of lipodystrophy. We therefore propose that interacting proteins, including those identified in this study, contribute to the molecular mechanism leading to the FPLD phenotype.

1 INTRODUCTION

1.1 The adipocyte

1.1.1 The adipocyte and adipose tissue

The human body consists of a multitude of diverse cell types, resulting in many different tissues. Each of these specific cells contributes a set of unique functions to the organism and allows the survival and healthy maintenance of the body. The single most important ability of any organism is to assimilate, store and use energy; it is also necessary for that organism to be capable of releasing energy from body stores upon demand, or prevent energy usage in times of energy excess. In the human body, energy is obtained from the breakdown (metabolism) of catabolites. These catabolites are obtained by the release of high-energy compounds from food and liquids in the digestive tract. The principal catabolite in humans is in the form of lipids or fat. Fat can be absorbed through the large intestine and can be utilised by virtually all cell types in the body. Fat and lipids are primarily stored in specialised cells known as adipocytes. Tissues predominantly composed of adipocytes are known as adipose tissues.

1.1.1.1 Adipocyte structure

Histologically, adipocytes are recognised from other cells by their intracellular storage of fat. Adipocytes constitute two distinct types of tissue, white adipose tissue (WAT) and brown adipose tissue (BAT). WAT and BAT are termed based upon their colour *in vivo*; they are also described as unilocular and multlilocular respectively, due to the presence of a single lipid droplet or multiple lipid droplets within the cell. BAT is present in humans during fetal development and diminishes during childhood. Its main function is to provide heat from the breakdown of lipids. There is little BAT in the human adult. On the other hand WAT is widely distributed in the human body and is the main site for the storage of lipids.

Adipocytes from WAT are large and can range from 20-200 μm in diameter, the vast majority averaging 100 μm across [Ross *et al.*, 1995; Fruhbeck *et al.*, 2001]. Upon isolation an adipocyte appears spherical, however when packed together in adipose tissue they are oval or polyhedral (Figure 1). The size of the cell is attributed to its internal content, a single lipid droplet averaging roughly 90% of the cell volume. This huge accumulation of lipid creates the appearance of a swollen cell. The presence of the

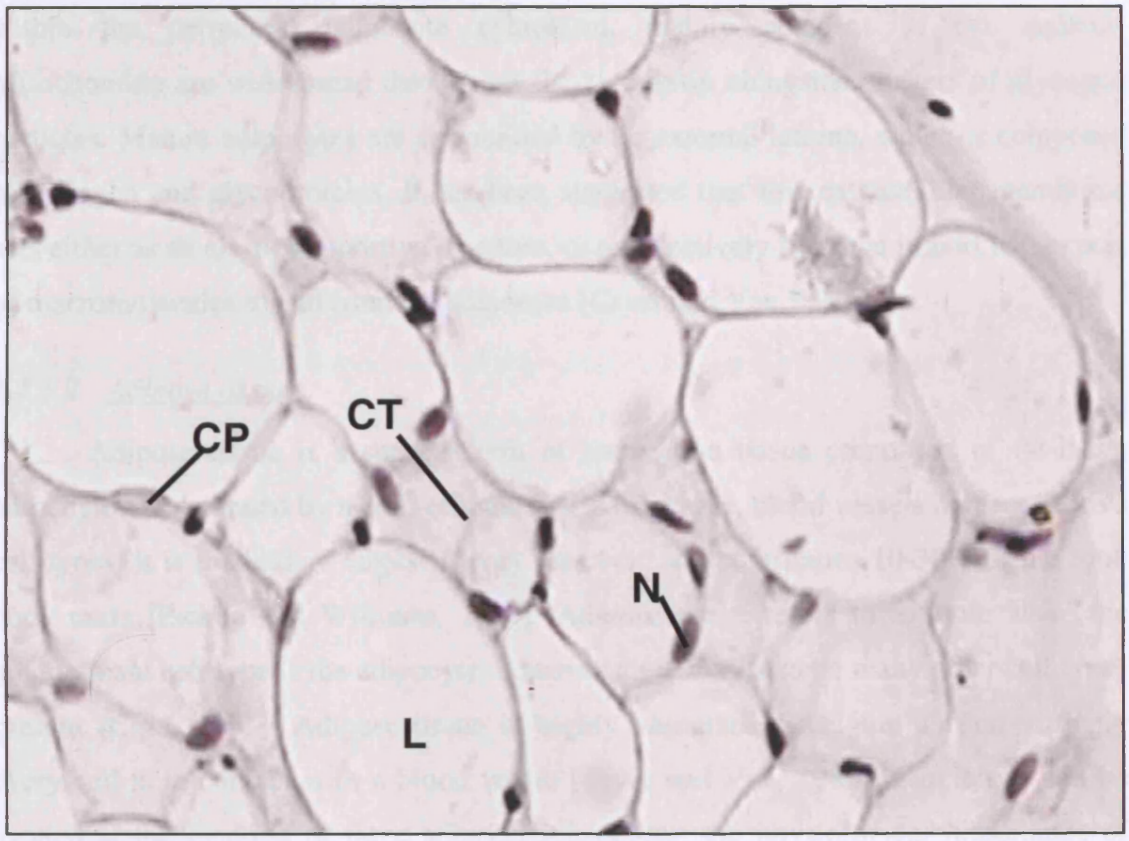

Figure 1. Histological appearance of white adipose tissue. L – lipid mass, N – nucleus, CT – connective tissue, and CP – capillaries. Note the squashed nucleus forced to the plasma membrane by the large lipid mass and the high degree of vascularisation. Stained with haematoxylin and eosin.

large lipid volume pushes all other organelles, including the nucleus, to the periphery of the adipocyte. The result of which makes adipose tissue easily identifiable, with the large lipid centre surrounded by the cytoplasm, a thin dark layer containing the flattened nucleus. The lipid organelle within the adipocyte has been examined with the transmission electron microscope (TEM) [Ross *et al.*, 1995]. The interface between the lipid and the cytoplasm has two components, a 5 nm thick layer of lipid reinforced by a 5 nm layer of microfilaments. This division is necessary to divide the lipid droplet and the hydrophilic cytoplasm. Organelles present in other mammalian cells are also located within the peripheral adipocyte cytoplasm, mainly adjacent to the nucleus. Mitochondria are widespread throughout the cytoplasm alongside clusters of glycogen particles. Mature adipocytes are surrounded by an external lamina, which is composed of collagen and glycoproteins. It has been suggested that this extracellular membrane acts either as an elastic supportive structure, or to selectively filter the import and export of macromolecules to and from the adipocyte [Cryer and Van, 1985].

1.1.1.2 Adipose tissue

Adipose tissue is a special form of connective tissue composed of fat-laden adipocytes, surrounded by a collagenous matrix of nerves, blood vessels and connective cell types. It is the body's largest energy reservoir and contributes 10-30% of the total body mass [Pickup and Williams, 1997]. Adipose tissue refers to a tissue when the predominant cell type is the adipocyte, however there may also be many other cell types present [Cinti, 2001]. Adipose tissue is highly vascularised (Figure 1) and virtually every cell is in contact with a blood vessel [Cryer and Van, 1985]. Capillaries can be located at the junction of three adjacent adipocytes, the physiological importance of which suggests the necessity of access for every adipocyte to the circulation enabling rapid absorption and release of lipids.

Other cells present in adipose tissue include macrophages, fibroblasts, mast cells and in concert constitute the connective tissue producing the extracellular matrix. The latter of which aids in the interconnection of these cell types with each other. The white adipose tissue is organised into lobules, which are supported by loose connective septa. The junction between adjacent adipocytes is not a simple cell-cell interface, but interspersed with collagen filaments and occasionally disrupted by fibroblast extensions between adipocytes [Cryer and Van, 1985].

1.1.1.3 Adipose tissue distribution

Adipose tissue under the skin is known as the *panniculus adiposus*. Typically, adipose tissue is located in the subcutaneous compartment around the lower part of the abdomen. It is also found under the skin in the buttocks, axilla and thigh. Internally, adipose tissue is deposited in a number of sites including the omentum, peritoneal, retroperitoneal and surrounding abdominal organs. Fat deposition is also recognised in the retro-orbital space, face and neck and within muscle. Subcutaneous adipose tissue surrounding the muscle and under the skin contains the majority of the body's adipose tissue. Although it is now accepted that the adipocyte is a metabolic tissue, initially fat was thought to be necessary for protection of the body from shock. Adipose tissue is likely to perform this role as well, as it is also found in regions requiring shock absorption, including those already mentioned such as the back of the eye, the buttocks and around the kidneys, heart and soles of the feet [Stevens and Lowe, 1997]. In support of this, these adipose tissues do not lose their structure and cushioning role during periods of lipid mobilisation in comparison to other adipose tissues [Ross *et al.*, 1995].

The relative amount of adipose tissue in each of these sites is variable. This is especially evident with gender differences, resulting in significantly different body contours [Arner, 1997]. Both sexes are able to accumulate adipose tissue in the breast, hips and gluteal regions, however females preferentially develop significantly more adipose tissue at these sites resulting in a 'gynoid' appearance. Males, in contrast, accumulate adipose tissue around the abdomen, intra-abdominally and subcutaneously, resulting in an 'android' appearance. Thus the accumulation of adipose tissue at specific sites is highly regulated and significant between human males and females. Vague [Vague, 1956] was the first to suggest that body fat distribution correlated with various health problems. The localisation of adipose tissue in the body can have drastic effects on metabolism [Bjorntorp, 1991], resulting in the development of diseases such as type 2 diabetes mellitus, hyperlipidaemia and other associated disorders.

1.1.1.4 Development

White adipose tissue formation begins during embryonic development. The totipotency of stem cells within the foetus decreases as growth continues and each diverging group of stem cells becomes increasingly committed to specific lineages. The adipocyte is derived from a multipotent stem cell, a mesodermal progenitor, which also has the potential to develop into muscle and cartilage cells [Cornelius *et al.*, 1994].

Mesenchymal cells become unipotent upon development into adipoblasts. These cells are morphologically identical to fibroblasts but are only capable of developing into adipocytes. Once committed to adipocyte development the adipoblast differentiates into a preadipocyte, a cell that expresses markers of an adipocyte, but has not started to accumulate lipid. It is still unknown whether all adipoblasts have progressed to preadipocytes upon birth, or if adipoblasts remain in the body throughout life [Ailhaud, 2001]. The preadipocyte cell matures into the distinctive adipocyte by progressive lipid accumulation, forming large spherical cells, dominated by a unilocular lipid mass.

Although the adipocyte development initiates in the human foetus, the majority of differentiation occurs soon after birth, in fact human neonates are relatively obese compared to other mammals. This excess of fat is thought to provide a constant source of energy during infancy [MacDougald and Lane, 1995]. This adipose tissue expansion results from increased adipocyte cell size (hypertrophy) and increased fat cell number (hyperplasia). Thus the potential to develop new adipocytes remains after birth and even in to the adult stage of life. To support this, adipocyte hyperplasia has been observed in human obesity. The relative contribution of adipocyte cell size and number to adipose tissue in obese individuals has not been determined [Gregoire *et al.*, 1998].

1.1.1.5 In vitro *models of adipocyte development*

The study of adipocytes *in vivo* is difficult. Adipose tissue is diffuse in the body, is a mixture of many cell types and the adipocyte precursor cell, the preadipocyte is indistinguishable from surrounding fibroblasts. *In vitro* models of adipocyte differentiation have been shown to be powerful alternatives to *in vivo* studies. The isolation and immortalisation of cells from adipose tissue has permitted the identification of the stages of adipocyte differentiation; thus it has been possible to determine the stage of commitment to the adipocyte and the transition through the preadipocyte to the mature adipocyte.

Two classes of cell lines have been recognised, multipotent mesenchymal precursors and unipotent adipoblasts [Gregoire *et al.*, 1998]. Murine multipotent cell lines include 10T1/2 and Balb/c 3T31246 and are capable of differentiating into mesodermal lineages such as myocytes, chondrocytes, fibroblasts and adipocytes [Taylor and Jones, 1979]. Adipoblast cell lines were isolated by Green and colleagues from mouse Swiss 3T3 embryos [Green and Meuth, 1974]. The most commonly used models are the 3T3-L1 and 3T3-F422A cells which are morphologically identical to

fibroblasts, but are committed to become adipocytes [Ntambi and Young-Cheul, 2000]. These cell lines can be cultured as fibroblast-like adipoblasts or induced to differentiate into adipocytes.

Conversion of confluent 3T3-L1 cells into adipocytes is mediated by administering an adipogenic cocktail. The three components to this cocktail include insulin, a substance that elevates cAMP levels (isobutylmethylyxanthine – IBMX) and glucocorticoids (dexamethasone). The initial stage of adipocyte conversion is temporary growth arrest, achieved by contact inhibition; the addition of the cocktail promotes a further round of mitosis known as clonal expansion. After 48 hours of differentiation, the cells complete the postconfluent cell division and enter into total growth arrest, coinciding with the expression of adipogenic transcription factors, peroxisome proliferator-activating receptor γ (PPARγ) and CCAAT/enhancer binding protein α (C/EBPα) [Ntambi and Young-Cheul, 2000], as discussed in Section 1.1.3. The cells are now considered to be preadipocytic, with the appearance of fibroblasts but expressing a set of adipogenic-specific proteins. This second growth arrest is terminal, the preadipocytes begin to accumulate lipid in the large lipid vacuole and remain in this state, as mature fat cells cannot divide [Ailhaud, 2001]. The remaining fates for the adipocyte are limited, either increased storage of triglycerides (increase in volume), mobilisation of fatty acids from triglyceride stores (decrease in volume), or apoptosis.

1.1.2 Function of adipose tissue in lipid metabolism

There are various catabolites in the body available for the production of energy in the form of ATP. Energy produced as a consequence of oxidation of triglyceride is 38.9 kJ/g, which is over twice the amount of energy obtained from the same amount of carbohydrate or protein (both 17.2 kJ/g) [Klaus, 2001]. Although glucose provides a source of rapid energy to virtually all of the body's tissues, if it were the main form of energy storage in the body (as glycogen) the increased mass would interfere with the organism's mobility. It is thought that the use of triglyceride as the major energy store has allowed the evolution of mobile organisms due to the anhydrous, condensed nature of triglyceride in adipose tissue [Unger *et al.*, 1999]. These three metabolites are all derived from the diet and absorbed through the intestine; those nutrients that are not immediately required for energy must be stored so that they may be released upon controlled demand during periods of low nutritional abundance. It is the role of the

adipocyte to store lipids in the body as triglyceride and mobilise this energy source as needed [Flier, 1995].

1.1.2.1 Transport of lipid

Lipids are a group of organic biomolecules, which are soluble in organic solvents and insoluble in water. These include fats, oils, triglycerides, phospholipids, cholesterol and fatty acids amongst many others. The most important of which are the fatty acids and their storage counterparts, the triglycerides.

Fatty acids are weak acids that have a single carboxyl group at the end of a hydrocarbon chain. The major fatty acids in the human body have 16-20 carbon residues and can be saturated (lacking carbon-carbon double bonds, e.g. stearic acid), or unsaturated (containing one or more carbon double bonds, e.g. oleic acid). Triglycerides are formed from the esterification of three molecules of fatty acid and one molecule of glycerol (which has been converted to glycerol 3-phosphate). Fatty acids not incorporated in triglyceride are known as non-esterified fatty acids (NEFA). Triglycerides are also known as neutral fats due to the loss of their carboxyl groups and considering that their flexible side-chains allow more efficient packing of molecules together, the storage of energy as triglyceride is more preferable to that of glycogen.

Lipids circulate in the blood in one of two ways, as NEFA or triglyceride. NEFA is transported as a sodium salt bound to the plasma protein, albumin, which neutralises it acidic effects. Triglyceride is transported in lipoprotein particles. Plasma lipoproteins are classified based on their distinct fractions following ultra-centrifugation, high-density lipoproteins (HDLs), low-density lipoproteins (LDL), very low-density lipoproteins (VLDL) and chylomicrons [Cryer and Van, 1985]. These transport vehicles have triglyceride or cholesterol rich cores and are surrounded by amphipathic lipids such as phospholipids and a range of apoproteins, which aid in the solublisation of the particles. There are numerous apoproteins, possessing different properties. As discussed they transport lipid by stabilising lipoproteins, but also act as ligands for specific receptors at tissue-blood interfaces, thus enabling the regulated release and uptake of lipid from the blood into tissue. The four plasma lipoproteins each carry different cargoes; the highest triglyceride content is in chylomicrons (85%) and VLDL (60%), whereas HDL is predominantly composed of protein. Cholesterol is transported mainly in LDL, constituting 50% of the total composition [Thabrew and Ayling, 2001].

Lipid enters the circulation by absorption of triglyceride in the intestine and is transported in chylomicrons either directly to the adipocyte, liver or to other tissues with a demand for lipid. Triglyceride is removed from chylomicrons at the capillaries of tissues by the action of the enzyme lipoprotein lipase (LPL). At the liver, triglyceride is released from chylomicrons and broken down into NEFA and glycerol, cholesterol is also liberated at this stage. It is the liver that is responsible for utilisation of NEFA and cholesterol, or the subsequent packaging of these molecules into the lipoproteins, VLDL, LDL and HDL [Thabrew and Ayling, 2001]. The purpose of which is to shuttle these metabolites to tissues such as the muscle where they can be used, or to the adipocyte for storage.

1.1.2.2 Uptake and storage of fatty acids by adipocytes

Triglyceride in lipoproteins (mainly as chylomicrons and VLDL) circulates in the blood until it is hydrolysed at specific endothelial sites by LPL. LPL is an enzyme, which is secreted by adipocytes and attaches to the surface of endothelial cells surrounding blood capillaries [Wion *et al.*, 1987]. Triglyceride-laden lipoproteins contain the apolipoprotein C-II on the surface, this small protein is necessary to activate LPL in the vascular endothelium [Olivecrona and Beisiegel, 1997], thus LPL can specifically hydrolyse triglyceride presented within these lipoproteins. NEFAs are released and taken up by adjacent adipocytes. NEFA may also be directly absorbed from circulating fatty acid-albumin complexes [Hamilton, 1998]. At this stage lipogenesis occurs in adipocytes, esterifying NEFAs with glycerol-3-phosphate (obtained from glycolysis) to form storage triglyceride which will be deposited in the lipid droplet within the fat cell. The lipogenic pathway involves several steps [Kahn, 2000]; in brief, this is the conversion of glycerol-3-phospate to phosphatidate, subsequently to diglyceride and finally to triglyceride mediated by the enzyme acyl CoA:diacylglycerol transferase (DGAT). The final step was considered to be carried out solely by DGAT as this is the only committed step of lipogenesis, however *Dgat*-deficient mice are capable of maintaining normal levels of triglyceride and are resistant to diet induced obesity [Smith *et al.*, 2000]. The conclusions of which suggest there are other compensatory mechanisms of triglyceride synthesis and storage.

1.1.2.3 Release of fatty acids from adipocytes

Release of fatty acids and glycerol from triglyceride (lipolysis) initiates the mobilisation of stored fat within the adipocyte. A multifunctional enzyme, hormone-sensitive lipase (HSL), which has broad substrate specificity, performs lipolysis [Osterlund, 2001]. HSL was cloned [Holm *et al.*, 1988] and shown to be activated by phosphorylation at serine residues [Shen *et al.*, 1998]. HSL is a cytosolic protein and upon activation, it repositions as a dimer [Shen *et al.*, 2000] at the periphery of the lipid droplet, exerting its lipolytic effects [Brasaemle *et al.*, 2000]. It is capable of hydrolysing tri-, di- and monoglycerides [Saltiel, 2000]. Liberated fatty acids enter the circulation and are transported to other tissues in the body for metabolism, such as muscle. Fatty acids produced this way also temporarily reside in adipocyte intracellular pools of fatty acid, composed of incoming and outgoing molecules. In this way the fatty acids may also be reincorporated into triglyceride in the adipocyte. On the other hand, the other product of lipolysis, glycerol, cannot be re-esterified as adipocytes lack the enzyme, glycerokinase and is thus released into the circulation, for eventual absorption by the liver [Saltiel, 2000].

Upon triglyceride hydrolysis in adipocytes, fatty acids are released and bound by small proteins, known as fatty acid-binding proteins (FABP4/aP2) [Hertzel and Bernlohr, 2000]. These are responsible for the intracellular trafficking of NEFA. Recent experiments have shown that FABP4 interacts with HSL [Shen *et al.*, 1999], suggesting these lipid chaperones be specifically involved in fatty acid clearance following lipolysis [Hertzel and Bernlohr, 2000]. A mouse knockout of HSL resulted in male sterility but not obesity as expected [Osuga *et al.*, 2000]. The conclusions of which suggest a compensatory mechanism of lipolysis [Saltiel, 2000].

1.1.2.4 Regulation of lipogenesis and lipolysis

The lipogenesis-lipolysis cycle is tightly regulated so that in response to the body's demands, lipogenesis may exceed lipolysis, or *vice versa*, relative to periods of excess energy uptake or excess energy expenditure respectively. Equally, during periods of balanced energy uptake and energy expenditure, both processes occur without either net gain or loss of triglyceride from the lipid droplet of the adipocyte. Factors that determine the relative lipogenic-lipolytic balance include the effects of insulin, catecholamines and regional location of adipose tissue.

1.1.2.4.1 Insulin

The effect of insulin on adipose tissue has been recognised since the restoration of fat in the bodies of wasted diabetic patients following insulin therapy [Frayn and Coppack, 1992]. Insulin promotes lipogenesis, by increasing lipogenic enzymes, namely acetyl CoA carboxylase, increasing uptake of glucose and increasing transcription of LPL. Secondly, insulin is known to inhibit lipolysis, by preventing HSL phosphorylation [Frayn and Coppack, 1992]. The consequence of insulin action is a decreased supply of NEFA to other body tissues, alternatively perceived as a conservation of energy.

Insulin directly increases the activity of LPL gene transcription and post-translational modification [Fried *et al.*, 1993]. This has the effect of escalating triglyceride clearance from circulating lipoproteins and increasing availability of NEFA within the adipocyte. As previously discussed (Section 1.1.2.1), glucose is necessary for lipogenesis, after conversion to glycerol-3-phospate. Insulin stimulates glucose uptake into the adipocyte via the GLUT4 transporter [Fukumoto *et al.*, 1989]. In brief, insulin binds to its receptor at the cell surface and is internalised by endocytosis causing insulin receptor autophosphorylation, which has a cascade effect mediated via several enzymes, ultimately resulting in protein kinase B phosphorylation [Boschmann, 2001]. The result of which assists GLUT4 translocation to the cell surface. The newly recruited glucose is subsequently available for triglyceride synthesis. Furthermore, insulin not only increases the availability of raw materials for triglyceride synthesis, but also stimulates the process of lipogenesis by activating enzymes involved in the pathway, including fatty acyl synthetase and acetyl CoA carboxylase [Pickup and Williams, 1997].

The antilypolytic effects of insulin are as important as its lipogenic effects. The lipolytic enzyme HSL is activated by cAMP-dependent phosphorylation and insulin has the effect of lowering cAMP levels, mediated via a cAMP phosphodiesterase [Holm *et al.*, 1997]. Reduction in active HSL inhibits NEFA production and release.

1.1.2.4.2 Catecholamines

The catecholamines are a group of chemicals which act as neurotransmitters or hormones and include adrenaline, noradrenaline and corticotropin. They are powerful lipolytic stimuli increasing the catabolism and release of NEFA by activation of HSL. Catecholamines bind to adrenergic receptors (α_1 and α_2, or β_1, β_2 and β_3 adrenoreceptors) on the surface of adipocyte [Boschmann, 2001]. These receptors are

coupled to GTP-binding proteins that either stimulate or inhibit adenylyl cyclase. Activation of adenylyl cyclase increases cellular cAMP levels and promotes protein kinase A (PKA) phosphorylation and subsequent activation of HSL [McKnight *et al.*, 1998].

The most abundant protein of adipocyte lipid droplets is perilipin [Greenberg *et al.*, 1991]. It can be phosphorylated by PKA and is thought to pose a barrier for HSL attachment onto the lipid droplet [Osterlund, 2001]. A contemporary theory of catecholamine-regulated lipolysis, is that perilipin resides on the lipid droplet periphery, acting as a barrier to HSL, upon phosphorylation of both of these proteins, perilipin moves away from the lipid surface and permits translocation and attachment of HSL at this site [Osterlund, 2001].

1.1.2.4.3 Regional location of adipose tissue

The two main sites for adipose tissue in humans are abdominal or gluteal-femoral, of which the abdominal can be further subdivided into intra-abdominal or subcutaneous. Vague was the first to observe that males and females have different fat depots over the body [Vague, 1956]. It is now accepted that these different sites of adipose tissue respond in a non-uniform manner. Catecholamines are most active in visceral fat, less active in abdominal subcutaneous fat and least active in gluteofemoral fat [Arner, 1997]. Wahrenberg and colleagues investigated the relative levels of α and β adrenoreceptors in abdominal and gluteofemoral sites in both males and females [Wahrenberg *et al.*, 1989]. The results demonstrated that fat cells from the abdomen were more responsive to lipolytic stimuli than those from the gluteal, in which there was a greater difference in females than males. These differences were attributed to the variation in adrenoreceptors. Additionally, insulin exerts a greater effect on lipolysis in subcutaneous tissue compared to intra-abdominal, most likely associated with the levels of insulin receptor [Bolinder *et al.*, 1983]. In conclusion, intra-abdominal adipose tissue is much more responsive to lipolysis than subcutaneous tissue. The metabolic consequences of which are numerous, but essentially involve the reduced clearance of NEFA from the circulation into peripheral tissues and direct drainage of NEFA into the liver [Frayn and Coppack, 1992].

1.1.2.5 Adipose tissue as an endocrine organ

The adipocyte has long been established as a depot for lipid, sensitising the body's energy status. Recently the adipocyte has exceeded these roles and acquired further functions in the overall process of energy homeostasis [Flier, 1995]. Currently there is evidence that adipose tissue is capable of acting as an endocrine organ, secreting hormones, growth factors and cytokines [Flier, 1995]. A range of signals produced by the adipocyte have been identified as a consequence of several investigations, including the positional cloning of leptin, the gene underlying the cause of the *ob/ob* mouse, a murine model of diabetes and obesity [Zhang *et al.*, 1994]. Other secreted molecules include tumor necrosis factor-α (TNF-α), interleukin-6 (IL-6), angiotensinogen, adipsin and AdipoQ [Fruhbeck *et al.*, 2001].

TNF-α is a cytokine commonly associated with macrophages. The finding that TNF-α expression was positively correlated to obesity initiated studies in this field [Hotamisligil *et al.*, 1995]. The biological effects of TNF-α expression include, LPL inhibition and C/EBPα and PPARγ down-regulation (Section 1.1.3), the consequence of which is shut-down of fat cell differentiation and maintenance [Fruhbeck *et al.*, 2001]. This contrasting finding suggested that possibly TNF-α be produced in large adipose tissues in an effort to decrease fat mass, by an apoptotic mechanism, similar to its role in tumor cells [Prins *et al.*, 1997]. It is also considered that upon the adipocyte reaching a critical size, TNF-α expression is elevated, enhancing growth factor responsiveness in the fat cell [Fruhbeck *et al.*, 2001].

Leptin is an adipocyte-specific secreted molecule, released into the blood as a 16 kDa protein following proteolytic cleavage from the plasma membrane [Chehab, 2000]. Mutation of this gene caused obesity and diabetes in the *ob/ob* mouse [Zhang *et al.*, 1994]. Leptin is secreted by adipocytes and binds to its receptor in the hypothalamus, informing the brain of the amount of body fat and thus links feeding behaviour, metabolism and endocrine function [Fruhbeck *et al.*, 2001]. However, there are now doubts about the major role of leptin in the body [Trayhurn *et al.*, 2001]. Regardless, the amount of adipose tissue in the body is the main determinant for the levels of circulating leptin, thus the function of leptin is positively associated with fat cell signalling [Fruhbeck *et al.*, 2001].

Adipsin is a serine protease secreted by adipocytes and found to be a member of the alternative complement pathway [Min and Spiegelman, 1986]. Adipsin levels are

dramatically reduced in several models of rodent obesity [Flier, 1995]. Adipsin is expressed, so the adipocyte may control the rate of *de novo* triglyceride synthesis and esterification [Sniderman and Cianflone, 1994].

The identification that these three factors, alongside others, have regulatory roles upon secretion from fat cells suggested that fat tissue is central in energy balance, not only a simple storage organ as initially thought.

1.1.3 Genetic control of adipogenesis

During differentiation of the preadipocyte to mature adipocyte there is a temporal cascade of adipogenesis specific gene expression. Many of these genetic factors have been elucidated from *in vitro* studies using the 3T3-L1 and 3T3-F422A preadipocyte cell lines (Section 1.1.1.5) [Green and Meuth, 1974]. Following post-confluent growth arrest of preadipocytes, a mixture of adipogenic stimulants is administered to induce the adipogenic program. This developmental program can be partitioned into distinct stages consisting of; 1) confluence; 2) hormonal induction; 3) permanent growth arrest; 4) adipocyte maturation. From one stage to the next, there is a co-ordinate expression of genes involved in the mediation of a precursor to a mature adipocyte. These adipogenic genes all have the ability to regulate other adipocyte developmental genes at the level of gene transcription. These transcription factors have been known for little over a decade and since their identification, there has followed an explosion of scientific interest in this field. Primarily these adipogenic transcription factors are divided into three distinct classes; peroxisome proliferator-activated receptor γ (PPARγ); CCAAT/enhancer binding protein (C/EBP); and adipocyte determination and differentiation factor 1 (ADD1) or its human homologue, sterol regulatory element binding protein 1(SREBP1).

1.1.3.1 C/EBP

Studies directed towards identifying nuclear factors which bound to the promoters of two adipocyte differentiation-induced genes, FABP4 and stearoyl-CoA desaturase resulted in the recognition of C/EBP [Christy *et al.*, 1989]. C/EBPs are members of a family of basic leucine zipper (b-Zip) transcription factors and include C/EBPα, C/EBPβ, C/EBPδ, C/EBPε and C/EBPζ, [Wu *et al.*, 1999]. These proteins form homo- or heterodimers via the leucine zipper in their carboxyl terminus. Three of the C/EBP members, C/EBPα, C/EBPβ and C/EBPδ are involved in adipocyte

differentiation [Cowherd *et al.*, 1999]. C/EBPβ and C/EBPδ are expressed early following hormonal induction, whereas C/EBPα is expressed late in adipogenesis and persists in the mature adipocyte.

C/EBPβ and C/EBPδ expression is thought to be involved in initiating and directing the differentiation process [Ntambi and Young-Cheul, 2000]. Expression of C/EBPβ in 3T3-L1 cells is sufficient to direct adipogenesis in the absence of hormonal inducers [Yeh *et al.*, 1995] and expression of C/EBPδ contributes to adipogenesis (yet still requires hormonal induction). Interestingly, the greater adipogenic potential of C/EBPβ has also been shown to promote adipogenesis in NIH-3T3 fibroblasts and thus C/EBPβ not only increases adipogenesis but also commits undifferentiated cell lines down an adipogenic pathway [Wu *et al.*, 1995]. In these experiments the expression of C/EBPβ and C/EBPδ increased the transcription of PPARγ (Section 1.1.3.2). The role of these two proteins in adipogenesis is also supported by transgenic mice studies. Mice deficient in either C/EBPβ or C/EBPδ have fully differentiated white fat cells with normal morphology; however, compound homozygous knockouts have a more dramatic phenotype [Tanaka *et al.*, 1997]. Approximately 15% of mice survive and have a reduction in white adipose tissue. The reduction in fat cells appeared to be a result of decreased cell number as opposed to atrophy. The levels of PPARγ were not affected in the fat which did develop and suggests that *in vivo* there exists alternative pathways during the initiation of adipogenesis [Rangwala and Lazar, 2000].

Progression of early adipogenesis into late differentiation correlates with a reduction in C/EBPβ and C/EBPδ concomitant with an increase in C/EBPα expression [Cao *et al.*, 1991]. Interestingly, the C/EBPα promoter contains a functional C/EBP binding site and is thought to be a target of C/EBPβ. Once activated C/EBPα would be able to regulate its own expression in a positive autoregulatory feedback loop [Yeh *et al.*, 1995]. Definitive proof that C/EBPα has a role in adipogenesis was obtained by expression of antisense C/EBPα [Lin and Lane, 1992] in preadipocytes, resulting in prevention of adipocyte differentiation. C/EBPα is also able to determine and differentiate non-committed fibroblasts down an adipogenic program [Freytag *et al.*, 1994]. In keeping with these results is the finding that C/EBPα knockout mice fail to develop white fat [Wang *et al.*, 1995]. An interesting investigation would be to identify which adipocyte markers the preadipocyte express in these mice, to define the stage at which adipogenesis becomes arrested or if the preadipocytes have even initiated

adipogenesis [Gregoire *et al.*, 1998]. C/EBPα expression increases from undetectable in the preadipocyte, to high in the mid to late stages of adipogenesis, remaining high in the mature adipocyte. The role of C/EBPα is central in adipogenesis and is considered a master regulator alongside PPARγ, a second C/EBPβ/ C/EBPδ target.

1.1.3.2 PPARγ

Several PPAR isoforms exist and have the ability to act as nuclear hormone receptors. PPARγ is expressed predominantly in adipose tissue and heterodimerises with a second nuclear receptor, the retinoid X receptor (RXR), directing transcription of many fat-specific genes.

Promoter analysis of the FABP4 gene identified an adipocyte regulatory factor (ARF6) which interacted with the adipocyte response element (ARE). Cloning of this factor revealed its identity, a heterodimer of PPARγ and RXR [Tontonoz *et al.*, 1994a]. PPARγ exists as two transcripts through the use of alternative promoters. PPARγ2 is the major form in adipose tissue and contains an extra 30 amino acids at the amino terminus [Tontonoz *et al.*, 1995]. The difference in PPARγ isoform function is currently unknown [Wu *et al.*, 1999].

To substantiate the role of PPARγ in adipogenesis, Tontonoz and colleagues retrovirally expressed PPARγ in mouse fibroblasts [Tontonoz *et al.*, 1994b]. Consistent with its proposed function, PPARγ was able to promote adipogenesis, however this was dependent on the supplementation of lipid activators. PPARγ has also exhibited its potency in adipogenesis by conversion of myoblasts into adipocytes [Hu *et al.*, 1995]. Furthermore, transgenic mice studies have revealed the necessity of PPARγ in adipogenesis. Although the homozygous knockout is embryonic lethal [Barak *et al.*, 1999], different groups have circumvented this to analyse PPARγ ablation in specific tissues. The most impressive of these studies was performed by Rosen and colleagues [Rosen *et al.*, 1999], in which they created chimeric mice derived from both normal and PPARγ (-/-) embryonic cells. Tissues requiring PPARγ would be completely composed of wild-type cells, whereas those tissues which have no need for PPARγ would be composed of a mixture of wild-type and PPARγ (-/-) cells. The outcome illustrated the necessity of PPARγ in adipose tissue, which was composed solely of wild-type cells, compared to tissues such as heart and spleen, which exhibited no preference.

As with other nuclear hormone receptors, PPARγ is modular in structure, possessing a DNA binding domain, trans-activation domain and a dimerisation domain. The latter is necessary for the complex to be transcriptionally active [Rosen *et al.*, 2000]. A carboxy terminal ligand-binding domain is also present, presumably only allowing dimerisation upon ligand binding. Natural and synthetic ligands have been identified for PPARγ. The natural ligand 15 deoxy-$\Delta^{12,14}$ prostaglandin J_2 is able to bind PPARγ and promote adipogenesis when added to PPARγ expressing cells [Forman *et al.*, 1995]. It is considered that other fatty acid high-affinity ligands are yet to be identified [Wu *et al.*, 1999; Ntambi and Young-Cheul, 2000]. Synthetic ligands include the thiazolidinediones (TZDs), a novel class of antidiabetic drugs [Lehmann *et al.*, 1995]. These drugs were developed for their ability to increase insulin-sensitivity and thus used in the treatment of type 2 diabetes mellitus, then subsequently shown to activate PPARγ. TZDs are currently the most potent ligands for PPARγ possessing high binding affinities, much greater than the natural prostaglandin ligand.

1.1.3.3 ADD1/SREBP

ADD1 was identified as a basic-helix-loop-helix (bHLH) transcription factor. A transcription factor binding DNA motif, known as an E-box present in the promoter of the fatty acid synthase (FAS) gene, was used to screen a rat adipocyte expression library, resulting in isolation of ADD1 [Tontonoz *et al.*, 1993]. The human homologue has been independently cloned from human HeLa cells on its ability to bind a second regulatory motif, the sterol response element (SRE-1) [Yokoyama *et al.*, 1993]. The factor, known as SRE binding protein (SREBP1), binds SRE-1 in the promoters of several genes involved in cholesterol homeostasis [Yokoyama *et al.*, 1993]. There are two isoforms of SREBP1, SREBP1a and SREBP1c which are alternative transcripts of the same gene and differ at their amino terminus. SREBP1a contains an additional unique 29 amino acids and SREBP1c only 5 amino acids extra. ADD1 corresponds to the SREBP1c isoform, which is the major isoform in animal tissues [Shimano *et al.*, 1997a]. The mode of action for ADD1/SREBP1 is novel. Full-length protein contains approximately 1150 residues and is bound to the membrane of the endoplasmic reticulum by virtue of two transmembrane domains. At periods of sterol depletion the full-length protein is cleaved to release an active N-terminal 500 amino acids. This activated cleavage product, once released from the membrane is able to translocate to the nucleus and direct the expression of genes under the transcriptional control of E-

boxes or SRE-1 sites [Brown and Goldstein, 1997]. This process has been solely determined for sterol responsiveness in liver metabolism, the action of ADD1/SREBP1 cleavage and activation with regard to the adipocyte remains to be determined [Rosen and Spiegelman, 2000].

Association of ADD1/SREBP1 with adipogenesis was first discovered by the observation of the dramatic induction of ADD1/SREBP1 following adipogenic initiation in 3T3-L1 preadipocytes and bears similarity to the expression profile of PPARγ [Kim and Spiegelman, 1996]. Overexpression of ADD1/SREBP1 in 3T3-L1 cells enhances hormonal induction compared to control cells and is responsible for induction of fatty acid synthase and lipoprotein lipase, both of which are critical for adipocyte development [Kim and Spiegelman, 1996]. Unlike PPARγ, ADD1/SREBP1 alone is unable to induce adipogenesis in undifferentiated fibroblasts. To further corroborate ADD1/SREBP1 in adipogenesis, a dominant-negative protein, which abolished ADD1/SREBP1 function, was expressed in preadipocytes and resulted in complete inhibition of adipogenesis. The conclusions of this work suggest that ADD1/SREBP1 is required for adipocyte differentiation, but whose actions are not as potent as PPARγ.

Targetted disruption of ADD1/SREBP1 in mice produced mortalities from 50%-80%. The mice which survived were normal in terms of their adipose mass and expression of adipocyte genes [Shimano *et al.*, 1997b]. A third member of the ADD1/SREBP family exists, SREBP2, derived from a different locus. In ADD1/SREBP1 knockout mice that survive and appear normal, SREBP2 expression is elevated and considered to be compensating for ADD1/SREBP1 loss.

The most plausible role for ADD1/SREBP1 in adipogenesis was discovered by two important experiments. Firstly, medium from cells expressing ADD1/SREBP1 was able to activate PPARγ gene transcription [Kim *et al.*, 1998]; and secondly, the block of adipogenesis using a dominant-negative ADD1/SREBP1 could be overcome by the addition of TZD ligand for PPARγ. Both of these results suggest that the role of ADD1/SREBP1 in adipogenesis is the production of endogenous ligand for PPARγ [Fajas *et al.*, 1999].

1.1.3.4 Cascade of adipogenic transcription

Although C/EBPs, PPARγ and ADD1/SREBP1, are considered to be the key determinants in adipogenesis, several other proteins exist which contribute to the overall process of adipocyte development. Considered together, all of these factors create a sequential cascade of gene expression which directs adipogenesis and is summarised in Figure 2.

Preadipocyte cell lines enter a regulated progression of transcription factor expression following hormonal induction. The first genes to respond are the proto-oncogenes *c-fos* and *jun-B* which peak a few hours post-induction [Rangwala and Lazar, 2000]. The expression of these genes is believed to have a mitogenic effect on the preadipocyte, initiating the second post-confluent mitosis and ultimately directing the cells towards adipogenic commitment [Ntambi and Young-Cheul, 2000]. The levels of these genes dissipate shortly after this initial activity. The first adipocyte-specific genes expressed are C/EBPβ and C/EBPδ, involved in the direct response of the exogenous hormones, dexamethasone and IBMX. Considering their rapid expression, these two factors are thought to be responsible in directing and initiating the differentiation process [Darlington *et al.*, 1998]. The expression of C/EBPβ and C/EBPδ precede that of PPARγ and C/EBPα and thus the effects of C/EBPβ and C/EBPδ are likely to result in activation of the latter transcription factors. This is supported by the finding of a functional CCAAT enhancer in the promoters of the genes encoding C/EBPα and PPARγ [Yeh *et al.*, 1995]. Once expressed these genes are capable of positive auto-regulation and so the need for C/EBPβ and C/EBPδ diminishes, as does the level of expression. [Darlington *et al.*, 1998]. Interestingly, C/EBPβ and C/EBPδ deficient cells are unable to differentiate into adipocytes, whereas ectopic expression of C/EBPα was able to circumvent this block and allow adipogenesis to proceed as normal. The conclusions of which are that C/EBPβ and C/EBPδ are necessary for the initiation of the adipogenic motor by C/EBPα activation and C/EBPα, once induced, conducts the remainder of the adipogenic program.

The delayed response of C/EBPα expression may be attributed to the transcriptional dominant-negative factor, C/EBPζ also known as CHOP-10. C/EBPζ was isolated from an adipocyte cDNA library on its ability to interact with C/EBPβ [Ron and Habener, 1992]. C/EBPζ is capable of forming heterodimers with C/EBP isoforms, but prevents DNA binding and thus represses under the control of

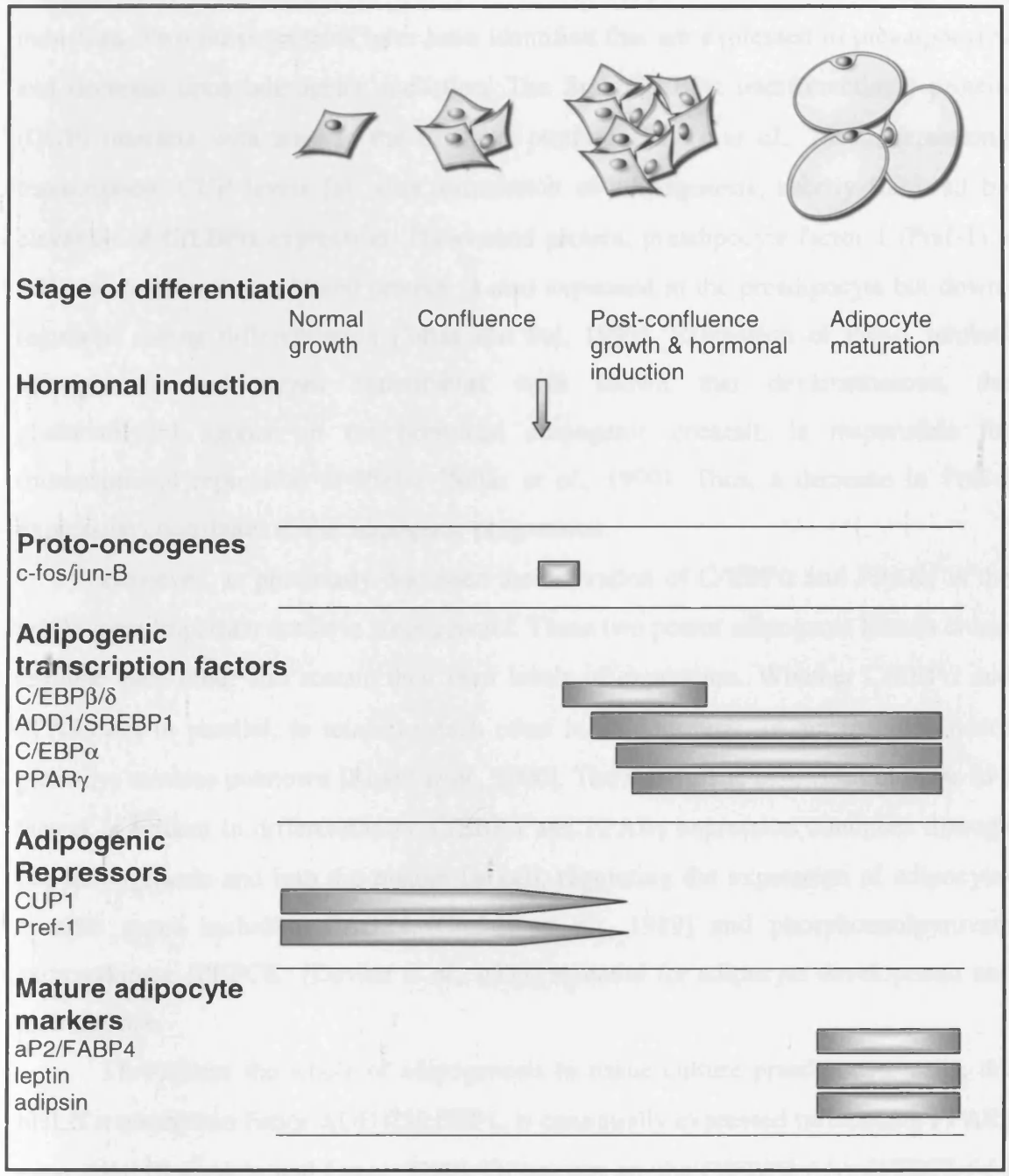

Figure 2. Transcriptional control of adipogenesis. Schematic representation of the timing of gene expression in the formation of adipocytes. Fibroblast-like preadipocytes grown in culture can be hormonally stimulated to proceed down a adipogenic pathway. Upon stimulation these cells express a range of transcription factors in a cascade manner. Firstly, adipogenic repressors are turned off, and after a brief period of proto-oncogene expression, several well-established adipogenic transcription factors are expressed. Ultimately this results in the expression of genes which enable the accumulation of lipid in the adipocyte.

CCAAT elements. This transcriptional repression could be overwhelmed by competitive dimerisation of elevated levels of C/EBPβ and C/EBPδ after hormonal induction. Two other proteins have been identified that are expressed in preadipocytes and decrease upon adipogenic induction. The first, C/EBPα undifferentiated protein (CUP) interacts with sites in the C/EBPα promoter [Tang *et al.*, 1997], repressing transcription. CUP levels fall after stimulation of adipogenesis, shortly followed by elevation of C/EBPα expression. The second protein, preadipocyte factor 1 (Pref-1) a cell surface, membrane bound protein, is also expressed in the preadipocyte but down-regulated during differentiation [Smas and Sul, 1993]. Expression of Pref-1 inhibits adipogenesis and recent experiments have shown that dexamethasone, the glucocorticoid agonist in the hormonal adipogenic cocktail, is responsible for transcriptional repression of Pref-1 [Smas *et al.*, 1999]. Thus, a decrease in Pref-1 expression contributes to the adipogenic progression.

However, as previously discussed the activation of C/EBPα and PPARγ is the single most important factor in adipogenesis. These two potent adipogenic factors cross-regulate each other and sustain their own levels of expression. Whether C/EBPα and PPARγ act in parallel, to reinforce each other in adipogenesis, or act in independent pathways remains unknown [Rosen *et al.*, 2000]. The synergistic behaviour of these two factors is evident in differentiation. C/EBPα and PPARγ expression continues through late adipogenesis and into the mature fat cell, regulating the expression of adipocyte-specific genes including FABP4 [Christy *et al.*, 1989] and phosphoenolpyruvate carboxykinase (PEPCK) [Devine *et al.*, 1999] essential for adipocyte development and maintenance.

Throughout the whole of adipogenesis in tissue culture preadipocyte cells, the bHLH transcription factor ADD1/SREBP1, is continually expressed influencing PPARγ expression [Rangwala and Lazar, 2000]. Of interest are the C/EBPβ (-/-), C/EBPδ (-/-) double knockout mice, approximately 15% [Tanaka *et al.*, 1997] of transgenic mice survive, of which all had a reduced fat mass. Expression of PPARγ and C/EBPα in adipose tissue of these survivors is, surprisingly, not compromised and thus suggests the existence of an alternative pathway in the activation of these adipogenic directors [Rangwala and Lazar, 2000]. Given that medium from ADD1/SREBP1 transfected cells is sufficient to promote adipogenesis through PPARγ activation [Kim *et al.*, 1998] and together with the fact that ADD1/SREBP1 can compensate for C/EBPβ, C/EBPδ

absence, ADD1/SREBP1 activates PPARγ-mediated transcription by production of endogenous ligand.

Levels of ADD1/SREBP1 are also maintained in the mature adipocyte and although implicated in PPARγ gene expression, there is also the possibility for a direct role of adipocyte-directed transcription. ADD1/SREBP1 has been shown to induce the expression of two essential fat cell proteins, fatty acid synthase and lipoprotein lipase [Kim and Spiegelman, 1996].

1.2 Lipodystrophies

The lipodystrophies are a group of heterogeneous disorders characterised by a reduction of adipose tissue. Typically, loss of adipose tissue, especially in subcutaneous depots, results in an accentuated muscular appearance accompanied with a number of metabolic disturbances. The first description of lipodystrophy was documented by Mitchell in 1885 [Mitchell, 1885] and since then there have been over 500 reported patients [Garg, 2000]. There are various forms of lipodystrophy, classified as either inherited or acquired, both of which can be subdivided on the basis of either a partial or total distribution of adipose tissue absence. Other types of lipodystrophy exist including localised lipodystrophy, affecting small sites on the body, or HIV antiretroviral treated lipodystrophy.

1.2.1 Acquired non-inherited lipodystrophies

Non-inherited forms of lipodystrophy have been identified and are characterised as either generalised (complete or total), or partial.

1.2.1.1 Acquired generalised lipodystrophy (AGL) – Lawrence syndrome

Lawrence described patients with a normal fat distribution at birth but developed lipodystrophy of all adipose tissue [Lawrence, 1946]. Approximately 50 reports of AGL have been documented [Garg, 2000]. There is a preponderance of female AGL cases. Usually the onset of adipose tissue loss is during childhood or early adolescence, followed by rapid completion of total fat loss, over weeks, months or years [Garg, 2000]. Temporary states of partial lipodystrophy have been observed, before total adipose tissue loss occurs. Adipose tissue is lost in all subcutaneous areas of the body, including those areas requiring mechanical fat, such as the soles of the feet and palms of the hands. Approximately four years after total adipose tissue loss diabetes mellitus

develops [Pickup and Williams, 1997]. AGL patients also have elevated triglyceride, NEFA and insulin levels in the blood, usually accompanied with a resistance to the effects of circulating insulin (insulin resistance) [Golden *et al.*, 1985; Klein *et al.*, 1992]. No reported study thus far has described the absence of internal abdominal fat. Analysis of fat from AGL patients suggested that adipose tissue was being destroyed, as opposed to a failure in maintenance or development [Pickup and Williams, 1997] and therefore thought to be an autoimmune disease [Billings *et al.*, 1987].

1.2.1.2 Acquired partial lipodystrophy (APLD) – Barraquer-Simons syndrome

At the beginning of the twentieth century Barraquer and Simons described a disorder of adipose tissue absence from the face to the abdomen, but with normal adipose tissue distribution around the pelvic girdle and lower limbs [Barraquer Ferre, 1949]. APLD has a higher incidence in females, developing during childhood or early adolescence [Peters *et al.*, 1973; Garg, 2000; Porter *et al.*, 2000]. The lipodystrophy initiates on the face and spreads to the necks and shoulders, eventually reaching the abdomen [Garg, 2000]. The time course for the progression of APLD is not as rapid as AGL and occurs over eighteen months to several years. The adipose tissue surrounding the pelvis and on the lower parts of the body is rarely affected, however post-pubertal females may sometimes deposit excess adipose tissue around the thighs [Garg, 2000; Porter *et al.*, 2000]. MRI visualisation was used to identify the regions of lipodystrophy in an APLD male; subcutaneous adipose tissue was absent in the face, neck, chest and abdomen, however gluteal and intra-muscular fat levels were normal, as was fat around the internal organs [Yuh *et al.*, 1988].

APLD is the exception in the association of lipodystrophies with metabolic abnormalities. Insulin resistance, diabetes mellitus and hyperlipidaemia rarely occur [Garg, 2000]. However, 20-50% of APLD cases have been reported to suffer from mesangiocapillary glomerulonephritis, a state of blood capillary proliferation in the Bowmans capsule of the kidney resulting in proteinuria, as revealed by renal biopsies [Peters *et al.*, 1973; Edelson, 1997]. Typically, renal dysfunction presents approximately ten years after the lipodystrophy [Garg, 2000]. The other interesting manifestation of APLD is hypoproteinaemia, including low serum levels of C3 complement protein. This is attributed to the presence of an autoantibody (C3 nephritic factor) against C3 convertase enzyme. Whilst C3 levels are low other alternative complement factors are high, suggesting continual activation of the complement

pathway. It has been proposed that adipocyte lysis by complement activation is the likely pathogenic mechanism for the regional lipodystrophy [Garg, 2000]. To support this hypothesis, C3 nephritic factor is capable of promoting adipocyte lysis [Mathieson *et al.*, 1993] and furthermore, another protein in the immune-complement response (adipsin) has been shown to be secreted by adipocytes [Flier, 1995].

1.2.2 Inherited familial lipodystrophies

As with acquired lipodystrophies the familial lipodystrophies can be classified as generalised – affecting the whole of the body, or partial – affecting all of the body with exception of the face and neck.

1.2.2.1 Congenital generalised lipodystrophy (CGL) – Berardinelli-Seip syndrome

Berardinelli [Berardinelli, 1954] and Seip [Seip, 1959] were the first to describe an inherited syndrome of total fat loss. It is extremely rare and estimated to affect less than 1 in 12 million people [Garg, 2000]. CGL is inherited as an autosomal recessive trait. The most striking and distinguishing feature of CGL is complete adipose tissue loss from birth continuing throughout life. If diagnosis is missed at birth it is made no later than the age of two, with equal incidence in the sexes [Edelson, 1997].

An invaluable study was documented by Seip and Trygstad on seven patients with CGL over a period of nearly forty years [Seip and Trygstad, 1996]. Insulin resistance is common in these CGL patients, manifesting as hyperinsulinaemia, hyperlipidaemia and type 2 diabetes mellitus. As with other syndromes of insulin resistance, the diseases of acanthosis nigricans (a darkening and hardening of the skin) and mild hirsutism in women are also recognised in CGL. Voracious appetite accompanies and worsens an increased metabolic rate, advanced bone age and accelerated growth in early childhood. However, final adult height remains normal. Organomegaly is observed alongside hypertrophy of the heart. This hypertrophic cardiomyopathy may become lethal in adulthood; three of Seip and Trygstads' patients died from cardiac defects at the ages of 24, 32 and 37. One further patient alive in 1996, suffered from stenocardia. Circulating levels of leptin are low in CGL patients, consistent with absence of adipose tissue, the leptin producing tissue [Garg, 2000].

Interestingly, the majority of the Seip and Trygstad families in which CGL segregates live in adjacent municipalities of southwestern Norway. The incidence of

consanguinity is common in CGL families and aids in the development of recessive inheritance. The localisation of the CGL families suggests a common founder mutation which has descended through each of the families, furthermore genealogical studies propose the mutation must have occurred at least 400 years ago [Gedde-Dahl *et al.*, 1996].

Whole body MRI was utilised to study the distribution of adipose tissue in three CGL patients [Garg *et al.*, 1992]. Adipose tissue was almost completely absent in subcutaneous sites, intra-abdominal and intra-thoracic. However, adipose tissue was present in odd locations, such as the optic orbits, buccal region, tongue, palms and soles. Garg proposed that CGL patients suffer from absence of metabolic adipose tissue, but retain mechanical adipose tissue, in regions of shock absorption.

As with other forms of lipodystrophy, the absence of subcutaneous adipose tissue results in prominence of the musculature and subcutaneous veins. In most cases the musculature is accentuated by an increase in skeletal muscle mass. The nature of the muscle hypertrophy has recently been investigated in CGL [Garg *et al.*, 2000]. Muscle biopsies support the hypothesis that increased muscle mass is due to an increase in muscle fibres or hyperplasia and not muscle hypertrophy. The mechanism for muscle hyperplasia is unclear.

A candidate gene approach was performed to exclude genes associated with adipocyte biology [Vigouroux *et al.*, 1998]. Garg and colleagues performed linkage analyses on seventeen CGL families and mapped the CGL1 locus to chromosome 9q34 [Garg *et al.*, 1999a]. Statistical scores localised the CGL1 locus nearest to the marker *D9S1818*. Haplotype analyses of disease chromosomes positioned the critical interval between markers *D9S1818* and *D9S1826*, an 8.7 cM genetic distance. Two of the seventeen families were found to be unlinked to 9q34, sequencing of the PPARγ gene revealed no mutations in these two families. However, this did provide proof of heterogeneity for CGL, with CGL1 at 9q34 and CGL2 unmapped in this study.

A recent study localised the CGL2 locus to chromosome 11q13 and identified the gene for CGL [Magré *et al.*, 2001]. Initial linkage analysis and subsequent gene identification were significantly aided by ascertainment of families from only two geographical locations, Lebanon and Norway. Homozygosity mapping refined the CGL2 locus to a 2.5 cM region at 11q13 between the markers *D11S4076* and *D11S480*. A deletion of microsatellite *CA10* in one family suggested a chromosomal deletion of this genomic segment. Upon database screening an unknown expressed sequence tag

(EST) was found to localise close to *CA10*. This gene was designated *CGL* and is the human homologue of the murine gene, G-protein gamma 3 subunit-linked gene (*Gng3lg*). Twelve genetic alterations were identified in the CGL families including, five missense mutations, six small deletions resulting in frameshift mutations and a single large deletion of 258 bp. *Gng3lg* spans 14 kb of genomic sequence and split into eleven exons. The protein product has been termed seipin, is composed of 398 amino acids and has a predicted mass of 43.8 kDa. Northern analysis revealed two mRNA species of 2.4 kb and 1.8 kb in most tissues, with an intermediate 2 kb transcript in the brain. The expression of *Gng3lg* is weak in most tissues, although the brain and testis have high relative expression. Unexpectedly, adipose tissue appears to have little or no *Gng3lg* expression. Modelling of seipin suggests two transmembrane domains. Magré and co-workers suggest that seipin has a role in homeostatic signalling between the brain and anabolic sites.

1.2.2.2 Familial partial lipodystrophy (FPLD) – Dunnigan-Köbberling syndrome

McKusick's group were the first to report a second inherited lipodystrophy, with patients devoid of subcutaneous fat over the body, however, distinct from CGL as the face and neck appeared to have normal to excessive levels of adipose tissue present [Ozer *et al.*, 1973]. Subsequently, Dunnigan and Köbberling described families suffering from a disorder of fat accumulation around the face, neck and shoulders with a lipodystrophy of the upper and lower extremities involving the truck [Dunnigan *et al.*, 1974; Kobberling *et al.*, 1975]. FPLD is an autosomal dominant disorder and the incidence is estimated to be less than 1 in 15 million, rarer than its autosomal recessive cousin CGL [Garg, 2000].

Dunnigan examined several members from two families, both of which lived in northern Scotland [Dunnigan *et al.*, 1974]. In the first family the propositus, a girl of nineteen years in age and her mother showed symmetrical lipodystrophy of the trunk and limbs with a full, rounded face. Tubero-eruptive xanthomata, acanthosis nigricans, hyperlipidaemia and type 2 diabetes mellitus were also diagnosed. As with CGL, the absence of adipose tissue in these patients results in exposed musculature and visible subcutaneous veins. The deceased maternal grandmother and great-aunt of the propositus were said to have a similar appearance. The propositus of the second family was a 49 year-old woman, again exhibiting partial lipodystrophy of the body, with exception in the face and neck, a similar phenotype is observed in Figure 3. Her

Figure 3. Affected FPLD female. Note the absence of subcutaneous adipose tissue, the prominence of the musculature and subcutaneous veins, the fat face and neck and acanthosis nigricans under the armpits and in the groin.

deceased mother and maternal grandmother were thought to both suffer from lipodystrophy. In both families the age of onset of the lipodystrophy is estimated to be during early adolescence. Interestingly, no males were reported to be lipodystrophic from either family.

Dunnigan and Köbberling proposed that FPLD be classified as either type 1 or type 2. Type 1 involves an absence of fat confined to the extremities, with trunk and abdomen adipose tissue appearing normal, or in some cases modestly obese (also referred to as FPLD-Köbberling type) [Köbberling and Dunnigan, 1986]. Type 2 or FPLD-Dunnigan type is characterised by complete body and limb lipodystrophy with normal to excessive adipose tissue deposition in the face and neck.

The absence of affected males, with female only transmission led the investigators to believe the mode of inheritance was X-linked with dominant transmission, whereby the disorder is lethal in the hemizygous state (XY) [Köbberling and Dunnigan, 1986]. Coincidentally the following paper reported the identification of a male with FPLD [Burn and Baraitser, 1986]. The identification of an FPLD male was critical as the disorder was inherited from the paternal grandmother to the father and onto the daughter. All females exhibited classical features of FPLD, whereas the male was described as possessing a muscular physique despite any effort towards his physique. Metabolically, the FPLD male suffered from hyperlipidaemia and hyperinsulinaemia. The authors suggested that the female preponderance in FPLD be because the absence of fat and revealed musculature is not considered dysmorphic in males.

In 1997 a further FPLD family was described [Jackson *et al.*, 1997]. A single large pedigree consisting of several affected males and females was presented. Cross-sectional MRI was used to confirm the absence of subcutaneous adipose tissue in a male and a female. Subcutaneous adipose tissue was completely absent from the chest and abdomen, however adipose tissue was present in intra-abdominal sites and also in the optic orbits. The segregation of FPLD in this family provided evidence of autosomal dominant inheritance and suggested that previous FPLD preponderance in females to be a consequence of misdiagnosis in FPLD males.

The association of lipodystrophy with the metabolic consequences of insulin resistance is common. A study directed towards elucidating insulin action in FPLD patients was conducted [Ursich *et al.*, 1997]. Adipocytes from both neck and subcutaneous abdominal regions were isolated and assessed for cell size, insulin

binding, insulin receptor number and glucose transport and oxidation. Surprisingly, adipocytes taken from the abdomen (the lipodystrophic site) were significantly larger than those isolated from the neck (the non-lipodystrophic site), they were, however more fragile upon isolation. It was proposed that the lipodystrophy might be a consequence of reduced fat cell size, this however is not supported by these data. Insulin activity and insulin-receptor binding were not significantly different to control values. Glucose uptake and oxidation were both severely impaired in both neck and abdominal adipocytes. These data suggest that insulin resistance in the adipocytes of FPLD patients is post insulin-receptor binding.

Localisation of adipose tissue in FPLD subjects is confined to a few specific sites in the body. Subcutaneous adipose tissue is always lost from the limbs and around the abdomen, however the posterior of the abdomen exhibits some retention of adipose tissue [Garg *et al.*, 1999b]. Regions of adipose tissue deposition include the face, neck and shoulders, sometimes giving the appearance of a buffalo hump; fat gain is also observed intra-abdominally, within muscle masses, bone marrow and in the females, in the labia.

Linkage analysis in several FPLD families indicated a FPLD locus at chromosome 1q21 [Jackson *et al.*, 1998; Peters *et al.*, 1998]. The FPLD critical interval was mapped to the genetic region flanked by the microsatellite markers *D1S305* and *D1S1600*, a genetic distance of 5.3 cM. Most interestingly there was no evidence of genetic heterogeneity, supporting the contribution of a single gene to FPLD. This interval contains many genes including *LMNA* [Wydner *et al.*, 1996], encoding nuclear lamins A and C and one potential candidate *CRABP2*, encoding cellular retinoic acid binding protein 2 [Flagiello *et al.*, 1997].

1.2.3 HIV-associated protease inhibitor lipodystrophy

The use of retroviral protease inhibitors (PI) in the treatment of human immunodeficiency virus (HIV)-infected patients has proven to be an effective therapy in decreasing HIV RNA levels and increasing CD4 (white blood cell antigen) count. Metabolic side effects have been reported including, hyperglycaemia, insulin resistance and hyperlipidaemia. The appearance of PI treated HIV patients drastically alters; approximately 16-24 months after beginning retroviral protease inhibitor therapy a severe lipodystrophic appearance is noticeable, accompanied with intra-abdominal fat deposition [Panse *et al.*, 2000]. Carr presented images of an HIV-protease inhibitor

treated male [Carr and Cooper, 1998]. These features are typical of a growing number of reports in this field [Garg, 2000]. Three to seven months after the start of protease inhibitor indinavir therapy, lipodystrophy of the face, arms, buttocks and legs with prominent subcutaneous veins was evident. These changes were concomitant with a central-abdominal obesity and the accumulation of a buffalo hump. Panse described a further four males receiving similar treatment, all developed lipodystrophy and a pseudo-athletic appearance. Skin biopsies from these patients demonstrated thinning of adipose tissue, however, the adipose tissue present was morphologically normal. Computed tomographic (CT) scans illustrated adipose tissue thinning in the face, cheek and other subcutaneous sites. Intra-abdominal fat accumulation was also shown this way. HIV-PI lipodystrophy is reminiscent to FPLD sharing the features of subcutaneous fat loss, with intra-abdominal and back of the neck fat gain. However FPLD patients have normal to excessive levels of fat in the face and chin, HIV-PI patients do not.

The molecular mechanism for HIV-PI lipodystrophy is unknown, although expected to be associated with inhibition of proteases involved in directing adipogenesis or lipid metabolism [Panse *et al.*, 2000].

1.2.4 Mouse models of lipodystrophy

Two models of lipodystrophy have recently been generated. Two independent groups have generated transgenic mice with alterations in the genes associated with adipocyte biology and development, C/EBP [Moitra *et al.*, 1998] and SREBP1 [Shimomura *et al.*, 1998].

Moitra and co-workers created a dominant negative protein, termed A-ZIP/F, which prevented the DNA binding of the C/EBP transcription factors. C/EBPβ, C/EBPδ and C/EBPα all have roles in adipogenesis (Section 1.1.3.1) [Moitra *et al.*, 1998]. In order to ablate white adipose tissue in mice, the investigators sought to create a protein that interferes in the transcriptional control of adipogenesis. A chimeric gene was created, under the control of a fat specific promoter, aP2. The gene was modified resulting in a protein which would bind to C/EBP transcription factor mediated by the leucine zipper domain, however a basic domain was replaced by an acidic domain. The two basic domains in a wild-type C/EBP dimer permit DNA binding. In the case of the mutant heterodimer, the basic domain interacts with the transgenic acidic domain and DNA binding is abolished. The transgenic mouse line expressing A-ZIP/F possessed sixteen copies of the transgene. Dissection of transgenic mice revealed no white adipose

tissue. Absence of adipocytes in these mice may be attributable to lack of adipocyte development or to adipocyte death. To assess this, mice were examined at different prenatal and postnatal stages. Subcutaneous adipose tissue was present in control animals at birth but completely absent in A-ZIP/F mice. In adult mice intra-abdominal adipose tissue was also absent, however, the transgenic mice did exhibit organomegaly including fatty infiltration of the liver. Metabolically these mice suffered from type 2 diabetes mellitus, accompanied with hyperglycaemia, hyperinsulinaemia and hyperlipidaemia. Leptin levels were also reduced as compared to control mice.

The second mouse model of lipodystrophy was created by genetic manipulation of the ADD1/SREBP1c gene [Shimomura *et al.*, 1998]. ADD1/SREBP1c is the most common isoform found in mouse tissues [Shimomura *et al.*, 1997] and shown to enhance adipogenesis and lipid accumulation in 3T3-L1 cells [Kim and Spiegelman, 1996]. The N-terminus of ADD1/SREBP1c, termed nSREBP1c, is the active transcription factor and translocates to the nucleus directing gene expression in an unregulated manner. This dominant positive active nSREBP1c was generated under the control of an adipocyte-specific promoter, aP2 [Ross *et al.*, 1990]. The result of which would be the forced over-expression of active nSREBP1c within adipocytes specifically, with the expectation that transgenic mice would gain adipose tissue, accompanied with a possible obese phenotype. Shimomura and colleagues generated two lines of transgenic aP2-nSREBP1c mice. Unexpectedly, mice exhibited a phenotype resembling human lipodystrophy. All mice generated were hemizygous for the transgene and at seven days after birth appeared normal apart from a large mass composed of large bilobed fat pad in the interscapular region. Submandibular brown fat was also enlargened and resembled white adipose tissue. The abdomen was distended, a consequence of a massively enlargened liver. The amount of white adipose tissue in omental and subcutaneous sites was equal in both wildtype and transgenic mice. Transgenic mice developed normally and gained adipose tissue, yet this ceased at 7-12 weeks of ages, omental fat was much smaller in transgenic over wild-type littermates. The liver remained large and the pancreas, spleen and abdominal lymph nodes all became enlargened. Histological examination of the liver, white fat and brown fat, revealed swollen fat-laden hepatocytes and brown adipocytes which appeared pale and resemble white adipose tissue. White fat was mainly composed of immature adipocytes. Circulating NEFA levels were normal and so were triglycerides. At 9-11 months of age the transgenic mice became hyperlipidaemic compared to wild-type littermates.

Hyperglycaemia and hyperinsulinaemia were both noted and as a result these mice were insulin resistant, although not at the level of the muscle. Numerous northern analyses illustrated aP2-nSREBP1c mice have normal expression of endogenous SREBP1, SREBP2 and C/EBPβ in adipose tissue, however adipogenic markers C/EBPα and PPARγ were either reduced or completely absent. The mature fat cell markers adipsin, leptin and FABP4/aP2 were all significantly reduced. Two adipogenesis inhibitors TNF-α and Pref-1 were elevated in the fat of transgenic animals.

These two models of forced lipodystrophy share features with the human lipodystrophies. The C/EBP A-ZIP/F mice are likely to represent CGL, with respect to the complete absence of all adipose tissue from birth and extreme metabolic disturbances. Shimomura and co-workers compared their mouse model to CGL aiso, likening disordered differentiation of adipose tissue, organomegaly and metabolic manifestations. However, given that these mice exhibit adipose tissue at birth and develop the lipodystrophy around seven weeks later, this is more reminiscent of FPLD. In support of this the aP2-SREBP1c mice have an enlarged interscapular fat pad, this is in a site similar to that of the buffalo hump in FPLD and HIV-PI lipodystrophy patients. Shimomura also report the identification of prominent submandibular fat mass, possibly resembling the fat neck in FPLD.

1.3 Lamins A/C and the nuclear lamina

The genetic interval on chromosome 1q21-22, the region containing the gene responsible for FPLD, harbours the *LMNA* gene. The *LMNA* gene has been mapped to 1q21.3 using fluorescence *in-situ* hybridisation (FISH) [Wydner *et al.*, 1996]. The genomic organisation of the *LMNA* gene has been determined and is composed of twelve exons spanning approximately 24 kb of genomic DNA sequence [Lin and Worman, 1993]. The *LMNA* gene accounts for several alternatively spliced transcripts in mammals, the most common of which are lamin A and lamin C. Lamins A and C are two of the major components of the nuclear lamina, a proteinaceous structure underlying the inner nuclear membrane (INM) [Stuurman *et al.*, 1998].

1.3.1 The nuclear lamina

The major distinguishing factor between eukaryotic and prokaryotic cells is the presence of a nuclear compartment separating the DNA from the rest of the cell. The genetic information in eukaryotes is packaged into large structures called chromosomes.

These chromosomes become discrete units at the time of cell division (mitosis) in these organisms; however, in the non-dividing or interphase state these chromosomes become dispersed and separated. The nuclear envelope is required to encompass these dispersed chromosomes (chromatin) and compartmentalise the DNA within the cell. The nuclear envelope consists of three main components; a continuous outer and inner membrane, nuclear pore complexes and the nuclear lamina.

The inner and outer nuclear membranes are easily identifiable in all nucleated cells. The double membrane is also continuous with the rough and smooth endoplasmic reticulum (ER) and sometimes associated with ribosomes [Gerace and Burke, 1988]. The presence of the nuclear envelope surrounding the whole of the nucleus poses difficulties for the trafficking of molecules to and from the nucleus (nucleo-cytoplasmic transport). Circular holes in the double membrane are the sites of molecule transport and their isolation has resulted in their classification as nuclear pore complexes (NPC) [Franke, 1974]. NPCs have been isolated and extensively studied by electron microscopy, resulting in the identification of annuli, or rings surrounding eight radial spokes and a central hollow [Gerace and Burke, 1988]. The isolation of NPCs from rat liver nuclear envelopes has been accompanied with the isolation of a 150 Å thick lamina [Aaronson and Blobel, 1975]. NPCs were bound to large lattice sheets of structural protein, which extended over large areas. The further purification of the lamina and subsequent electrophoresis revealed three major proteins of approximate mass 69, 68 and 67 kDa. These were later classed as lamin A, lamin B and lamin C respectively [Gerace and Blobel, 1980]. Transmission electron microscopy of the nuclear lamina revealed its structure (Figure 4). Filaments approximately 10 nm in diameter were arranged in a meshwork like structure, in some areas appearing tetragonal in shape. The lamina is present within the inner nuclear membrane only and attached to NPCs. However, this supramolecular protein structure is dynamic and breaks down during mitosis. Concomitant with nuclear envelope breakdown during mitosis the lamina dissolves and disappears, resulting in the release of monomeric lamin polypeptides; of which lamin A and lamin C solubilise and lamin B remains attached to membrane fragments of the nucleus [Gerace and Blobel, 1980]. Upon formation of daughter nuclei, the cell repolymerises the monomeric lamin polypeptides to form the new lamina.

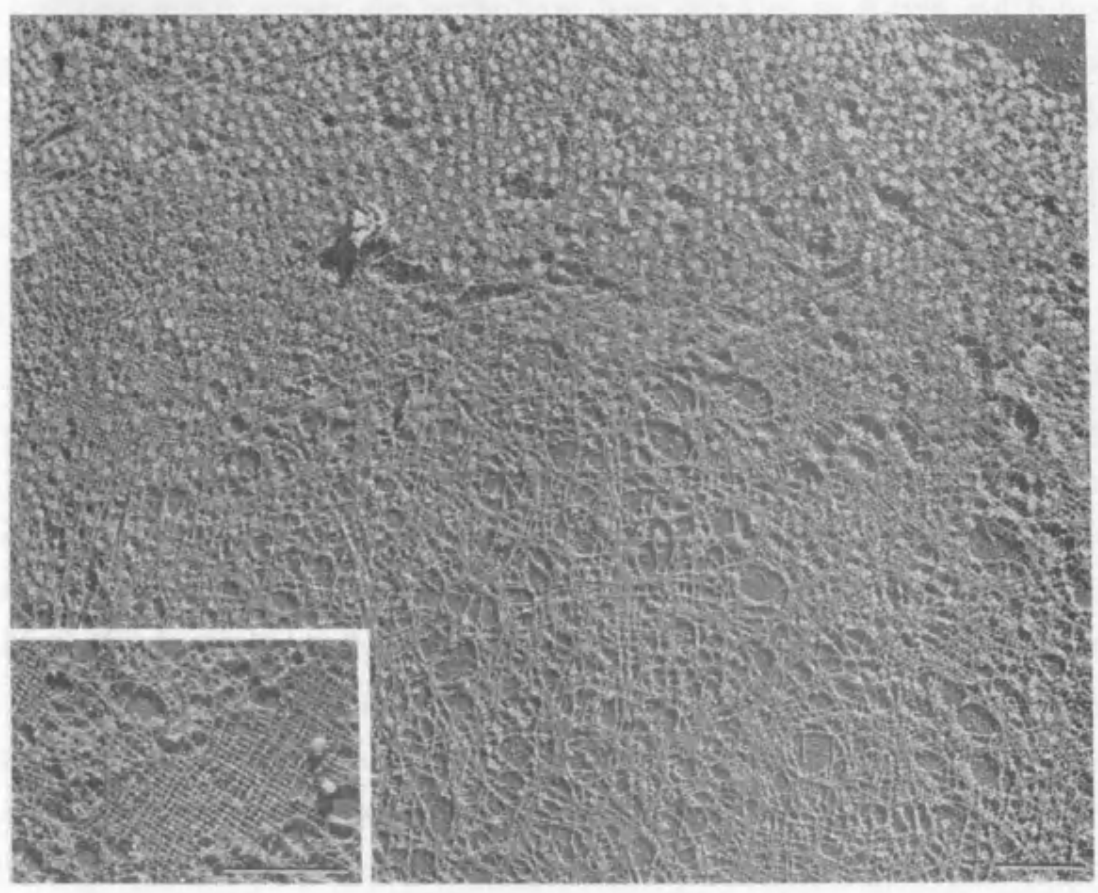

Figure 4. Supramolecular structure of the nuclear lamina. Prepared nuclear lamina extracts were viewed using transmission electron microscopy. Larger picture illustrates the vast expanse of interlinking lamin filaments forming the meshwork-like structure known as the lamina. Inset shows a high magnification view of this meshwork, revealing the regular orthogonal lattice of the lamina (bar represents 1 μm). Reproduced with permission by Nature [Aebi *et al.*, 1986].

1.3.2 Lamins

The structural basis for the nuclear lamina assembly was unveiled by the cloning of the genes that give rise to the lamin polypeptides. Although only three lamin proteins were initially identified in the nuclear lamina, further isoforms have been reported which add to the family of lamins. The four main lamin proteins are lamin A, lamin B1, lamin B2 and lamin C [Broers *et al.*, 1997]. On the basis of structural similarities and localisation during mitosis, the lamins have been classified as A-type and B-type [Stuurman *et al.*, 1998]. A-type lamins become soluble during mitosis, whereas B-type lamins remain associated with nuclear membranes [Gerace and Blobel, 1980]. A-type lamins consist of lamin A and lamin C, B-type lamins consist of lamin B1 and lamin B2.

1.3.2.1 Lamin structure and assembly

The cloning of the genes that give rise to the lamin proteins provided crucial information about their structure and function [Fisher *et al.*, 1986]. Lamin A and lamin C cDNAs were isolated and sequenced, revealing their homology to each other and the intermediate filament (IF) proteins. The intermediate filaments are structural proteins associated with the cytoskeleton. Lamin A and lamin C are identical for the first 566 amino acids, from this residue onwards lamin A consists of a further 98 amino acids (a total of 664 amino acids) and lamin C consists of an additional 6 unique amino acids (a total of 572 amino acids). The most striking structural feature of these two proteins was the presence of a large extended α-helical rod domain, from residue 31 to 388, see Figure 5a. This region also bore the strongest homology to the IF proteins and to the B-type lamins. The α-helical rod domain of these lamins contained a heptad repeat, with regular occurrence of hydrophobic resides, a characteristic of α-helical structures [Chothia, 1984]. This rod domain was broken at three positions resulting in four continuous coils 1a, 1b, 2a and 2b with three small linker peptides. The polypeptide sequence of lamin A and lamin C also demonstrates a small amino terminal 'head' domain of approximately 30 amino acids and a carboxyl terminal 'tail' domain of either 275 or 183 amino acids in lamin A and lamin C respectively. Lamin B1 and lamin B2 are highly homologous and cloning of the respective cDNA clones has permitted the identification of those domains common in the A-type lamins [Peter *et al.*, 1989; Hoger *et al.*, 1990]. The partial similarity of the DNA sequence for lamin A and lamin C

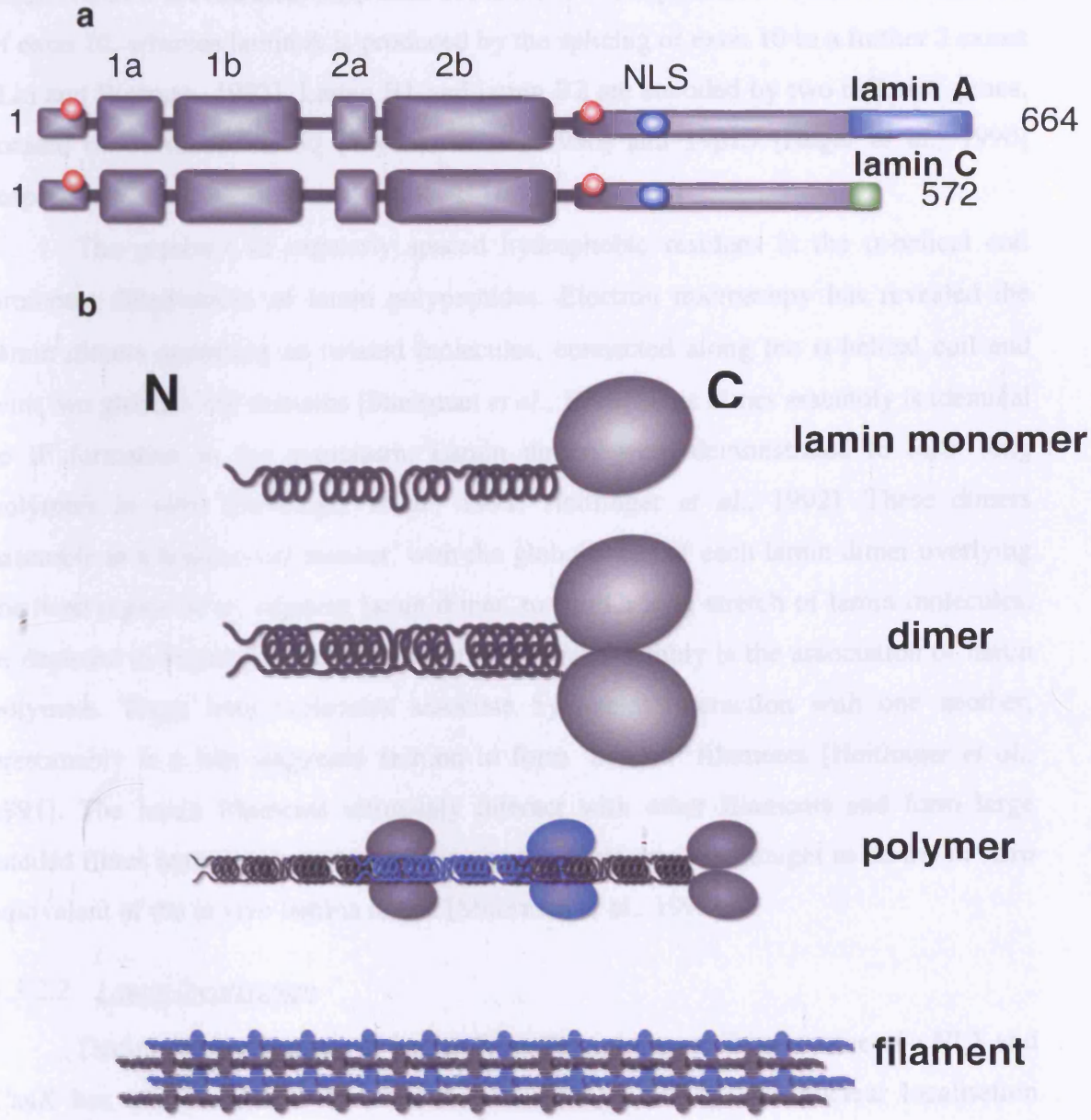

Figure 5. Lamin A/C. (a) Polypeptide representation of lamin A (upper) and lamin C (lower). Large boxes represent α-helical domains, red spots represent phosphorylation sites, blue spot shows the position of the nuclear localisation signal (NLS), blue box is the region specific to lamin A, green box is the region unique to lamin C. (b) Predicted protein structure, top model illustrates the small N-terminus, four α-helical coils, and the C-terminus globular region, next models demonstrate the dimerisation of lamin monomers at their α-helical domain and the 'head to tail' assembly of a lamin polypeptide. Lower diagram shows the lateral assembly of lamin polypeptides to form lamina filaments.

suggested that these two cDNAs were alternative transcripts from the same gene. Genomic mapping of lamin A and lamin C revealed the presence of 12 exons of which lamin A and C are identical until exon 10; lamin C is the product of a small continuation of exon 10, whereas lamin A is produced by the splicing of exon 10 to a further 2 exons [Lin and Worman, 1993]. Lamin B1 and lamin B2 are encoded by two different genes, located on chromosome 5q [Wydner *et al.*, 1996] and 19p13 [Hoger *et al.*, 1990] respectively.

The presence of regularly spaced hydrophobic residues in the α-helical coil promotes dimerisation of lamin polypeptides. Electron microscopy has revealed the lamin dimers appearing as twisted molecules, connected along the α-helical coil and with two globular tail domains [Stuurman *et al.*, 1998]. This dimer assembly is identical to IF formation in the cytoplasm. Lamin dimers were demonstrated to form long polymers *in vitro* [Heitlinger *et al.*, 1991; Heitlinger *et al.*, 1992]. These dimers assemble in a head-to-tail manner, with the globular tail of each lamin dimer overlying the head region of an adjacent lamin dimer, to form a long stretch of lamin molecules, as depicted in Figure 5b. The next level of lamina assembly is the association of lamin polymers. These long molecules associate by lateral interaction with one another, presumably in a half-staggered fashion to form 'beaded' filaments [Heitlinger *et al.*, 1991]. The lamin filaments ultimately interact with other filaments and form large banded fibres resulting in paracrystalline arrays. This array is thought to be the *in vitro* equivalent of the *in vivo* lamina lattice [Stuurman *et al.*, 1998].

1.3.2.2 Lamin localisation

Distinguishing features of lamins from IF proteins are the presence of a NLS and CaaX box at the extreme carboxyl terminus [Nigg, 1992]. The nuclear localisation signal (Lys-Lys-Arg-Lys-Leu-Glu) located at residues 417-422 in lamin A/C is capable of directing the translocation of the protein to the nucleus [Fisher *et al.*, 1986]. Disruption of this NLS in the lamin proteins results in the localisation of lamins with cytoplasmic membranes and formation of lamina structure within the cytoplasm [McKeon, 1991]. The successful localisation of lamins to the nucleus is the first step of lamina formation. The next step is the inclusion of these proteins into the lamina.

Lamin A, lamin B1 and lamin B2 all have a feature at the extreme carboxyl terminus of the polypeptide known as a CaaX box, where C is a cysteine residue, a is an aliphatic amino acid and X is any amino acid. This CaaX box is a site for post-

translational modification of the protein, composed of three stages; isoprenylation of the cysteine, proteolytic removal of the terminal three amino acids, then carboxyl-methylation of the isoprenylated cysteine [Kitten and Nigg, 1991]. The purpose of these modifications is now known to be the generation of a lipid hydrophobic tail in a hydrophilic protein. This enables membrane association and since the lamins have already been localised to the nucleoplasm the nearest membrane to become attached to is the INM. The combination of the NLS and CaaX motifs promote lamin formation at the periphery of the nucleoplasm. The attachment of B-type lamins with nuclear membrane fragments during mitosis is consistent with this process, however lamin A becomes soluble at this period. Additional studies with lamin A revealed that upon its incorporation into the lamina the final 15 amino acids of the prenylated protein are removed by a specific lamin A endoprotease located in the inner nuclear membrane [Kilic *et al.*, 1999]. In overview, the localisation of the lamins is determined firstly by their NLS, secondly by creation of a hydrophobic tail which inserts in the INM, lamina formation occurs at this time, after which lamin A only is further cleaved producing a lamina-associated non-membrane attached lamin molecule. The exception to this above process is lamin C which bears no CaaX motif [Fisher *et al.*, 1986] and its sub-nuclear localisation is dependent on direct incorporation into the preformed lamina. Considered together, newly translated lamin A, lamin B1 and lamin B2 can independently incorporate into the nuclear lamina, however lamin C is dependent on a preformed lamina. In mitosis lamin B1 and lamin B2 remain associated with membrane fragments and lamin A (now deficient in prenylated cysteine) and lamin C become soluble. In a state of nuclear membrane reassembly the B-type lamins firstly create the foundation of the lamina after which lamin A and lamin C may become incorporated.

The exact timing of assembly and disassembly of the lamina during mitosis is crucial with respect to the other dynamic changes which also occur at this time. Initial studies demonstrated that the lamina is depolymerised into monomeric subunits at mitosis and that these monomeric lamin units are reincorporated into the nuclear lamina of daughter nuclei [Gerace and Blobel, 1980]. The disassembled lamins were shown to be hyperphosphorylated and then dephosphorylated upon reassembly. The sites of phosphorylation were determined as serine 22 and serine 392 of lamin A and lamin C [Ward and Kirschner, 1990]. Interestingly, these two serine residues are positioned exactly five amino acids from the ends of the α-helical rod domain (Figure 5a) and conserved in all lamins from all species [Heald and McKeon, 1990]. Both of these

serine residues are positioned between two proline residues and it was therefore considered that phosphorylation induces a conformational change at these sites and ultimately affects the ability of the α-helical rod to promote dimer assembly. Mutation analysis of these two serine sites were shown to impair lamina dissassembly at mitosis, with marked persistence of the nuclear lamina at stages of chromosome condensation [Heald and McKeon, 1990]. The removal of the two serine/proline domains resulted in mitotic arrest in transfected cells, with virtually all transfected cells in an interphase state. In addition a region of 33 amino acids and a region of 32 amino acids at the beginning and end of the α-helical domain respectively were shown to be crucial for the formation of the lamina. The phosphorylation of nuclear lamins is mediated by cdc2 kinase, a major regulator of the eukaryotic cell cycle [Peter *et al.*, 1990] and is central to the formation of lamin dimers. However, another kinase was demonstrated to act on serine 16 on chicken lamin B2 and found to be crucial in the head to tail longitudinal assembly of dimers [Peter *et al.*, 1992].

1.3.2.3 Lamin expression

Discrimination between A-type and B-type lamins is also achieved by considering their expression profiles. In general, B-type lamins are expressed in virtually all somatic cells, while A-type lamins are absent from early embryos and undifferentiated cells, but expressed in most other cell types [Gerace and Burke, 1988]. The expression of lamins has been addressed in human tissues and mammalian cell lines [Broers *et al.*, 1997; Lin and Worman, 1997]. Lamin B1 expression is low but detectable in all human tissues, however lamin A/C expression is variable [Lin and Worman, 1997]. Both lamin A and lamin C are highly expressed in the heart, placenta and skeletal muscle, other tissues show little or no lamin A/C expression. The expression of A-type lamins in cell culture is also highly variable, in contrast to lamin B1 expression, which is generally high. This supported an earlier study whereby lamin A and lamin C is completely absent from a human T lymphoblastic cell line, but lamin B1 was present; hence it was believed that lamin B1 is sufficient for nuclear lamina formation [Guilly *et al.*, 1987]. A-type lamin expression was assayed in mouse tissues, from a very early stage of embryogenesis to adulthood [Rober *et al.*, 1989]. Lamin A/C was completely absent from all tissues in the embryo until the 11^{th} embryonic day. The mesenchyme and connective tissue show the earliest signs of lamin A/C expression, with the skeletal muscle exhibiting high levels of lamin A/C. Most other tissues begin to

express lamin A and lamin C around birth and postnuptially. From these studies it was apparent that once a cell type is committed, it maintains lamin A/C expression. A thorough analysis of A and B-type lamin expression in human tissues was performed by Broers and co-workers [Broers *et al.*, 1997]. Lamin B2 expression was found in all tissues analysed, however lamin B1 expression was much more restricted, being absent in some skin endothelium cells, cells in the kidney and urinary bladder, neuroendocrine cells such as the thyroid and all types of muscle. Lamin A/C expression was found to be variable but present in most cell types, with absence in immune-response cells. Lamin A and lamin C expression was not assayed in adipose tissues.

The absence of lamin A and lamin C from developing cells and near ubiquitous expression from terminally differentiated cells suggests the association of lamin A and lamin C expression with the commitment of cell differentiation [Stuurman *et al.*, 1998]. The developmental specificity of A-type lamin expression is considered to be under transcriptional regulation [Lin and Worman, 1997]. Lamin A and lamin C are alternative transcripts of the *LMNA* gene, possessing the same 5' ends and thus the same initiation codon under control of the same promoter [Lin and Worman, 1997]. Sequencing of the lamin A/C promoter allowed the identification of a retinoic acid-responsive element [Okumura *et al.*, 2000], the biological implications of which are predicted to be involved in developmental lamin A/C expression.

1.3.3 Lamina-associated and lamin-interacting proteins

The A-type and B-type lamins are the major contributors to the nuclear lamina, however since their identification other lamina and lamin associated proteins have been recognised. The localisation and relationship of these proteins with the lamina is shown in Figure 6.

1.3.3.1 Lamin B receptor (LBR)

LBR was the first protein found to interact with the lamin proteins [Worman *et al.*, 1988]. The chicken LBR protein is composed of 637 amino acids and consists of eight transmembrane domains and an amino-terminal 200 amino acid nucleoplasmic projection [Ye and Worman, 1994]. The transmembrane region spans the inner nuclear membrane and the amino-terminal domain has two potential interaction sites. The first, positioned between residue 1 and 60 is considered to be involved in lamin binding and the region from residue 97 to 174 binds chromatin [Chu *et al.*, 1998]. LBR binds

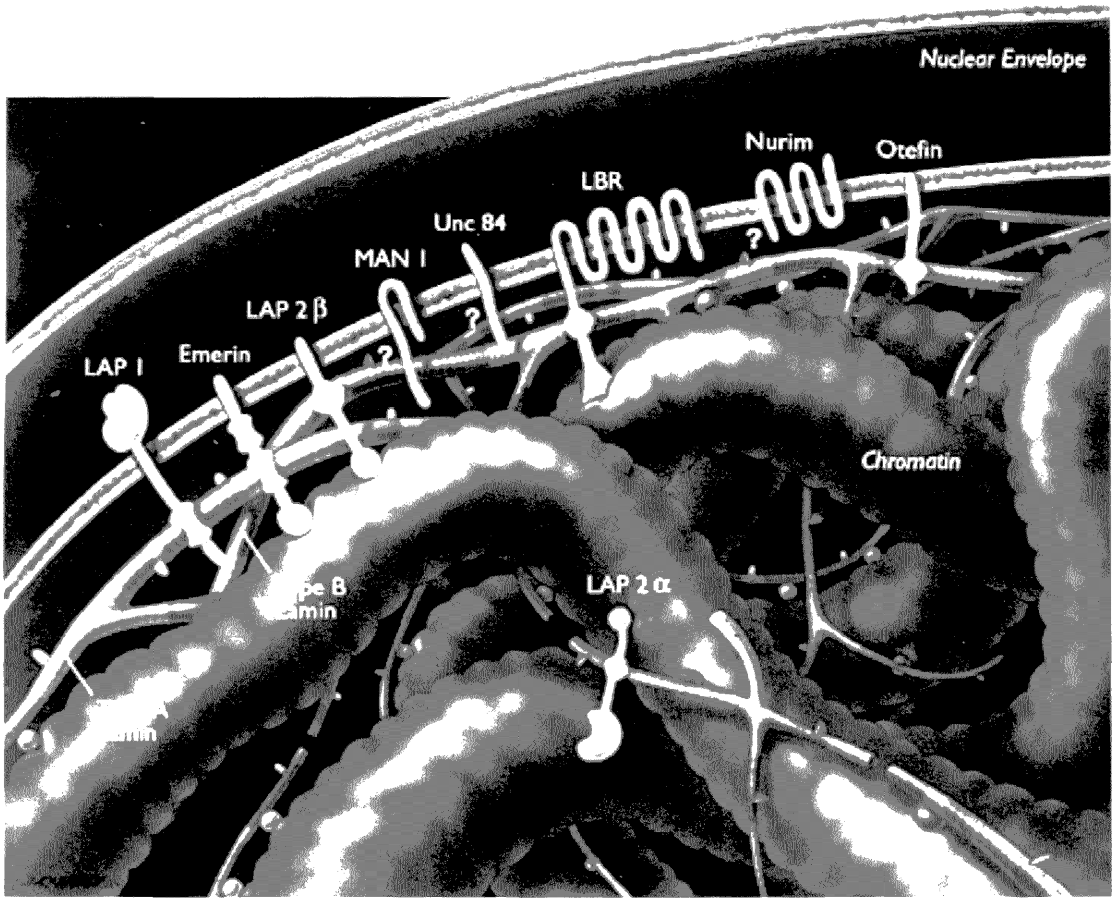

Figure 6. Hypothetical illustration of interactions with the lamina at the nuclear periphery. The outer and inner nuclear membranes are depicted as double membranes. The lamin binding proteins all span the INM (with the exception of LAP2α) and interact with A-type or B-type lamins and chromatin. Reproduced with permission by Trends in Biochemical Sciences [Cohen *et al.*, 2001].

strongly to both lamin B and DNA *in vitro* [Worman *et al.*, 1988; Ye *et al.*, 1997]. Heterochromatin is tightly packed DNA, rarely required for transcription. In higher eukaryotic nuclei, heterochromatin is associated with the nuclear lamina. A heterochromatin-associated protein (HP1) binds to LBR and mediates the chromatin binding [Ye *et al.*, 1997].

1.3.3.2 Lamin associated proteins (LAPs)

The LAPs were identified using antibodies that localised to the nuclear periphery [Senior and Gerace, 1988]. The LAPs were classified as LAP1 or LAP2 on the basis of immunological detection.

Three related forms of LAP1 (LAP1A, LAP1B and LAP1C) are likely to be products of alternative splicing from the same gene [Stuurman *et al.*, 1998]. All LAP1 isoforms bind chromatin *in vitro* [Foisner and Gerace, 1993], however only LAP1A and LAP1B bind lamins A, C and B1. In contrast LAP1C does not bind lamins. The LAP1 isoforms range in size from 55-75 kDa and the cloning of LAP1C showed the presence of 506 amino acids [Martin *et al.*, 1995]. LAP1C possesses a single transmembrane domain, the inability of lamin binding was not elucidated. Interestingly, LAP1A and LAP1B are abundant in differentiated cells only and it is speculated that these two proteins interact with A-type lamins in a developmentally regulated manner [Chu *et al.*, 1998].

There are several isoforms of LAP2 in mammals (α, β, γ, δ, ε and ζ) [Foisner and Gerace, 1993], all alternative transcripts from the same gene [Harris *et al.*, 1995]. All of the LAP2 isoforms share a common amino terminal domain (residues 1-187). Beyond this region LAP2α is completely different from the other isoforms, possessing no transmembrane domain, whereas the other LAP2 isoforms all contain a single transmembrane domain near the carboxyl terminus [Chu *et al.*, 1998]. The domain (1-85) common to all LAP2 isoforms is responsible for interactions with chromatin, a domain adjacent to the TM spanning region interacts with B-type lamins [Furukawa *et al.*, 1998], this region is absent in LAP2α. LAP2α has a unique 507 amino acids, which is neither involved in transmembrane spanning, or interactions with B-type lamins. A recent investigation demonstrated that LAP2α was able to directly bind A-type lamins *in vitro* and *in vivo* [Dechat *et al.*, 2000]. The extreme carboxyl terminus of LAP2α binds lamin C specifically in the globular-tail domain, common to lamin A and lamin C.

1.3.3.3 Emerin

Emery-Dreifuss muscular dystrophy (EDMD) is a human disorder characterised by slow progressive muscle wasting and cardiac conduction defects [Emery, 1989]. It has been recognised as either an X-linked or autosomal dominant form. The X-linked form is caused by mutations in the STA gene [Bione *et al.*, 1994], which encodes an inner nuclear membrane protein with homology to LAP2 [Nagano *et al.*, 1996]. Emerin is a protein of 254 amino acids and contains a single transmembrane domain. Co-localisation of emerin with A-type lamins suggested that these two proteins interact [Manilal *et al.*, 1998]. Subsequent protein interaction analysis with lamin A and emerin has proven this direct association [Clements *et al.*, 2000; Sakaki *et al.*, 2001]. The region from 1-188 of emerin is capable of binding lamin A [Clements *et al.*, 2000] and the interaction with lamin A is stronger than with lamin C [Sakaki *et al.*, 2001].

1.3.3.4 Other lamin binding proteins

Several other proteins have been found to either localise to the nuclear lamina, or bind to lamins. These include nurim [Rolls *et al.*, 1999], otefin [Ashery-Padan *et al.*, 1997], Narf [Barton and Worman, 1999], MAN1 [Lin *et al.*, 2000], Nup153 [Smythe *et al.*, 2000] and Rb [Mancini *et al.*, 1994]. The human protein nurim (nuclear rim protein) localises to the nuclear periphery and has a predicted mass of 29 kDa, with 5 potential transmembrane domains [Rolls *et al.*, 1999]. Otefin is a *Drosophila* protein localised to the INM, biochemically it is not a transmembrane protein, however there is a region of hydrophobicity in the polypeptide [Ashery-Padan *et al.*, 1997]. Using lamin A in a yeast two-hybrid screen to identify lamin A interacting proteins, a novel protein, Narf, was isolated [Barton and Worman, 1999]. Narf only interacts with prenylated prelamin A and is considered to be pivotal in mature lamin A formation. Narf is a protein of 456 amino acids with no predicted TM domains. MAN1 was isolated by the virtue of being localised to the INM [Lin *et al.*, 2000]. The protein is 82 kDa in mass and contains two transmembrane domains located towards the carboxyl terminus. Comparison of the amino acid sequence of MAN1 to emerin and LAP2 revealed the conservation of a 43-residue motif, termed the LEM module (LAP2, emerin, MAN1) near the amino terminus, corresponding to the nucleoplasmic projections. This LEM domain is likely to form two α-helices, its function is unknown.

The association of Nup153 with the lamina demonstrates the anchoring of nuclear pores on the lamina. Nup153 is a nucleoporin protein and part of the nuclear

pore complex [Radu *et al.*, 1995]. Co-immunoprecipitation of Nup153 with lamin B3 (an alternatively spliced isoform of lamin B2) confirms this [Smythe *et al.*, 2000]. The interaction of Nup153 with other lamins has not been investigated.

Finally, the finding that the retinoblastoma protein (Rb) interacts with lamin proteins suggested possible functions of the lamina in gene transcription [Mancini *et al.*, 1994; Ozaki *et al.*, 1994]. Rb is a 110 kDa tumor suppressor protein and can repress gene transcription. It is a DNA binding protein and is differentially phosphorylated during the cell cycle. Experiments *in vivo* and *in vitro* have demonstrated the direct interaction between Rb and the A-type lamins.

1.3.4 Functions of the nuclear lamina

Although the discovery of the lamina was achieved by isolation of lamina with nuclear pore complexes [Aaronson and Blobel, 1975] and this association was considered to be the function of the lamina, a multitude of other roles have now been assigned to this proteinaceous mesh at the periphery of the nucleoplasm.

The most extensively studied area of lamin function is its role in nuclear architecture of chromatin and effects on gene transcription. Transcriptionally inactive heterochromatin is known to localise near the lamina [Blobel, 1985]. The finding that LBR binds a protein of heterochromatin HP1 [Ye *et al.*, 1997] and that the α-helical domain [Glass *et al.*, 1993], in addition to a region in the carboxyl terminus (residues 396-430 of lamin C) [Taniura *et al.*, 1995] of both A and B-type lamins possesses a chromatin binding site strongly implicates the lamina in chromatin organisation. The latter report specifically determined that the lamins were capable of interacting with core histones, components of higher order chromatin structure. The chromatin binding of lamins, LAPs and LBR imply that the nuclear lamina exerts effects on the organisation of chromosomes in the interphase nucleus. However, the observation that B-type lamins are retained on INM fragments during mitosis, whereas A-type lamins become soluble and eventually surround the condensing chromosomes in anaphase [Gerace and Blobel, 1980] suggests that the lamina is necessary for nuclear envelope formation around daughter chromosomes [Nigg, 1992]. The presence of A-type lamins on chromosomes may polymerise with B-type lamins and mediate assembly of the nuclear membrane around the two new nuclei in the post-mitotic cell [Hutchison *et al.*, 1994].

The association of the lamina with chromatin is also considered to be relevant in DNA replication during interphase [Hutchison *et al.*, 1994]. In a post-mitotic cell the DNA must replicate before another cell division can occur. DNA replication initiation occurs at regular intervals along the genome and disruption of the lamina has been shown to inhibit DNA replication initiation [Ellis *et al.*, 1997] and elongation [Moir *et al.*, 2000].

The most recognised function of the lamina is that of providing structural rigidity to the nuclear envelope and stabilising nuclear envelope structures [Hutchison *et al.*, 1994]. The lamina is arranged as a well-connected scaffold [Stuurman *et al.*, 1998], that either directly interacts with the INM or is anchored by other proteins (Figure 6) [Cohen *et al.*, 2001]. Experiments which have disrupted lamina formation have also caused morphological changes in the nuclear envelope [Schirmer *et al.*, 2001]. The positioning and spacing of nuclear pores is also a highly probable role of the lamina, especially considering the interaction of lamin with nuclear pore proteins [Radu *et al.*, 1995]; in support of this, lamina disruption and clustering also results in the clumping of nuclear pores [Schirmer *et al.*, 2001].

The specific biological function of the A-type lamins is likely to be involved in developmental and terminal differentiation of cells. The expression of lamin A and lamin C is absent from non-differentiated cells and some haematopoietic cells, however highly expressed in differentiated cells and tissues [Guilly *et al.*, 1987; Rober *et al.*, 1989; Broers *et al.*, 1997]. An increase in A-type lamin expression has been observed in cellular quiescence and thus provides additional evidence for the role of lamin A and lamin C in cell-specific development and maintenance.

1.4 Approaches towards disease gene identification and characterisation

The deciphering of the genetic code by solving the crystal structure of DNA [Watson and Crick, 1953] and the advent of new molecular genetic techniques [Saiki *et al.*, 1985] has permitted the accelerated growth in the understanding of molecular biology. The co-ordinated use of a vast range of molecular genetic techniques is pivotal in human disease genetics and toward understanding associated pathological consequences of gene dysfunction. Many distinct techniques aid in the identification of genes responsible for disease, many additional methods allow the elucidation of the molecular roles of these genes.

1.4.1 Disease-gene identification by positional cloning

The recognition of a familial basis for a human disease is the beginning of a task devoted to the ultimate identification of the gene(s) which when mutated cause a given genetic condition. With the exception of a few cases most disease loci and genes have been identified in the last two decades only [Strachan and Read, 1996]. Inheritance patterns for simple mendelian traits may be classified as autosomal dominant (disease manifests in the heterozygous state), autosomal recessive (disease only occurs in the homozygous state), or X-linked (disease is inherited in a sex associated manner) [Chung and Gardiner, 1996]. The identification of a causative gene can be achieved using one of four methods, functional and candidate gene cloning, or positional and positional-candidate gene cloning.

Functional cloning requires the absence/presence of a dysfunctional protein product. This altered protein responsible for the disease needs to be isolated and partially sequenced in order to map the protein back to the mutated gene, as illustrated in the cloning of the haemophilia A gene [Gitschier *et al.*, 1984]. Candidate-gene approaches in human disease require an understanding of the biochemical pathway which is disrupted in the disorder [Strachan and Read, 1996]. Identification of a locus or chromosome is not essential for this method as it relies entirely on the biochemical relatedness of a gene to the disorder. An example of this is the identification of mutations in the rhodopsin gene in patients with retinitis pigmentosa (RP). Firstly rhodopsin was characterised as a pigment in the rods of the retina, subsequently the search for the gene underlying RP, a disorder of eye pigment clumping, focused on rhodopsin. Mutations were identified shortly after [Dryja *et al.*, 1990].

Positional cloning is the identification of a disease-causing gene with no prior knowledge about pathology or disease mechanism. Essentially this method requires large families and uses a range of molecular genetic techniques to localise the genetic region containing the disease gene (locus). Positional-candidate cloning utilises the 'homing-in' of positional cloning whilst also considering biological candidates. These stages involved in positional cloning are described below and depicted in Figure 7.

1.4.1.1 Recombination analyses

Upon ascertainment of affected individuals and their relatives all family members are genotyped for genetic markers which are approximately evenly distributed over the whole genome. The vast majority of these markers are cytosine and adenine dinucleotide repeats $(CA)_n$ (termed microsatellites) [Weber and May, 1989] and the

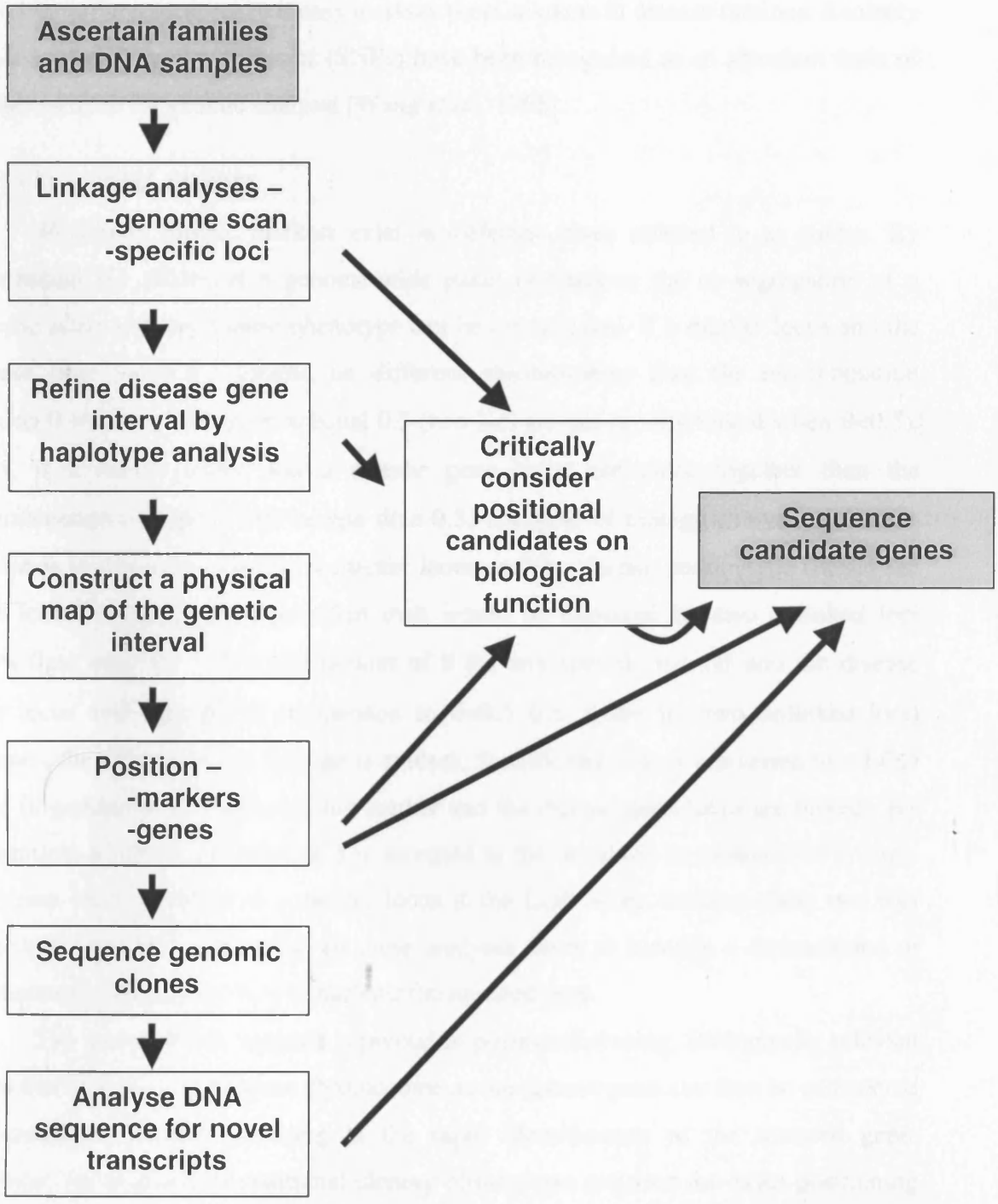

Figure 7. Overview of positional-candidate gene cloning. The whole positional cloning process is initiated with the input of DNA samples and results in the identification of mutations in a candidate gene (grey boxes). Each box represents a critical step in the methodology. Before the construction of a physical map the candidate genes are firstly considered with regard to biological candidacy before sequence analysis; whereas, positional candidates are chosen specifically with regard to their localisation and used directly in sequence analysis.

length of repeat varies greatly. The high degree of polymorphism and their simple molecular arrangement make it easy to assay these markers in disease families. Recently single-nucleotide polymorphisms (SNPs) have been recognised as an abundant form of marker suitable for genetic analysis [Wang *et al.*, 1998].

1.4.1.1.1 Linkage analyses

Molecular genetic markers exist in different states referred to as alleles. By determining the alleles of a genome-wide panel of markers the co-segregation of a specific allele and the disease phenotype can be investigated. If a marker locus and the disease gene locus are located on different chromosomes then the recombination fraction θ would be expected to equal 0.5 (two loci are genetically linked when $\theta<0.5$). Thus, if a marker locus and a disease gene locus are close together then the recombination fraction θ will be less than 0.5. The goal of linkage analysis in human disease is to determine whether a marker locus and the disease phenoytype (hence the gene locus) co-segregate more often than would be expected for two unlinked loci [Terwillger and Ott, 1994]. Calculation of θ for any specific marker and the disease gene locus and subsequent comparison to $\theta=0.5$ (i.e. value for two unlinked loci) indicates the likelihood that linkage is evident. Statistically, this is converted to a LOD score (logarithm of the odds that the marker and the disease gene locus are linked). By convention, a LOD score value of 3 is accepted as the threshold as evidence of linkage. A disease locus is linked to a marker locus if the LOD score between these two loci exceeds a value of 3. The result of these analyses serve to identify a chromosome or subchromosomal region likely to harbour the mutated gene.

The power of this analysis is pivotal in positional cloning. Biologically relevant genes that also map to the same chromosome as the disease gene can then be considered as candidates, possibly resulting in the rapid identification of the mutated gene. However, the majority of positional cloning efforts have required the exact positioning of a disease locus using haplotype analyses.

1.4.1.1.2 Haplotype analyses

Genome-wide searches for linkage use widely distributed markers and thus only define a broad locus for the disease gene. Upon the identification of a locus the disease locus must be saturated with all available polymorphic markers. The genotyping of these markers in all family members allows the construction of the distribution of alleles

on maternal and paternal chromosomes (haplotypes) with respect to offspring and parents. The generation of haplotypes allows the identification of meiotic recombinations within the disease interval. This reveals the section of the haplotype which confers disease susceptibility. The disease locus is now located within a critical genetic interval and the positioning of additional markers is essential in the fine mapping of the proximal and distal boundaries of this interval. Concurrently, all genes within this region should be considered as candidates. It is apparent that the use or construction of a genetic and physical map is crucial to the process of positional disease-gene cloning.

1.4.1.2 Construction of genetic and physical maps

The success of the human genome project has required the generation of high quality genetic and physical maps. Both forms of map are generated using genes, markers or other DNA segments, however a genetic map is constructed using the recombination coefficient as an indicator of relative distance, whereas a physical map uses genomic DNA fragments to assemble a continuous set of DNA sequence incorporating markers and genes.

1.4.1.2.1 Genetic maps

In 1987 the first genetic linkage map was published using 403 polymorphic markers (most of which were RFLPs) [Donis-Keller *et al.*, 1987]. The difficulty in RFLP typing and their limited informativity required the construction of additional genetic maps using the more evenly distributed, highly polymorphic microsatellites. Laboratories in France rapidly produced microsatellite based linkage maps, initially of 813 markers [Weissenbach *et al.*, 1992], eventually increased to 5,264 [Dib *et al.*, 1996]. Microsatellites were isolated and then typed in panels of radiation hybrids. Statistical linkage analysis indicated relative position and distance. Further genetic maps were constructed based on other types of microsatellites, for example the Co-operative Human Linkage Center (CHLC) constructed maps using the already published markers by Weissenbach and colleagues and identified other unique tri- and tetranucleotide markers (e.g. GATA) [Murray *et al.*, 1994].

These maps consisting of ordered markers became essential in rapid linkage and haplotype analyses (Section 1.4.1.1) and critical in the generation of physical maps.

1.4.1.2.2 Physical maps

The first physical maps were identified by karyotype analysis, physically partitioning DNA into discrete units called chromosomes and by the observation of *p* (*petite*) and *q* (*que*) arms. Giesma staining of metaphase chromosomes also allowed subchromosomal regions to be identified. The advent of recombinant DNA techniques in the 1980s allowed the construction of physical maps by cloning of genomic sections. This was initially performed using yeast artificial chromosomes (YACs) [Cohen *et al.*, 1993]. Although YACs have the potential to harbour large sections of genomic DNA, 33,000 were needed to cover 75% of the human genome [Chumakov *et al.*, 1995]. Polymorphic microsatellites and non-polymorphic markers (sequence-tagged sites, STSs) were amplified by the polymerase chain reaction (PCR) [Saiki *et al.*, 1988] in these YACs to determine STS content. The YACs were also analysed by restriction enzyme digestion to assess the degree of overlap of the cloned genomic DNA.

Another approach to segmented genomic mapping was also developed alongside the use of YACs. This involved the radiation-induced cleavage of total human genomic DNA, followed by the random rescue of different fragments by a rodent cell line. Roughly 100 radiation-hybrid (RH) lines were created, each possessing a selection of human genomic DNA sections [Walter and Goodfellow, 1993; Walter *et al.*, 1994]. These cell lines were screened by PCR to determine STS content, which, in turn allowed the production of a linear map of RH clones. RH calculated marker distances are measured in centiRays (cR) because the resolution of these maps is dependent on the dosage of radiation administered to cleave the genomic DNA [Strachan and Read, 1996].

The formation of YAC and RH based maps became the foundations or framework maps for all other physical maps that followed. Disadvantages in both YAC and RH panels associated with direct sequencing, large insert size and chimeras prompted geneticists to develop new cloning vectors which were capable of carrying relatively large inserts of high-quality DNA. These vectors were not susceptible to chimeras and also easy to manipulate, sequence and screen using a variety of methods. These new efficient genomic tools were known as bacterial artificial chromosomes (BACs) and bacteriophage P1 artificial chromosomes (PACs), both developed at Roswell Park Cancer Institute (RPCI) [Shizuya *et al.*, 1992; Ioannou *et al.*, 1994]. Both of these vectors carry on average between 100-200 kb of foreign DNA and propagate as plasmids in *E. coli*. BACs and PACs can be grown easily and DNA extraction is

straightforward. DNA can be used for direct PCR based STS content mapping, or for STS hybridisation mapping. Both techniques require the use of a library of BAC or PAC genomic DNA clones whereby the DNA from every clone is bound to a nylon filter. STS markers are radioactively labelled using PCR then hybridised against the library filters. Library filters are scored for the presence or absence of hybridised STS against each genomic clone. STS content mapping permits the assembly of overlapping clones over the region under investigation.

The assembly of large overlapping genomic clones to form contigs of continuous DNA is central in the physical mapping process and pivotal in the human genome mapping effort. From the aspect of positional cloning the formation of a contig of clones has many functions; correct ordering of current polymorphic markers used in haplotype analysis; ascertainment of new polymorphic markers to aid in fine-mapping of the disease critical interval; the placement of known genes or uncharacterised partial gene transcripts (expressed sequence tags, ESTs); and the direct DNA sequencing to find novel genes. All of these functions also apply to the role of the physical map in the human genome project.

Physical mapping in the 1980s and 1990s resulted in the sequencing or contig assembly of small regions of the human genome, usually those regions implicated in positional cloning efforts. The human genome mapping project was well underway in the late 1990s when some academic institutions combined their positional cloning projects with the physical mapping genomic sequencing centres. The completion of the human genome project this year will reduce the necessity for a physical mapping stage of any positional cloning project as all of the human genome is now bioinformatically available. Today the rate-limiting step in positional cloning has changed from the generation of a physical map to the identification and characterisation of genes by bioinformatic analyses.

1.4.1.3 Sequence variant detection

The identification of a disease locus by linkage analyses, the fine-mapping of the disease critical interval by haplotype studies and the construction of a physical map to identify new markers and position candidate genes all lead to the necessity for detection of mutations and sequence variants in the mutated gene. Either direct sequencing of candidate genes or the indirect search for sequence variants using single stranded conformational polymorphism analysis (SSCP) or denaturing high performance liquid

chromatography (DHPLC) achieves this. All of which require the use of the polymerase chain reaction [Saiki *et al.*, 1985] to amplify coding sequences of the candidate gene.

SSCP was first used in 1989 to detect DNA mutations [Orita *et al.*, 1989]. Gene coding sequences are amplified by PCR, denatured, the single stranded DNA molecules are electrophoresed on a non-denaturing gel and the banding pattern observed. DNA strands from each PCR will adopt a three-dimensional conformation dependent on the primary sequence. Presence of a heterozygous mutation will change the primary sequence and in turn affect the three-dimensional conformation as will be revealed by an altered banding pattern on the gel. Those PCR products with different migration patterns must then be sequenced to reveal the nature of the sequence variation. SSCP detects 70-95% of mutations in PCR products of 200 bp or less [Iwahana *et al.*, 1992].

The principle of SSCP relies on the three-dimensional structure of single strands of DNA, in contrast DHPLC relies on the three-dimensional structure of double stranded DNA molecules. PCR products of gene sequences are denatured then slowly allowed to re-anneal. If only wild-type sequence is present then the DNA strands anneal to each other perfectly, however, if a mutation exists then wild-type and mutated DNA strands will form a nearly perfect match apart from a mismatch "bubble" at the site of mutation. Perfectly matched strands are termed homoduplex and mismatched strands are termed heteroduplex. The separation of homoduplex and heteroduplex DNA is performed on a WAVE™ DNA Fragment Analysis System, using the technique of high-performance liquid chromatography [Oefner and Underhill, 1995]. DNA fragments are injected alongside triethylammonium ions (TEA) through a narrow column which is packed with alkylated polystyrene particles. Positively-charged TEA interacts with negatively charged DNA and mediates interactions with the hydrophobic tails of the solid-phase particles. Homoduplexes have a stronger binding affinity with the column matrix than heteroduplexes and thus following a increasing set of stringency washes the homoduplex DNA is retained on the column longer than heteroduplex. The result of which is the observation of changes in DNA molecule retention with mutated DNA compared to wild-type DNA. DHPLC has been successfully used in the identification of mutations in a gene which causes migraine and ataxia [Ophoff *et al.*, 1996]. DHPLC is extremely useful with large sample sets, as 96 well plates of PCRs can be automatically loaded through the packed column for analysis. PCR products which yield altered retention times are subsequently analysed for sequence changes using direct sequencing.

The above methods all have varying efficiencies at detecting sequence changes, but are unable to precisely define the nature of a DNA sequence variation. Direct sequencing of PCR products reveals the molecular change and thus is necessary as the final step in positional cloning. Sequencing technologies were developed over two decades ago [Maxam and Gilbert, 1977; Sanger *et al.*, 1977], of which the Sanger method is still employed today in academic institutions and large-scale genome sequencing centres. Candidate gene coding sequences are amplified and used as single stranded templates in a dideoxy chain termination reaction or sequencing reaction. A DNA polymerase synthesises a complementary strand to the single-stranded template incorporating normal deoxynucleotide triphosphates (dNTPs), however a low concentration of dideoxynucleotide triphosphates (ddNTPs) are also added to the reaction. Each nucleotide is represented by one of four fluorescently labelled ddNTPs and upon limited incorporation of a ddNTP in the replicated strands the extension ceases. This yields a population of molecules which differ in length by one base and each have a different dye terminator which has caused the termination of that strand. Electrophoresis of these molecules results in the size dependent detection of migrating molecules past a detection laser. This information is used to create a computerised gel image, which can be analysed using suitable software. This automated technology was adapted from the Sanger method [Smith *et al.*, 1986] and made commercially available by companies such as Perkin Elmer-Applied Biosystems. Direct sequencing is 100% efficient and will detect homozygous as well as heterozygous mutations. More importantly it can reveal the exact molecular change which is much more informative than just knowing that there is a sequence alteration. The high cost of fluorescent ddNTPs makes this technique less suitable for high throughput sequencing, however with small samples the advantages of sequencing outweigh those of alternative sequence variant detection.

1.4.2 Approaches towards understanding the molecular mechanism of disease

The identification of a mutated gene responsible for a genetic disease is the ultimate goal of a positional cloning project. It is, however, the beginning of a completely new project – the elucidation of a molecular mechanism for the disease in question. Typically, mutations in a given gene will result in reduced or no function of the protein (loss-of-function), or the generation of a novel or abnormal protein (gain-of-function). Autosomal dominant diseases are caused as a consequence of an altered

function in one allele, with another non-affected functional allele. There are several mechanisms in which the mutated allele manifests itself as a disease, based upon either loss-of, or gain-of function.

In dominant disorders one allele is mutated and the other is unaffected. Disease may result from one of three mechanisms. Haploinsufficiency describes the scenario whereby the disease is caused by a reduction in normal levels of functional protein. Thus the dosage of the protein product within the cell is considered critical. The second mechanism is known as dominant-negative. This effect occurs when an altered protein not only loses its own function, but exerts inhibitory effects over the normal functional protein. The final mechanism involves a gain-of function, whereby the mutated protein acquires a novel function.

1.4.2.1 Comparison of molecular mechanisms in other autosomal dominant diseases

Occasionally, a disease gene is evidently related functionally to the disease (e.g. RP and rhodopsin; Section 1.4.1), in other cases, studies may link the gene and disease together. However, the majority of positional cloning projects have revealed causative genes that bear no functional relationship to the disorder. In these cases a number of specific cell-biological molecular analyses can be carried out to determine the mechanism of disease. In such situations of site-specific mutations in disease-causing genes a disruption of a protein-protein interaction may be the underlying molecular mechanism, which results in a disease phenotype. The following examples illustrate how a protein-protein interaction may be involved with the pathogenesis of disease.

Alzheimers disease is an autosomal dominant neurodegenerative disorder associated with missense mutations in any one of at least three genes, namely the amyloid precursor protein (APP), presenilin 1 (PS1) or presenilin 2 (PS2) [Czech *et al.*, 2000]. The molecular mechanism of Alzheimers has not been elucidated, however recently a protein from the brain was found to interact with PS2 [Stabler *et al.*, 1999]. It was identified as an apoptotic protein and has now become of much interest, with relevance to the selective degeneration of neurological tissues.

Huntingtons disease (HD) is also an autosomal dominant neurodegenerative disease, caused by expansion of a triplet repeat $(CAG)_n$ in the gene *huntingtin* [The Huntington's Disease Collaborative Research Group, 1993], resulting in extended polyglutamine stretches in the 350 kDa protein (Htt). Interestingly, huntingtin is ubiquitously expressed and thus is intriguing as to why only selective cell loss is

and mutant Htt are both primarily localised to the cytoplasm [Wood *et al.*, 1996]. Considering the apparent normal subcellular localisation several groups redirected studies towards identifying interacting partners of Htt. Two proteins were found to interact at the polyglutamine stretch of Htt and expressed at high levels in the brain [Li *et al.*, 1995; Wanker *et al.*, 1997]. A contemporary hypothesis for the molecular basis of disease requires Htt aggregation via the polyglutamine stretch, of which may modulate aberrant protein-protein interactions [Reddy *et al.*, 1999]. In addition, Htt has recently been shown to interact with transcription factors only in an extended polyglutamine state and predicted to perturb gene expression [Steffan *et al.*, 2000].

Many technologies exist to determine if a protein-protein interaction exists. These include co-immunoprecipitation and *in vitro* protein complex pull-down assays of proteins. These techniques detect the interaction of two or more known proteins, whereas the yeast two-hybrid screen is a technique which allows the detection of unknown cellular proteins that bind to a protein of interest. With consideration of the above examples and many others, e.g. [Gallagher *et al.*, 2000; Kawamata *et al.*, 2001] the yeast two-hybrid has proven vital towards elucidation of disease mechanisms. In many cases, the yeast two-hybrid has identified novel interactions, but has also allowed the study of known protein-protein interactions to determine the effect of disease mutations.

1.4.2.2 Yeast two-hybrid system

The increased understanding of eukaryotic gene transcription led to the appreciation of the role of transcription factors. It was established in the 1980s that transcription factors were modular in structure, with two separable domains, one to bind the DNA and another to recruit the RNA polymerase holoenzyme [Brent and Finley, 1997]. Pioneering experiments in this field were based on the fusion of one DNA-binding domain (DBD) to a second unrelated transcription activation domain. A bacterial DBD was fused to a eukaryotic activation domain and the chimeric protein was assessed for its function in yeast; the hybrid transcription factor bound to a bacterial promoter element and activated transcription of a Gal4 responsive gene [Brent and Ptashne, 1985]. It was the concurrent work by Fields and Song that resulted in the development of a protein interaction assay [Fields and Song, 1989]. The yeast Gal4 transcription factor was split into the DBD and activation domain and these were fused to two proteins which were known to interact. The creation of an engineered reporter

gene (*lacZ*) in a yeast strain and the co-transformation of plasmids encoding these two hybrid genes revealed that the ability of the Gal4 to operate as a transcription factor was re-established when the fusion proteins interacted with each other.

The next significant advancement in this field was a study by Chien and colleagues, demonstrating that the assay could be utilised to identify new protein interactions [Chien *et al.*, 1991]. The method consisted of making a 'bait' protein, whereby the Gal4 DBD was fused to a protein of interest and expressed in yeast. A library of cDNAs were fused to the Gal4 activation domain and transformed into the Gal4 DBD expressing yeast strain. The *lacZ* reporter gene was used to assess those clones that interacted, by the presence of a blue colouration in the colony (a consequence of *lacZ* activation). Revealing the identity of the expressing cDNAs in the interacting clones confirmed the interaction of known protein binding partners, but also permitted the identification of novel protein interactions.

The final modification to the yeast two-hybrid assay was the construction of multiple reporters, of which were growth selective. Clones that contained interacting proteins activated transcription of auxotrophic genes permitting the growth of that particular clone on nutritionally deficient media. This changed the yeast two-hybrid screen to a selection, whereby either the *LEU2* or *HIS3* gene forms the selective reporter and yeast are plated onto media lacking leucine or histidine respectively [Vojtek *et al.*, 1993]. Confirmation of a protein interaction could then be performed using the second reporter, *lacZ*.

Many variations of the yeast two-hybrid are currently available [van Criekinge and Beyaert, 1999]. However, James and co-workers modified the host yeast strain and the DBD and activation domain plasmids to create a highly efficient protein interaction assay [James *et al.*, 1996]. Three reporters were constructed in the yeast PJ69-4a, using the *HIS3*, *ADE2* and *lacZ* genes. Clones that contained interacting proteins were plated onto media lacking histidine, those clones which grew were streaked onto media deficient in histidine and adenine (a more stringent promoter, permitting no 'leaky' transcription). Clones that survive these two selective tests are finally assayed using the *lacZ* reporter.

Over the last decade the yeast two-hybrid screen has developed from a pioneering experiment to a well-established functional biological technique and has in many cases defined molecular pathways and mechanisms in the cell.

1.5 Aims and objectives

The initial aims of this project were to focus on the positional cloning of the gene responsible for FPLD. This continued on from initial clinical and molecular genetic studies conducted by Dr. Steve Jackson and included the fine mapping of the critical interval of the FLPD locus, at chromosome 1q21-22 [Jackson *et al.*, 1998]. The automated genotyping of microsatellite markers in pre- and newly-ascertained FPLD families from northern Europe aided in the reduction of the FPLD genetic interval. Upon the identification of a restricted genetic interval a physical map was constructed, using all known markers, genes and transcripts previously mapped to the 1q21 region. This map was generated using genomic clones, with the aim of producing a complete physical representation of the FPLD genetic interval. These contiguous sets of clones were used to correctly position markers and genes at 1q21 and ultimately submitted for sequencing at the Sanger Centre, thus contributing to the human genome-mapping project.

The identification of the gene mutated in FPLD, permitted the analysis of inheritance of mutations in affected individuals in ascertained FPLD kindreds. Mutation screening techniques were also used to screen for FPLD mutations in clinically related phenotypes, including diabetes and hyperlipidaemia.

To further understand the molecular mechanisms underlying the pathogenesis of FPLD, protein interaction technologies were utilised. The yeast two-hybrid system is one potential system to screen for interacting partners of the FPLD gene, and resulted in the identification of several lamin interacting proteins. By considering their potential biological function, these protein-protein interactions have allowed further speculation on the molecular mechanism for FPLD.

2 MATERIALS AND METHODS

2.1 Materials

2.1.1 General Reagents

All chemicals and reagents were purchased from Sigma-Aldrich (Poole, UK), BDH (Poole, UK), or Fisher (Loughborough, UK) apart from those listed below.

α [^{32}P]-dCTP	Amersham Pharmacia Biotech Inc. (Little Chalfont, UK)
α [^{33}P]-dCTP	Amersham Pharmacia Biotech Inc. (Little Chalfont, UK)
100 bp DNA ladder	New England Biolabs UK Ltd. (Hitchin, UK)
1 kb DNA extension ladder	Life Technologies Ltd. (Paisley, UK)
Agarose	Bio Gene (Kimbolton, UK)
Ampicillin	Melford Laboratories (Suffolk, UK)
Dextran sulphate	Amersham Pharmacia Biotech Inc. (Little Chalfont, UK)
dNTPs	Amersham Pharmacia Biotech Inc. (Little Chalfont, UK)
Glutathione-Sepharose 4B	Amersham Pharmacia Biotech Inc. (Little Chalfont, UK)
IPTG	Melford Laboratories (Suffolk, UK)
L-[^{35}S] methionine	Amersham Pharmacia Biotech Inc. (Little Chalfont, UK)
Long Ranger acrylamide	FMC Bioproducts (Chicago, USA)
MDE SSCP gel solution	FMC Bioproducts (Chicago, USA)
Nonidet P-40	ICN Biomedicals (High Wycombe, UK)
Hybond N+ nylon membrane	Amersham Pharmacia Biotech Inc. (Little Chalfont, UK)
Poly (dA-dC)-Poly (dG-dT)	Amersham Pharmacia Biotech Inc. (Little Chalfont, UK)
ProtoGel	National Diagnostics (Hull, UK)
SequaGel-6	National Diagnostics (Hull, UK)
SequaGel-complete	National Diagnostics (Hull, UK)
X-Gal	Melford Laboratories (Suffolk, UK)
YNB	Qbiogene (Harefeld, UK)

2.1.2 Enzymes

All enzymes and enzyme buffers were purchased from Life Technologies Ltd. (Paisley, UK), or New England Biolabs UK Ltd. (Hitchin, UK) apart from those listed below.

AmpliTaq DNA polymerase	ABGene (Epsom, UK)
Klenow DNA polymerase	Amersham Pharmacia Biotech Inc. (Little Chalfont, UK)
Pfu DNA polymerase	Stratagene (La Jolla, USA)

2.1.3 Oligonucleotides.

All oligonucleotides were purchased from Interactiva (Germany), 5' fluorescently labelled oligonucleotides were purchased from Applied Biosystems (Foster City, USA). PCR primers for STS probes were made at the Sanger Centre on an ABI 3948 DNA synthesiser (Foster City, USA).

2.1.4 Molecular Biology Kits

BigDye terminator	Applied Biosystems (Foster City, USA)
Gel purification kit	Qiagen (Crawley, UK)
Midiprep kit	Qiagen (Crawley, UK)
Miniprep Kit	Qiagen (Crawley, UK)
PCR purification kit	Qiagen (Crawley, UK)
Quikchange Site-Directed mutagenesis	Stratagene (La Jolla, USA)
TNT® Quick Coupled transcription/translation System	Promega (Madison, USA)
Yeast plasmid rescue kit	Zymo Research (Orange, USA)

2.1.5 Patient samples

Venous blood samples (10 ml) were taken from patients and collected in EDTA tubes. Blood was stored at -80°C.

2.1.6 Recipes

2.1.6.1 Common recipes

6× sucrose loading dye

6× TBE

35% (w/v) sucrose

0.25% (w/v) bromophenol blue

0.25% (w/v) xylene cyanol

10× PCR buffer

750 mM Tris-HCl pH8.8

200 mM $(NH_4)_2SO_4$

0.1% (v/v) Tween 20

10× TBE

890 mM Tris-base

890 mM boric acid

20 mM EDTA-NaOH pH8.0

20× SSC

3 M NaCl

0.3 M Trisodium citrate

Adjust pH to 7.0 with HCl

BAC prep solution I

50 mM glucose

25 mM Tris-base

1 mM EDTA

BAC prep solution II

0.2 M NaOH

1% SDS

BAC prep solution III

3.5 M KOAc

Church hybridisation buffer [Church and Gilbert, 1988]

0.5 M Na_2HPO_4 pH 7.2

1% (w/v) BSA

1 mM EDTA

7% (w/v) SDS

Denaturing PAGE loading dye

95% (v/v) formamide

0.1% (w/v) dextran blue

LacZ buffer

60 mM Na_2HPO_4

40 mM NaH_2PO_4

10 mM KCl

1 mM $MgSO_4$

50 mM β-mercaptoethanol

Adjust pH to 7

Paraffin block extraction buffer

5 mM KCl

1 mM Tris-HCl pH8.3

250 μM $MgCl_2$

0.5 mg/ml proteinase K

0.45% (v/v) Nonidet P-40

0.45% (v/v) Tween 20

Protein digestion buffer

10 mM Tris-base

0.1 mM EDTA

0.75 mM NaCl

2.5% (w/v) SDS

Adjust pH to 10.5 with NaOH

Strip solution II

0.1× SSC

0.2 M Tris-base

1% (w/v) sarcosyl

Sucrose lysis buffer

11% (w/v) sucrose

10 mM Tris-HCl pH7.5

5 mM $MgCl_2$

1% (v/v) Triton-X

TE

10 mM Tris-HCl pH7.4

1 mM EDTA pH8

$T_{0.1}E$

10 mM Tris-HCl pH7.4

0.1 mM EDTA pH8

Transformation buffer

15 mM $CaCl_2$

250 mM KCl

10 mM PIPES

55 mM $MnCl_2$

Adjust pH to 6.7 with HCl

2.1.6.2 Protein analysis

1× PBS

137 mM NaCl

2.7 mM KCl

4.3 mM Na_2HPO_4

1.4 mM KH_2PO_4

2× protein sample buffer

62.5 mM Tris-HCl pH6.8

5% (v/v) β-mercaptoethanol

20% (v/v) methanol

2% (w/v) SDS

0.2% (w/v) bromophenol blue

10% (v/v) glycerol

10× SDS-PAGE running buffer

250 mM Tris-base

1.92 M glycine

1% (w/v) SDS

Destain

40% (v/v) methanol

10% (v/v) glacial acetic acid

GST binding buffer (NETN)

0.5% (v/v) Nonidet P-40

1 mM EDTA

20 mM Tris-HCl pH8

100 mM NaCl

SDS-PAGE lower buffer

1.5 M Tris-HCl pH8.8

0.4% (w/v) SDS

SDS-PAGE upper buffer

0.5 M Tris-HCl pH6.8

0.4% (w/v) SDS

SDS-PAGE stain

40% (v/v) methanol

10% (v/v) glacial acetic acid

0.025% (w/v) coomassie blue

Transfer buffer

25 mM Tris-base

192 mM glycine

20% (v/v) methanol

2.1.6.3 Media

10× Amino acids [Parchaliuk *et al.*, 1999]

20 µg/ml arginine

33 µg/ml inositol

30 µg/ml isoleucine

30 µg/ml lysine

3 µg/ml p-aminobenzoic acid

50 µg/ml phenylalanine

100 µg/ml homoserine

40 µg/ml tryptophan

30 µg/ml tyrosine

150 µg/ml valine

10× YNB

6.7% (w/v) yeast nitrogen base with ammonium sulphate

LB agar

1% (w/v) tryptone

0.5% (w/v) yeast extract

0.85 M NaCl

2 mM NaOH

1.5% (w/v) agar

LB broth

1% (w/v) tryptone

0.5% (w/v) yeast extract

0.85 M NaCl

2 mM NaOH

YPD agar

1% (w/v) yeast extract

2% (w/v) peptone

2% (w/v) glucose

3% (w/v) agar

YPD broth

1% (w/v) yeast extract

2% (w/v) peptone

2% (w/v) glucose

Yeast minimal media

1× amino acid mix

1× YNB

2% (w/v) glucose

2.2 Methods

2.2.1 Patient DNA extraction

2.2.1.1 Human blood

Blood samples (10 ml) were chilled on ice for 30 min. Ice cold sterile dH_2O was added to a volume of 50 ml (or 5× the sample volume); following brief vortexing the samples were centrifuged in 50 ml tubes at 2000×*g*, 4°C for 10 min. The supernatant was discarded and the pellet gently resuspended in 25 ml of ice-cold sucrose lysis buffer and incubated on ice for 10 min. Samples were centrifuged at 2000×*g*, at 4°C for 10 min, the supernatant was then discarded and the pellet gently resuspended in 3 ml of protein digestion buffer containing proteinase K (0.2 mg/ml). The samples were incubated at 37°C overnight. 2 ml of 6 M NaCl were added, and the samples agitated for 20 sec, after which they were centrifuged at 3500×*g*, at 4°C for 30 min. The supernatant was collected and 10 ml of 100% ethanol (RT) was added; following repeated inversion of the sample a DNA precipitate appears. This was spooled out using a pipette tip and placed in 1 ml of 70% ethanol in a 1.5 ml centrifuge tube. After centrifugation at 800×*g* for 10 min, the supernatant was removed and the pellet air-dried. The DNA was resuspended in 500 µl of TE. A 500-fold dilution of the DNA was quantified at a wavelength of 260 nm. The DNA concentration was calculated using the equation, 1 OD_{260} unit equals 50 µg/ml.

2.2.1.2 Human pathological specimens embedded in paraffin

Paraffin blocks were cut into 6 µm sections and placed in a centrifuge tube. 1 ml of xylene was added and incubated at room temperature for 5 min. Samples were then centrifuged at 16000×*g* for 3 min, after which the supernatant was removed, and the samples washed a further two times using xylene. The resulting pellet was washed three times with 1 ml of 100% ethanol, incubating after each wash at RT for 2 min, and subsequently centrifuged at 16000×*g* for 3 min. The pellet was vacuum dried for 10 min, and resuspended in 400 µl of paraffin block extraction buffer plus 0.5 mg/ml proteinase K and incubated at 58°C overnight. The following day the sample was heated at 96°C for 15 min to denature the proteinase K.

2.2.2 Oligonucleotide design

2.2.2.1 Genomic DNA

Polymorphic microsatellites were selected from the Généthon linkage map [Dib *et al.*, 1996]. Those located in or surrounding the FPLD critical interval were chosen. Oligonucleotide primer sequences for the markers were obtained from the Généthon database (www.genethon.fr). Other tetranucleotide repeat markers also located within the same interval were selected from the Co-operative Human Linkage Centre (www.chlc.org). The novel microsatellite *D1S3759* was identified 100 bp downstream of *LMNA* gene within BAC 54H19 (RPCI-11). PCR primers were generated for this marker using Primer 3 software (www-genome.wi.mit.edu/cgi-bin/primer/primer3_www.cgi). Each 5' primer for each microsatellite amplicon was labelled with a fluorophore dye (see Table 1). PCR primers for *LMNA* gene coding sequence were created using Primer 3 software (www-genome.wi.mit.edu/cgi-bin/primer/primer3_www.cgi) with reference to *LMNA* genomic structure [Lin and Worman, 1993].

2.2.2.2 BAC end STS

BAC end clone sequence required for chromosome walking was retrieved from The Institute for Genome Research (TIGR) database (www.tigr.org/tdb/humgen/bac_end_search/bac_end_search.html) [Kelley *et al.*, 1999]. BAC end sequence (from the T7 or Sp6 cloning site) was screened for repetitive elements using BLAST database searches (Section 2.2.13). Oligonucleotides for PCR primers were generated against non-repetitive BAC end sequence using Primer 3 software (www-genome.wi.mit.edu/cgi-bin/primer/primer3_www.cgi).

2.2.2.3 Cloning oligonucleotides

To generate restriction enzyme sites within a cloned DNA sequence, oligonucleotides were designed for PCR. In general, approximately 20 bases at the 3' end of the oligonucleotide corresponded to the template DNA. Within the 5' end of the oligonucleotide a restriction enzyme site was inserted 4 nucleotides from the 5' terminal phosphate.

Marker	Repeat	Genetic distance to next marker	Sense primer 5'- 3'	Antisense primer 5'- 3'	Hetero-zygosity	5' dye	T_a °C	[Mg]	Size (bp)	Origin
D1S2345	CA	2.7	CAAGCTCCGTCTCAAAC	CATCTTCCCAATCTACAGG	80	TET	52	1.5	140	www.genethon.fr
D1S2346	CA	0.6	TATCTTGCCCTGCACC	AAGTGGGTCTCCCCAG	83	FAM	60	1.5	100	www.genethon.fr
D1S305	CA	0	CCAGCTCGGTATGTTTTTACTA	CTGAAACCTCTGTCCAAGCC	82	TET	50	1.5	150	www.genethon.fr
D1S2715	CA	1.6	CACAGGATTCTGCGTCTAACT	TGCTCCAAGAACTGAAGTGA	72	HEX	57	1.5	160	www.genethon.fr
D1S303	CA	0	CGACAAGAGCGAAACTCCAT	GCTTCCCAGAGGCTAGGATT	52	HEX	62	1.5	185	www.genethon.fr
D1S2777	CA	0	GCACCACGGAACTCCAGTAT	CACCACTGTGCCCAGCTAAT	63	TET	60	1.0	260	www.genethon.fr
D1S2714	CA	0	ATGAATTGCTTGAGCCCA	AGCTATCCTCCCACCTCAGA	61	FAM	62	1.5	175	www.genethon.fr
D1S2140	GATA	-	GCTGAAAAGACACTTCAGTGG	ATGGTATGAACCTGGAGGTG	93	FAM	50	1.5	250	www.chlc.org
D1S3757	CA	-	AATGAGCAGGAGGATGCAGT	GGTTTTGGCAAACGCTAAAG	-	TET	55	1.5	250	www.gdb.org
D1S2721	CA	1.6	TTGCTCGGCCAGAGTCT	ACGCATCACACCTGGCTAGT	71	HEX	52	1.5	240	www.genethon.fr
D1S2624	CA	0.1	GGCGAGCACATCGTTA	TCCTGCACAGAGTCCAA	69	TET	50	1.5	205	www.genethon.fr
D1S506	CA	2.9	GGGCCTATGGCTGGAA	GGCTATGCTGGGGCAA	57	FAM	48	1.5	111	www.genethon.fr
D1S1600	GATA	-	TGTCACTGATTTGGGTAGCA	GTTTTCTTAATTTCTTTTGCAGG	69	HEX	55	1.5	155	www.chlc.org

Table 1. Microsatellite markers. Each microsatellite was amplfied by PCR using the corresponding sense and antisense primers at the stated annealing temperature and $MgCl_2$ concentration. The sense primer of each microsatellite was labelled with a 5' fluorophore dye (FAM, HEX or TET).

2.2.3 PCR

Based on the initial description of PCR [Saiki *et al.*, 1988], a general method for PCR was utilised. Using the appropriate primer pairs, PCR reactions were set up as shown below. A PCR reaction premix was made for each primer pair and aliquoted to a series of DNA samples.

Basic 1× PCR premix:	10× PCR buffer	1 µl
	15 mM $MgCl_2$	1 µl
	2 mM dNTPs	1 µl
	Forward primer (5 µM)	0.5 µl
	Reverse primer (5 µM)	0.5 µl
	ABGene Amplitaq	0.5 U
	Genomic DNA	50 ng
	Add dH_2O to 10 µl	

PCR reactions were placed in a 96 well microtitre plate (ABGene. Epsom, UK), covered with an adhesive lid (ABGene. Epsom, UK) and placed in a DNA Engine Thermal Cycler (MJ Research Inc. Waltham, USA). The PCR programs for each primer pair were based on the general program, which follows, selecting an optimal annealing temperature (T_a) for each primer pair.

General PCR

STEP	TEMP	TIME (min:sec)	PROCESS
1	96°C	5:00	Initial template DNA denaturation
2	96°C	0:30	Amplicon DNA denaturation
3	45-65°C	0:30	T_a oligonucleotide annealing temperature
4	72°C	0:30	DNA polymerase extension
5	-	-	Go to STEP 2, 34 times

The resulting PCR reactions were stored at -20°C until needed. Modifications to this general PCR technique were made depending on the requirements for further analysis (Sections 2.2.3.1 to 2.2.3.4).

2.2.3.1 PCR of microsatellites

Microsatellite PCRs were performed as above using the oligonucleotides for each marker at the optimal conditions (Table 1), however, a final extension period at 72°C for 10 min was added, to consistently add 3' adenine residues to all PCR products. Fluorescent PCR primers and products were stored in the dark.

2.2.3.2 PCR generation of radioactive probes

PCR reactions were performed using the oligonucleotide primers for each STS (Table 1, Appendices I and II) as above apart from the substitution of dNTPs with 0.4 µl of 5 mM dATG and 0.4 µl of either α [^{32}P]-dCTP or α [^{33}P]-dCTP. All PCR reactions using radioactive dCTP were performed under mineral oil.

2.2.3.3 PCR for genomic sequencing

PCRs used for direct DNA sequencing were performed as above, although the reaction was scaled-up to 40 µl, using 100 ng of genomic DNA. The *LMNA* gene coding sequence was amplified using the oligonucleotide primers listed in Table 2.

2.2.3.4 PCR for cloning

PCRs for cloning were performed differently to above. Oligonucleotide primers used for each construct are described in Table 3. In brief, 10 µl of 10× *Pfu* buffer (Stratagene. La Jolla, USA), 10 µl of 2 mM dNTPs, 5 µl of each primer (5 µM), 2.5 U of *Pfu* DNA polymerase, and 1 ng of template plasmid DNA were mixed and adjusted to 100 µl with dH_2O. The general PCR program was used with the modification of adjusting the length of time for the 72°C extension step (allowing 2 min/kb of amplicon). PCR reactions were stored at -20°C.

2.2.4 Agarose gel electrophoresis

DNA (PCR or plasmid) samples were analysed by taking 5 µl of sample, adding 1 µl of 6× sucrose loading dye and loaded on a 2% agarose gel (for amplicons <1 kb) or 0.8% agarose gel (amplicons >1 kb or plasmid digests), containing 50 ng/ml of ethidium bromide. Large scale cloning PCRs or plasmid digests (in general 30 µl) were combined with 5 µl of 6× sucrose loading dye and loaded on 0.8% agarose gels. All gels were run at 10 V/cm in 1× TBE for 30-60 min and finally viewed using a UV trans-illuminator.

Exon	Sense primer 5' - 3'	Antisense primer 5' - 3'	T_a °C	Product size
LMNAex1	CCCAGATCCCGAGGTCCGAC	CCTCTCCACTCCCCGCCA	67	577
LMNAex2	CAGACTCCTTCTCTTAAATC	CCTAGGTAGAAGAGTGAGTG	52	270
LMNAex3	GCTTCCTTCAAGTTCTTGTG	GCGAGCTCTGACACAGCTGG	58	281
LMNAex4	TTGGCCTCCCAGGAACTAAT	GTAAGGGTAGGGCTGCCAAG	60	290
LMNAex5	GCAGTGATGCCCAACTCAGG	CCTGCGTTCCAGCCTGCATC	65	273
LMNAex6	CTACACCGACCCACGTCCCTC	CCAGAGGACACTGCCAGCAC	65	343
LMNAex7	GTGCTGGCAGTGTCCTCTGG	CCACTCTCTCCCTGATGCAG	64	347
LMNAex8	TCAATTGCAGGCAGGCAGAG	GCTCCCATCGACACCCAAGG	64	261
LMNAex9		CCTCCGATGTTGGCCATCAG	64	475
LMNAex10	GTAAGCAGCAGGCCGGACAAAG	CACAGGAATATTCCATGGCATC	58	460
LMNAex11	GCACAGAACCACACCTTCCT	CCTACCCCTCGATGACCAG	67	455
LMNAex12	AGATGCTACCTCCCTTCTAG	TCCCATGACGTGCAGGGCAG	60	207

Table 2. *LMNA* exon primer sequences. Primer pairs were used for PCR using the optimised annealing temperature. Exon 9 was amplified using exon 8 sense primer with exon 9 antisense primer.

PCR based cloning

	Sense primer 5' - 3'	Antisense primer 5' - 3'	PCR Digest	Acceptor sites	Template	Host vector
pCDSREBP1aTF	GATCGGATCCATGGACGAGCCACCCTTCAG	GTCAGTCGACGCGGGAGCGGTCCAGCATGCC	*Bam*HI & *Sal*I	*Bam*HI & *Xho*I	IMAGE 2230916	pCDNA3
pCDSREBP1cTF	GATCGGATCCATGGATTGCACTTTCGAAGACATG CTTCAGCTTATCAACAACC	GTCAGTCGACGCGGGAGCGGTCCAGCATGCC	*Bam*HI & *Sal*I	*Bam*HI & *Xho*I	IMAGE 2230916	pCDNA3
pCILMNAmyc	CACGAATTCATGGAGCAGAAGCTGATCTCCGAGG AGGACCTGAACATGGAGACCCCGTCCCAGCG	CCAGCGAGCGCACACGGTCG	*Acc*I & *Eco*RI	*Acc*I & *Eco*RI	pCILMNA	pCI-neo
pCDSREBP1:227TF	GACGGATCCACCATGGTAACGACCACTGTGACCT CG	GTCAGTCGACGCGGGAGCGGTCCAGCATGCC	*Bam*HI & *Sal*I	*Bam*HI & *Xho*I	IMAGE 2230916	pCDNA3
pGBDULMNA389	GATCGAATTCCTGTCCCCCAGCCCTACCTCGC	GATGGATCCTTACATGATGCTGCAGTTCTGG	*Bam*HI & *Eco*RI	*Bam*HI & *Eco*RI	IMAGE 897544	pGBDUc1
pGBDULMNC389	GATCGAATTCCTGTCCCCCAGCCCTACCTCGC	CACTGGATCCTCAGCGGCGGCTACCACTCACATG GTGGTGATGGAGCAGGTC	*Bam*HI & *Eco*RI	*Bam*HI & *Eco*RI	pGBDULMNA389	pGBDUc1
pGBDUmLmna379	AGAATTCCTGCTGGAGGGCGAGGAGGAG	TAAGATCTGGCCCAGCCTGGCAGGTCCCA	*Bgl*II & *Eco*RI	*Bgl*II & *Eco*RI	pBS-Lmna	pGBDUc1
pGBDUmLmna389	GATCGAATTCCTGTCCCCCAGCCCTACCTCG	TAAGATCTGGCCCAGCCTGGCAGGTCCCA	*Bgl*II & *Eco*RI	*Bgl*II & *Eco*RI	pBS-Lmna	pGBDUc1
pGBDUSREBP1aFL	GATCGGATCCATGGACGAGCCACCCTTCAG	GTCAGTCGACTAGCTGGAAGTGACAGTGGTCC	*Eco*RI & *Sal*I	*Eco*RI & *Sal*I	IMAGE 2230916	pGBDUc1
pGEXLMNA389	CCCGAATTCTGTCCCCCAGCCCTACCTCGC	GAGATGGTGCACGATGCACAG	*Eco*RI & *Sal*I	*Eco*RI & *Sal*I	pGBDULMNA389	pGEX4T3

Table 3. PCR based cloning methodology. Inserts were prepared using PCR with the above primers with the corresponding template DNA. The resulting product was digested using the PCR digest enzymes and ligated into the acceptor sites in the host vector. Image template vectors were obtained from the HGMP resource [Lennon *et al.*, 1996], pBS-Lmna (mouse lamin A in pBluescript-SK) was kindly provided by Noboru Nakajima (BERI. Osaka, Japan).

2.2.5 Genotyping of microsatellite markers

To increase throughput of microsatellite markers, PCR amplicons of differing size and fluorescent label were pooled together for each DNA sample. This was achieved by first diluting the PCR products 15-fold in dH_2O, then combining 1.5 µl of each PCR in a fresh microtitre plate, to which 1.5 µl of denaturing loading dye and 0.3 µl TAMRA™ size standard (Applied Biosystems. Foster City, USA) was added. This was denatured at 96°C for 2 min and held on ice. Polyacrylamide gels were made using 12 cm well-to-read ABI Genescan plates. A 6% gel mix was made using 20 ml of SequaGel-6, 5 ml of SequaGel complete and 100 µl of 10% ammonium persulphate (APS), then allowed to polymerise for 2 hours. Fluorescent PCR samples were loaded on the gel and electrophoresed in 1× TBE on an ABI377 DNA fragment analyser (Applied Biosystems. Foster City, USA). Raw data gels were saved for later analysis on an Apple computer (Apple. Cupertino, USA). Gel images were analysed using the Genescan Package v3.1 (Applied Biosystems. Foster City, USA) and the peak heights of each microsatellite determined using Genotyper v2.0 software (Applied Biosystems. Foster City, USA). Microsatellite allele sizes were estimated and checked for correct inheritance within the families. Alleles for each microsatellite were entered into Cyrillic 2.0 (Cherwell Scientific. Oxford, UK) in order to create haplotypes.

2.2.6 Fluorescent DNA sequencing of PCR products and plasmids

35 µl of large scale sequencing PCRs were column purified using a Qiagen PCR purification kit following the manufacturer's protocol. Purified PCR products were eluted in 30 µl of dH_2O. PCR products or plasmid DNA were then used for direct DNA sequencing with primers used to generate the PCR or using nested internal primers to the amplicon or plasmid, following the method below.

Basic sequencing reaction:	BigDye terminator mix	4 µl
	Primer (5 µM)	0.64 µl
	PCR template/plasmid	200 ng
	Add dH_2O to 10 µl	

Sequencing reactions were placed in a 96 well microtitre plate (ABGene. Epsom, UK), covered with an adhesive lid (ABGene. Epsom, UK) and placed in a DNA

Engine Thermal Cycler (MJ Research Inc. Waltham, USA). Cycle sequencing was performed as follows:

Sequencing program

STEP	TEMP	TIME (min:sec)	PROCESS
1	96°C	0:05	DNA template denaturation
2	60°C	0:10	oligonucleotide annealing
3	72°C	4:00	DNA polymerase extension
4	-	-	Go to STEP 1, 28 times

The resulting sequencing reactions were stored in the dark at -20°C until needed. The 10 µl sequencing reactions were precipitated by addition and thorough mixing of 64 µl of 100% ethanol and 26 µl of dH_2O, then left at RT in the dark for 30 min. Samples were subsequently centrifuged at 3500×*g* for 30 min and the supernatant was removed by inverting the sample onto non-fluorescent tissue paper. Residual ethanol was removed by brief centrifugation of the inverted sample at a minimal velocity. Pellets were dried and resuspended in 5 µl of denaturing PAGE loading dye. This was denatured at 96°C for 2 min and held on ice. Polyacrylamide gels were made using 36 cm well-to-read ABI plates. A 5% gel mix was made using 10.8 g of urea, 3 ml of Long Ranger® acrylamide, 3 ml 10× TBE, 15.6 ml of dH_2O, 150 µl of 10% APS and 21 µl of TEMED and allowed to set for 2 hours. Fluorescent sequencing samples were loaded on the gel and electrophoresed using 1× TBE on an ABI377 DNA fragment analyser (Applied Biosystems. Foster City, USA). Raw data gels were saved for later analysis on an Apple computer (Apple. Cupertino, USA). Gel images were analysed using the Sequencing Analysis v3.4.1 Package (Applied Biosystems. Foster City, USA).

2.2.7 Genomic BAC fingerprinting

BAC clones were restriction enzyme analysed using the published method of fluorescent fingerprinting of genomic clones [Gregory *et al.*, 1997]. BAC clone DNA (approximately 200 ng) was used for digestion. To the DNA a fingerprinting mixture was added, composed of 2.8 U of *Hind*III, 3 U of *Sau*3AI, 3.7 U Thermo Sequenase, 1 µl of NEB buffer 2, 0.2 µl of fluorescent dideoxy adenosine triphosphate ddATP (10 µM; Applied Biosystems. Foster City, USA) and the final volume was adjusted to 20 µl

with $T_{0.1}E$. A set of three clones were analysed together. The fingerprinting reaction for each was performed as described, however each of the three clones was fingerprinted using a different fluorophore labelled ddATP (the first clone was labelled with HEX ddATP, the second with TET ddATP and the third with NED ddATP). Reactions were incubated at 37°C for 1 hr. Digest products were precipitated by adding 7 µl of 0.3 M NaOAc and 40 µl of 100% ethanol. This mixture from three differently labelled BAC clone digests was pooled and centrifuged at 3000×*g* for 20 min at 20°C. The supernatant was discarded and the pellet washed in 100 µl of 70% ethanol, centrifuged at 3000×*g* for 10 min at 20°C, air-dried and resuspended in 5 µl of $T_{0.1}E$. To each pooled sample, 2 µl of marker solution was added and then denatured at 80°C for 10 min and held on ice. Samples were electrophoresed on an ABI377 DNA fragment analyser (Applied Biosystems. Foster City, USA), using 12 cm well-to-read, 4.5% denaturing polyacrylamide gel. Raw data gels were saved for later analysis using Sanger 'in-house' fingerprinting software. In brief, this entailed the analysis of the gel image using Image software (www.sanger.ac.uk/Software/Image), whereby the package produces a normalised banding image for each restriction digest. These standardised digest patterns were subsequently interpreted using FPC software v4.0 (www.sanger.ac.uk/Software/FPC), an interactive program which builds contigs from fingerprinted clones after they have been standardised with Image software [Soderlund *et al.*, 2000].

2.2.8 Hybridisations

Tertiary screen BAC nylon filters were made as follows. BAC clones were picked from a glycerol stock and used to inoculate 1 ml of LB broth supplemented with 25 µg/ml chloramphenicol, then grown at 37°C in a shaking incubator for 16 hr. Using an 'in-house' gridding robot, the cultures were used to inoculate a gridding hedgehog (sterile 96 pin tool) and spotted onto a Hybond N+ nylon membrane. Filters were placed, inoculum side up, on LB agar supplemented with chloramphenicol (25 µg/ml), and grown at 37°C for 16 hr. Filters were removed from the media and placed colony side up onto Whatman 3MM paper (pre-soaked in 10% SDS) and left for 4 min. Filters were subsequently transferred to Whatman 3MM paper soaked in 0.5 M NaOH/1.5 M NaCl and incubated for 10 min, after which the filters were placed on a dry piece of 3MM Whatman paper and left for a further 10 min. The filters were neutralised by

submerging in 0.5 M Tris-HCl pH 7.4/1.5 M NaCl for 5 min, and gently agitated in an orbital shaker. This step was repeated. A series of washes were performed by agitation in 2× SSC/0.1% SDS for 5 min, 2× SSC only for 5 min and finally rinsing twice in 50 mM Tris-HCl pH 7.4 for 5 min. The filters were air-dried (colony side up) on dry 3MM Whatman paper. When nearly dry, the DNA was fixed onto the filters by UV treatment using a Stratalinker 2400 (Stratagene. La Jolla, USA).

Library screen or tertiary screen filters were pre-hybridised in Church hybridisation buffer [Church and Gilbert, 1984] and incubated for 3 hr at 65°C with gentle rocking. Radioactive PCR probes were generated using the described method (Section 2.2.3.2).

For library screens, PCR probes were pooled for each STS bin (Appendix I). To the combined probes, a competition mixture was added, composed of 125 µl of total human placental DNA (10 mg/ml), 125 µl of 20× SSC and 5 µl of Poly (dA-dC)-Poly (dG-dT) (1 mg/ml). The final volume was adjusted to 500 µl with dH_2O. The probe mixture was denatured at 96°C for 5 min, held on ice for 2 min then added to the pre-hybridising filters. The probe mixture was left to hybridise to the filters overnight at 65°C with gentle agitation.

For tertiary screens, each probe individually was combined with the competition mix and incubated with one tertiary filter only.

All filters were subjected to stringency washes the following day. In brief, the filters were washed twice in 2× SSC (RT), twice in 0.5× SSC/1% SDS for 30 min at 65°C with agitation and finally twice in 0.2× SSC (RT). Filters were covered in Saran wrap and exposed to Fuji Medical X-ray film for 2 days at -80°C.

Probes were stripped from the filters by placing in 0.4 M NaOH and incubating at 42°C for 40 min with agitation. The filters were then placed in stripping solution II and again incubated at 42°C for 40 min with agitation. Filters were briefly rinsed in 0.2× SSC and air-dried. Filters were stored at room temperature.

2.2.9 Sequence variant screening

2.2.9.1 SSCP

Genomic PCRs (10 µl) were performed as described in Section 2.2.3. PCR sample (3 µl) was combined with 5 µl of denaturing PAGE loading dye and the final

volume adjusted to 10 µl with dH_2O. This mixture was denatured at 96°C for 5 min and chilled on ice prior to loading on a 6% polyacrylamide gel. Gels were made using 5 ml of MDE (mutation detection) solution, 1.2 ml of 10× TBE, 1 ml of glycerol (100%), 14 µl of TEMED, 100 µl of APS and the final volume adjusted to 20 ml with dH_2O. Gels were allowed to polymerise for 2 hr at RT. PCR samples were electrophoresed on the gel in 0.6× TBE using a Maxi Slab apparatus (ATTO Corporation. Tokyo, Japan) at RT, 150 V for 6 hr. DNA was visualised by silver staining. Gels were fixed for 10 min in 10% (v/v) ethanol/0.5% (v/v) glacial acetic acid, rinsed in dH_2O, stained for 10 min in 0.1% (w/v) silver nitrate, rinsed again in dH_2O, developed in 0.375 M NaOH/0.1 % (v/v) formaldehyde for 20 min, rinsed a further time in dH_2O and finally fixed for 10 min in 0.07 M Na_2CO_3.

2.2.9.2 DHPLC

Genomic PCRs (20 µl) were performed as described in Section 2.2.3. using the PCR primers LMNAex8F and LMNAex8R (Table 2). The PCR samples were subsequently denatured (96°C for 5 min) and slowly cooled (-1°C/min) to allow heteroduplex formation. 5 µl of the heteroduplex PCRs were combined with 5 µl of dH_2O and analysed on the WAVE™ Fragment Analysis System (Transgenomic Inc. San Jose, USA). The WAVE system had previously been optimised to successfully detect known mutations in the *LMNA* exon 8 amplicon. A method was developed involving a separation temperature of 62°C which allowed efficient detection of heteroduplex DNA. Detection of DNA, as it was released from the alkylated surface of the column, was achieved using an 'in-system' UV laser set at λ= 260 nm. The length of retention time was compared to the detection of DNA in the eluate.

2.2.10 Cloning methods

2.2.10.1 Preparation of ultra chemically-competent E. coli

E. coli (DH5α or BL21) were made chemically competent using the Inoue method [Inoue *et al.*, 1990]. An overnight culture of *E. coli* was grown in 2 ml of LB broth at 37°C, shaking at 300 rpm. 1 ml of this culture was used to inoculate 500 ml of LB broth supplemented with 2.5 ml of 2 M $MgCl_2$. This culture was grown at 20°C shaking at 100 rpm for 15-24 hr or until OD_{600} = 0.3-0.6. Bacteria were centrifuged at

2500×*g* for 10 min at 4°C, the supernatant was discarded and the pellet gently resuspended in 150 ml of transformation buffer (4°C). The suspension was re-centrifuged at 2500×*g* for 10 min at 4°C, the supernatant discarded and the pellet resuspended in 40 ml of transformation buffer containing 3 ml of 100% DMSO. Resuspended bacteria were aliquoted into a series of centrifuge tubes and 'snap-frozen' in liquid nitrogen. Tubes were stored at -80°C until needed.

2.2.10.2 Digestion of plasmid and insert

Cloning PCRs were generated as described in Section 2.2.3.4. PCR (95 µl) was column-purified using a Qiagen PCR purification kit following the manufacturer's protocol. Purified PCR products were resuspended in 30 µl of dH_2O. Either PCR products or plasmids containing the required insert were digested with the appropriate restriction enzymes (Table 3 and 4), along with the acceptor vector. In general, 3 µl of a 10× restriction enzyme buffer (compatible for both enzymes) and 5 U of each enzyme were combined with 2 µg of plasmid DNA or 26 µl of purified PCR and the final volume adjusted to 30 µl with dH_2O. Reactions were incubated at 37°C for 2-3 hr, then electrophoresed on an agarose gel (Section 2.2.4). Insert and vector DNA were viewed on a trans-illuminator and excised with a scalpel. DNA was purified using a Qiagen gel purification kit following the manufacturer's protocol. Digested DNA was resuspended in 30 µl of dH_2O and stored at -20°C. DNA was quantified using gel electrophoresis by comparing band intensity to a quantified standard.

2.2.10.3 DNA ligation and bacterial transformation

Approximately 20 ng of vector DNA was used in a ligation reaction. Insert was combined with vector to give a 3:1 insert:vector ratio (with respect to available termini for phosphodiester bond formation). Insert and vector DNA were incubated with 4 µl of 5× T4 ligation buffer and 1 U of T4 ligase in a final volume of 20 µl (adjusted with dH_2O) at 16°C for 12 hr.

Circular plasmids (1 ng) or ligation reactions (10 µl) were transformed into chemically competent *E. coli* DH5α or BL21 (for protein expression only). *E. coli* were made competent using the method described (Section 2.2.10.1). 100 µl aliquots of competent bacteria were slowly thawed and incubated on ice with plasmid for 30 min. Bacteria were subsequently 'heat-shocked' at 42°C for 90 sec, held on ice for a

(i) Site-directed mutagenesis based cloning

	Sense primer 5' - 3'	Antisense primer 5' - 3'	Extension	Template	Host vector
pGADGHLipa-Xba	TTGCTTGAATGCATAAAGTCTAGAAGCAGATAG GCTGGCAG	CTGCCAGCCTATCTGCTTCTAGACTTTATGCAT TCAAGCAA	23 minutes	pGADGHLipa (Y2H67)	pGADGH
pGBDULMNA389K486N	ACCGGTTCCCACCAAATTTCACCCTGAAGGCTG GG	CCCAGCCTTCAGGGTGAAATTTGGTGGGAACCG GT	10 minutes	pGBDULMNA389	pGBDUc1
pGBDULMNA389R453W	GGAGGGCAAGTTTGTCTGGCTGCGCAACAAGT	ACTTGTTGCGCAGCCAGACAAACTTGCCCTCC	10 minutes	pGBDULMNA389	pGBDUc1
pGBDULMNA389R482W	TCCCTTGCTGACTTACTGGTTCCCACCAAAGTT CA	AACTTTGGTGGGAACCAGTAAGTCAGCAAGGGA TC	10 minutes	pGBDULMNA389	pGBDUc1
pGBDUmLmna379R482W	TTGATGACCTATTGGTTCCCACCGAAG	CTTCGGTGGGAACCAATAGGTCATCAA	10 minutes	pGBDUmLmna379	pGBDUc1
pGBDUSREBP1aFL+1	GGAATTCCCCGGGGGATCCCATGGACGAGCCAC CCTTCA	TGAAGGGTGGCTCGTCCATGGGATCCCCCGGGG AATTCC	20 minutes	pGBDUSREBP1aFL	pGBDUc1

(ii) Sub-cloning

	Donor vector	Acceptor vector	Digest of insert	Acceptor sites	Host vector
pCILipa	pGADGHLipa-Xba	pCI-neo	*Eco*RI & *Xba*I	*Eco*RI & *Xba*I	pCI-neo
pCILMNA	IMAGE 897544	pCI-neo	*Sal*I & *Not*I	*Sal*I & *Not*I	pCI-neo
pCISREBP1aFL	pGBDUSREBP1aFL	pCI-neo	*Eco*RI (partial) & *Sal*I	*Eco*RI & *Sal*I	pCI-neo
pBSGal4mLmna379	pGBDUmLmna379	pBS-SK	*Hind*III (partial) & *Bgl*II	*Hind*III & *Bgl*II	pBS-SK
pGADGHSREBP1aFL	pGBDUSREBP1aFL+1	pGADGH	*Bam*HI & *Sal* I	*Bam*HI & *Xho*I	pGADGH

Table 4. Further cloning methodology.(i) Site-directed mutagenesis based cloning was achieved using overlapping sense and antisense primers with the engineered nucleotide change. With these primers a polymerase-based reaction was performed using the relevant vector DNA as template, adjusting the extension time according to the size of the plasmid. (ii) Subcloning methodology was utilised to transfer a cDNA insert from one vector (donor) to a second vector (acceptor) using the corresponding restriction enzymes.

further 2 min, then plated onto LB agar media containing the appropriate selective antibiotic (50 μg/ml ampicillin or 30 μg/ml chloramphenicol). Bacteria were incubated at 37°C overnight. Bacterial plates were stored at 4°C until needed.

2.2.10.4 Growth and storage of bacteria

Bacterial colonies were picked from transformed LB agar plates using a sterile tip and used to inoculate LB media. For screening recombinant plasmids several colonies were picked and grown in 5 ml LB broth plus appropriate antibiotic at 37°C, shaking at 300 rpm for 16 hr. To grow bacteria harbouring a plasmid with a confirmed DNA insert, a single colony was used to inoculate 50 ml of LB broth plus appropriate antibiotic, and grown at 37°C, shaking at 300 rpm for 16 hr. For long-term storage, the bacterial over-night culture (750 μl) was combined with 250 μl of 80% glycerol and stored at -80°C.

2.2.10.5 Preparation of plasmid DNA

2.2.10.5.1 Small-scale plasmid preparation

1.5 ml of overnight bacterial culture harbouring the desired plasmid was transferred to a centrifuge tube and centrifuged at 16000×*g* for 1 min at RT. The supernatant was discarded and the bacterial pellet used to obtain plasmid DNA, using the Qiagen miniprep kit following manufacturer's protocols. Purified plasmid DNA was resuspended in 50 μl of dH_2O, then stored at -20°C.

2.2.10.5.2 Large-scale plasmid preparation

Large-scale plasmid extraction was performed by centrifuging 50 ml of overnight bacterial culture at 3300×*g* for 15 min at RT. The supernatant was discarded and the bacterial pellet used to obtain plasmid DNA using a Qiagen midiprep kit according to manufacturer's protocols. Purified plasmid DNA was resuspended in 200 μl of TE, then stored at -20°C. A 100-fold dilution was quantified at a wavelength of 260 nm. The DNA concentration was calculated using the equation, 1 OD_{260} unit equals 50 μg/ml.

Following purification all plasmids were confirmed by restriction enzyme digestion using the appropriate enzymes (Table 3 and 4) and direct DNA sequencing (Section 2.2.6).

2.2.10.5.3 BAC clone plasmid preparation

BAC DNA was extracted using a modified method based on the alkaline lysis procedure of Birnboim and Doly [Birnboim and Doly, 1979]. Bacterial cultures were grown as described (Section 2.2.10.4) and 250 µl were transferred to a 'U'-bottom microtitre plate and cells centrifuged at 1000×*g* for 4 min. The supernatant was discarded and the pellet resuspended in residual supernatant by gentle agitation. 25 µl of BAC prep solution I were added and carefully mixed. 25 µl of BAC prep solution II were then added, mixed as before and incubated at RT for 5 min. 25 µl of BAC prep solution III (4°C) was added, mixed and incubated for a further 5 min at RT, after which the entire sample was transferred to a 2 µm filter-bottomed microtitre plate (Millipore. Bedford, USA), which was placed over a second 'U'-bottom microtitre plate containing 100 µl of isopropanol. The microtitre plates containing the BAC DNA samples were centrifuged at 1300×*g* for 2 min at 20°C. The filter plate was removed and the microtitre plate containing flow-through was incubated at room temperature for 30 min, before centrifugation at 3500×*g* for 20 min at 20°C. The supernatant was removed and DNA pellet briefly dried before washing in 100 µl of 70% ethanol, followed by centrifugation at 3500×*g* for 10 min at 20°C. The supernatant was removed and residual ethanol allowed to dry before resuspending the pellet in 5 µl of $T_{0.1}E$.

2.2.11 Yeast two-hybrid techniques

2.2.11.1 Growth and maintenance of yeast

The host yeast strain PJ69-4a [James *et al.*, 1996] was streaked onto YPD agar and incubated at 30°C for 3-5 days. Yeast colonies that appeared were stored at 4°C. Liquid cultures of yeast were made by taking an inoculum of a freshly streaked yeast colony and placing in YPD media, then growing for 30°C at 200 rpm for 16 hr.

Yeast harbouring a plasmid were maintained on minimal media supplemented with 40 µg/ml uracil, 60 µg/ml leucine, 20 µg/ml histidine and 40 µg/ml adenine. One or more of these latter four amino acids was omitted from the media, depending on the combinations of plasmids present and the reporter gene assay used (Section 2.2.11.4). Yeast grown on minimal media agar were incubated at 30°C for 5-7 days.

Yeast stocks were made by combining 750 µl of overnight liquid culture with 250 µl of 80% glycerol and were stored at -80°C.

2.2.11.2 Yeast transformation

Yeast were transformed using the lithium acetate/single-stranded DNA/polyethylene glycol method [Agatep *et al.*, 1998]. Yeast were grown in 5 ml of appropriate media at 30°C for 16 hr. The OD_{600} was noted using a 1 in 10 dilution and the cell density calculated (1 OD_{600} unit $\approx 1 \times 10^7$ cells/ml). The overnight culture was used to inoculate 50 ml of pre-warmed YPD to give a starting cell titre of 0.5×10^6 cells/ml. This culture was grown at 30°C, shaking at 200 rpm for 5 hr (or until $OD_{600} \approx 2$). The culture was transferred to a sterile tube and centrifuged at 3000×*g* for 5 min at RT. The supernatant was discarded and the pellet resuspended in 25 ml of dH_2O and recentrifuged at 1000×*g* for 5 min. The supernatant was again discarded and the pellet resuspended in 900 µl of dH_2O, transferred to a centrifuge tube and centrifuged at 16000×*g*. The supernatant was discarded and the pellet resuspended in approximately 700 µl of 0.1 M LiOAc (or sufficient to adjust the final suspension to 1 ml). The suspension was incubated at 30°C for 10 min, after which the cells were pipetted in 100 µl aliquots. Each aliquot was centrifuged at 16000×*g* for 1 min and the supernatant removed. Transformations were performed by adding the following constituents to each cell pellet in the order stated:

Transformation set-up

1. 240 µl of 50% (w/v) PEG_{4000}
2. 36 µl of 1M LiOAc
3. 50 µl of ss-Herring Sperm DNA (2 mg/ml)
4. 100 ng of plasmid DNA
5. add dH_2O to a final volume of 360 µl

This mixture was gently pipetted to thoroughly mix the constituents and incubated at 30°C for 30 min. Yeast cells were subsequently heat-shocked by incubating the mixture at 42°C for 30 min. The cells were centrifuged at 16000×*g*, the supernatant removed and the pellet resuspended in 200 µl of dH_2O. The transformed yeast were plated onto appropriate media.

2.2.11.3 Library screen

Using varying amounts of 3T3-L1 cDNA library DNA (100 ng – 1 μg), an optimal transformation (performed as described in Section 2.2.11.2) efficiency of 1× 10^5 transformants/μg was obtained using 1 μg of library DNA in a 1× scale transformation (Appendix III).

PJ69-4a harbouring the bait plasmid was grown in 50 ml of selective medium lacking uracil for 16 hr at 30°C shaking at 200 rpm. The next day, the yeast were diluted in 300 ml of pre-warmed YPD (30°C) to give a starting cell titre of 0.5 × 10^6 cells/ml. The culture was incubated at 30°C shaking at 200 rpm until $OD_{600} \approx 2$. The culture was transferred to a centrifuge tube and centrifuged at 3000×*g* for 5 min at RT, the supernatant was discarded and the pellet washed in 150 ml of dH_2O. The cells were recentrifuged at 1000×*g* for 5 min and the pellet resuspended in sufficient dH_20 to give a final volume of 6 ml. This suspension was centrifuged 16000×*g* for 5 min, the supernatant discarded and a transformation mix was added as described in Section 2.2.11.2, except that all of the constituents were scaled up sixty times and 60 μg of library DNA were used. Subsequent incubations and heat-shock routines were carried as described above and the final pellet resuspended in 20 ml of dH_2O. This transformation reaction was split into 4 and plated out onto four 24 × 24 cm plates containing minimal agar medium lacking uracil, leucine and histidine, supplemented with 10 mM 3-AT. Plates were incubated at 30°C for 10 days, after which they were stored at 4°C.

2.2.11.4 Reporter gene assays

2.2.11.4.1 Selective growth assay

Transformed yeast colonies were picked from solid media plates and streaked onto selective media. Generally, the selective medium lacked the amino acids required for maintaining plasmids (uracil, leucine or both) and was additionally deficient in either of the auxotrophic reporter amino acids, histidine, adenine or both. When histidine was omitted from the medium, 10 mM 3-AT was added to reduce background growth.

2.2.11.4.2 β-galactosidase assay

Transformed yeast colonies were picked from solid media plates and used to inoculate 5 ml selective liquid media, then incubated at 30°C shaking at 200 rpm for 18

hr (or until OD ≈ 1-2). Cells were centrifuged at 1100×*g* for 5 min and the supernatant discarded, then resuspended in 110 µl of fresh lacZ buffer. Following a 1 in 100 dilution in lacZ buffer, the OD_{600} was noted. 100 µl of cell suspension were added to a further 900 µl of lacZ buffer, 10 µl of 0.1% (w/v) SDS and 20 µl of chloroform. The sample was vigorously vortexed for 10 sec then incubated at 30°C for 15 min. 200 µl ONPG (4 mg/ml in 0.1 M K_2PO_4) was added and briefly vortexed for 5 sec. The samples were incubated at 30°C and the time noted. Upon the development of a yellow colouration, the reaction was stopped by the addition of 200 µl of 1 M Na_2CO_3. The time of reaction was noted. The sample was centrifuged at 1100×*g* for 5 min and the OD_{420} of the supernatant was recorded. β-galactosidase activity was expressed as specific units and was calculated using the formula below.

$$U = \frac{1000 \times OD_{420}}{(t) \times (v) \times OD_{600}}$$

where t = time of reaction in minutes

v = volume of cells used in assay (ml)

OD_{420} (absorbance of *o*-nitrophenol)

OD_{600} (cell density at start of assay)

2.2.11.5 *Plasmid rescue*

Yeast cells were grown at 30°C in YPD or appropriate selective media shaking at 200 rpm. 1 ml of culture was centrifuged at 600×*g* for 2 min, and the supernatant removed. A yeast plasmid rescue kit was utilised to extract plasmid DNA from the yeast cell pellet using zymolyase to lyse the cells. Plasmid samples were resuspended in 35 µl TE. 5 µl of this sample were used to transform *E. coli* DH5α (Section 2.2.10.3).

2.2.12 Protein methods

2.2.12.1 In vitro *translation of plasmids*

The TNT® Quick Coupled transcription/translation system was used to *in vitro* translate plasmid borne cDNA sequences downstream of a T7 promoter. Purified plasmid (1 µg) was combined with 2 µl of L-[^{35}S] methionine, 40 µl of TNT® master

mix and the final volume adjusted to 50 µl with nuclease-free dH_2O. Samples were incubated at 30°C for 90 min then stored at -80°C until needed.

2.2.12.2 GST protein expression and purification

E. coli BL21 was transformed with pGEX4T3 expression plasmid or the engineered construct pGEXLMNA389 (Table 3). A single colony was used to inoculate 5 ml of LB media supplemented with ampicillin (50 µg/ml) and grown at 200 rpm, 37°C for 16 hr. The culture was used to inoculate 45 ml of pre-warmed LB plus ampicillin (50 µg/ml), then grown for 2 hrs at 37°C shaking at 300 rpm. IPTG was added to a final concentration of 0.5 mM and the bacteria grown under the same conditions for a further 1 hour. The bacterial culture was transferred to a sterile tube and centrifuged at 3300×*g* for 10 min at 4°C. The supernatant was removed and the pellet resuspended in 5 ml of 1× PBS (4°C). Cells were sonicated twice for 10 sec, followed by centrifugation at 15000×*g* at 4°C for 10 min. The supernatant was collected and 1 ml of 50% glutathione-Sepharose 4B (prepared following manufacturer's instructions) was added. The mixture was incubated at RT for 30 min with rotation. The sample was centrifuged at 500×*g* at 4°C for 5 min and the supernatant discarded. The beads were washed in 5 ml of NETN buffer and centrifuged at 500×*g* at 4°C for 5 min. This wash was repeated a further two times. The beads were resuspended in 500 µl of NETN buffer (4°C), aliquoted into 100 µl volumes and stored at 4°C until needed.

2.2.12.3 GST pull-down

100 µl of GST purified protein, coupled to sepharose beads (Section 2.2.12.2) were incubated with 20 µl of *in vitro* translated protein (Section 2.2.12.1). The final volume was adjusted to 500 µl with NETN buffer (4°C). All samples were incubated at 4°C on a rotating wheel for 15 hr. Samples were centrifuged at 16000×*g* for 1 min, the supernatant discarded and the beads washed in 500 µl of fresh NETN buffer (4°C). This was performed a total of three times. All samples were dried in a speedivac centrifuge under a vacuum, using heat for 10-15 min until residual buffer had been removed. 20 µl of 2× protein sample buffer were added to the beads and heated to 96°C for 5 min. Samples were stored at -80°C until needed.

2.2.12.4 SDS-PAGE analysis of proteins

Protein samples resuspended in 2× SDS-PAGE loading dye were heated at 96°C for 3 min prior to gel electrophoresis. SDS polyacrylamide gels were cast in 10 × 7 cm glass plates using the Protean III casting apparatus (Biorad. Hercules, USA). Gels were made in two sections, an upper 4% stacking gel and a lower section high-percentage separation gel. For a 7.5% gel, the lower gel was made using 1.5 ml of lower buffer, 1.5 ml of protogel, 3 ml of dH_2O, 75 µl of 10% APS and 5 µl of TEMED; for a 10% gel the same volumes were added with the exception of 2 ml of protogel and 1 ml of dH_2O. Gels were overlaid with isopropanol to ensure level setting and left to polymerise for 30 min. The isopropanol was washed off using dH_2O and the stacking gel poured on top of the lower gel. The stacking gel was composed of 325 µl of protogel, 625 µl upper buffer, 1.5 ml dH_2O, 75 µl APS and 5 µl of TEMED and left to polymerise for a further 30 min. Protein samples (up to 25 µl) were loaded on the appropriate percentage SDS-PAGE gel and electrophoresed at 150 V for 1 hr in 1× SDS-PAGE running buffer.

Gels were fixed in SDS-PAGE stain, with gentle agitation for 20 min and washed in destain several times for 30 min, or until background blue staining disappeared. Gels were dried on Whatman 3MM paper using a gel drying apparatus (Biorad. Hercules, USA).

2.2.13 Database analyses

All computerised analyses were carried out using an Apple G4 computer (Apple. Cupertino, USA). In general, DNA and protein single-letter code sequence (Appendix IV) was manipulated in a text-editing program, and analysed using Genejockey software (Biosoft. Cambridge, UK). Genejockey was used to identify restriction enzyme sites in DNA sequence and to translate DNA sequence into amino acid sequence.

Retrieval of DNA and protein sequence was achieved using the Entrez database at NCBI [Wheeler *et al.*, 2001]. Comparison of sequences was carried out using the nucleotide and protein BLAST server databases [Altschul *et al.*, 1990].

Amino acid sequence was analysed for motifs and domains using a range of software available on the Internet (Appendix V).

3 GENETIC REFINEMENT OF THE FPLD LOCUS AND CONSTRUCTION OF A PHYSICAL MAP AT 1q21

3.1 Recombination-based refinement of the FPLD critical interval

3.1.1 Introduction

The advent of molecular biology techniques and the identification of a new class of markers, the highly polymorphic microsatellites [Weber and May, 1989], is central to rapid identification of disease causing genes by positional cloning [Collins, 1995]. The abundance of these markers and their simple analysis (using the cost-effective method of PCR) permits the swift identification of a disease locus using linkage-based analyses and the subsequent refinement of a large genetic interval.

Initial linkage analyses are performed to identify a chromosomal segment which harbours the mutated gene. Large pedigrees in which the disease gene segregates are extremely useful. Each meiosis provides information which aids in the identification of a disease-associated locus. The procedure entails the genotyping of equally spaced genetic markers to determine their allelic state; followed by statistical analysis to identify those alleles which segregate with the disease phenotype [Chung and Gardiner, 1996]. The identification of an allele or set of alleles (haplotype) that is inherited with the disease from parent to offspring indicates the proximity of the defective gene to these markers. These linkage analyses serve to identify a chromosome or subchromosomal region; thereupon a critical survey of genes in the interval is performed to identify an attractive biological candidate. Marfan syndrome was mapped by linkage analyses to the long arm of chromosome 15 [Kainulainen *et al.*, 1990], to which the fibrillin gene had also recently been mapped [Magenis *et al.*, 1991]. This gene was considered to be a good biochemical candidate for disease and subsequently mutations were identified within it [Dietz *et al.*, 1991]. However, in most cases, a biological candidate gene has not been mapped to the chromosome associated with the disease and further analyses are necessary to pinpoint the genetic interval containing the defective gene. The follow-up investigation of a linkage-based study requires the recognition of a group of markers which are consistently inherited with the disorder. The analysis of every genetic marker within and surrounding this interval is necessary and should be performed in all available members from every affected family. The

construction of haplotypes will indicate the haplotype which is likely to be harbouring the disease gene. Careful observation should then be employed to determine when a recombination has occurred and when a section of the disease haplotype is transmitted with or without the disease. Recombinations aid in the identification of proximal and distal boundaries for the disease critical interval and can dramatically reduce the size of the disease gene-harbouring segment. These techniques are pivotal in the localisation of the mutated gene and allow the systematic consideration of mapped genes, which might have previously been thought not to be causative to the studied disorder.

3.1.2 Linkage of FPLD to 1q21-22

FPLD, although initially considered to be X-Linked [Kobberling and Dunnigan, 1986], was later recognised to be an autosomal dominant disorder [Jackson *et al.*, 1997]. Jackson and colleagues ascertained two multigenerational FPLD families from the UK [Jackson *et al.*, 1998]. A second group from the USA also identified five extended FPLD families [Peters *et al.*, 1998]. Both groups performed linkage analyses using a genome-wide panel of microsatellite markers and mapped the FPLD locus to the long arm of chromosome 1. Haplotype analysis defined a 21.2 cM interval at 1q21 between the proximal marker *D1S2881* and the distal marker *D1S484*. Subsequent studies identified a smaller critical interval also at 1q21, between the markers *D1S305* (proximal) and *D1S1600* (distal), an estimated 5.3 cM region [Peters *et al.*, 1998]. Comparison of two genetic maps [Murray *et al.*, 1994; Dib *et al.*, 1996] positioned the latter critical interval within the interval identified by Jackson and colleagues.

3.1.3 Patient ascertainment

Two previously reported families (Fam 1 and Fam 2) were used for genotyping of microsatellites saturated in the 1q21 region [Jackson *et al.*, 1998]. A further 7 families (Fam 3-9) were ascertained and all patients underwent detailed auxological examination. Skin fold thickness, muscle hypertrophy and phlebactasia (accentuated appearance of subcutaneous veins) were considered reliable phenotypic criteria. All families used in reducing the critical interval by haplotype analyses are described in Table 5. Blood samples were obtained from family members and used for microsatellite analysis.

Number	Origin	Number of affected members
Fam 1	Leicester, UK	11
Fam 2	Bristol, UK	8
Fam 3	Bristol, UK	4
Fam 4	Norfolk, UK	3
Fam 5	Northampton, UK	8
Fam 6	Norwich/Blackpool, UK	5
Fam 7	Maastrict, NL	8
Fam 8	Hanover, Germany	3
Fam 9	Rotterdam, NL	3

Table 5. Nine FPLD families ascertained from north Europe. Each family was numbered as chronologically ascertained. The most prevalent family location, alongside the number of individuals suffering from FPLD in each family was noted.

3.1.4 Construction of haplotypes for FPLD pedigrees

In this study, every member of the 9 FPLD families (Table 5) was fluorescently genotyped for the microsatellite markers listed in Table 1. In each family a disease haplotype was identified and correlated with the presence of the FPLD phenotype.

The identification of a disease haplotype in each family substantiated linkage of the FPLD locus to 1q21. The saturation of markers above, between and below the microsatellites *D1S305* and *D1S1600* confirmed that the critical interval localised between these two markers.

3.1.5 Identification of proximal and distal recombinants

Families 7 and 8 (Figures 8 and 9 respectively) provided two recombination events at 1q21 which permitted the reduction of the FPLD critical interval. The proximal (centromeric) recombination was identified in individual II:6 in Family 7. The parents of this individual were not available for study and thus their haplotypes were inferred by the frequency of haplotype combinations observed in generation II. The disease haplotype was constructed using genotypes from individuals III:1, III:2 and II:2. This haplotype was consistently found in all FPLD patients. Individual II:6 has a recombination between markers *D1S2346* and *D1S305*. *D1S305* was homozygous in the mother and thus is uninformative for mapping the precise location of the recombination event. The recombination provides a new proximal boundary for the FPLD gene in this cohort.

The distal recombinant was observed in individual III:4 of Family 8. This female, despite being young at the time of ascertainment (age 8 years), on detailed examination, had unequivocal evidence of lipodystrophy. The construction of haplotypes in this family revealed the presence of a recombination event between *D1S2721* and *D1S2624*. These data establish a new distal recombinant further reducing the minimum interval for the FPLD locus. Although *D1S2624* was approximately 3 cM centromeric to *D1S1600*, precise localisation proved difficult, as these two markers had been alternatively positioned on two different genetic maps [Murray *et al.*, 1994; Dib *et al.*, 1996]. Taken together the observation of two novel recombinations at chromosome 1q21 in these two families reduced the FPLD critical interval from a 5.3 cM interval bordered by *D1S305* and *D1S1600* to a 3.8 cM interval between the markers *D1S305* and *D1S2624*.

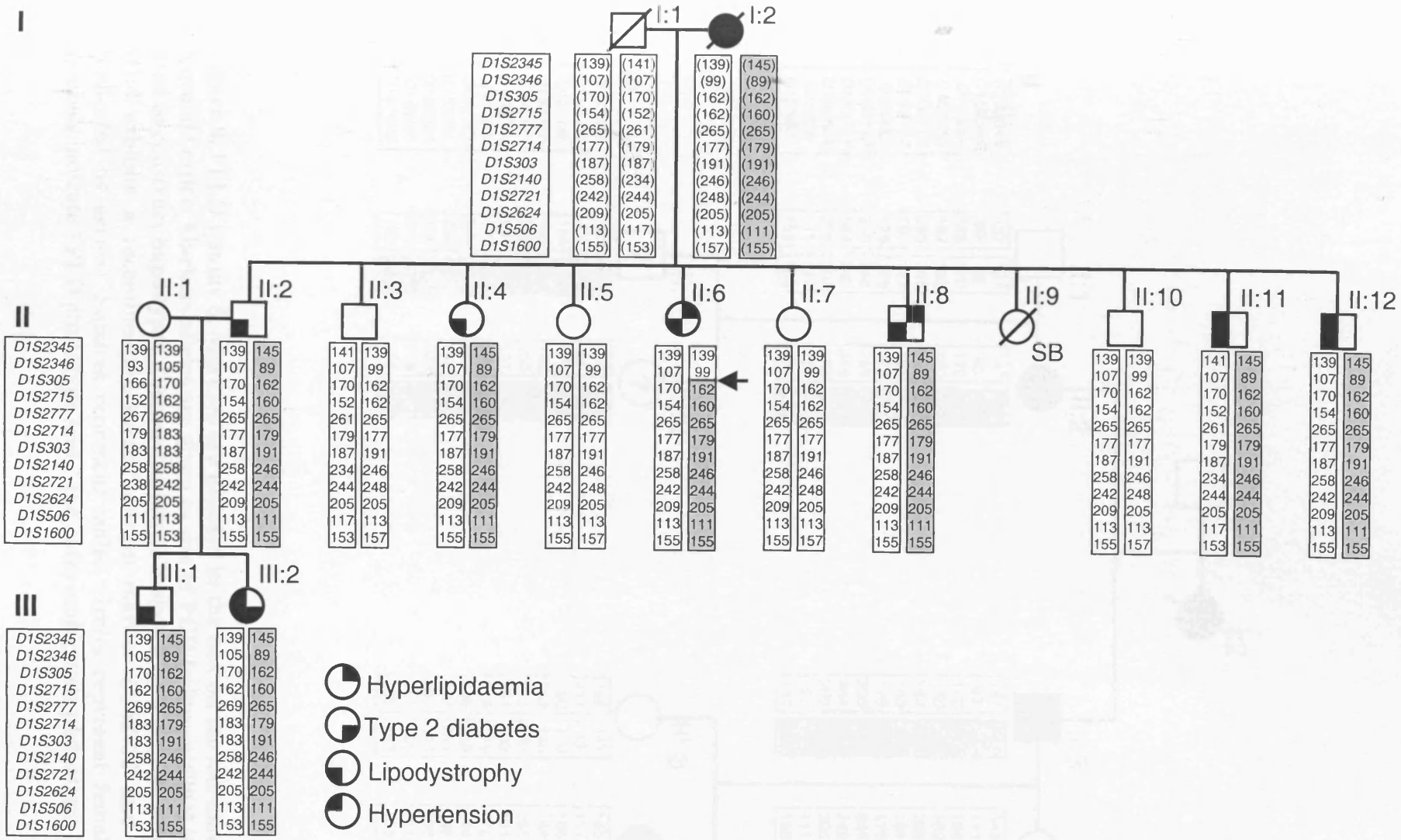

Figure 8. FPLD Family 7. Markers are denoted in the boxes on the left-hand side, in a genetic order. Marker alleles are given as size of PCR (microsatellite) in bp, and used to construct haplotypes. Disease haplotype is shown by a grey box. Individual II:6 exhibits a recombination event between marker *D1S2346* and *D1S2715* (*D1S305* is uninformative), marked by the arrow. Individuals I:1 and I:2 were not genotyped but their haplotypes were inferred. Squares represent males and circle represent females, partial shading of the symbols corresponds to a disease phenotype, see key.

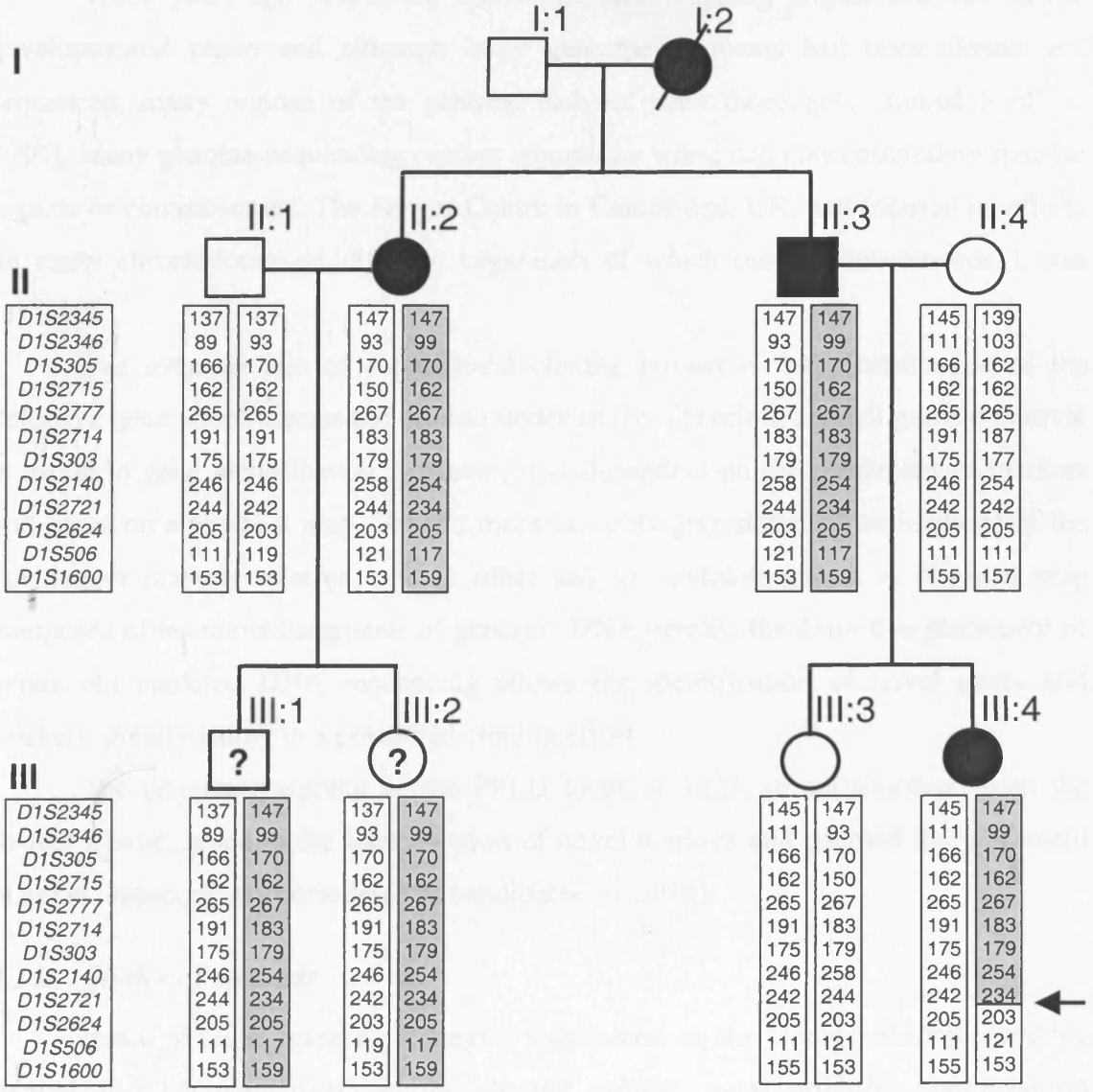

Figure 9. FPLD Family 8. Markers are denoted in the box on the left-hand side, in a genetic order. Markers alleles are given as size of PCR (microsatellite) in bp, and used to construct haplotypes. Disease haplotype is shown by a grey box. Individual III:4 exhibits a recombination event between marker *D1S2721* and *D1S2624* (indicated by arrow). Squares represent males, circles represent females, filled symbols indicate FPLD phenotype and ? indicates ambiguous phenotype.

3.2 Construction of a physical map at 1q21

3.2.1 Introduction

Three years ago (1998) the human genome mapping project was still in the developmental phase and although large genomic segments had been cloned and sequenced, many regions of the genome had not been thoroughly studied [Collins, 1995]. Many genome-sequencing centres around the world had concentrated on specific regions or chromosomes. The Sanger Centre in Cambridge, UK, had focused its efforts on many chromosomes in different organisms of which human chromosome 1 was included.

The eventual aim of a positional cloning project is the identification of the defective gene which causes the disease under study. Therefore a small genetic interval is useful in gene identification; however, it is dependent on the placement of markers and genes on a physical map. Genetic maps can only give statistical estimations of the position of markers relative to each other and to candidate genes. A physical map composed of assembled segments of genomic DNA permits the definitive placement of genes and markers. DNA sequencing allows the identification of novel genes and markers, greatly aiding in a positional cloning effort.

The physical mapping of the FPLD locus at 1q21, in collaboration with the Sanger Centre, aided in the identification of novel markers and enabled the placement of genes, subsequently considered as candidates for FPLD.

3.2.2 Choice of methods

Initial physical mapping strategies were based on the cloning of large genomic regions (0.1-1.5 megabases) in the cloning vectors, yeast artificial chromosomes (YACs) [Chumakov *et al.*, 1995]. A total of 33,000 YAC clones were obtained, analysed and found to cover 75% of the human genome. These YACs were assembled primarily on STS content as determined by PCR based assays. Genetically positioned STSs [Weissenbach *et al.*, 1992; Hudson *et al.*, 1995] were screened against YAC clone DNAs and the data used to assemble the YACs into contiguous sequence.

Although YAC clones are capable of carrying large inserts, there are several limitations ranging from low transformation efficiency, difficulty in subsequent sequence analysis using bacterial cloning techniques, a high degree of insert instability

and abundance of chimeric clones [Green *et al.*, 1991]. These drawbacks prompted the use of large-insert bacterial cloning vectors and a bacteriophage P1 cloning system was developed (P1 artificial chromosomes – PACs) [Ioannou *et al.*, 1994]. PACs can accept inserts in the 70 to 100 kb range. However, a second set of bacterial based vectors, the bacterial artifical chromosomes (BACs) were created and able to harbour inserts of up to 300 kb [Osoegawa *et al.*, 2001]. Both of these bacterial systems allowed quick preparation of DNA and straightforward sequence analysis by subcloning into more convenient vectors. They were thus, considered superior to the YAC system even though they were typically one-tenth the size. However, the development of PACs and BACs did not make the initial YAC maps redundant. In many cases the YAC maps were used as a 'framework' map to help in the grouping of STSs, a consequence of which was the correct choice of physically placed STSs to screen for PAC or BAC clones.

As mentioned previously the YAC maps were composed of many chimeric clones and the correct grouping of STSs proved difficult. As an alternative to the YAC framework maps, a second type of framework map was developed, the radiation hybrid (RH) map (Section 1.4.1.1.2). RH maps were considered superior to YAC framework maps, as they were not subject to chimeras and deletions [Walter and Goodfellow, 1993; Walter *et al.*, 1994]. Furthermore, altering the dose of radiation administered to the DNA could control the resolution of these maps. The use of these improved resources permitted the correct positioning of STSs into discrete chromosomal regions (also referred to as bins).

The construction of a physical map at 1q21 was achieved with the use of the Sanger Centre maps and techniques. Genemap98 formed the foundation of the Sanger chromosome 1 RH map [Deloukas *et al.*, 1998]. The final map was composed of approximately 5,500 chromosome 1 specific sequence tag sites, many identified from public databases [Murray *et al.*, 1994; Dib *et al.*, 1996; Wheeler *et al.*, 2001]. Using this RH resource, STSs from chromosome 1q21 were divided into four bins (Appendix I). These STSs were used to screen the enhanced BAC library (RPCI-11) developed by Pieter de Jong [Osoegawa *et al.*, 2001] and standard hybridisation techniques were used to identify STS positive clones. STS content was then determined for each clone and the novel approach of fluorescent restriction enzyme digest fingerprinting used to order the BAC clones into overlapping contigs [Gregory *et al.*, 1997].

3.2.3 Identification of BAC clones which map to 1q21

The STSs in each pool (Appendix I; primer sequences available from www.sanger.ac.uk) were amplified by PCR against genomic DNA to verify that each PCR product corresponded to the predicted size for that STS. Radioactive PCR probes were made and combined for each 1q21 pool. The 25 (pool 1 or 2) or 26 (pool 3 or 4) STS probes were incubated against the RPCI-11 library filters. Positive clones were identified and recorded on the chromosome 1 specific database **1ace**, which is used to update the publicly available database **webace** every week (www.sanger.ac.uk). The use of 102 STSs in library screens identified 812 positive BAC clones from the RPCI-11 library, which were representative of the entire 1q21 genomic interval. These 812 BACs were isolated from the other clones in the library and used to create a set of chromosome 1q21 specific nylon filters. The 812 clones were grown on a single filter and 60 copies were made. An example of one of these filters is shown in Figure 10a.

3.2.4 STS content mapping of 1q21 BAC clones

Sixty 1q21 filters were made to reduce the number of times each filter had to be used. It was intended that the 102 original 1q21 STSs be put against the filters individually, in addition to any other markers or genes known to map near to 1q21, thus each filter would only be used two or three times. These screens were termed tertiary screens and each STS was individually used to probe the 812 BACs by hybridisation to determine the exact STS content of each clone. The 102 STSs were mapped against these tertiary filters and scored for their presence or absence (e.g. Figure 10b). As before, all data were recorded on the 1ace database. The polymorphic microsatellites used for genotyping also acted as STSs and were probed against the 1q21 filters (Table 1). Hence, each marker was positioned on the 1q21 BAC clones. On average a single STS hybridised to 5-10 BAC clones.

3.2.5 Contig assembly

The robust method of fluorescent fingerprinting was the predominant technique used in contig assembly [Gregory *et al.*, 1997]. This method provides reliable data for building contigs, using the restriction digest pattern for each specific section of cloned genomic DNA. The 812 BAC DNAs were prepared and fluorescently fingerprinted. The raw data gels were analysed using Sanger fingerprinting software (FPC) and the fingerprint pattern for each BAC saved for later analysis [Soderlund *et al.*, 2000].

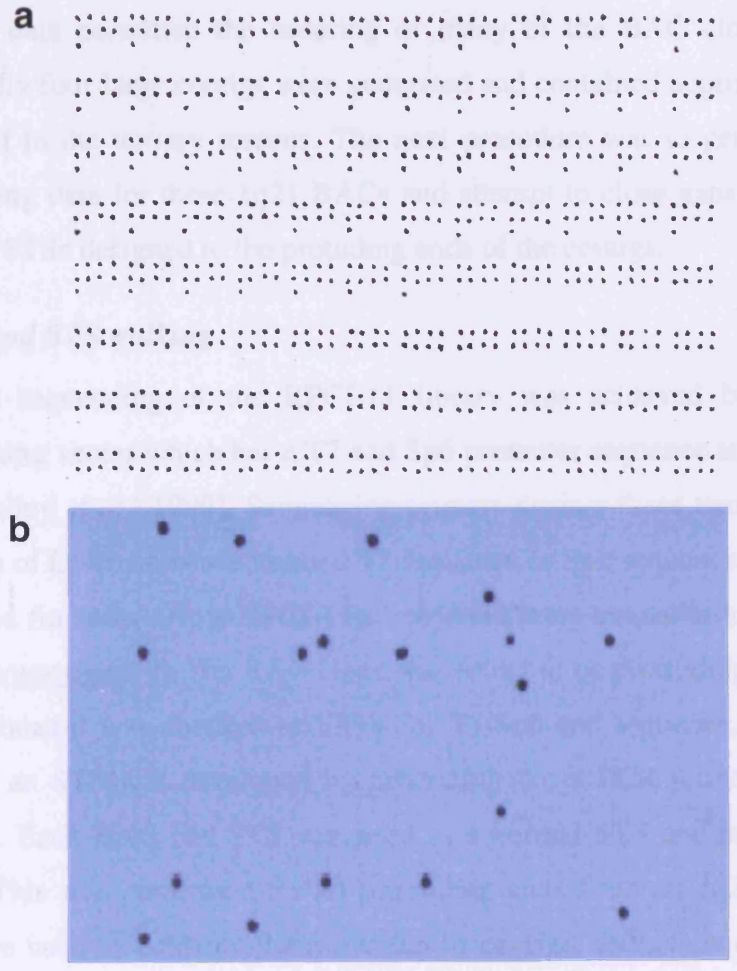

Figure 10. Example of STS mapping using a 1q21 BAC filter. (a) Nylon filter (120 × 80 mm) showing the positions of the 812 1q21 BACs. (b) Autoradiograph identifying the positive BACs for stSG28025, an EST from the disease gene interval. The autoradiograph was placed on top of the filter and the positive BACs scored. All data were saved in the Sanger Centre chromosome 1 database, 1ace.

Once all fingerprints were obtained for the 1q21 BACs, the fingerprint patterns were used to identify clones which shared segments of genomic DNA. This was converted into a digital representation indicating the degree of overlap between adjacent BACs. These maps were verified by checking the STS content of the BACs. Analysis of one STS was expected to highlight those BACs lying directly underneath. Discrepancies were attributed to scoring errors of the autoradiograph against the 1q21 filters.

These data permitted the ordering of many of the BAC clones into several contigs. Initially four large contigs were generated and contained approximately 50% of the STSs used in the tertiary screens. The next procedure was to generate more STS content mapping data for these 1q21 BACs and attempt to close gaps between contigs by generating STSs designed to the protuding ends of the contigs.

3.2.6 BAC end STS walking

Partial sequencing of the RPCI-11 library was achieved by exploiting the pBAC3.6 cloning vector which has a T7 and Sp6 promoter sequence at either end of the insert site [Kelley *et al.*, 1999]. Sequencing primers against these two sites resulted in 300-500 bases of DNA sequence, termed T7 sequence or Sp6 sequence. Sequences have been generated for most of the RPCI-11 library and were available to download from the Internet (www.tigr.org). If a BAC clone was found to be protruding from the end of a contig of clones it was checked at TIGR for T7/Sp6 end sequence. If end sequence was available an STS was developed by generating novel PCR primers (Appendix II) for both ends. Each BAC end STS was used as a normal STS and probed against the 1q21 filters. This was performed for all protruding ends from all 1q21 contigs. These new data were used to confirm clone overlap in contigs, recruit more previously un-contigged clones or to remodel entire contigs on the strength of the new information. The initial tertiary screens resulted in 5 contigs and 23 BAC end clone STSs were developed to close these gaps. This was subsequently referred to as walk 1. After this the 4 new contigs were reviewed and a further 10 BAC end STSs generated for walk 2. This increased the size of the contigs and reduced the overall number to 3. Walk 3 used 8 BAC end STSs and resulted in only 2 large contigs of clones. The final walk was achieved using only 4 BAC end STSs. The final physical map was composed of two large contigs consisting of approximately 300 BACs from which a minimum tiling pathway of 30 BACs was selected. Those clones chosen to represent the minimum set

were done so with reference to the bioinformatic fingerprinting data and correlation with STS mapping data (Figure 11).

3.2.7 Integration of FPLD physical map with pre-existing maps

The markers *D1S2345* and *D1S2346* were not used in the original library screens, but were used in the screens against the 1q21 BACs. These two markers were at the centromeric end of the FPLD interval and needed to be physically mapped. A small physical map spanning 2.5 Mb of DNA had been previously constructed by a group searching for genes involved in epidermal growth [South *et al.*, 1999]. This contig was composed of 36 clones positioned adjacent to 1q21 and had been submitted for sequencing at the Sanger Centre. DNA was prepared from these clones and used in a direct PCR based assay to determine if the markers *D1S2345* and *D1S2346* were contained within this interval. The marker *D1S1664* (www.genethon.fr) was used as a positive control as it had previously been placed on this map. *D1S2346* was successfully positioned on the map and prompted the placement of the next two telomeric markers *D1S305* and *AFMa082wc1* (www.genethon.fr). *D1S305* was not placed on this map, but *AFMa082wc1* was situated at the very telomeric end of the map and additionally mapped to several BAC clones from the 812 chromosome 1q21 BACs. This new data was used to review the fingerprints of all of these *AFMa082wc1* associated clones and a connection was made between these two independently generated physical maps (Figure 11).

3.2.8 Physical order of microsatellite markers and known genes

The placement of microsatellite markers on the physical map prompted comparison to the published genetic order. The position of the proximal and distal markers remained constant whereas those, which had little or no genetic distance between them, were significantly reordered (Figure 11).

Marker *D1S305* was not placed on either of these two large contigs. This marker should have been mapped onto clones between *D1S2346* and *D1S2715*. Secondly, the block of markers *D1S2777*, *D1S2714* and *D1S303* were thought to be ordered as listed. However the physical map demonstrated that the true order was *D1S303*, *D1S2777* and finally *D1S2714*. Other uncertainties were also resolved. The tetranucleotide marker *D1S2140* had previously not been placed on an integrated map; thus the assumed location of *D1S2140* proximal to *D1S2721* was found to be correct.

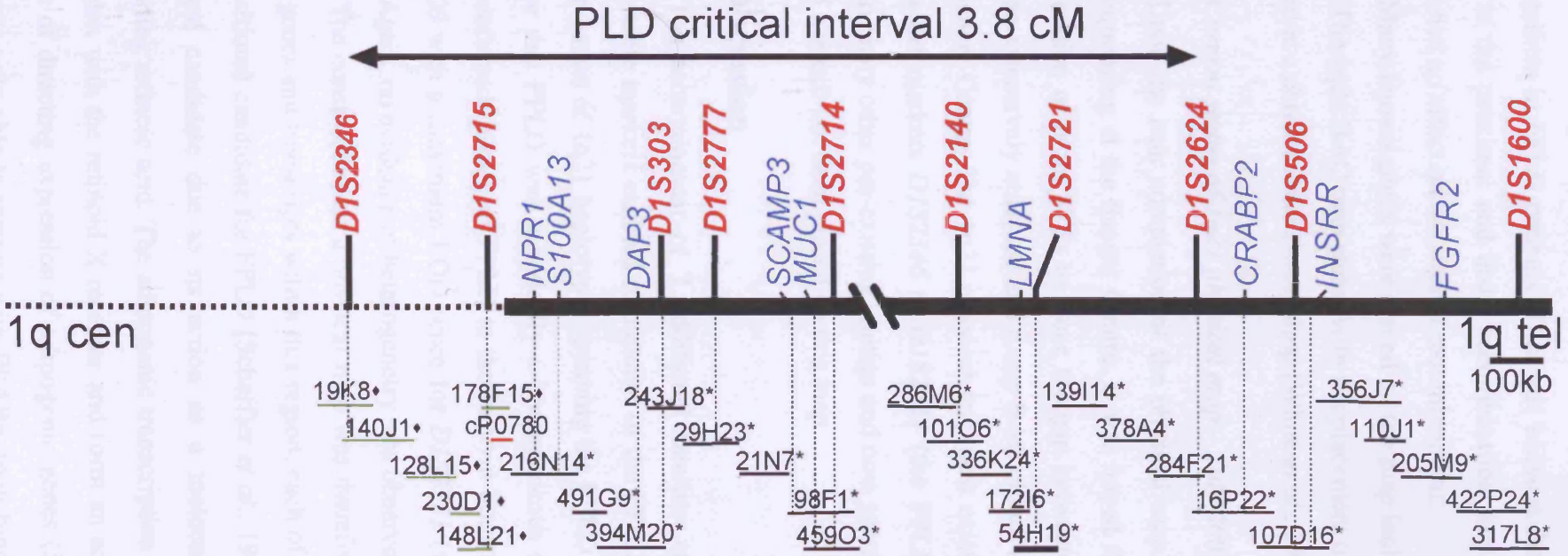

Figure 11. Physical map at 1q21. Two large contigs of clones are shown with a small gap. Microsatellite markers are shown in red, genes are shown in blue. Large black solid lines indicate the BAC clones generated with the 1q21 STS probes. Dotted line represents a pre-existing contig of clones [South *et al.*, 1999]. The minimum tiling path of genomic clones is shown, each with their specific clone identifier. BACs are marked with * and PACs marked with ♦and shown in green, the single cosmid is shown as a red line. BAC 54H19 is shown as a bold line.

The finding of an altered marker order had no effect on the genotyping of microsatellites in FPLD patients. This was because the marker order was found to be correct at the proximal and distal recombination sites whereas the reordered central markers had no effect on the sites of recombination.

Many known genes were placed on the map including *NPR1*, *DAP3*, *LMNA* and *INSRR*. The 1q21 BAC map status with the placement of known markers and genes was presented at a chromosome 1 workshop [White *et al.*, 1999].

3.2.9 Current status of 1q21 physical map – July 2001

Upon the near completion of the physical map, BAC clones were selected for direct sequencing at the Sanger Centre. It was hoped that new sequence would enable the generation of more STSs to close the gap between the two contigs. The map has now been extensively analysed and many BAC clones are in various sequencing stages at the Sanger Centre. The 1q21 physical map now exists as a single extensive map and includes the markers *D1S2346* to *D1S2624* (the FPLD critical interval). It has been joined to many other pre-existing contigs and now spans 8.1 Mb of DNA. Interestingly, *D1S305* has still not been placed on this map.

3.3 Discussion

The ascertainment of 7 additional families and genotyping of all available microsatellite markers enabled refinement of the FPLD locus from 5.3 cM to 3.8 cM. Co-segregation of 1q21 haplotypes spanning the FPLD critical interval provided strong evidence that FPLD was genetically a homogeneous disorder. A further independent study confirmed linkage of FPLD to the interval bordered by the markers *D1S305* and *D1S1600* with a maximum LOD score for *D1S2721* (see Figure 11) [Anderson *et al.*, 1999]. Again, no evidence of heterogeneity was observed.

The construction of a physical map was therefore essential in order to place all known genes and transcripts within this region, each of which could then be considered as a positional candidate for FPLD [Schaffler *et al.*, 1999]. CRABP2 was considered a biological candidate due to its action as a molecular chaperone within the cell, transporting retinoic acid. The adipogenic transcription factor PPARγ is known to form a complex with the retinoid X receptor and form an active transcription factor, ARF6, capable of directing expression of adipogenic genes (Section 1.1.3.2). The retinoid X receptor is only able to interact with PPARγ upon binding of the ligand, retinoic acid.

Thus a defect in CRABP2 could reduce retinoic acid availability and affect transcription of adipogenic genes. The positioning of *D1S2624* proximal to the potential candidate *CRABP2* (Figure 11) excluded its role in FPLD.

Thirty characterised genes were placed in the estimated 3 Mb interval between *D1S2346* and *D1S2624*. Systematic consideration of all of these genes was carried out to identify a potential candidate with respect to adipocyte differentiation. This was achieved by reviewing the expression profiles, physical localisation and biological candidacy. At this stage the possibility of mutations in a novel transcript were not excluded and the generation of 1q21 DNA sequence was important in facilitating the prediction of novel genes.

Individual II:8 from Fam 7 (Figure 8) has marked hyperlipidaemia and intriguingly the locus for familial combined hyperlipidaemia (FCHL) had also been recently located to chromosome 1q21 [Pajukanta *et al.*, 1998], implying that FPLD and FCHL might indeed be allelic disorders of the same gene.

The overall purpose to the fine mapping of a disease locus and construction of a physical map is to define the number of genes considered as causative for the disorder. Fine mapping of the FPLD locus excluded all candidate genes in a 1.5 cM region at the distal end of 1q21 including the candidate *CRABP2*. The physical map provided the resolution of marker order and was used as a resource to map other candidate genes. The eventual generation of the 1q21 DNA sequence will aid in the prediction of novel genes and permit their characterisation with relevance to adipocyte function.

Finally, the generation of the BAC resource at 1q21 has contributed greatly to the human genome-sequencing project on chromosome 1 and thus will enhance future studies in human and medical genetics.

4 MUTATION DETECTION IN *LMNA*

4.1 Introduction

A reduction of the FPLD critical interval identified and defined positional candidate genes between the markers *D1S305* and *D1S2624*. Candidate genes located close to *D1S2721* were prioritised as this marker had been shown to be very highly associated with the FPLD phenotype [Anderson *et al.*, 1999]. This marker had been placed on the BAC clone 54H19 (RPCI-11) alongside the *LMNA* gene. During the search for candidate genes, a single missense sequence variant was identified in a large multigenerational family with FPLD [Cao and Hegele, 2000]. The *LMNA* gene had been chosen as a candidate for FPLD because of the relatedness of FPLD with an inherited disorder proven to be caused by mutations in *LMNA* [Bonne *et al.*, 1999]. This disorder is known as the autosomal dominant variety of Emery-Dreifuss muscular dystrophy (EDMD-AD). It was hypothesised that the degeneration of myocytes in EDMD patients was analogous to the degeneration of adipocytes in FPLD individuals. Sequence analysis of the 12 exons of *LMNA* revealed a heterozygous mutation at codon 482 (CGG→CAG) in exon 8 resulting in the amino acid change, arginine to glutamine (R482Q). Five Canadian families had been independently ascertained and all found to harbour the R482Q mutation, in each case occurring on the same 1q21 microsatellite haplotype. These data suggest a founder mutation to account for the segregation of FPLD in these families. To exclude the possibility that the sequence variant might represent a polymorphism rather than a disease causing mutation, a large cohort of control subjects were screened (1000 individuals or 2000 chromosomes). No sequence variants were found.

This observation of the R482Q sequence alteration by Cao and Hegele and the positioning of *LMNA* within the critical interval close to marker *D1S2721* in this study (Figure 11), provided compelling evidence to prompt the analysis of the *LMNA* gene in the 9 FPLD families from north Europe.

4.2 Detection of mutations within *LMNA* in 1q21-linked FPLD families

The *LMNA* gene had been previously mapped to chromosome 1q21 [Wydner *et al.*, 1996] and its placement on the 1q21 BAC physical map confirmed it as a candidate

for FPLD. The genomic structure of *LMNA* had been reported [Lin and Worman, 1993] and was used to design intronic PCR primers to amplify the whole coding sequence of the gene (Table 2). Initially, a proband from each of the nine families was sequenced for all 12 exons of *LMNA*. Missense mutations were found in probands from each family and exhibited highly site-specific clustering within exon 8. Heterozygous missense mutations were present in either codon 482 or codon 486 of *LMNA*. Four different missense mutations were observed, three localised to codon 482 and one to 486 (Figure 12). The heterozygous mutation at codon 482 (CGG→TGG) results in the amino acid substitution arginine to tryptophan (R282W) and was observed in Families 1, 2, 4, 7, 8 and 9. Mutation at the same codon (CGG→CAG), resulting in the substitution of arginine with glutamine (R482Q), was observed in Fam 3 only. Mutation of CGG→CTG (codon 482) changed the amino acid from arginine to leucine (R482L) and was identified in Fam 5. These three different mutations at codon 482 were observed in a total of 8 FPLD families. The second codon found to be mutated was codon 486. The wild-type sequence AAG (lysine) was mutated in Fam 6 to AAC (asparagine). This mutation was identified in one family only.

To confirm the causal relationship of the codon 482 and 486 mutations with FPLD, their segregation within families was investigated. Codon 482 (CGG) forms part of a *Hpa*II/*Msp*I restriction enzyme palindrome – CCGG. Variation in this sequence (i.e. in the case of all codon 482 sequence changes) destroys the sequence symmetry; hence the *Hpa*II/*Msp*I site is lost, resulting in an altered digest banding pattern (Figure 13a). All individuals (affected, unaffected and married-in) from all 9 FPLD families (with the exception of Fam 6) were amplified by PCR for *LMNA* exon 8 only, digested with *Hpa*II and electrophoresed on an agarose gel. Figure 13b shows the presence of a 167 bp band in affected individuals in a subset of FPLD families. The 167 bp band was present in all FPLD patients who belonged to the same family in which an R482 mutation had been identified. Several patients had not developed FPLD yet harboured a disease haplotype, these individuals all had a mutation at codon 482.

Family 6 possessed a K486N mutation, which did not create or destroy a restriction enzyme palindrome. Thus, segregation of this mutation with FPLD was observed by direct sequencing (Figure 13b).

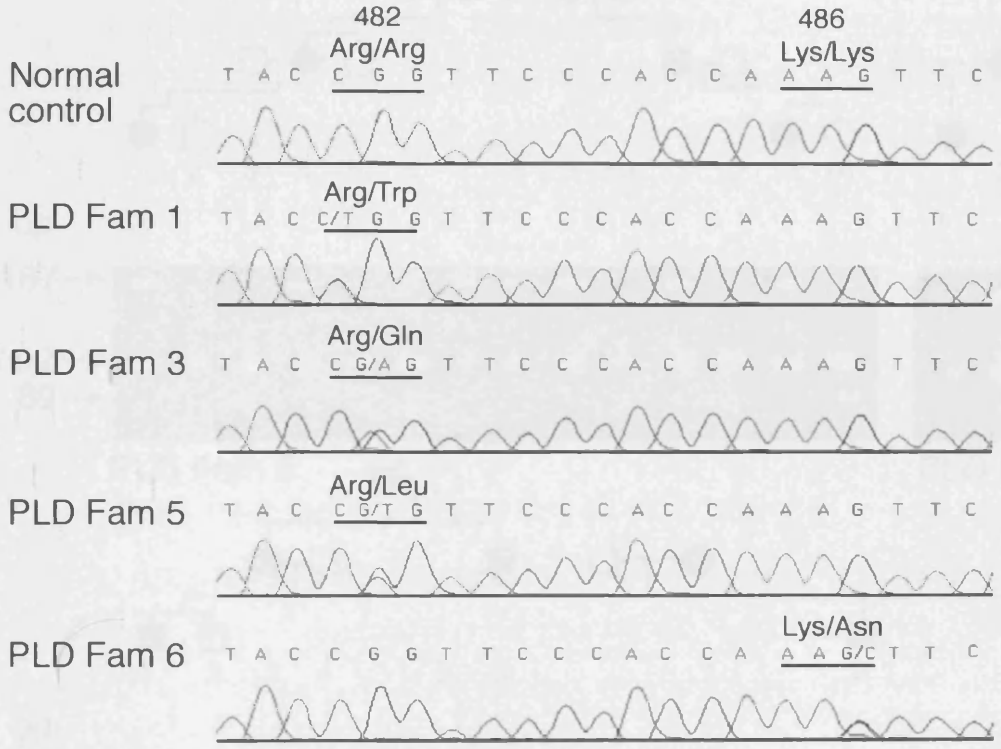

Figure 12. Sequence chromatograms of codon 482 and 486 alterations detected in exon 8 of the *LMNA* gene. Three different single nucleotide mutations were observed in codon 482 (dual peaks), resulting in the amino acid change from arginine to tryptophan, glutamine, or leucine. Only one mutation was identified in codon 486 in Fam 6.

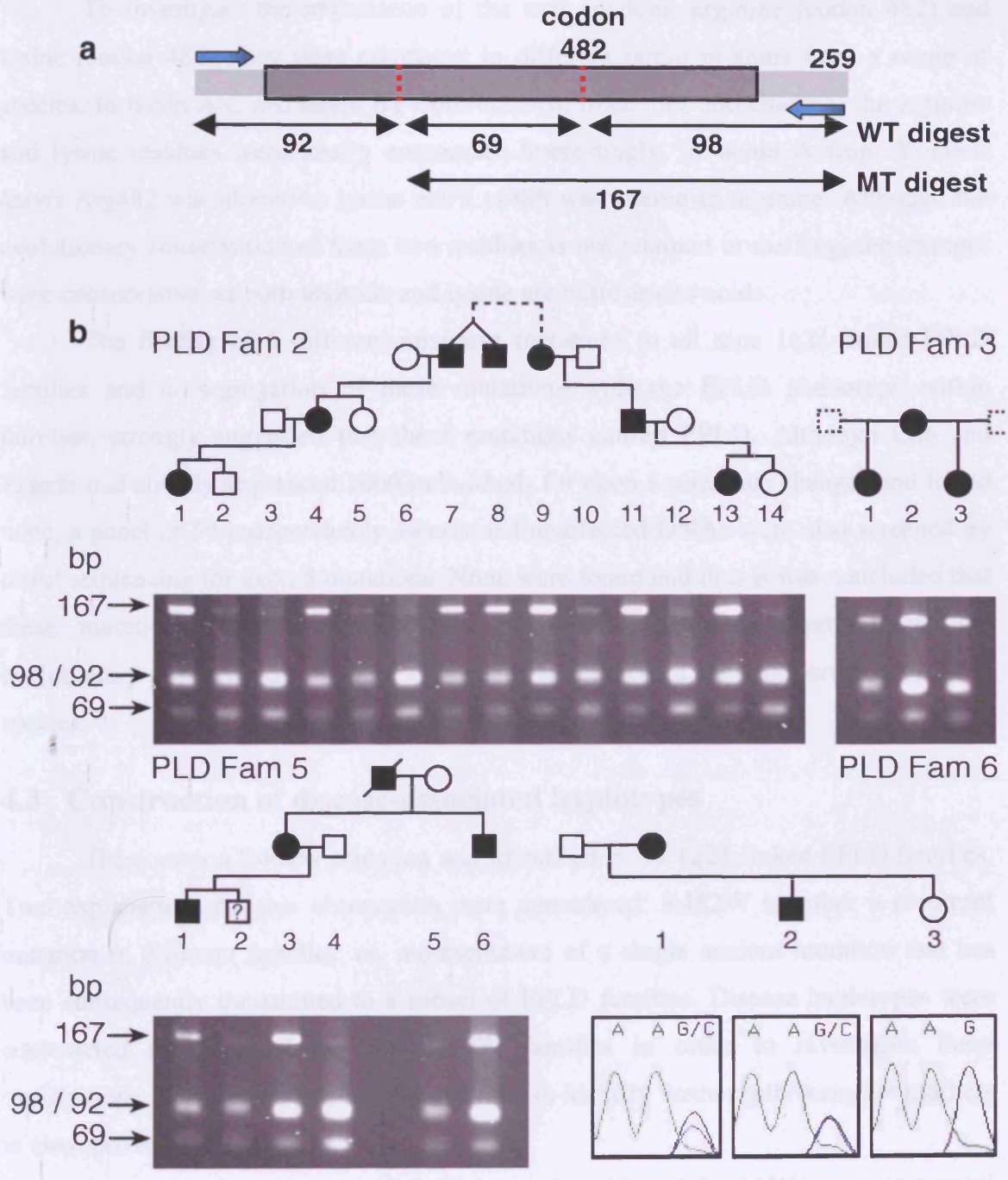

Figure 13. Co-segregation of *LMNA* codon 482 and 486 mutations with the FPLD phenotype. (a) Representation of *LMNA* exon 8 (dark grey box) located between intronic sequence (light grey boxes). Blue arrows show the position of PCR primers used to amplify exon 8, and red dotted lines show the location of *Hpa*II sites. The second *Hpa*II site is mutated in FPLD patients and is not cleaved by *Hpa*II giving rise to altered digest product sizes. (b) Segregation of each type of FPLD mutation in FPLD families. R482W segregates in Family 2, R482Q segregates in Family 3, R482L segregates in Family 5. The larger 167 bp band is present in those individuals with FPLD only. Family 6 have a K486N mutation which does not create or destroy a palindrome sequence and the mutation is shown to segregate by direct DNA sequencing.

To investigate the importance of the two residues, arginine (codon 482) and lysine (codon 486), they were compared in different lamin proteins from a range of species. In lamin A/C and lamin B1 from humans, mice, rats and chickens the arginine and lysine residues were totally conserved. Interestingly, in lamin A from *Xenopus laevis* Arg482 was altered to lysine and Lys486 was altered to arginine. Although the evolutionary conservation of these two residues is not retained in the frog, the changes were conservative, as both arginine and lysine are basic amino acids.

The finding of 4 different missense mutations in all nine 1q21-linked FPLD families and co-segregation of these mutations with the FPLD phenotype within families, strongly suggested that these mutations caused FPLD. Although Cao and Hegele had already sequenced 1000 individuals for exon 8 sequence changes and found none, a panel of 50 independently ascertained unaffected DNAs were also screened by direct sequencing for exon 8 mutations. None were found and thus it was concluded that these mutations were responsible for the FPLD phenotype. Furthermore, the evolutionary conservation of these two residues implicated their importance in other species.

4.3 Construction of disease-associated haplotypes

The common R482W mutation was identified in six 1q21-linked FPLD families. Two explanations for this observation were considered; R482W is either a recurrent mutation in different families, or, representative of a single ancient mutation that has been subsequently transmitted to a subset of FPLD families. Disease haplotypes were constructed for each of the six R482W families in order to investigate these explanations. Toward this goal, it was essential to identify further microsatellite markers in close proximity to the gene.

The physical mapping of the 1q21 interval positioned the *LMNA* gene on several BAC clones (Figure 11), of which clone 54H19 had been fully sequenced. A genome-sequencing effort (Washington University, USA) had incorrectly mapped BAC 54H19 to a region on chromosome 16. Bioinformatic BLAST database searches with the *LMNA* cDNA sequence against the HTGS resource (high-throughput genome sequence) identified the sequence from BAC 54H19 [Altschul *et al.*, 1990]. Of the 812 BAC clones in the 1q21 interval, the clone 54H19 had been used to generate BAC end sequence STSs at the T7 and Sp6 cloning sites. This had allowed the orientation of the clone within the 1q21 physical map, which aided in the orientation of the *LMNA* gene.

BLAST2 homology analyses localised *LMNA* to the centromeric end (T7) of the 164 kb clone [Tatusova and Madden, 1999], with exon 1 positioned centromeric relative to exon 12. The BAC clone 54H19 was screened for additional polymorphic microsatellites. Direct sequence analysis identified two $(CA)_n$ microsatellites, both telomeric to exon 12. One was identified as *D1S2721* and situated 40 kb downstream from *LMNA*. The other microsatellite was determined to be novel and situated only 100 bp downstream to exon 12. The generation of PCR primers (one of which was fluorescently labelled; Table 1) to amplify the novel microsatellite and subsequent agarose gel electrophoresis revealed it to be highly heterozygous. The sequence was submitted to the Genome Database (www.gdb.org) [Letovsky *et al.*, 1998] and a recognised marker identifier, *D1S3757* obtained. The physical map had now been used to correctly order the genetic markers and place the *LMNA* gene relative to these sites.

Haplotypes were constructed using this true marker order as shown in Table 6. In the six R482W families three distinct haplotypes were observed and suggested the occurrence of three ancestral mutation events. Thus, the CGG→TGG alteration in R482W is recurrent and this is supported by the likely mechanism of mutation. The cytosine in a CG run is often modified by methylation. Sites containing 5-methylcytosine provide hotspots for mutation as this modified base may incorrectly be deaminated and converted to thymine, resulting in a mismatched G/T base pair. Upon DNA replication this results in one strand containing wild-type sequence G/C and the other, containing mutated T/A.

These three haplotypes encompassed the *LMNA* gene and it remains a possibility that the allele 265 at marker *D1S3757* shared by Families 7, 9, 4 and 8 represents an earlier ancestral mini-haplotype. However, definitive data was confined to three independent mutational events.

4.4 Screening of additional families and sporadic individuals

The identification of codon 482 and 486 mutations in all FPLD families prompted the direct sequencing of the *LMNA* gene in other FPLD families, previously considered too small for haplotype analysis. The first family (Fam 10) was ascertained from Birmingham, UK and consisted of an affected girl, her unaffected brother and affected father. Sequence analysis of the 12 exons of *LMNA* revealed a recurrent missense mutation at codon 482, R482W (CGG→TGG; Figure 14a). This was identified in the girl and her father and not in the unaffected brother.

	Fam 1	Fam 2	Fam 7	Fam 9	Fam 4	Fam 8
Marker	Leicester UK	Bristol UK	Maastrict NL	Rotterdam NL	Norfolk UK	Hanover Germany
D1S2346	99	99	89	99	93	99
D1S305	162	162	162	162	160	170
D1S2715	162	162	160	160	162	162
D1S303	183	183	179	179	179	179
D1S2777	269	269	265	265	269	267
D1S2714	183	183	191	191	183	183
D1S2140	254	254	246	246	254	254
LMNA	R482W	R482W	R482W	R482W	R482W	R482W
D1S3757	241	241	265	265	265	265
D1S2721	242	242	244	244	234	234
D1S2624	203	203	205	205	205	205

Table 6. 1q21 haplotypes for FPLD families harbouring an R482W mutation. The 10 microsatellite markers which were used for haplotype construction are listed with allele sizes for each marker on the disease chromosome. Family 1 and Family 2 share an identical haplotype over the whole locus, Families 7 and 9 share the majority of the 1q21 markers, and Families 4 and 8 have a small haplotype in common. All three haplotypes are distinct from each other and span the *LMNA* gene. The dotted box encloses a possible founder haplotype.

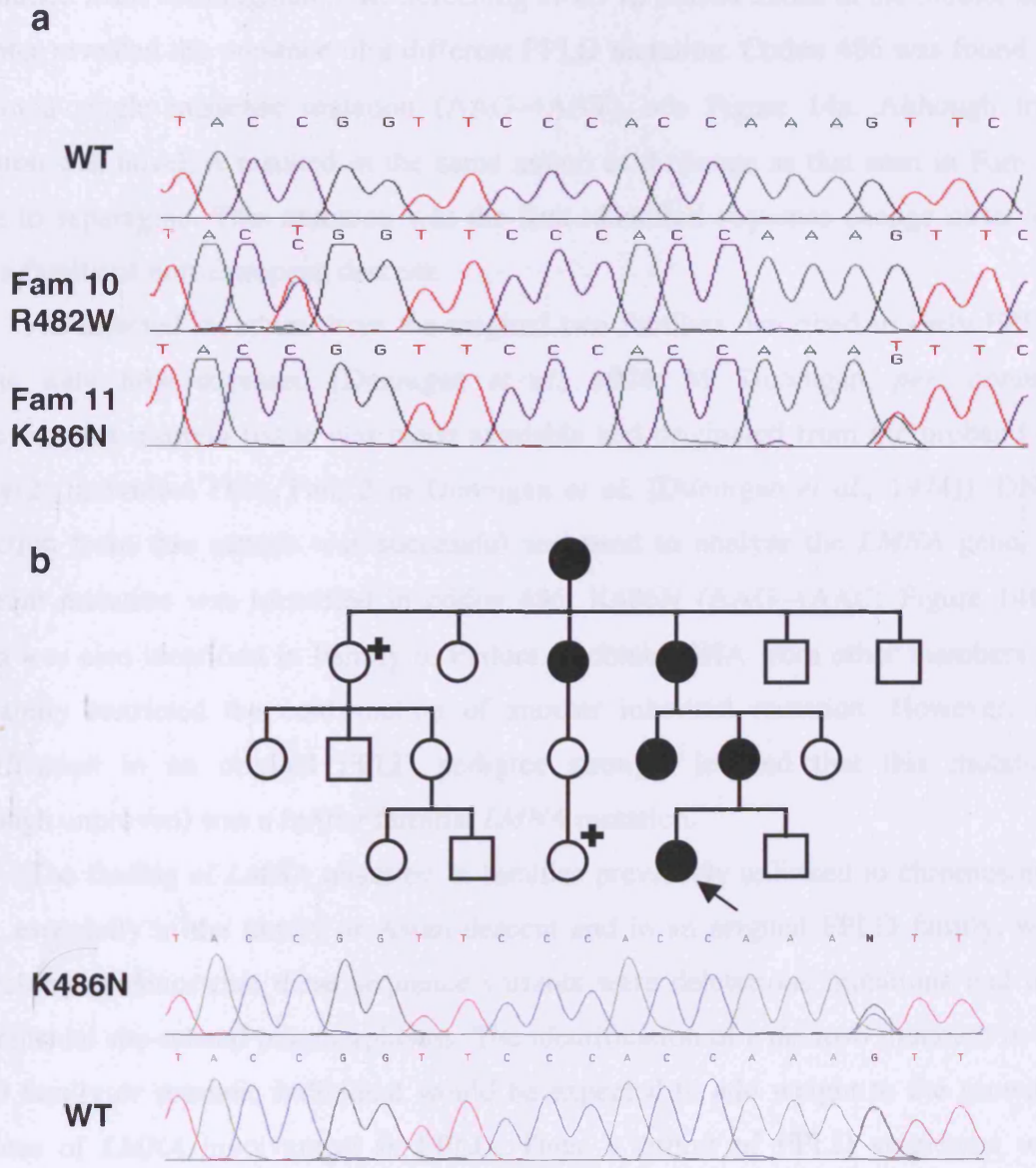

Figure 14. Identification of further familial mutations. (a) Identification of a recurrent mutation R482W (CGG→TGG) in a previously, 1q21 un-linked family. Identification of a novel mutation K486N (AAG→AAT) in a family of Asian descent. (b) Identification of a recurrent mutation K486N (AAG→AAC) identified in post-mortem tissue from the proband (arrow) from Dunnigan's original family 2 from Inverness. Pedigree shows affected individuals (filled symbols), squares represent males and circles represent female, small cross refers to type 2 diabetes.

The second family (Fam 11), originally of Pakistani descent, was also ascertained from Birmingham, UK. Screening of all 12 *LMNA* exons in the mother and daughter revealed the presence of a different FPLD mutation. Codon 486 was found to contain a single missense mutation (AAG→AAT), see Figure 14a. Although this mutation was novel, it resulted in the same amino acid change as that seen in Fam 6, lysine to asparagine. This mutation was the first identified sequence change observed from a family of non-European descent.

All affected members from the original two families described in early FPLD reports were now deceased [Dunnigan *et al.*, 1974; M. Dunnigan, *pers comm*]. However, post mortem tissue was made available and originated from the proband of family 2 (individual IV:4, Fam 2 in Dunnigan *et al.* [Dunnigan *et al.*, 1974]). DNA extraction from this sample was successful and used to analyse the *LMNA* gene. A recurrent mutation was identified in codon 486, K486N (AAG→AAC; Figure 14b), which was also identified in Family 6. Failure to obtain DNA from other members of the family restricted the confirmation of another inherited mutation. However, its identification in an original FPLD pedigree strongly implied that this mutation (although unproven) was a further familial *LMNA* mutation.

The finding of *LMNA* mutation in families previously unlinked to chromosome 1q21, especially in the family of Asian descent and in an original FPLD family, was compelling evidence that these sequence variants were deleterious mutations and not co-incidental site-related polymorphisms. The identification of a *de novo* mutation in an FPLD family or sporadic individual would be expected to add weight to the growing evidence of *LMNA* involvement in FPLD. Thus, a cohort of FPLD singletons was screened for the whole of the *LMNA* gene.

Twenty-one singleton FPLD patients were screened for the 12 exons of *LMNA*. DNA samples from all of these patients were sent by clinicians from the UK, with the exception of one sample from Israel. In many cases the familial status of these samples had not been investigated and their FPLD phenotype was described as 'unconfirmed' or 'possible'. Such ambiguous FPLD samples were routinely screened. Of these 21 samples only 4 mutations were observed in the *LMNA* gene, all within exon 8 and all recurrent, R482W (CGG→TGG). Three of these patients were considered as exhibiting a definite FPLD phenotype; the fourth was described as possibly suffering from FPLD with an unknown family history. Those considered as definite FPLD patients did not all

have a verified familial background. Two were known to have affected fathers but DNA samples from these individuals were unavailable for study. The other patient had an unknown family history. Thus, in the screening of 21 further FPLD patients another 4 recurrent mutations were identified, of which two are thought to be familial and two unknown.

The inherited basis for these two final mutations was not elucidated, as parental DNA samples were unavailable. These mutations may either represent *de novo* mutations or add to the list of familial mutations.

Of the remaining 17 singleton samples no mutations were identified. This was not considered significant as many of the samples were obtained from clinicians, uncertain about the FPLD phenotype. However, several samples were analysed and known to be from unequivocal FPLD patients. These four definite FPLD samples were from families in which relatives also exhibited FPLD. The FPLD phenotype in these patients was not considered atypical, making the absence of *LMNA* mutation surprising given the identification of *LMNA* mutations in all known FPLD families to date. However, as other family samples were unavailable, linkage to 1q21 using microsatellite markers was unachievable. Thus, it was not determined if these FPLD patients were linked to 1q21 and the *LMNA* gene. It is unlikely that a second FPLD locus exists given the absence of heterogeneity in linkage studies [Jackson *et al.*, 1998; Peters *et al.*, 1998] and the successful identification of exon 8 specific mutations in the described FPLD families. Potential promoter or intronic mutation could not be excluded by sequence analysis of the coding region of *LMNA*.

4.5 Collaborative screening of *LMNA* in other European FPLD families

As part of a collaborative effort, the *LMNA* gene was analysed in a cohort of patients ascertained by a group headed by Jacqueline Capeau in Paris, France. They identified six FPLD families from France and Italy, in whom the *LMNA* gene was directly sequenced for all 12 exons [Vigouroux *et al.*, 2000]. In all of the six families, the recurrent heterozygous R482W (CGG→TGG) missense mutation was identified and consistently segregated with the disease. Mutational analysis of *LMNA* in a singleton with characteristic features of FPLD revealed a further recurrent mutation, R482Q (CGG→CAG). Although this patient's parents were unavailable for study,

lipodystrophy had been described in the mother, suggesting that the mutation was familial.

This group continued non-collaborative screening of the *LMNA* gene in other FPLD patients. Of significant interest was a singleton whose mother was thought to be lipodystrophic. Sequencing of exon 8 revealed no deleterious missense mutations. However, sequencing of exon 11 revealed a CGC→CAC transition at codon 584. The predicted effect would be the substitution of arginine for histidine (R584H). Unfortunately, the inherited basis of this mutation was not elucidated, as other family members were not available for study and the segregation of this mutation with the FPLD phenotype could not be established. Thus the causal role of the R584H variant in FPLD was not definitive. In an attempt to demonstrate R584H was responsible for FPLD, a cohort of 100 unrelated control subjects were screened for this mutation. No sequence variants were detected and therefore the R584H sequence alteration was thought unlikely to represent a polymorphism. This study increased the frequency of exon 8 recurrent mutations and also provided a novel FPLD missense mutation, at a novel locus, in exon 11. Although 2 singletons were found to harbour disease mutations (R482Q and R584H), the proof of a *de novo* mutation was not obtained and, again, these individuals were considered likely to have an FPLD parent.

4.6 Cohort screening of *LMNA*

Other inherited genetic disorders share some phenotype overlap with FPLD. With regard to appearance, CGL and HIV-PI patients present with similar morphological features as FPLD patients. Furthermore, the metabolic disturbances seen in FPLD are also associated with other more common western world diseases. These include hyperlipidaemia and type 2 diabetes mellitus. The screening of representative cohorts of these four diseases was achieved by direct DNA sequencing of PCR products and the high throughput heteroduplex detection method of DHPLC (Section 1.4.1.3).

4.6.1 CGL

Congenital lipodystrophic patients exhibit similar characteristics compared to FPLD patients (Section 1.2.2.1). Although most CGL families have been linked to chromosome 9q34, some evidence of genetic heterogeneity has been observed [Garg *et al.*, 1999]. It was postulated that unlinked 9q34 CGL might be an allelic disorder caused by mutations in *LMNA*. Four representative patients from CGL families were analysed

for the whole of the *LMNA* gene coding sequence. No mutations were identified and it was, thus, concluded that CGL is not an allelic disorder of *LMNA*.

In support of this study, others have also reported an absence of *LMNA* mutation in CGL patients [Vigouroux *et al.*, 2000; Kazlauskaite *et al.*, 2001]. Taken together with these two reports, 18 CGL patients have now been screened for mutation in the *LMNA* gene and none have been identified.

Subsequent reports have now identified a second CGL locus and observed mutations in a novel gene at 11q13 (Section 1.2.2.1) [Magré *et al.*, 2001]. This provides additional support for the lack of *LMNA* involvement in CGL.

4.6.2 HIV-Lipodystrophy

HIV protease inhibitor-associated lipodystrophy develops in HIV infected individuals who are treated with protease inhibitors (Section 1.2.3). The appearance of these individuals after prolonged PI treatment resembles the FPLD phenotype. It was speculated that a mutation in *LMNA* may present a genetic susceptibility towards developing lipodystrophy upon PI treatment. A cohort of sixteen DNA samples from individuals exhibiting HIV-lipodystrophy was analysed by direct sequencing, for mutations in the *LMNA* gene. No mutations were identified, leading to the conclusion that the *LMNA* gene does not underpin the development of lipodystrophy in protease inhibitor treated HIV patients [Behrens *et al.*, 2000].

4.6.3 FCHL

Hyperlipidaemia is characterised by an elevation of circulating triglycerides and/or cholesterol. The inherited disorder familial combined hyperlipidaemia (FCHL) is notable for elevated levels of both triglycerides and cholesterol and is linked to chromosome 1q21 [Pajukanta *et al.*, 1998]. The phenotype overlap of FPLD and FCHL with respect to elevated lipid levels in the circulation prompted the sequence analysis of the *LMNA* gene in FCHL patients. DNA samples from 15 independently ascertained FCHL patients were obtained and direct sequence analysis was carried out on exon 8, the apparent 'hot-spot' of FPLD mutation. No sequence variation from wild-type sequence was identified in any of the 15 samples, implying that FCHL is not a result of mutation in the coding sequence of *LMNA* exon 8.

4.6.4 Type 2 diabetes mellitus

The low success rate of FPLD identification in males and the presence of insulin resistance and type 2 diabetes mellitus impelled the analysis of the *LMNA* gene in diabetic patient cohorts. A resource maintained at the Hammersmith Hospital in London, UK, was utilised; this was composed of DNA samples from families with type 2 diabetes mellitus. These DNA samples were ascertained during the period 1995-1998, through six research centres in the UK [Wiltshire *et al.*, 2001].

DHPLC was used for high-throughput screening of mutations in these DNA samples. The analysis of heteroduplex identification in *LMNA* exon 8 was optimised using the WAVE™ machine (Transgenomic. Omaha, USA). Several different PCR samples were generated for exon 8 only against different template DNA. One PCR was performed on an R482W harbouring patient, another on a K486N patient and a final PCR on an unaffected wild-type sample. These three different samples were passed through the DHPLC column and the retention patterns of the DNA samples observed at different column temperatures. At a column temperature of 62°C a significant change in retention was observed for all three samples (Figure 15). The WT sequence is detected as a single sharp peak, whereas the R482W sequence appears as two equally high peaks and the K486N mutation appears as a single large peak preceded by two smaller peaks of equal height.

All 386 of the diabetic samples were amplified for *LMNA* exon 8. The samples were subsequently denatured and slowly cooled to permit heteroduplex formation. PCR samples were plated into 96 well microtitre plates and placed on the DHPLC machine. The machine is self-loading and fully automated. Following a sixteen-hour run of 96 samples the retention plots were analysed for the presence of heteroduplex DNA. Of the 386 samples, there was 3% PCR dropout, as determined by flat retention plots. Sixteen samples gave altered retention plots, but these did not correlate with the standardised R482W or K486N plots. In most cases the altered retention plots appeared towards the end of a run of 96 samples. Regardless, these 16 samples were subsequently PCR amplified and used for direct sequencing. No mutations were identified.

A second cohort of diabetic samples were made available by Prof. S. O'Rahilly (Addenbrooks Hospital. Cambridge, UK). These samples were all independently ascertained and known to have a familial background. Fifty DNA samples were

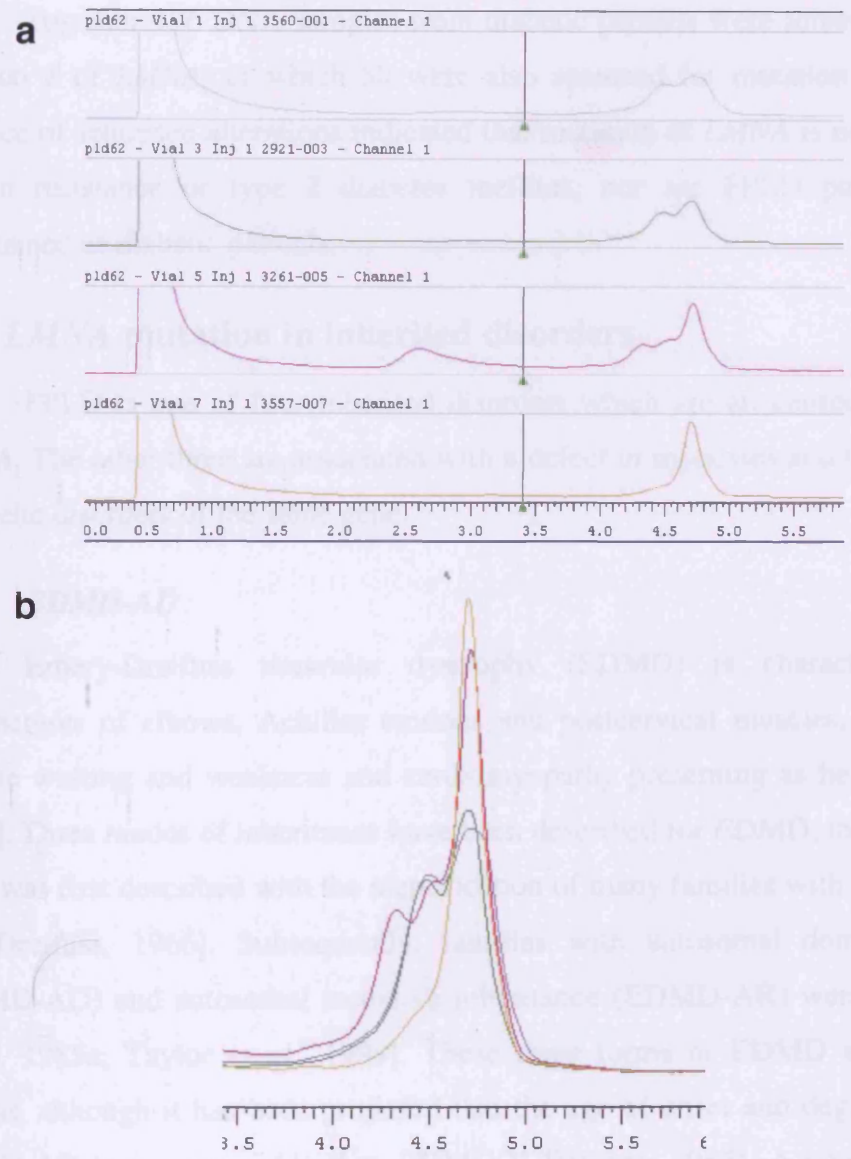

Figure 15. Optimisation of DHPLC column temperature on *LMNA* exon 8 amplicons. (a) Retention plots of various *LMNA* exon 8 amplicons. A column temerature of 62°C was determined to be optimal for heteroduplex detection. X-axis is the retention time of the DNA within the column and the peaks show the time at which the DNA is eluted from the column. Each plot illustrates the effect of heterozygous mutation in exon 8 on retention time. Grey plot is an R482W mutation (CGG→TGG), green plot is an R482Q mutation (CGG→CAG), pink plot is a K486N mutation (AAG→AAC), and the yellow plot is wild-type sequence. (b) Overlay of each retention plot described above.

analysed by direct DNA sequencing for exons 8 and 11 of *LMNA*. Again, no mutations were identified.

Together 436 DNA samples from diabetic patients were screened for mutations in exon 8 of *LMNA*, of which 50 were also screened for mutation in exon 11. The absence of sequence alterations indicated that mutation of *LMNA* is not associated with insulin resistance or type 2 diabetes mellitus, nor are FPLD patients incorrectly ascertained as diabetic patients.

4.7 *LMNA* mutation in inherited disorders

FPLD is one of four inherited disorders which are all caused by mutations in *LMNA*. The other three are associated with a defect in myocytes and now considered to be allelic disorders of the same gene.

4.7.1 EDMD-AD

Emery-Dreifuss muscular dystrophy (EDMD) is characterised by early contractures of elbows, Achilles tendons and postcervical muscles, slow progressive muscle wasting and weakness and cardiomyopathy presenting as heart block [Emery, 1989]. Three modes of inheritance have been described for EDMD, the classic X-linked form was first described with the identification of many families with EDMD-X [Emery and Dreifuss, 1966]. Subsequently, families with autosomal dominant inheritance (EDMD-AD) and autosomal recessive inheritance (EDMD-AR) were reported [Miller *et al.*, 1985a; Taylor *et al.*, 1998]. These three forms of EDMD are clinically very similar, although it has been proposed that the age of onset and degree of severity for EDMD-AD is more variable than EDMD-X [Becker, 1986]. A comparative study of EDMD-X and EDMD-AD patients [Bonne *et al.*, 2000] led to the observation of a more severe and progressive muscle wasting of the bicep muscles and hypertrophy of the quadriceps in the latter. In general EDMD-X patients presented with early contractures whereas EDMD-AD patients presented with initial muscle weakness and difficulty in running.

The novel gene *STA* at Xp28 was identified by a positional cloning approach and found to be mutated in EDMD-X [Bione *et al.*, 1994]. Mutations were identified which resulted in premature truncation of the *STA* protein. The *STA* gene encodes a protein of 254 amino acids and is ubiquitously expressed, with the highest levels observed in skeletal muscle and heart. The protein product is termed emerin, possesses a single

transmembrane domain and spans the inner nuclear membrane (Section 1.3.3.3). Thus the importance of emerin in the composition of the nuclear lamina was considered significant with respect to EDMD.

EDMD-AD was mapped to 1q11-23, by use of linkage analyses on a large French EDMD-AD pedigree and further confirmed in four additional families [Bonne *et al.*, 1999]. Fine mapping positioned the EDMD-AD locus between *D1S2346* and *D1S2624* (exactly the same boundaries as the FPLD critical interval identified in this study). The approximate positioning of *LMNA* [Wydner *et al.*, 1996] to this interval and the identical cell localisation of lamin A/C as emerin, suggested *LMNA* be a strong candidate for EDMD-AD. Four different heterozygous mutations were identified in the five independently ascertained families: one nonsense mutation G6X (CAG→TAG) and three missense mutations R453W (CGG→TGG), R527P (CGT→CCT) and L530P (CTC→CCC). These mutations all segregated with disease in the families, with the exception of R453W that arose *de novo*. In sharp contrast to emerin, where all of the mutations caused protein truncation, the majority of the mutations in *LMNA* are missense mutations. Over 25 different EDMD-AD mutations have now been described in the literature and are illustrated in Figure 16 (also Table 7).

The sequencing of the *LMNA* gene in a diagnosed EDMD sporadic patient revealed a homozygous missense mutation H222Y (CAC→TAC) [Raffaele Di Barletta *et al.*, 2000]. This patient was described as exhibiting a severe form of muscular dystrophy, the parents were first cousins and both were noted to be heterozygous for the mutation, yet phenotypically normal. These data formed the basis of the first report that mutations in *LMNA* can also cause the autosomal recessive form of EDMD.

4.7.2 CMD1A

Dilated cardiomyopathy is a disorder of the heart characterised by dilatation of the cardiac chambers and impaired systolic contraction and accounts for many cases of heart failure world-wide. Approximately, one third of all dilated cardiomyopathy cases are familial and inherited as an X-linked or autosomal dominant disorder [Michels *et al.*, 1992]. Dilated cardiomyopathy is often accompanied by conduction system defects (CMD1A) and a disease locus has been identified at chromosome 1p1-q24 [Kass *et al.*, 1994]. The recognition that EDMD patients exhibit conduction system defects and cardiac complications implicated the *LMNA* gene in dilated cardiomyopathy. *LMNA* was thus sequenced in members from 11 CMD1A families [Fatkin *et al.*, 1999].

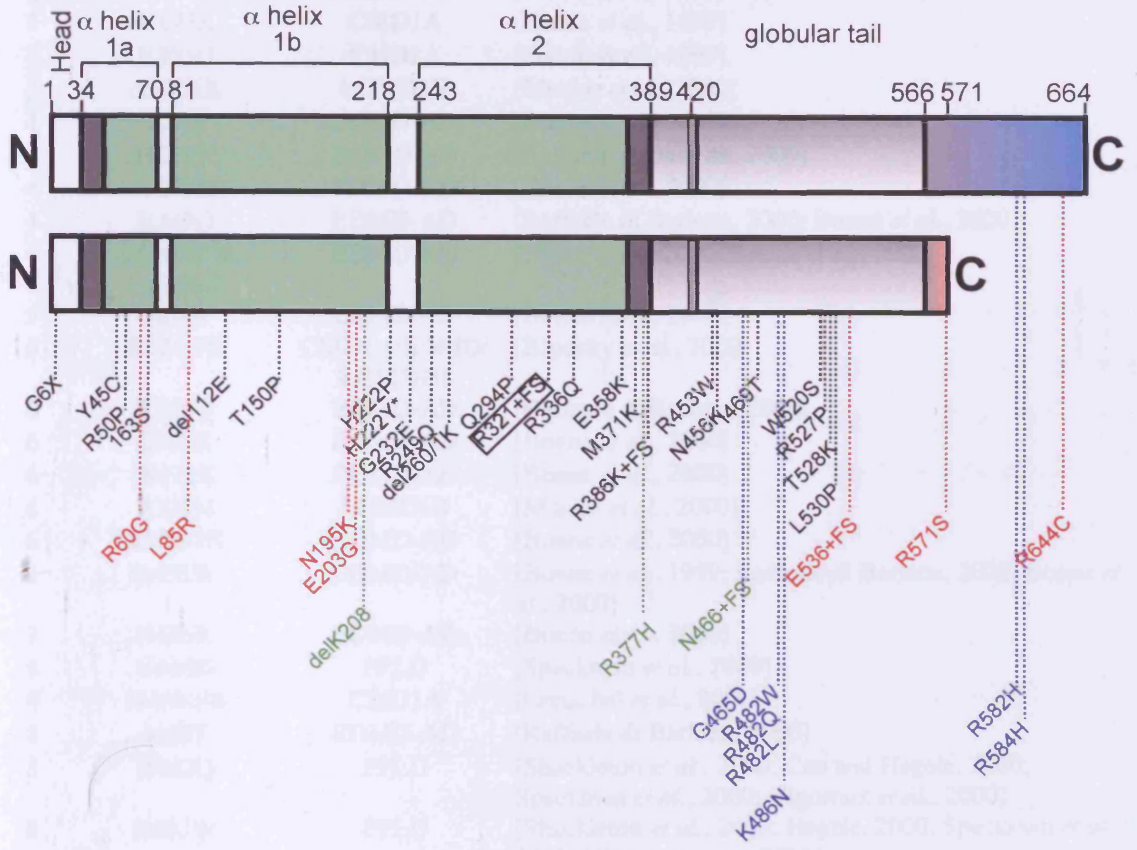

Figure 16. *LMNA* gene mutations. Polypeptide structure of lamin A (upper) and lamin C (lower) divided into the known functional domains. Dark grey boxes represent the highly conserved 30 amino acid residues at either end of the rod domain. The α-helices are divided into the main subdomains (green boxes); light grey shaded box refers to the tail domain common to both lamin A and lamin C and the two coloured boxes illustrate the lamin A (blue) and lamin C (red) specific domains. Below are all the known mutations at the time of writing (July, 2001). EDMD-AD/AR mutations are illustrated in black, LGMD1B in red, CMD1A in green and FPLD mutations in blue. The single EDMD-AR mutation is denoted with *, and the boxed mutation causes a range of myocyte and cardiomyocyte disturbances. Mutations are written using the single letter amino acid code (Appendix IV).

Exon	Mutation	Phenotype	Reference
1	Q6X	EDMD-AD	[Bonne *et al.*, 1999]
1	Y45C	EDMD-AD	[Bonne *et al.*, 2000]
1	R50P	EDMD-AD	[Bonne *et al.*, 2000]
1	R60G	CMD1A	[Fatkin *et al.*, 1999]
1	163S	EDMD-AD	[Bonne *et al.*, 2000]
1	L85R	CMD1A	[Fatkin *et al.*, 1999]
1	del112E	EDMD-AD	[Bonne *et al.*, 2000]
2	T150P	EDMD-AD	[Felice *et al.*, 2000]
3	N195K	CMD1A	[Fatkin *et al.*, 1999]
3	E203G	CMD1A	[Fatkin *et al.*, 1999]
3	del208K	LGMD1B	[Muchir *et al.*, 2000]
4	H222P	EDMD-AD	[Bonne *et al.*, 2000]
4	H222Y	EDMD-AR	[Raffaele di Barletta, 2000]
4	G232E	EDMD-AD	[Bonne *et al.*, 2000]
4	R249Q	EDMD-AD	[Raffaele di Barletta, 2000; Bonne *et al.*, 2000]
4	del260K or del261K	EDMD-AD	[Felice *et al.*, 2000; Bonne *et al.*, 2000]
5	Q294P	EDMD-AD	[Bonne *et al.*, 2000]
6	R321-FS	CMD1A/EDMD/ LGMD1B	[Brodsky *et al.*, 2000]
6	R336Q	EDMD-AD	[Raffaele di Barletta, 2000]
6	E358K	EDMD-AD	[Bonne *et al.*, 2000]
6	M371K	EDMD-AD	[Bonne *et al.*, 2000]
6	R377H	LGMD1B	[Muchir *et al.*, 2000]
6	R386-FS	EDMD-AD	[Bonne *et al.*, 2000]
7	R453W	EDMD-AD	[Bonne *et al.*, 1999; Raffaele di Barletta, 2000; Bonne *et al.*, 2000]
7	N456K	EDMD-AD	[Bonne *et al.*, 2000]
8	G465D	FPLD	[Speckman *et al.*, 2000]
8	N466-FS	CMD1A	[Genschel *et al.*, 2000]
8	I469T	EDMD-AD	[Raffaele di Barletta, 2000]
8	R482Q	FPLD	[Shackleton *et al.*, 2000; Cao and Hegele, 2000; Speckman *et al.*, 2000; Vigoroux *et al.*, 2000]
8	R482W	FPLD	[Shackleton *et al.*, 2000; Hegele, 2000; Speckman *et al.*, 2000; Vigoroux *et al.*, 2000]
8	R482L	FPLD	[Shackleton *et al.*, 2000]
8	K486N	FPLD	[Shackleton *et al.*, 2000]
8	K486N	FPLD	[Shackleton *et al.*, 2000]
9	W520S	EDMD-AD	[Bonne *et al.*, 2000]
9	R527P	EDMD-AD	[Bonne *et al.*, 1999]
9	T528K	EDMD-AD	[Raffaele di Barletta *et al.*, 2000; Bonne *et al.*, 2000]
9	L530P	EDMD-AD	[Bonne *et al.*, 1999]
9	E536-FS	LGMD1B	[Muchir *et al.*, 2000]
10C	R571S	CMD1A	[Fatkin *et al.*, 1999]
11	R582H	FPLD	[Speckman *et al.*, 2000]
11	R584H	FPLD	[Vigoroux *et al.*, 2000; Hegele, 2000]
11	R644C	CMD1A	[Genshel *et al.*, 2000; Speckman *et al.*, 2000]

Table 7. All reported mutations in the *LMNA* gene. *LMNA* mutations published were identified from several reports (above). Mutations are written using the single letter amino acid code (Appendix IV). Frameshift mutations are referred to with FS.

Five missense mutations were identified: R60G, L85R, N195L, E203G and R571S. The mutation R571S was identified in the 3 prime section of exon 10 which is specific to the lamin C isoform only. The phenotype in this family was reported to be milder than the other cases of CMD1A. Sequence variants were not detected in six CMD1A families.

The phenotypic overlap of CMD1A with EDMD prompted the clinical assessment of skeletal muscle in CMD1A patients. Those patients harbouring one of the five CMD1A-*LMNA* mutations did not suffer from skeletal-muscle dysfunction nor muscle weakness or joint contractures. These mutations and those described in more recent reports are listed in Table 7 and displayed in Figure 16.

4.7.3 LGMD1B

The term 'limb-girdle muscular dystrophy' (LGMD) refers to several disorders associated with slow progressive muscle wasting and weakness in the limbs and around the 'girdle' of the body. Several dominant (LGMD1) and recessive (LGMD2) forms have been identified. An autosomal dominant form (LGMD1B) has been described with additional age-related atrioventricular cardiac system defects, dilated cardiomyopathy and absence of early contractures [van der Kooi *et al.*, 1996]. Three LGMD1B families were used in a linkage study to identify a LGMD1B locus [van der Kooi *et al.*, 1997]. The markers *D1S305* and *D1S303* provided maximum LOD scores and facilitated the positioning of the LGMD1B locus at chromosome 1q21. The previous identification of *LMNA* mutations in the related muscular dystrophy (EDMD-AD) suggested *LMNA* mutation in LGMD1B and was thus analysed in three LGMD1B families [Muchir *et al.*, 2000]. Three novel mutations were identified in each of the families. The first was an in-frame deletion of codon 208 (delAAG) resulting in the loss of a lysine residue, del208K. The second was a mutation in the splice-donor site immediately after exon 9 (gtaag→gtaac). RNA transcript analysis revealed that with this splice-site mutation exon 9 is not spliced to exon 10, instead continues through intron 9. The aberrant transcript possesses the first 536 normal lamin A/C residues followed by 35 unique amino acids and a premature stop codon. The final mutation was a missense mutation CGC→CAC resulting in an arginine to histidine substitution (R377H). These three mutations co-segregated with the disease in each family and were absent from 200 normal chromosomes. All identified LGMD1B mutations are shown in Figure 16 (listed in Table 7).

These three disorders share clinical characteristics and are all associated with muscle degeneration or improper functioning. The disorders EDMD and LGMD1B are closely linked at the phenotypic level, by their shared characteristic of skeletal muscle wasting, observed amongst patients. However, LGMD1B and the disease CMD1A may be classed together due to the presence of cardiac dysfunction among patients with both disorders. These myopathies represent allelic forms of the same disorder with EDMD and CDM1A the two extreme phenotypes, and LGMD1B representative of an intermediate phenotype.

4.7.4 Additional FPLD reports

The identification of *LMNA* exon 8 and exon 11 specific mutations in FPLD patients encouraged the screening of *LMNA* in other FPLD families ascertained by groups from Europe and America. Ascertainment of a further five Canadian FPLD families by Hegele and co-workers permitted the identification of the R482Q, R482W and R584H recurrent mutations [Hegele *et al.*, 2000], which supports the identification of these same mutations in the UK and French studies (Sections 4.2, 4.4 and 4.5). Interestingly, upon sequencing the *LMNA* gene in an R482Q heterozygote, a second missense mutation was identified in exon 7 (GTG→ATG) corresponding to a valine to methionine substitution (V440M). This mutation was inherited from the unaffected parent. This V440M/R482Q compound heterozygote was described as exhibiting a severe FPLD phenotype, with profound insulin resistance, severe diabetes and cardiac defects. These symptoms may represent a severe FPLD phenotype or may, in fact, impinge on the characteristics of the other allelic disorders of *LMNA*. The pathogenicity of V440M is unclear as the unaffected father is heterozygous for V440M, yet is phenotypically normal.

A further study reported the analysis of the *LMNA* gene in 15 FPLD families [Speckman *et al.*, 2000]. The R482Q mutation (CGG→CAG) was identified in 5 families and the R482W mutation (CGG→TGG) in 7 families. Two novel mutations were also identified, each in only one family. The first was in exon 11, R582H (CGC→CAC), this sequence alteration was two codons proximal to the R584H mutation identified in two other studies. The genetic change in both mutations, was identical (CGC→CAC) [Hegele *et al.*, 2000; Vigouroux *et al.*, 2000]. The location of this variant relative to the position of the confirmed mutation R584H certified its role in FPLD. This was the third report of FPLD mutation outside of *LMNA* exon 8; however,

it was localised to a newly recognised FPLD mutation hotspot in exon 11. The second novel mutation was also unique, with regard to location within the *LMNA* gene. A heterozygous sequence change was identified at codon 465 within exon 8. The sequence was altered from GGC to GAC and resulted in a glycine to aspartic acid substitution (G465D) in the lamin A/C polypeptide. These two novel mutations were absent from 140 DNA samples. Ironically, the initial family identified by this group, F100, was not found to harbour any sequence variation from wild-type sequence, even though this family was linked to 1q21. Further analyses in the promoter region and the detection of large-scale genomic rearrangements are required to exclude *LMNA* mutation in this family.

4.8 *LMNA* knockout mouse

The generation of animal models of human disease can aid in the understanding of disease pathogenesis, as a result of genetic manipulations, breeding programs and medical and biological tests not possible in human subjects. The study of a mouse model suffering from a similar disease in humans can aid in the understanding of the genetic basis for disease. Equally possible is the genetic manipulation of a gene or pathway in order to observe the resultant phenotype. With these aims, Sullivan and colleagues generated transgenic mice in which A-type lamins were eliminated by gene targeting [Sullivan *et al.*, 1999]. Homologous recombination was used to delete a region of *Lmna* from exon 8 to exon 11. Western blot analyses demonstrated that lamin A/C proteins were not expressed in these mice. At birth, *Lmna* null (-/-) mice were indistinguishable from heterozygote or wild-type mice. Within 2-4 weeks the growth of the (-/-) mice was dramatically reduced and these animals were approximately 50% the weight of their littermates. At this time, the *Lmna* null mice had difficulty in walking and exhibited splayed hind legs with the appearance of a 'progressively more hunched posture'. By 8 weeks all (-/-) mice had died. Intriguingly, the heterozygotes (+/-) appeared phenotypically normal, muscular abnormalities were not noted, nor did the mice die prematurely compared to wild-type mice. Other phenotypic changes in the *Lmna* null mice included slight thymic atrophy and absence of adipose tissue. Detailed examination of skeletal muscle revealed myocyte degeneration. Examination of the cardiomyocytes showed the ventricular muscle was most severely compromised, with other myocytes clearly atrophic.

These mice appear to suffer from the murine form of EDMD. Many phenotypic characteristics are found in both mammals including muscular dystrophy and contraction and premature mortality. Unfortunately Sullivan *et al.* failed to describe the reason for death in the *Lmna* (-/-) mice. An interesting and expected cause would be associated with heart failure and would define these mice as true models of EDMD. To further investigate this similarity in phenotype the localisation of emerin was investigated. In lamin A/C (-/-) cells, emerin was not localised to the nuclear periphery but was diffuse in the nuclear and cytoplasmic compartments. Transfection of these cells with wild-type lamin restored emerin localisation at the nuclear periphery. It may be concluded that lamin A and emerin rely on each other for the correct positioning of both at the nuclear periphery. The absence of either one results in a defect in myocyte and cardiomyocyte maintenance and/or development. The description of adipose tissue absence in these mice also demonstrates the importance of *LMNA* in the development of a further cell type, adipocytes.

4.9 Discussion

Over 40 different mutations have been identified in the *LMNA* gene in the past two years. Mutations account for at least four allelic disorders, involving predominantly the myocyte, cardiomyocyte, or the adipocyte. EDMD-AD/AR and LGMD1B patients both have skeletal muscle abnormalities, sometimes observed in CMD1A. Furthermore, the cardiac defects common to CMD1A have also been identified in EDMD and LGMD1B. FPLD, a disorder involving subcutaneous adipocytes, also caused by *LMNA* mutation, is both intriguing and unexpected. The distinct difference between these three myocyte diseases and FPLD is, to some degree, reflected at the molecular genetic level. EDMD-AD/LGMD1B/CMD1A mutations are distributed over the whole of the *LMNA* coding sequence, with no striking similarity in mutation type or evidence of mutation clustering in each disease. In sharp contrast, the FPLD mutations are all missense and highly site-specific, affecting only 5 amino acids G465, R482, K486, R582 and R584.

The cloning of the gene causative of X-linked EDMD and the subsequent linkage of EDMD-AD to 1q21 led to the identification of EDMD-AD mutations in *LMNA*, on the basis of emerin and lamin A/C cellular localisation. EDMD-AD was the first disorder linked to a defect in lamin A/C function. Initially, five mutations were found in *LMNA,* distributed over the whole of the gene. Four of these were missense and mapped to both the α-helical rod and globular tail of lamin A/C. Of interest is the

fifth mutation, a null mutation – Glu6Stop. This mutation results in premature truncation and effectively, no functionally active protein is produced from this gene. Disease mechanism in dominant disorders requires either a dominant negative (deleterious protein interaction) or haploinsuffiency (quantitative loss of biologically active protein) defect. The loss of lamin A/C protein, in the case of the G6X mutation, strongly suggests that EDMD-AD is caused by haploinsufficiency. Thus, it may be proposed that lack of sufficient lamin A/C causes muscular defects as a result of reduced lamin A/C levels at the nuclear lamina within muscle cells. The lack of lamin A/C possibly effects the structure of the nuclear lamina. The lamina is normally composed of lamins A/B1/B2/C and the presence of only 50% of normal lamin A/C levels would reduce the overall size and composition of the lamina. It may be speculated that a threshold level of lamin protein is necessary for correct lamina formation or adequate structural integrity. Lamin proteins are classified as type V intermediate filaments and thus have a significant evolutionary conserved structural role in the cell [Cohen *et al.*, 2001]. Partial lamin loss may possibly result in reduced tensile strength of the lamina. This could have the effect of reducing nuclear envelope rigidity and general cell maintenance at the nuclear level. How these mutations only affect muscle, given their ubiquitous expression is also intriguing. A fascinating insight into this may be related not to lamin A/C expression, but to lamin B expression. An extensive study of lamin protein levels in many human tissues demonstrated expression of lamin B2 and lamin A/C in virtually all tissues [Broers *et al.*, 1997]. However, lamin B1 exhibited restrictive expression. Most notably, lamin B1 expression is absent in all types of muscle; skeletal, heart, interstitial heart fibres and smooth muscle. The absence of lamin B1 in these tissues may demand an absolute requirement of normal levels of lamin A/C protein. Thus, G6X would be predicted to reduce the amount of lamin available to muscle cells, already deficient in lamin B1 protein, and may explain why only muscle is affected by a loss of lamin A/C protein. It is also believed that only within the myocyte is the nuclear envelope and lamina subjected to mechanical stress as a consequence of muscle contraction and relaxation [Morris and Manilal, 1999]. The lamina is considered likely to play a role in ensuring the rigidity of the nuclear envelope. In the case of EDMD-AD, the weakened lamina may not perform its structural role correctly and putatively, allows the 'kneading' of the nucleus by contractile forces in the myocyte [Morris and Manilal, 1999]. It would therefore correlate that those muscles that are more frequently used exhibit severe myocyte

atrophy as opposed to muscles less commonly used. EDMD-AD patients develop muscle wasting with a humero-peroneal distribution and contractures in the Achilles tendons and neck. Thus, theoretically it is consistent that muscular dystrophy is present in muscle subjected to more persistent use. In keeping with this hypothesis, muscular weakness has also been reported in other commonly used muscles including the diaphragm, quadriceps and those on the hands and face [Bonne *et al.*, 2000].

The EDMD-AD missense mutations distributed over the remainder of *LMNA* either result in haploinsufficiency or dominant negative protein. Given the rationale that G6X causes EDMD-AD as a result of haploinsufficiency, it is logical to predict that other EDMD-AD mutations would lead to the EDMD-AD phenotype by a similar mechanism. Potentially, all other missense mutations render the lamin A/C protein defective in lamina formation and hence cannot be incorporated into the lamina correctly. This would resemble a haploinsufficient mechanism, whereby even though protein is present it cannot contribute to the structure of the lamina. Many other missense mutations have now been detected in EDMD-AD patients, mainly localised throughout the rod domain of lamin A/C. Presently, it is reasonable to conclude that these missense mutations can exert their effects in one of two ways; either by altering protein conformation in the α-helix and disrupting the heptad repeat structure (critical in helix formation) [Fisher *et al.*, 1986], or by altering peptide domains that are crucial in dimerisation and polymerisation of the lamins [McKeon, 1991]. In support of the former concept, several amino-acid deletions (3 base in-frame deletions) have been identified del112E, del261/262K. This form of mutation would affect the frame of the heptad repeat and alter the conformation in the α-helix, ultimately causing severe twists in the lamin polypeptide. For example, the globular tail domain may be slightly rotated relative to the rod domain and affect lamin dimerisation or polymerisation. Many missense mutations result in the substitution of proline (a large aromatic amino acid) in the place of smaller linear amino acids; these include R50P, H222P, Q294P, R527P and L530P. A consequence of proline replacement could involve the introduction of extreme structural 'kinks' in the protein. The characteristic feature of an α-helix is the presence of a heptad repeat of hydrophobic residues [Chothia, 1984]. Several of the EDMD-AD mutations correlate to hydrophobic residues, including Y45C, I63S and R249Q. Mutations that do not fit with these general rules of amino acid substitution (replacement by a larger amino acid, amino acid loss, or amino acid substitution at

putative hydrophobic residues) include a number in exon 6, exon 7 and exon 9. The exon 6 mutations E358K and M371K localise within the rod domain and although they do not affect hydrophobic residues or exert dramatic structural changes, they do localise to the 33 amino acid conserved domain at the end of the α-helix [McKeon, 1991]. This domain is known to be critical in helix formation [Hutchison *et al.*, 2001] and therefore, may also affect the internal structure of the lamin molecule. The EDMD-AD mutations in the lamin tail domain are clustered to a 10-residue site in exon 9 and include W520S, R527P, T528K and L530P. Two of these mutations are consistent with the previous hypothesis (change to proline). Thus, it may be possible that this site is essential to the correct folding of the protein. The lamin tail domains are believed to interact with each other, either in dimer formation or polymer formation. Therefore the residues 520-530 could be important in lamin-lamin interactions. Although these mutations localise outside the rod domain they may still have an affect on the strength of the nuclear lamina.

Further corroboration of this mechanism of correct lamin structure and self-interaction is provided by the discovery of two different mutations at the same codon. Histidine 222 is mutated to proline in EDMD-AD and to tyrosine in EDMD-AR. The more dramatic change is proline and is sufficient to cause disease in the heterozygous state. The other mutation H222Y has no effect in the heterozygous state, but precipitates EDMD-AR when homozygous. Thus, it may be argued that more subtle mutations are not deleterious when compensated by wild-type lamin.

Several mutations have been described which cause CMD1A and LGMD1B. Two CMD1A mutations, R60G and L85R are localised to the N-terminal conserved domain of the first α-helix and thus may disrupt the assembly of lamin dimers, known to be critical in dimer assembly [Moir *et al.*, 1991]. Two other mutations are localised to a domain in exon 3 corresponding to the end of helix 1b, adjacent to the short peptide linker between helices 1b and 2. Mutation at these residues may also effect the internal structure of the α-helix and cause rotation in the lamin molecule which is exaggerated, as it occurs just proximal to the linker segment. Intriguingly, two further missense mutations cause CMD1A and they both occur in either lamin A only (R644C) or lamin C only (R571S). Both of these mutations substitute arginine and lie adjacent to the extreme C-termini of both proteins. R571 is the penultimate amino acid in lamin C and R644 is the previous to penultimate amino acid in lamin A (upon lamin A maturation).

Thus, it may be concluded that an arginine residue at the very end of lamin A or C is important in cardiomyocyte maintenance. Taken together, the CMD1A mutations cluster in three domains: at the N-terminal conserved domain, at a site proximal to the linker peptide or at the very C-terminus. It is reasonable to suggest that these mutations may permit lamin dimer formation but may actually disrupt the formation of head-to-tail polymers. This difference may explain the phenotypic variation between EDMD and CMD1A. One range of mutations results in structural changes within the lamin protein and affects dimer formation and/or lateral assembly of the filaments, whereas the other mutations affect head-to-tail polymer formation.

LGMD1B shares phenotypic features with EDMD-AD and CMD1A, possessing defects in both skeletal muscle and cardiac function. The mutations associated with LGMD1B do not cluster within *LMNA*. One missense mutation has been identified (R377H) and is localised to the conserved domain at the distal end of the rod domain. An in-frame 3 bp deletion was detected and results in the loss of lysine at position 208 (del208K). This mutation localises to the end of rod 1b, proximal to the linker peptide, between rod 1b and 2. The third mutation was found in the intron 9 splice donor site. Analysis of the mature mRNA transcribed from this gene demonstrated the retention of intron 9 and a premature stop codon. Lamin A/C is predicted to be normal until amino acid 536 and followed by a unique 35 amino acids encoded by intron 9, to constitute a chimeric protein of 571 residues. This protein lacks the carboxy terminal half of lamin A tail domain and the corresponding carboxy terminal quarter of lamin C.

The phenotypic median of LGMD1B between EDMD and CMD1A is also reflected in the location and type of mutations; LGMD1B mutations have been identified near to both CMD1A and EDMD-AD mutations. The LGMD1B mutation, del208K, localises close to several CMD1A mutations. Furthermore, a second LGMD1B mutation, R377H is positioned central to a cluster of EDMD-AD mutations (E358K, M371K and R386K).

Brodsky and colleagues reported a fascinating mutation which was identified in a family suffering from dilated cardiomyopathy with skeletal muscle involvement [Brodsky *et al.*, 2000]. The mutation is a single base deletion in exon 6 that causes a frameshift from amino acid 321 onwards. The altered reading frame causes the addition of 158 novel amino acids before the occurrence of a stop codon. This mutation does not affect the majority of the α-helix, however adds nonsense amino acids from half way through rod 2. The conserved 33 amino acid domain at the end of the rod domain, the

NLS and the entire tail domain for both lamin A and C are lost. Five affected members were described with this mutation, one of whom was deceased. The other four individuals all suffered from variable degrees of cardiac defects. Interestingly, these patients also exhibited varying degrees of skeletal muscle abnormalities, ranging from weakness of the limb-girdle to slight rigidity of the elbow and Achilles tendon. Two patients were considered to have slight LGMD, with another diagnosed with mild EDMD. This discovery has been instrumental in the confirmation that EDMD-AD, LGMD1B and CMD1A are all phenotypically related and allelic disorders of the *LMNA* gene.

Two reports have documented the direct interaction of lamin A with emerin [Clements *et al.*, 2000; Sakaki *et al.*, 2001]. It is possible that lamin mutation interferes with this interaction, especially in the case of lamin missense mutation in the globular domain. The finding that emerin and lamin A dysfunction both lead to EDMD suggests that this interaction is critical in the proper functioning of the myocyte. The correct assembly of lamin dimers, lamina construction and lamina localisation at the nuclear envelope is defective in EDMD (both forms) and to a certain extent in CMD1A and LGMD1B, as illustrated by R321-FS. Thus the interaction of emerin is critical to recruit and position the nuclear A-type lamins (analogous to the recruitment of B-type lamins by LAP2β [Furukawa and Kondo, 1998]). The specificity of the lamina defect, is likely to be a result of one of two mechanisms: either a lack of lamin B1 in muscle that interferes with the positioning of A-type lamins at the nuclear envelope and thus, the lamina formation of A-type lamins or, alternatively, the weakened lamina is less efficient in stabilising nuclear structure in myocytes (cells which exert increased mechanical stress).

FPLD is distinct at the phenotypic and genetic level. FPLD mutations are all missense and localised to 5 amino acids in the globular tail of lamin A. These five mutations map to two different domains, of which one has been saturated with many recurrent mutations from different sources. Domain 1 is in exon 8 and the two residues affected are R482 and K486, the second domain is in exon 11 (residues R582 and R584) and specific to lamin A. Four independent groups have documented mutations in over 30 FPLD families, all of which map to these 4 amino acids with the exception of a single mutation identified once only, G465D (also in exon 8). The residues in exon 8 are frequently mutated (42 out of 45 FPLD families). It is considered that FPLD patients harbouring an exon 8 mutation (R482 or K486) exhibit a typical FPLD phenotype,

whereas those individuals with mutations outside these two residues possess an atypical FPLD phenotype [Garg *et al.*, 2001]. Atypical FPLD patients (heterozygous for R582H) exhibit reduced adipose tissue loss and normal levels of subcutaneous adipose tissue in the medial part of the thigh and gluteal regions. Other regions are described as being less lipodystrophic than similar sites in FPLD patients with R482 mutation. The authors hypothesise that adipocytes from the less affected lipodystrophic areas express more lamin C relative to lamin A and thus the mutations in exon 11 are less deleterious, however provide no evidence to support this idea.

Interestingly, the G465D mutation has been identified only once, compared with 40 independent findings of mutations in R482 or K486. Speckman and colleagues consider individuals with this mutation to present with typical FPLD. Given that this mutation is over 50 bases (17 amino acids) proximal to R482 it would be of interest to investigate the degree of lipodystrophy in these patients, compared to R482 patients. The sole occurrence of G465D compared to the frequent identification of other FPLD mutations would suggest that it is either at a site of rare mutation, or the phenotype in these patients is, in fact, less dramatic than in typical FPLD patients.

The contrasting mutations in FPLD compared to EDMD-AD/LGMD1B and CMD1A may represent two different disease mechanisms. The finding of null, frameshift and missense mutations in the α-helical domain and localised sites in the tail domain in disorders involving the myocyte could ultimately affect the self-interaction of lamins, their assembly and finally their overall structure and rigidity. The extreme site-specific nature of FPLD mutations in the tail domain may reflect the function of this globular tail, independent of the α-helical functions. Several roles have been assigned to the carboxy terminal globular domain. Its adjacency to a partner lamin tail in a lamin dimer suggests a role in the dimerisation of lamin filaments. Equally, the head-to-tail arrangement of lamin dimers also implicates the tail domain in dimer-dimer interactions and hence, polymer assembly. As previously discussed EDMD and CMD1A mutations possibly result in a perturbation of dimer or polymer assembly; thus, FPLD mutations would be expected to be distributed throughout the gene if they caused a defect in structural lamina conformation.

Other carboxy terminal tail roles include interactions with chromatin. Initially, chromatin binding was assigned to the α-helical rod [Glass *et al.*, 1993] but subsequent studies have identified chromatin binding domains in the tail of lamin A and C [Taniura

et al., 1995]. This has been demonstrated by *in vitro* and *in vivo* studies with *D. melanogaster* lamin Dm_0 and suggest that these interactions are mediated by histone proteins [Goldberg *et al.*, 1999]. Lamin-chromatin binding may have ramifications in the control of gene expression, by associating with nucleosomes in transcriptionally closed DNA (heterochromatin). Conflicting investigations report that chromatin is attached to the lamina at scaffold attachment regions in the DNA sequence (SARs and MARs) [Zhao *et al.*, 1996]. The chicken lysozyme gene is known to be controlled by SARs either side of the gene and can be envisaged as a transcriptionally accessible loop [Lewin, 1997]. It is possible that multiple chromatin attachment sites are present in lamin A/C and interact with both DNA sequence and proteins in nucleosomes. Mutation at these sites would perturb normal gene transcription and alter the regulation of gene expression, leading to a disruption of the normal biology of the cell.

Finally, the carboxy terminal globular domain of lamin A/C is reported to interact with many other cellular proteins [Cohen *et al.*, 2001] (Figure 6). The finding that emerin and lamin A dysfunction both lead to EDMD suggests that this interaction is critical in the biology of the myocyte. Although FPLD mutation may perturb lamin A and emerin interaction, it is unlikely as this mechanism appears to underlie the distinct muscular diseases. LAP2α has been shown to co-localise with lamin A, within discrete intranuclear foci [Dechat *et al.*, 2000]. These foci also consist of RNA splicing factors [Jagatheesan *et al.*, 1999]. Thus, specific lamin A/C mutation could cause a defect in translational regulation (in addition to transcriptional regulation as a consequence of chromatin binding). Again, many of these interacting proteins are ubiquitous and do not provide a clear explanation for adipocyte-specific failure in FPLD patients.

Transcription factors are recognised as cell-specific proteins capable of directing specific cellular development [Lewin, 1997]. It is therefore of interest that lamin A/C interacts, or at least co-localises with a number of transcription factors. The majority of these are repressors, although transcriptional activators have been shown to localise at the nuclear periphery [Cohen *et al.*, 2001]. It would be intriguing to determine if these transcription factors were expressed in adipocytes only and if FPLD lamin mutations disrupted the lamin-transcription factor interaction.

Lamin mutation has been found to cause four different inherited diseases, of which affect muscle and fat cells. With respect to the type, location and consequence of mutations, two molecular mechanisms can be considered. Firstly, those mutations which result in a reduced or weakened lamina lead to nuclear stress, specifically in myocytes.

et al., 1995]. This has been demonstrated by *in vitro* and *in vivo* studies with *D. melanogaster* lamin Dm_0 and suggest that these interactions are mediated by histone proteins [Goldberg *et al.*, 1999]. Lamin-chromatin binding may have ramifications in the control of gene expression, by associating with nucleosomes in transcriptionally closed DNA (heterochromatin). Conflicting investigations report that chromatin is attached to the lamina at scaffold attachment regions in the DNA sequence (SARs and MARs) [Zhao *et al.*, 1996]. The chicken lysozyme gene is known to be controlled by SARs either side of the gene and can be envisaged as a transcriptionally accessible loop [Lewin, 1997]. It is possible that multiple chromatin attachment sites are present in lamin A/C and interact with both DNA sequence and proteins in nucleosomes. Mutation at these sites would perturb normal gene transcription and alter the regulation of gene expression, leading to a disruption of the normal biology of the cell.

Finally, the carboxy terminal globular domain of lamin A/C is reported to interact with many other cellular proteins [Cohen *et al.*, 2001] (Figure 6). The finding that emerin and lamin A dysfunction both lead to EDMD suggests that this interaction is critical in the biology of the myocyte. Although FPLD mutation may perturb lamin A and emerin interaction, it is unlikely as this mechanism appears to underlie the distinct muscular diseases. LAP2α has been shown to co-localise with lamin A, within discrete intranuclear foci [Dechat *et al.*, 2000]. These foci also consist of RNA splicing factors [Jagatheesan *et al.*, 1999]. Thus, specific lamin A/C mutation could cause a defect in translational regulation (in addition to transcriptional regulation as a consequence of chromatin binding). Again, many of these interacting proteins are ubiquitous and do not provide a clear explanation for adipocyte-specific failure in FPLD patients.

Transcription factors are recognised as cell-specific proteins capable of directing specific cellular development [Lewin, 1997]. It is therefore of interest that lamin A/C interacts, or at least co-localises with a number of transcription factors. The majority of these are repressors, although transcriptional activators have been shown to localise at the nuclear periphery [Cohen *et al.*, 2001]. It would be intriguing to determine if these transcription factors were expressed in adipocytes only and if FPLD lamin mutations disrupted the lamin-transcription factor interaction.

Lamin mutation has been found to cause four different inherited diseases, of which affect muscle and fat cells. With respect to the type, location and consequence of mutations two molecular mechanisms can be proposed. Firstly, those mutations which result in a reduced or weakened lamina lead to nuclear stress, specifically in myocytes.

A null mutation in an EDMD patient would suggest haploinsufficiency as a molecular mechanism. Alternatively, point mutations in *LMNA* may result in an aberration in lamina incorporation or the prevention of WT lamin contribution to the lamina, as a consequence of mutant and WT heterodimer formation. Thus, these defects could be interpreted as both haploinsufficiency and dominant negative mechanisms.

Site-specific localisation of FPLD mutations to the lamin A tail domain implies the functional significance of these domains. These sites could result in loss of function and thus, haploinsufficiency as a molecular mechanism. It is unknown whether these mutations affect lamina assembly, DNA interactions, gene transcription and translation or specific interactions with other proteins in the nuclear compartment, including transcription factors.

5 YEAST TWO-HYBRID SCREEN WITH LAMIN A

5.1 Introduction

Identification of mutations in the *LMNA* gene in FPLD patients highlighted the importance of A-type lamins in the nuclear lamina of adipocytes. Additionally, the discovery of other mutations in *LMNA* that cause muscle-specific diseases suggested a crucial role for the nuclear lamina in the myocyte and cardiomyocyte. It is possible, yet unproven, that the absence of lamin B1 in muscle renders myocytes susceptible to nuclear envelope stress and, thus, necessitates normal levels of wild-type A-type lamins in this cell type. While this would explain the specificity of lamina dysfunction in the muscle disorders, it does not account for the adipocyte dysfunction observed in FPLD. The nature of the FPLD mutations may indicate the molecular mechanism underpinning the disease. In most cases the mutations have resulted in the replacement of a basic amino acid with either a hydrophobic, or hydrophilic un-charged amino acid, i.e. R482W, R482Q, R482L, K486N. Interestingly, an atypical FPLD patient suffering from a less severe form of lipodystrophy harboured an exon 11 mutation that resulted in an amino acid substitution of arginine (hydrophilic basic amino acid) with another basic residue, histidine. It is feasible that more subtle molecular changes may result in the less severe phenotype. Nonetheless, these FPLD mutations are considered likely to affect the charge of the mutated residue. Protein charge is known to be critical in protein interactions and these mutations may perturb interactions between lamin A and other cellular proteins. Another tantalising possibility is that these mutations affect a protein interaction specific to adipocytes.

In support of this idea, the FPLD mutations have recently been mapped to the surface of the lamin A globular domain. By comparison to the IF proteins, the three-dimensional structure for the lamin α-helix was determined [Fisher *et al.*, 1986]. No known structurally resolved proteins display homology to the lamin tail domain (residues 389-664 in lamin A); thus the three dimensional structure of the lamin A tail domain was resolved using X-ray crystallography [S. Shoelson, *pers comm*] and arranges into a symmetrical lattice composed of overlapping β-sheets (Figure 17). Of significant importance is the location of *LMNA* missense mutations. A subset of FPLD and EDMD-AD missense mutations have been positioned on this 3-D structure. EDMD-AD mutations all map to the interior of the structure, whereas the FPLD

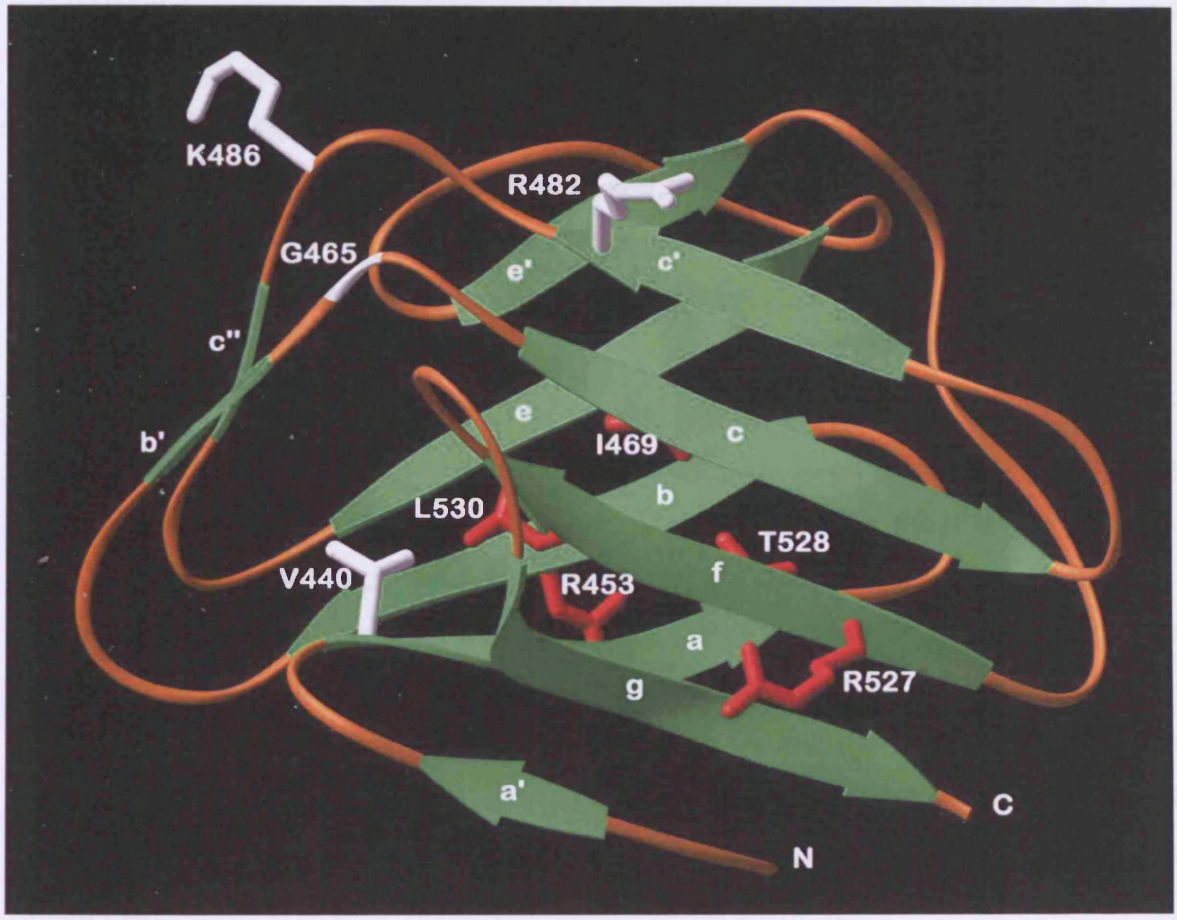

Figure 17. Three-dimensional structure of the tail domain of lamin A. Crystal structure resolution of human lamin A residues 389 to 664. Green ribbons refer to β-sheets. Disease-causing missense mutations are identified for both FPLD (white projections) and EDMD-AD (red projections). Provided by S. Shoelson.

mutations all map to the exterior. The exposure of these residues at the lamin A tail domain surface and their mutation which results in change of charge, strongly implies that this region of lamin A may provide an interface for interactions with other cellular proteins. It was also proposed that this site is involved in lamina formation, either by contributing to dimer, or polymer formation or interactions with the nuclear envelope proteins such as emerin [Holt *et al.*, 2001]. Because of the near-ubiquitous expression of both A-type lamins and emerin, this proposed site of interaction would not specifically affect adipocytes over other tissues.

With consideration to the above findings, it was speculated that lamin A interacts with an adipocyte-specific protein and this interaction is perturbed in FPLD patients. Further, it was conjectured that, using lamin A as a bait protein in a yeast two-hybrid screen against proteins from adipocytes, a lamin A adipocyte-specific interaction may be identified.

A yeast two-hybrid screen involves the interaction of two chimeric modular proteins (Section 1.4.2.2), one of which contains the gene under investigation (the bait) with the other protein being one of a library of transcripts (the prey; Figure 18a). A successful screen will identify only those proteins from the library that interact with the bait protein. Although the yeast two-hybrid technology is one of several techniques designed to investigate protein interactions [Brent and Finley, 1997], it is exemplary, as it is a technology designed to identify novel interactions and to specifically investigate interactions within specific cell types [Brent and Finley, 1997]. The yeast two-hybrid technique is a lengthy investigation composed of many sequential stages, overviewed in Figure 18b.

5.2 Ascertainment of an adipocyte cDNA yeast two-hybrid library

An enhanced yeast two-hybrid system was used [James *et al.*, 1996] (Figure 18a). This system uses the yeast strain PJ69-4a, which is auxotrophic for four amino acids, uracil, leucine, histidine and adenine and, accordingly, requires these amino acids to be supplied in the media, or synthesised from an exogenous source. The absence of uracil and leucine is compensated for by the introduction of plasmids harbouring genes capable of synthesising these amino acids. Uracil is synthesised from the *URA3* gene on the plasmid pGBDUc1, which is the vector containing the Gal4 DBD (after which the bait gene is inserted) and leucine is synthesised by the *LEU2* gene on the plasmid pGADGH (Clontech. Palo Alto, USA), which contains the Gal4 activation domain

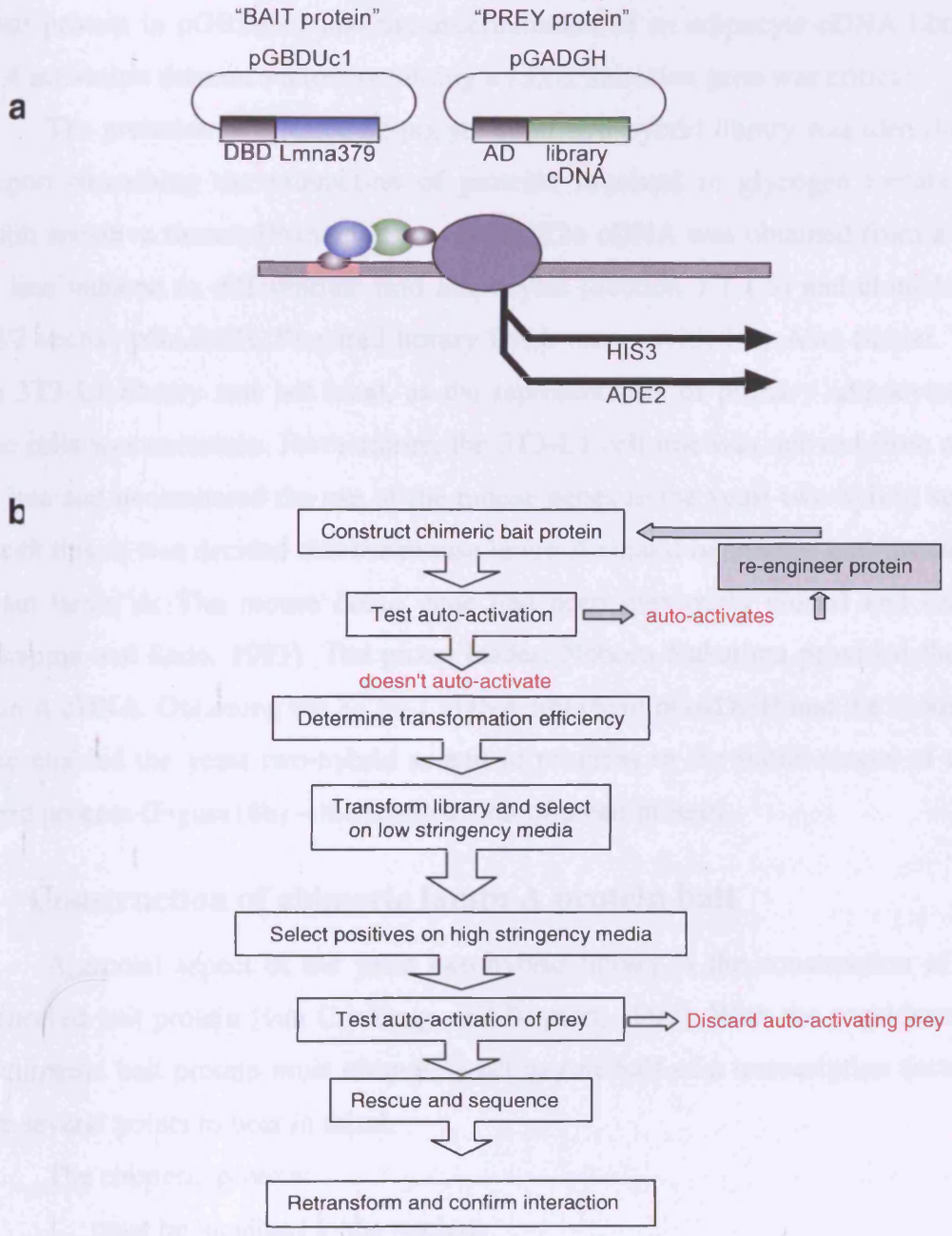

Figure 18. The yeast-two hybrid technique. (a) Schematic representation of the yeast two-hybrid process. The protein of interest 'bait' (blue box – in this case Lmna379-664) is cloned into a Gal4 DNA binding domain (DBD – grey box) vector and subsequently transformed into yeast. A library of transcripts from a desired cell type is cloned into a Gal4 activation domain (AD – green box) vector. All transcripts are transformed into the 'bait-containing yeast'. Those proteins which interact with the bait protein will result in the reconstitution of the Gal4 transcription factor (grey circles) and permit the binding of the protein complex at a Gal4 responsive element (red hatch) initiating transcription of the histidine (*HIS3*) and adenine (*ADE2*) genes. (b) Overview of the steps required in a yeast two-hybrid screen. A recognised drawback of the yeast two-hybrid technique is the autoactivation of a 'bait' protein (grey pathway).

(followed by a cloning site for inserting a library of transcripts). Construction of a lamin A bait protein in pGBDUc1 and the ascertainment of an adipocyte cDNA library in a Gal 4 activation domain vector containing a *LEU2* selection gene was critical.

The presence of a tested adipocyte yeast two-hybrid library was identified from a report describing the interaction of proteins involved in glycogen metabolism in insulin sensitive tissues [Printen *et al.*, 1997]. The cDNA was obtained from a 3T3-L1 cell line induced to differentiate into adipocytes (Section 1.1.1.5) and cloned into the *LEU2* vector, pGADGH. Prepared library DNA was provided by Alan Saltiel. The use of a 3T3-L1 library was not ideal, as the representation of primary adipocytes within these cells was uncertain. Furthermore, the 3T3-L1 cell line was derived from a murine cell line and necessitated the use of the mouse genes in the yeast two-hybrid screen. In light of this, it was decided that the mouse lamin A should be used as bait instead of the human lamin A. The mouse *Lmna* gene had been previously cloned and sequenced [Nakajima and Sado, 1993]. The group leader, Noboru Nakajima provided the mouse lamin A cDNA. Obtaining the 3T3-L1 cDNA library in pGADGH and the mouse *Lmna* clone enabled the yeast two-hybrid screen to progress to the initial stages of the two-hybrid process (Figure18b) – the construction of a bait protein.

5.3 Construction of chimeric lamin A protein bait

A crucial aspect of the yeast two-hybrid library is the construction of a well-engineered bait protein [van Criekinge and Beyaert, 1999]. With the consideration that the chimeric bait protein must ultimately act as one half of a transcription factor, there were several points to bear in mind.

The chimeric protein:

1. must be localised to the nucleus
2. must not be targeted elsewhere within the cell
3. must not be subjected to known proteolytic degradation
4. must not form complexes within the cell that would incorrectly localise the protein
5. must not require post-translational modifications critical for complex interactions, which occur in the true host organism, but not in the yeast host
6. must be soluble

With regard to the above, it was decided to modify the lamin A protein prior to fusion with the Gal4 DBD in pGBDUc1. Firstly, it was thought that as the lamin A

protein is localised to the nucleus by its nuclear localisation signal KKRK (417-420) [Fisher *et al.*, 1986; Nakajima and Sado, 1993] this would not inhibit nuclear localisation of the chimeric Gal4 DBD-lamin A protein but may, in fact, facilitate its correct localisation. Secondly, the inclusion of the CaaX proteolytic modification domain in lamin A was not thought likely to affect the chimeric protein. *Saccharomyces cerevisiae* are not known to possess nuclear lamins [Wilson, 2000] and, therefore, the enzymes involved in the CaaX box removal would not be present, permitting retention of the entire lamin A protein. Even in the event of proteolytic removal, only 18 residues would be removed which would have a limited, if any, effect on the two-hybrid screen.

The dimerisation ability of lamin A would presumably have a negative effect on the production of a sound transcription factor. Although yeast are devoid of lamins the chimeric protein consisting of the Gal4 DBD and the lamin A protein (residues 1-665 in mouse) could possibly interact with itself and form a dysfunctional transcription factor dimer with altered conformation that may not perform correctly at reporter loci. Protein dimerisation of this nature could impair binding at the Gal4 responsive element in the promoters of reporter genes. Furthermore, this hypothetical dimerisation could ultimately lead to polymerisation of these molecules into larger supramolecular structures, causing protein precipitates. This was considered a distinct possibility given the ability of lamin A to easily form paracrystalline structures *in vitro* [Moir *et al.*, 1991; Stuurman *et al.*, 1998]. On the basis of previous investigations, the dimerisation and polymerisation ability is most likely mediated by the α-helical rod domain (residues 1-379/389) [Heitlinger *et al.*, 1991; Moir *et al.*, 1991]. Hence, it was decided that removal of this section of lamin A would produce a more suitable protein. The C-terminal tail domain of lamin A, residues 379 to 665 was amplified and inserted in-frame after the Gal4 DBD in pGBDUc1. The omission of the α-helical domain was considered unlikely to affect the validity of the screen in the search for lamin A interacting proteins. This was because the NLS was retained in the C-terminal domain and the hypothesis was that an adipocyte specific protein would interact specifically with the tail domain of lamin A, as this was the site of FPLD mutations (residues 465, 482, 486, 582 and 584).

The Gal4-Lmna379 bait protein (hereafter referred to as Lmna379) was cloned as described in Table 3 and prepared from *E. coli*. The purified DNA plasmid was termed pGB-Lmna379 and used to transform the yeast strain PJ69-4a. The maintenance

of this plasmid was achieved by growing yeast on media deficient in uracil, upon which only yeast containing the plasmid (and thus the *URA3* gene) could survive.

Before the transformation of this strain with the adipocyte cDNA library several 'quality-controls' were performed to determine that the bait protein was a suitable target for interacting proteins in the yeast-two hybrid screen (Figure 18b). These consisted of checking that the bait protein was expressed in the yeast cell and did not auto-activate reporter genes.

5.4 Lamin A as a suitable bait: verification

Auto-activation is a phenomenon in the yeast two-hybrid screen that can often result in the premature termination of a screen. Its definition is the activation of reporter gene (in PJ69-4a this is histidine and adenine) by the chimeric bait protein in the absence of an interacting partner. The Gal4 DBD operates correctly, but the cloned gene under investigation harbours motifs that do not search for interacting proteins to help the survival of the selected yeast cell but instead directly recruit RNA polymerase to the promoters of the reporter genes. In these cases, simple transformation of the chimeric bait protein is sufficient to trigger the reporter genes and the selective reporters are rendered obsolete, as concerns the subsequent transformation of interacting proteins from a library of transcripts. Features of proteins that can cause auto-activation are known to include regions of acidic residues or stretches of highly charged amino acids capable of forming a multitude of complexes with other cellular proteins [van Criekinge and Beyaert, 1999]. Generally, transcription factors which already possess acidic activation domains are more likely to activate transcription when fused to the Gal4 DBD and, thus, result in poor chimeric bait proteins.

The yeast two-hybrid system generated by James and co-workers [James *et al.*, 1996] consists of two selective reporter genes, histidine and adenine. The use of adenine as a reporter gene was unique and had been generated for its superiority over the histidine reporter. Histidine, the classical yeast two-hybrid reporter is described as a 'leaky' reporter. Transcription initiated from the Gal4-histidine promoter is constantly activated, albeit at low basal levels. With the introduction of a chimeric Gal4 binding protein this basal level of transcription would rise dependent on the nature of the chimeric bait protein. Consequently, this allows the reporter to be activated and low levels of histidine to be produced which, in turn, permits the yeast cell to partially survive on media deficient in histidine. The chemical 3-aminotriazole (3-AT) inhibits

the histidine gene product and low levels of 3-AT are sufficient to eliminate the background 'leaky' transcription of histidine. However, high levels of 3-AT are deleterious and either overcome weak interactions identified in the yeast two-hybrid screen, or alternatively kill the yeast. Thus, it is important to determine the level of 3-AT that is just sufficient to suppress auto-activation. As mentioned above, the adenine reporter is not affected by high basal levels of transcription and no 'fine-tuning' with 3-AT or other chemicals is necessary.

To determine if Lmna379 caused auto-activation, the second vector, pGADGH (without a cDNA insert) was also transformed into PJ69-4a (already harbouring pGB-Lmna379). This was done to test for direct auto-activation of the bait protein Lmna379 and also to test that the bait protein didn't interact with the Gal4 activation domain and result in activation of the reporter genes. Several combinations of media deficient in histidine and adenine were made. In each set of media the amino acids uracil and leucine were omitted to maintain the two plasmids (pGBDUc1 and pGADGH). In addition to this, histidine was omitted and different plates were made with increasing levels of 3-AT (1 mM to 25 mM). A diluted yeast culture was spread on these plates and left to grow for several days. It was determined that levels of 3-AT less than 10 mM permitted growth, whereas 15 mM 3-AT suppressed all growth. It was concluded that a level of 10 mM 3-AT was sufficient to reduce background histidine product without over-suppressing weak interactions. However, the use of histidine and its presumed leaky transcription was also considered to be beneficial in the initial stages of the yeast two-hybrid screen as it would permit the detection of weakly interacting proteins [James, 1996 #238; P. James, *pers comm*]. Thus, the use of media deficient in uracil, leucine and histidine, supplemented with 10 mM 3-AT would be suitable selective agents in the initial library screen. The use of the more stringent adenine reporter would eventually be useful in the determination of true positive interacting proteins from the initial library screen. Therefore the auto-activation of Lmna379 on the adenine reporter was also investigated. PJ69-4a containing pGB-Lmna379 and pGADGH was plated onto media deficient in uracil, leucine, histidine and adenine and also supplemented with 10 mM 3-AT. After an incubation period of two weeks, with the apparent absence of growth, it was concluded that neither the adenine or histidine reporter genes could be auto-activated by Lmna379.

In addition to these tests, it was also necessary to check that Lmna379 was expressed in the yeast cells. Western blot analyses using a cross-species lamin A

antibody were performed on protein samples from liquid yeast cultures believed to express Lmna379. No chimeric proteins were identified by western blot leading to three possibilities: first, the protein was not expressed, second, the antibody epitope was compromised, or protein expression was at too low a level to be detected by western blot. The last explanation is supported by the fact that pGB-Lmna379 contains a truncated alcohol dehydrogenase promoter (ADH1). Full length ADH1 is 1500 bp in length and leads to high level expression of sequences under its control [van Criekinge and Beyaert, 1999]. A truncated ADH1 promoter has, since, been engineered (only 410 bp in length cf. 1500 bp) and results in low levels of gene expression. This has the advantage of increasing stringency in the yeast two-hybrid screen by providing just sufficient protein for the selective interaction. A clear disadvantage is the low levels of protein produced that are, sometimes, undetectable on western blot [van Criekinge and Beyaert, 1999]. In order to circumvent this obstacle of low protein expression, the chimeric protein, Gal4 DBD fused to lamin A (residues 379-665), was sub-cloned into an expression vector containing a T7 promoter. T7 promoters can be exploited using a commercial kit, the transcription and translation expression system (TNT® kit). A vector containing a complete cDNA sequence positioned downstream of the T7 promoter may be used to generate protein by performing an *in vitro* transcription and translation (IVT). This vector is incubated with the TNT® kit and supplemented with [^{35}S] methionine. Any protein generated during this incubation period will have [^{35}S] methionine incorporated. PAGE analysis and autoradiography will identify those proteins which are successfully expressed. In this case, the Gal4 DBD fused to Lmna 379-665 was cloned into the T7 expression vector pBS-SK (Table 4). PAGE and autoradiography revealed two protein bands, of approximate size 47-48 kDa and 37-39 kDa. Computerised analysis of the chimeric gene sequence (Gal4 DBD and Lmna379) predicted a molecular weight of 48 kDa. The larger of the two bands was considered to be the correctly expressed chimeric protein and the second, lower band either a degradation product or a transcript derived from a later methionine initiation codon. To investigate the second possibility, the chimeric protein sequence was analysed for internal methionines. Several were identified, one methionine codon (ATG) in particular was found to localise within a highly conserved Kozak consensus sequence [Kozak, 1984]. The predicted size of the protein, derived from this translational start site, was deduced using computerised analyses and estimated to be 39 kDa. It was, thus, concluded that the smaller band was a result of the later initiation methionine.

Although it was not directly proven that the chimeric bait gene was expressed in the yeast endogenously, it was demonstrated that the plasmid pGB-Lmna379 does generate a protein of the correct molecular size. Hence, it is likely that Lmna379 was produced in the yeast PJ69-4a, albeit at extremely low levels that, nonetheless, would be sufficient for a successful yeast two-hybrid screen.

5.5 Optimisation of transformation efficiency

The lithium acetate transformation method is considered a robust and efficient technique for the sequential transformation of library plasmid in the yeast two-hybrid system [Agatep *et al.*, 1998; van Criekinge and Beyaert, 1999]. Typically 1×10^5 transformants are obtained per microgram of plasmid DNA used, but this can vary significantly depending on several factors that include: the quality of DNA, the size of the plasmid, the strain of yeast, the growth stage of the yeast and quality of materials used in the transformation process. The aim of the yeast two-hybrid screen is to test the interaction capacity of every transcript in the library with the bait protein. The 3T3-L1 adipocyte cDNA library was predicted to be composed of 1×10^6 different transcripts all cloned into pGADGH [S. Chiang, *pers comm*]. It was advised that the most desirable number of transformants to screen was six times the complexity of the library [D. Gietz, *pers comm*], a total of 6×10^6 transformants. To obtain this number the transformation of PJ69-4a was optimised using varying amounts of library plasmid DNA. Transformation of small amounts of DNA result in higher transformation efficiencies compared to when larger amounts of DNA are utilised. Although transformation efficiency is higher when using small amounts of DNA, a lower number of transformants are generated overall.

Only 100 μg of 3T3-L1 adipocyte cDNA was provided and it was critical to optimise the transformation efficiency in order to obtain 6×10^6 transformants. To this end, pilot transformations were performed using the yeast PJ69-4a (already harbouring pGB-Lmna379) with varying amounts of library DNA to establish the optimal level of transformation (Figure 19). Using these calculated transformation efficiencies the exact amount of library DNA required was calculated at 60 μg (Appendix III).

In summary, the normal transformation procedure was scaled up sixty times using 60 μg of 3T3-L1 adipocyte DNA in order to attain a total of 6×10^6 transformants.

A graph demonstrating the increase in total transformants in the yeast strain PJ69-4a using increasing amounts of plasmid DNA

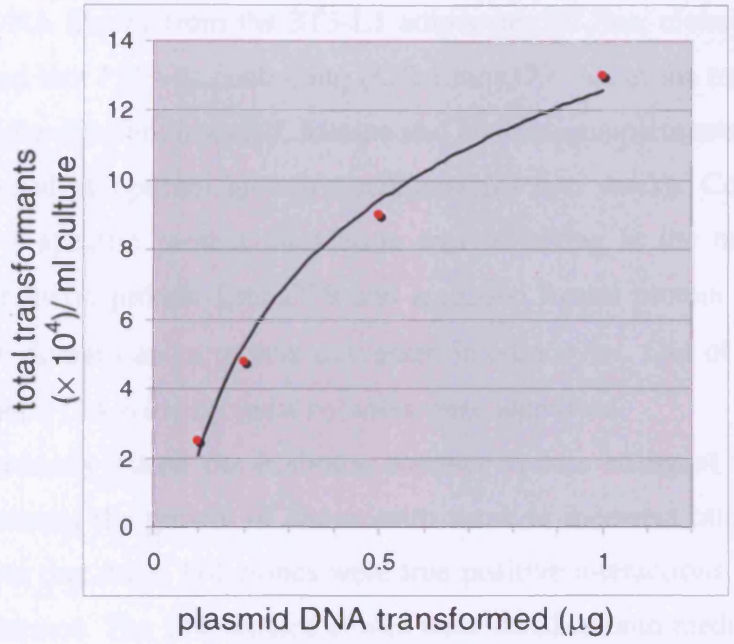

A graph demostrating the decrease in transformation efficiency in the yeast strain PJ69-4a using increasing amounts of plasmid DNA

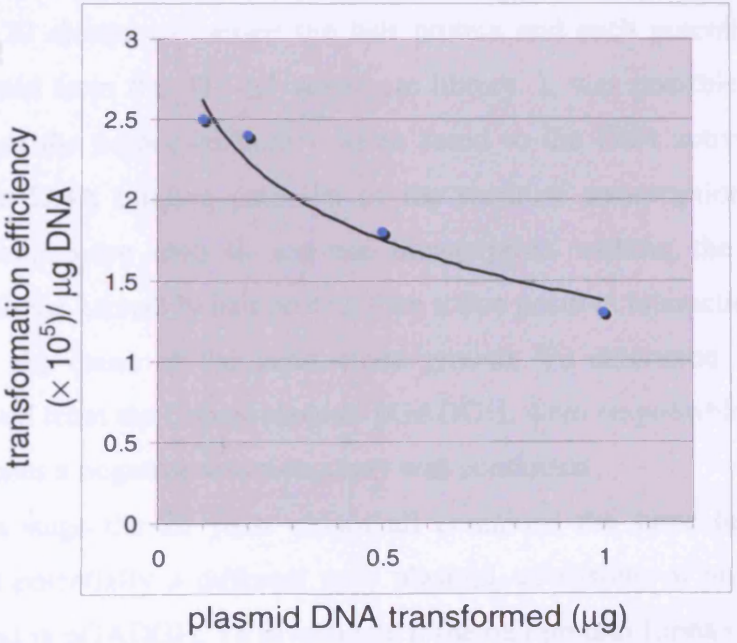

Figure 19. Optimisation of library plasmid transformation in PJ69-4a. Upper graph demonstrates the overall increase in total transformants with increasing amounts of 3T3-L1 adipocyte library DNA. Lower graph illustrates that a higher transformation efficiency is achieved using lower amounts of 3T3-L1 plasmid DNA.

5.6 Library transformation and functional analysis of positive clones

The cDNA library from the 3T3-L1 adipocyte cell line, cloned into pGADGH, was transformed into PJ69-4a containing pGB-Lmna379. All of the transformants were plated onto media deficient in uracil, leucine and histidine supplemented with 10 mM 3-AT and incubated at optimal growth conditions for two weeks. Colonies that grew indicated that a specific protein interaction was occurring at the histidine promoter between the chimeric protein Lmna379 and a second fusion protein composed of the Gal4 activation domain and a protein expressed in adipocytes. Out of an estimated 6×10^6 transformants, 114 growing yeast colonies were identified.

As previously stated the histidine reporter is less stringent than the adenine reporter and permits the growth of clones with weak or incorrect interactions (Section 5.4). To confirm that these 114 clones were true positive interactions a second reporter assay was performed. The 114 isolated clones were streaked onto media identical to that used in the initial library selection but, additionally, deficient in adenine. This subsequent selective measure identified 20 positive clones, with potentially strong interactions, from the initial 114 (Figure 20).

These 20 clones all carried the bait protein and each potentially harboured a different plasmid from the 3T3-L1 adipocyte library. It was possible that the random transcripts from the adipocyte library when fused to the Gal4 activation domain re-established the DNA binding potential of the modular transcription factor. If these chimeric proteins were able to activate transcription without the requirement for interaction with the Lmna379 bait protein then a true positive interaction with Lmna379 would not be the cause of the yeast clone growth. To determine if these chimeric proteins, derived from the library plasmid pGADGH, were responsible for activation of the reporter genes a negative selection assay was conducted.

At this stage the 20 yeast clones all contained the same bait plasmid pGB-Lmna379 and potentially a different prey plasmid, consisting of an unknown cDNA insert contained in pGADGH. To investigate if the bait protein Lmna379 was crucial for the interaction, it was selectively lost from the yeast clones. The resulting yeast, with only library plasmid pGADGH, would be exposed to media selection for positive interactions (media lacking histidine and adenine).

Figure 20. Authentication of positive interacting clones. (a) The 114 yeast clones that grew on media deficient in uracil, leucine and histidine (supplemented with 3-AT) were streaked onto identical media additionally deficient in adenine. Colony growth indicates the 20 positives competent in strong activation of the reporter genes. (b) The 20 positives clones identified in a) were re-plated onto similar media to confirm their candidacy as *bona fide* positive interactors.

The plasmid pGB-Lmna379 was auxotrophically maintained by plating onto media lacking uracil, as this plasmid harbours the *URA3* gene. Other investigations have revealed the *URA3* gene can be selected against. In addition to its role in uracil synthesis it can also alter the chemical 5-fluoro-orotic acid (5-FOA) to a lethal substance [Boeke *et al.*, 1987]. The 20 yeast clones were grown for several generations in liquid media lacking leucine only (to specifically select for the library plasmid) and supplemented with uracil (to allow the loss of pGB-Lmna379). Subsequently, the yeast were plated onto media lacking leucine but supplemented with uracil and 5-FOA. All 20 yeast clones grew on this media and, thus, each colony was believed to harbour the library plasmid only. To determine if the chimeric protein derived from this plasmid was capable of auto-activation, yeast colonies were streaked onto media lacking leucine, histidine and adenine. No yeast colonies grew and it was concluded that the maintenance of these 20 clones was dependent on a genuine interaction between the bait and prey proteins to permit growth on selective media.

5.7 Sequence identification of interacting clones

The identification of twenty positive clones, whose interaction properties had been confirmed prompted the sequence analysis of the adipocyte cDNA inserts. This was achieved using a technique known as plasmid rescue, involving obtaining small amounts of plasmid from the yeast strain and the subsequent transformation of these plasmids into competent bacteria. After this the DNA can be easily analysed and manipulated. The majority of the 20 plasmids were introduced into bacteria (plasmids from yeast clones Y2H24 and Y2H85 were not rescued using this technique). To confirm that the correct plasmids were obtained by the plasmid rescue procedure a plasmid digest was performed using a frequent cutting restriction enzyme. All 18 plasmids were digested with *Taq*I and the digests electrophoresed on an agarose gel (Figure 21a). Bands of identical size were common in all digests and indicated the presence of the vector DNA. Different banding patterns were observed for those with different inserts. Interestingly, similar banding patterns were noted in a proportion of the samples, suggesting that these vectors had the same, or related, inserts.

Sequencing primers were designed to pGADGH that flanked the cloning sites and were directed into the cDNA insert (Figure 21b). The first primer (ADF), designed to the Gal4 activation domain on the sense DNA strand, was anticipated to produce the coding strand sequence of the cDNA insert. The second primer (T7) was designed to a

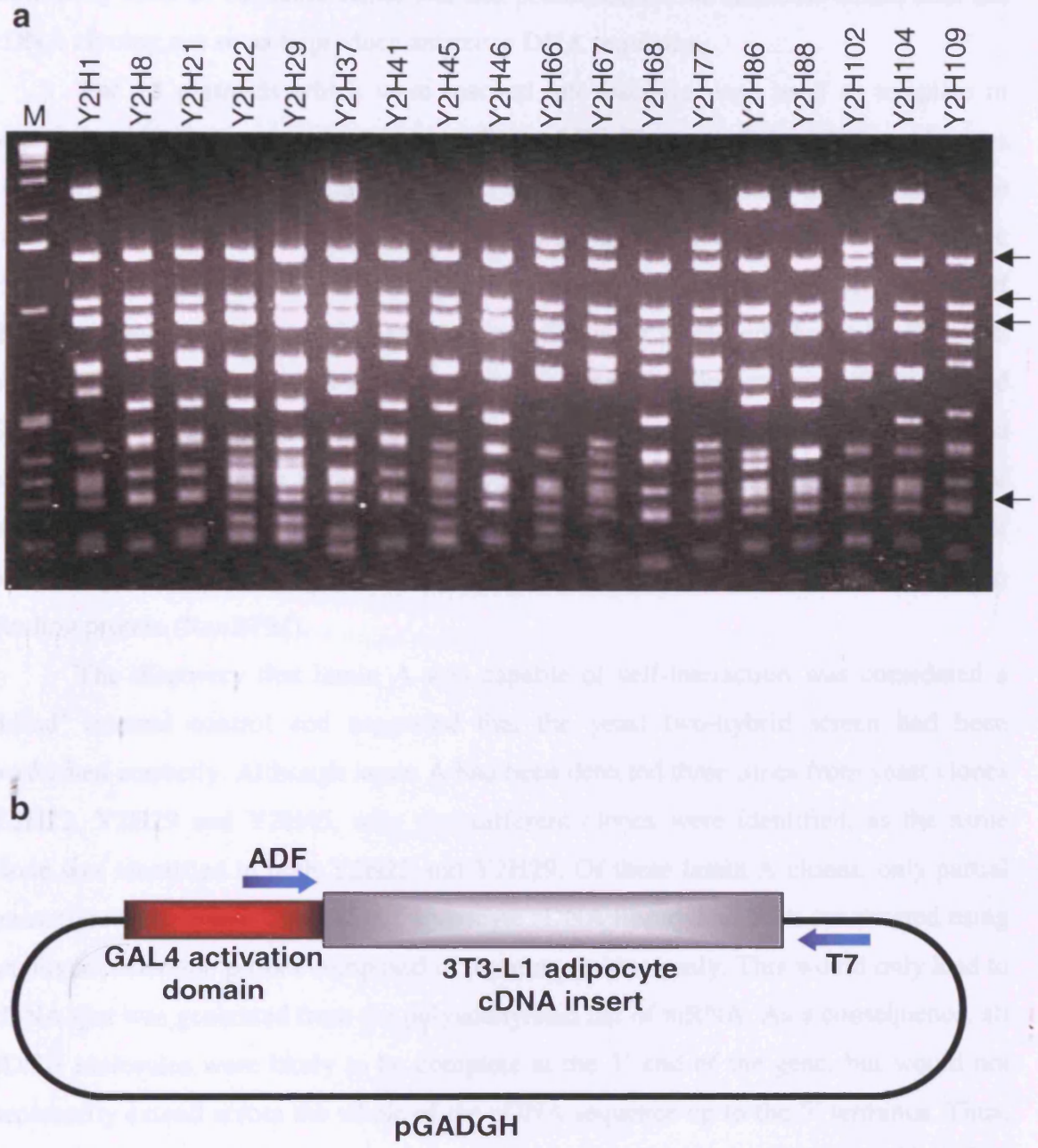

Figure 21. Insert characterisation of the yeast two-hybrid clones. (a) Eighteen of the twenty positive lamin A interacting clones were digested using the frequent-cleaving enzyme *Taq*I, and electrophoresed on a 1.0% agarose gel resulting in a fingerprint for each vector (M – marker). Vector bands common to all digests were identified (arrows) and many digest patterns were recognised several times (e.g. Y2H1, 37, 46, 86, 88 and 104) indicating the presence of identical inserts. (b) Diagram of the 'prey' vector, pGADGH. Red box identifies the Gal4 activation domain and the large grey box represents the unknown cDNA insert. The inserts were initially sequencing using the ADF and T7 primers (blue arrows).

commonly used T7 sequence donor site and positioned on the antisense strand after the cDNA cloning site so as to produce antisense DNA sequence.

The 18 plasmids which were rescued into bacteria were used as template in sequencing reactions using the primers ADF and T7. Thirteen of the 18 plasmids were successfully sequenced using both primers. Typically, 400-600 bases of DNA sequence were obtained. The identified DNA sequence was, subsequently, used in bioinformatic BLAST searches [Altschul *et al.*, 1990] to determine the identity of the cDNA insert. Of the 13 clones, four classes of interacting proteins were identified (Table 8). The first class was composed of seven sterol regulatory element-binding proteins (SREBP1 and SREBP2). The second class contained three lamin A proteins. The third class consisted of two cDNA sequences which had no significant homology to any known DNA or protein sequences in the databases and were determined to be novel. The final class of interacting proteins was composed of one protein only, which had homology to Ran binding protein (RanBPM).

The discovery that lamin A was capable of self-interaction was considered a 'blind' internal control and suggested that the yeast two-hybrid screen had been performed correctly. Although lamin A had been detected three times from yeast clones Y2H22, Y2H29 and Y2H45, only two different clones were identified, as the same clone was identified in both Y2H22 and Y2H29. Of these lamin A clones, only partial transcripts were found. The 3T3-L1 adipocyte cDNA library had been constructed using an oligoncucleotide primer composed of thymine residues only. This would only lead to cDNA that was generated from the polyadenylated tail of mRNA. As a consequence, all cDNA molecules were likely to be complete at the 3' end of the gene, but would not necessarily extend across the whole of the cDNA sequence up to the 5' terminus. Thus, it was feasible that cDNA inserts, truncated before the 5' end, would be identified. The sequence of the two lamin A clones was identical at the 3' end of the insert but differed, in length of sequence, at the 5' end. Using BLAST searches it was established that the first lamin A clone (Y2H22 and Y2H29) contained amino acids 288 to the poly-A tail and the second clone (Y2H45) contained amino acids 253 to the poly-A tail. It was concluded that a region in lamin between residues 288 and 665 was responsible for self-interaction with the globular tail domain of lamin A (residues 379-665).

The interaction between lamin A and RanBPM suggested a role for the lamina in the nuclear trafficking of macromolecules across the nuclear membrane. RanBPM had previously been shown to interact with Ran [Nakamura *et al.*, 1998]. Ran function is

Clone	Insert
Y2H1	SREBP1 residue 126-end
Y2H8	No sequence
Y2H21	No sequence
Y2H22	Lamin A residue 288-end
Y2H24	Unable to rescue
Y2H29	Lamin A residue 288-end
Y2H37	SREBP1 residue 135-end
Y2H41	No sequence
Y2H45	Lamin A residue 253-end
Y2H46	SREBP1 residue 227-end
Y2H66	RanBPM
Y2H67	Novel gene
Y2H68	No sequence
Y2H77	Novel gene
Y2H85	Unable to rescue
Y2H86	SREBP1 residue 80-end
Y2H88	SREBP1 residue 60-end
Y2H102	SREBP2 residue 5-end
Y2H104	SREBP1 residue 227-end
Y2H109	No sequence

Table 8. Sequence identification of the twenty yeast two-hybrid positive clones. Each clone was numbered when isolated from the initial yeast two-hybrid screen (114 positives in total). Those that also activated the *ADE2* reporter gene are listed above. Determination of the insert was achieved using BLAST database searches with the ADF and T7 generated sequence.

associated with nuclear translocation [Vasu and Forbes, 2001]. Although Ran is localised to the nucleus, RanBPM was positioned in the centrosome [Nakamura *et al.*, 1998]. The subcellular localisation of RanBPM did not suggest that it was capable of binding lamin A and, hence, it was considered a false positive.

The seven SREBP clones consisted of 6 SREBP1 clones and a single SREBP2 clone. SREBP1 and SREBP2 are both transcription factors that have been extensively studied (Section 1.1.3.3). Initially identified as genes capable of directing cholesterol biosynthesis, they have been subsequently implicated in adipogenesis. Furthermore, transgenic mice containing transcriptionally active SREBP1c have been developed resulting in a murine model of lipodystrophy (Section 1.2.4) [Shimomura *et al.*, 1998]. In light of this information, it was of significant biological interest that this protein had been identified as an interacting partner of lamin A. Hence, the characterisation of this particular interaction was considered pivotal towards elucidation of the molecular mechanism of FPLD.

5.8 Functional analysis of the lamin A and SREBP interaction

The seven SREBP clones were sequenced in their entirety using a progressive set of nested sequencing primers. This sequencing was performed for three reasons. Firstly, the whole cDNA sequences for the murine orthologues of the SREBP genes had not been previously characterised as no reference of these sequences were found in the literature or on the publicly available databases (www.ncbi.nlm.nih.gov). Secondly, it was necessary to find which part of the SREBP protein interacted with lamin A (as determined by defining the site of truncation of the cDNA sequence). Finally, it was necessary to check that the clones were not composed of chimeric or deleted genes.

The complete sequencing of the Y2H102 clone revealed the cDNA sequence of mouse SREBP2. Almost the entire cDNA coding sequence was obtained and it was predicted that only the first four amino acids of the protein would be absent from the chimeric protein. The other six clones were all identified as SREBP1. Five different library clones were identified, the 5' end of the cDNA sequence was absent in all and, thus, it was predicted that the proteins would lack the N-terminal domain of the SREBP1 protein. The shortest of these clones was Y2H104 and corresponded to SREBP1 amino acids 220 to 1129. This suggested that the site responsible for interaction with lamin A was between these residues in all of the proteins identified in the screen. The comparison of these six truncated proteins with the predicted full-length

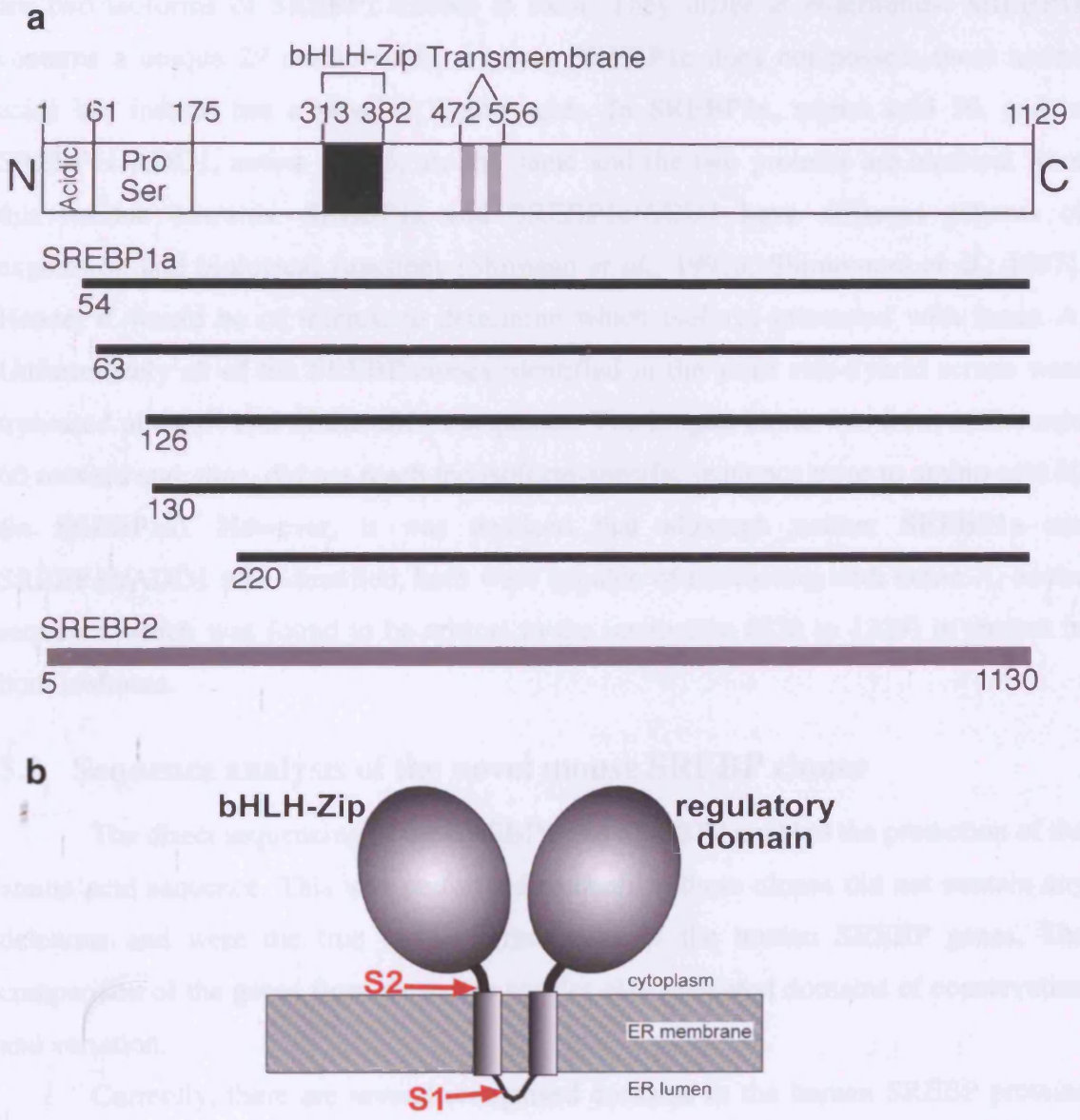

Figure 22. Mouse SREBP clones identified in the yeast two-hybrid screen. (a) Full length SREBP1a, annotated with the residues which demarcate specific domains. SREBP1a contains an acidic and proline/serine rich domain at the N-terminus. A bHLH-Zip is also present (black box) followed by two transmembrane domains (grey boxes). Six SREBP clones were identified in the yeast two-hybrid screen and all were truncated at the 5' terminus (clone 220 was isolated twice). SREBP2 was identified once (horizontal grey line) with only 4 amino acids absent from the 5' end. (b) Model of SREBP in the membrane of the endoplasmic reticulum. The two larger domains of SREBP reside within the cytoplasm of the cell, whereas the small domain between the two transmembrane domains projects into the ER lumen. Upon activation, SREBP is cleaved at site 1 and site 2 (red numerals) and the bHLH domain translocates to the nucleus.

protein is diagrammatically represented in Figure 22a. SREBP1a and SREBP1c/ADD1 are two isoforms of SREBP1 known to exist. They differ at N-terminus; SREBP1a contains a unique 29 amino acids, whereas SREBP1c does not possess these amino acids but instead has a novel 5 amino acids. In SREBP1a, amino acid 30, and in SREBP1c/ADD1, amino acid 6, are the same and the two proteins are identical from this residue onwards. SREBP1a and SREBP1c/ADD1 have different patterns of expression and biological functions [Shimano *et al.*, 1997a; Shimomura *et al.*, 1997]. Hence, it would be of interest to determine which isoform interacted with lamin A. Unfortunately all of the SREBP clones identified in the yeast two-hybrid screen were truncated at the 5' end of the cDNA sequence. The longest clone was from amino acid 60 onward and, thus, did not reach the isoform-specific sequence prior to amino acid 30 (in SREBP1a). However, it was deduced that although neither SREBP1a nor SREBP1c/ADD1 was identified, both were capable of interacting with lamin A, as the sequence which was found to be critical in the interaction (220 to 1129) is present in both isoforms.

5.9 Sequence analysis of the novel mouse SREBP clones

The direct sequencing of the SREBP1 and SREBP2 enabled the prediction of the amino acid sequence. This was performed to confirm these clones did not contain any deletions and were the true mouse orthologues of the human SREBP genes. The comparison of the genes from these two species also indicated domains of conservation and variation.

Currently, there are several recognised domains in the human SREBP proteins that are known to confer certain properties (Figure 22a) [Sato *et al.*, 1994]. The SREBP proteins are tripartite in structure and are bound to membranes of the endoplasmic reticulum (ER) in a hairpin orientation (Figure 22b). The N-terminal domain, of approximately 480 amino acids, contains a basic helix-loop-helix leucine zipper (bHLH-Zip) transcription factor domain. This is followed by a transmembrane segment, a short loop of approximately 30 amino acids which projects into the ER lumen, and then by a second transmembrane domain. The C-terminal cytoplasmic projection consists of approximately 590 amino acids and is involved in the binding of a regulatory protein known as SREBP cleavage activation protein (SCAP) [Brown and Goldstein, 1997]. SCAP initiates a sequential two-step cleavage of the SREBP proteins at two specific sites by site-1-protease (S1P) and site-2-protease (S2P) [Brown and Goldstein,

1999]. The result of this cleavage is the release of an active N-terminal transcription factor, that translocates to the nucleus and activates transcription of genes involved in cholesterol and fatty acid biosysthesis and more interestingly, adipogenesis [Tontonoz *et al.*, 1993; Yokoyama *et al.*, 1993].

The amino acid sequence of mouse SREBP1 (this study) was compared to human SREBP1 [Yokoyama *et al.*, 1993] using a computational algorithm [Thompson *et al.*, 1994] and is illustrated in Figure 23 and Figure 25a. This was also performed for SREBP2 [Hua *et al.*, 1993] (Figure 24 and Figure 25b). The bHLH-Zip domains are highly conserved in both SREBP proteins and the critical residues, as previously defined [Hua *et al.*, 1993; Tontonoz *et al.*, 1993; Yokoyama *et al.*, 1993], are completely conserved in both SREBP1 and SREBP2. These include the consensus sequence of the bHLH, the leucine residues of the leucine zipper and the tyrosine (at residue 325 in human SREBP1a and 342 in human SREBP2), critical in the recognition of two regulatory elements in promoters of genes under the transcriptional regulation of SREBP [Kim *et al.*, 1995]. The transmembrane domains are highly conserved in SREBP2 but in SREBP1 the amino acids are less conserved, although they do retain hydrophobic properties. The two motifs which are cleaved by the two proteases (RSVL for S1P [Duncan *et al.*, 1997], DRSR and NP for S2P [Hua, 1996 #353; Ye, 2000 #20] are both conserved. The acidic domains at the extreme N-terminus of the SREBP proteins are highly conserved (to a lesser degree in SREBP1a), thus, indicating that their roles in transcriptional activation are of importance. The adjacent proline and serine domains are the least conserved domains in the proteins. It was suggested that this region could be involved in binding of other transcriptional co-activators [Brown and Goldstein, 1999]; however, given the low degree of conservation in both SREBP1 and SREBP2, this function may not be as critical as initially thought.

SREBP1 and SREBP2 are very similar and possess the same domains. The distinguishing feature of SREBP2 is the presence of a glutamine rich region proximal to the bHLH domain, which is absent in SREBP1. This glutamine rich domain is also considered to be involved in binding transcriptional co-activators [Hua *et al.*, 1993]. The high, almost identical (98%), conservation between mouse and human SREBP2 proteins in this segment suggests this domain is of strong functional significance. The glutamine rich region is postulated to confer different properties to SREBP2 [Hua *et al.*, 1993]. Intriguingly, SREBP2 is more highly conserved than SREBP1 (91% and 79%

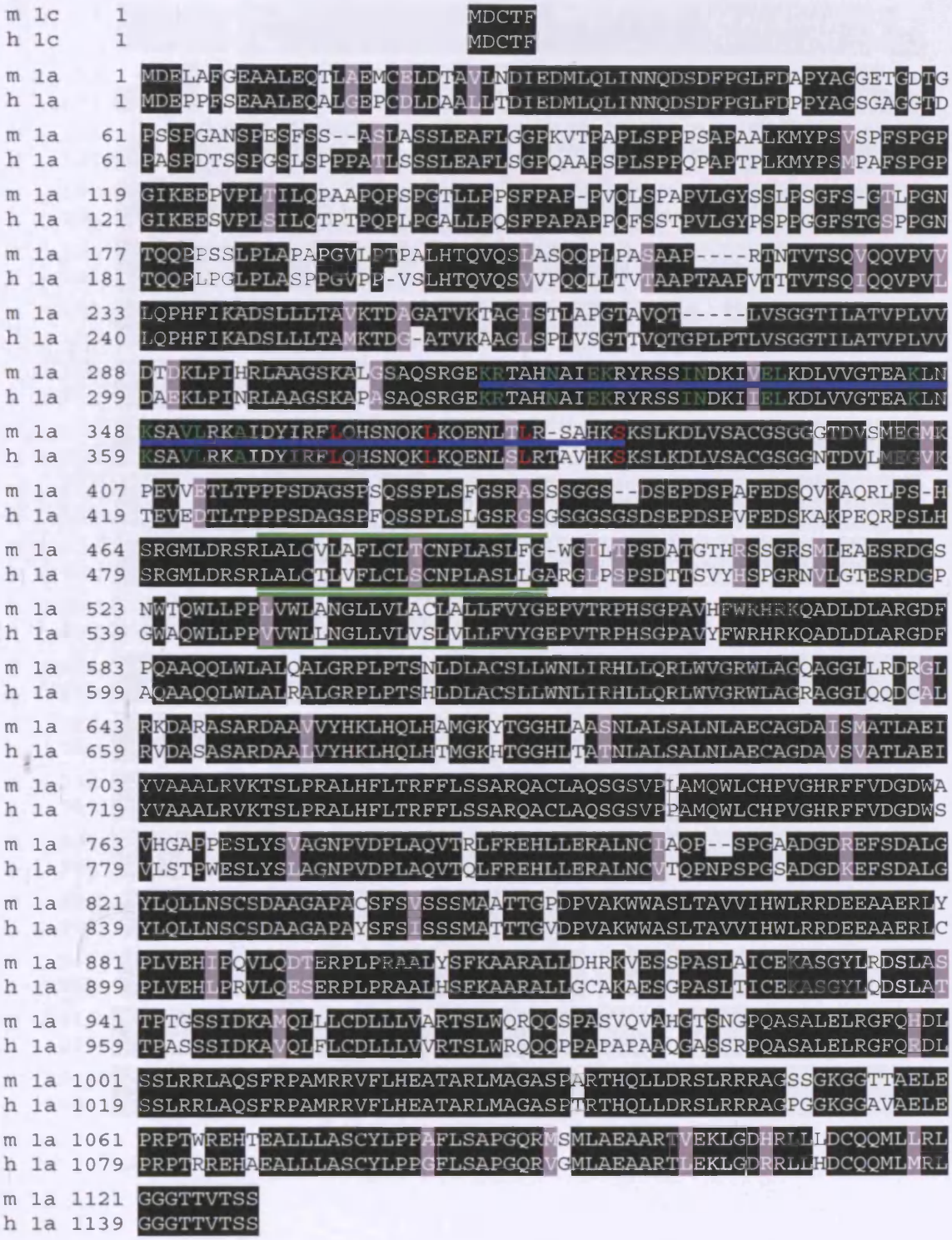

Figure 23. SREBP1 amino acid comparison. Deduced mouse (m) and human (h) SREBP1a/1c amino acid sequences are aligned using Clustal W [Thompson *et al.*, 1994]. Amino acids are written in single letter code (Appendix IV), and the relative residue position at the start of each line. Identical amino acids are indicated by black boxes and amino acids of similar function by grey boxes. The basic helix-loop-helix domain is shown by the blue line and critical residues coloured (green for the bHLH consensus and red for the leucine residues in the leucine zipper consensus). The two transmembrane domains are shown by the green boxes.

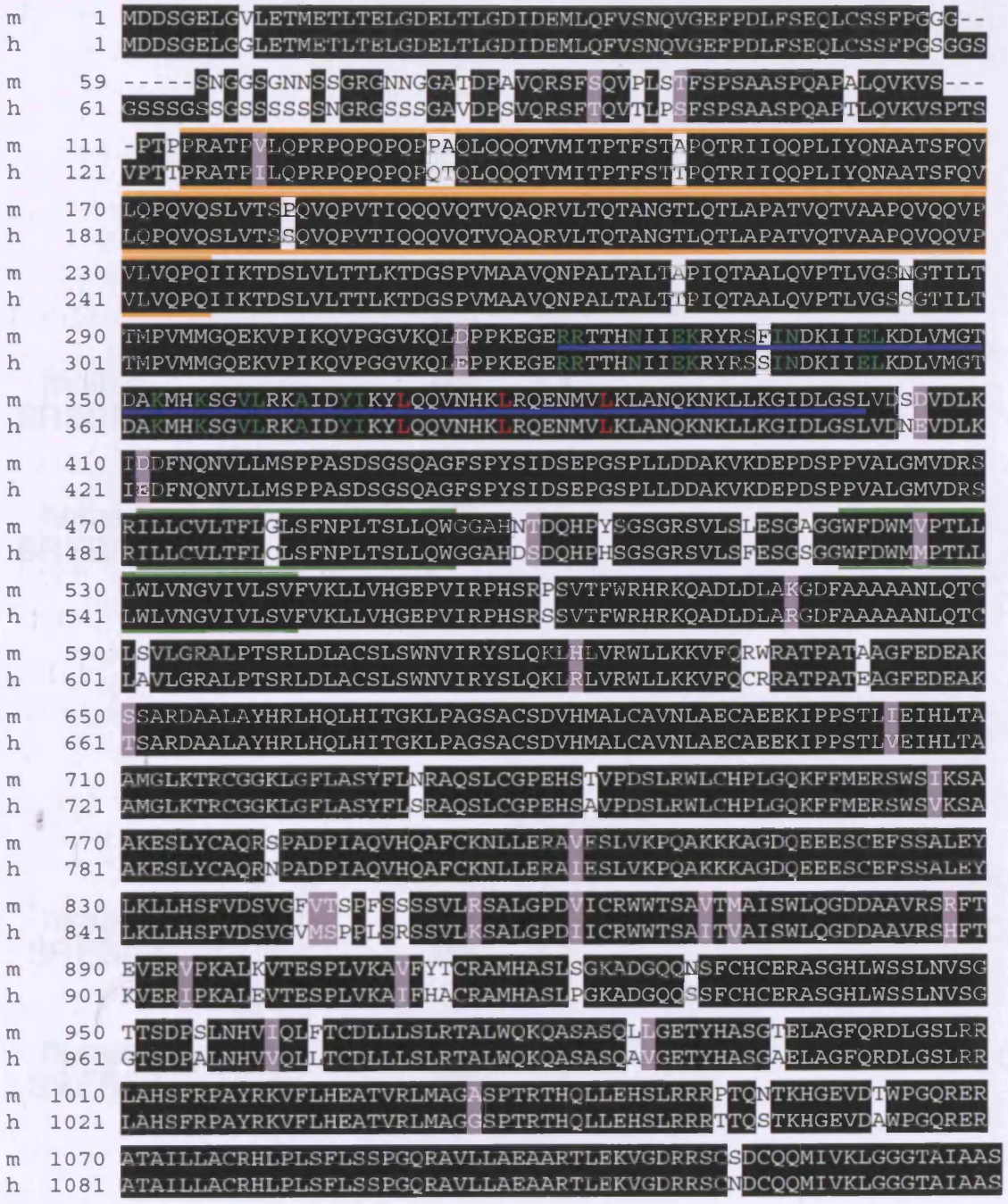

Figure 24. SREBP2 amino acid comparison. Deduced mouse (m) and human (h) SREBP2 amino acid sequences are aligned using Clustal W [Thompson *et al.*, 1994]. Amino acids are written in single letter code (Appendix IV) with the relative residue position at the start of each line. Identical amino acids are indicated by black boxes and amino acids of similar function by grey boxes. The glutamine rich domain is demarcated by the orange box. The basic helix-loop-helix domain is shown by the blue line and critical residues coloured (green for the bHLH consensus and red for the leucine residues in the leucine zipper consensus). The two transmembrane domains are shown by the green boxes.

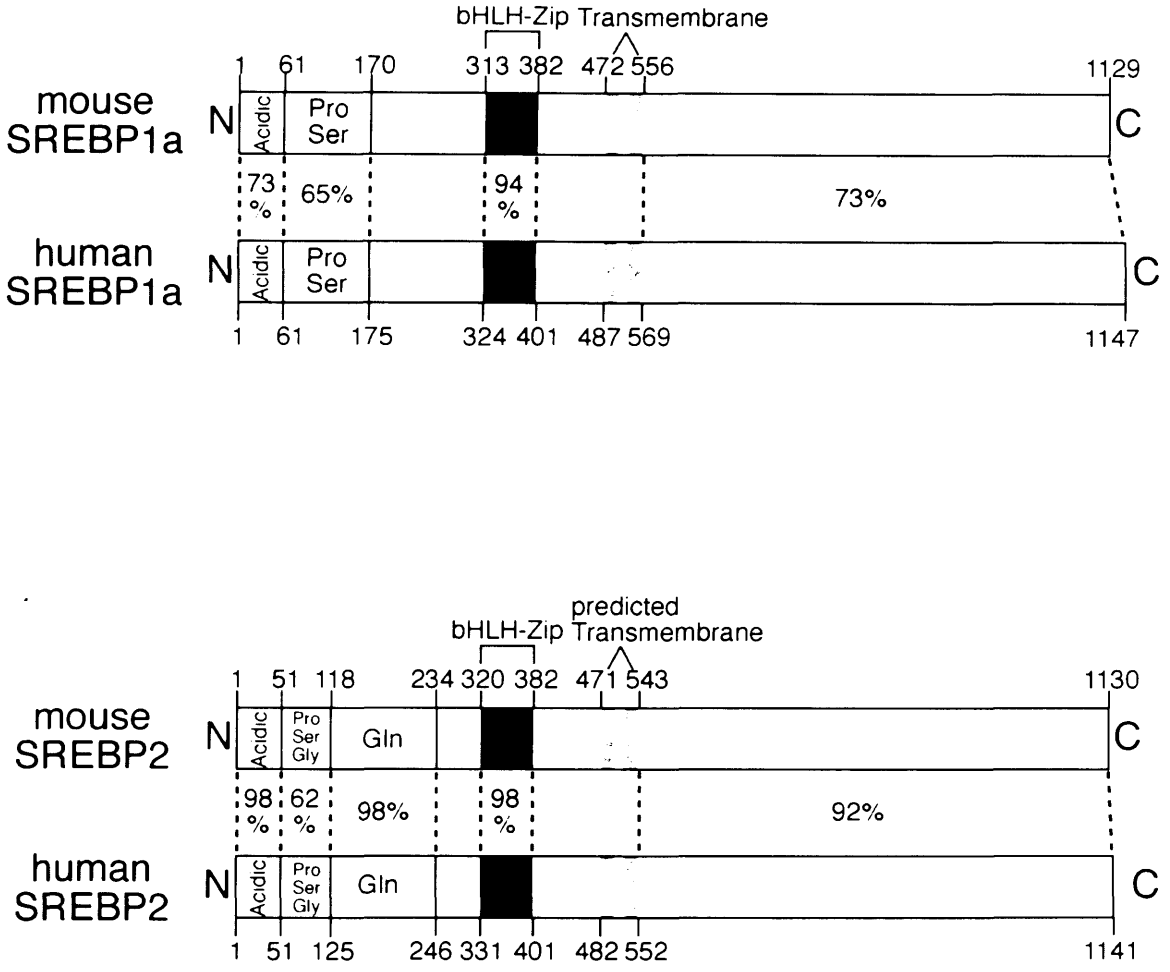

Figure 25. Comparison of mouse SREBP1a and SREBP2 with their human orthologues. (a) SREBP1a amino acid sequence is compared to human SREBP1a, bHLH-Zip domain is indicated by the black box and the transmembrane domains are shown as grey lines. Amino acid identities between the two proteins are indicated as percentages between the two proteins. (b) As for SREBP1a, apart from the additional presence of the glutamine rich domain.

respectively). The functional significance of this observation is unknown, but possibly related to their relative importance within the cell.

5.10 Yeast two-hybrid analysis of the human lamin A and SREBP1a interaction

To confirm that lamin A and SREBP1 interacted, a direct yeast two-hybrid assay was performed using human lamin A and human SREBP1a. Human lamin A (residues 389-664) was fused to the Gal4 DBD and human SREBP1a was fused to Gal4 activation domain. These two proteins were introduced into yeast and the interaction analysed. Yeast expressing both proteins was streaked onto reporter media lacking histidine and adenine. Simultaneously, a negative and positive control was set-up. The negative control consisted of yeast containing human lamin A fused to Gal4 DBD and a human protein involved in centrosome function, Nek2 [Fry and Nigg, 1995] fused to the Gal4 activation domain. These two proteins are considered not to interact. The positive control used the lamin A chimeric protein and previously identified lamin A binding protein, Narf [Barton and Worman, 1999], which was fused to the Gal4 activation domain. To further characterise the specificity for SREBP1 to interact with the A-type lamins, a Gal4 DBD fusion protein was created using the tail domain of human lamin C (residues 389-572).

Human lamin A failed to interact with Nek2 but did interact with SREBP1a and Narf (Figure 26). This confirmed that human lamin A was not ubiquitously interacting with proteins fused to the Gal4 activation domain but specifically interacted with Narf and SREBP1a. The tail domain of lamin C also failed to interact with SREBP1a using the yeast two-hybrid system. This result suggests that SREBP1a binding is unique to the lamin A specific region, or the whole of lamin A is necessary for strong interaction with SREBP1a.

The observation that lamin A interacted with SREBP1 from both humans and mice substantiated this potential interaction.

5.11 *In vitro* analysis of the lamin A SREBP1 interaction

To further confirm this novel interaction, a second set of experiments were performed using *in vitro* synthesised and bacterially expressed proteins. A technique known to as the GST pull-down was utilised (Figure 27). This technique was developed originally to aid in the investigation of transcription initiation complexes [Chen *et al.*,

Lamin A 389-664
+
Narf

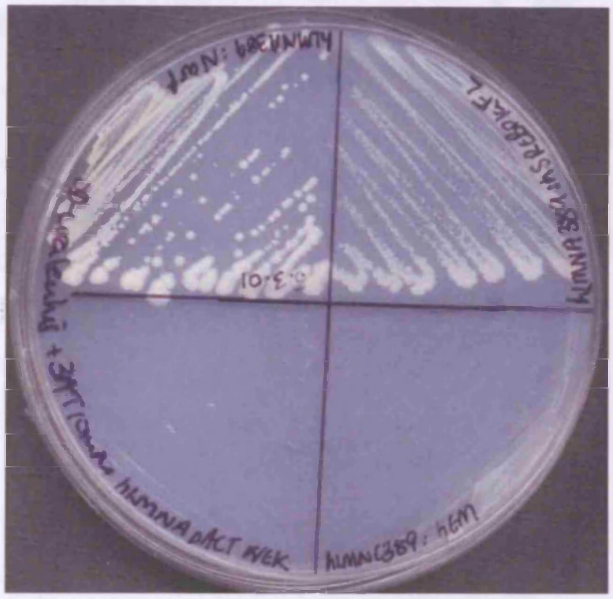

Lamin A 389-664
+
SREBP1a

Lamin A 389-664
+
Nek2

Lamin C 389-572
+
SREBP1a

Figure 26. Yeast two-hybrid analysis of the human lamin/SREBP1a interaction. Combinations of bait and prey plasmids were transformed in the yeast strain PJ69-4a and streaked onto minimal media lacking uracil, leucine, adenine and histidine, supplemented with 10 mM 3-AT. Lamin A 389-664 was tested for its interaction with Nek2, Narf, and SREBP1a; lamin C 389-572 was tested for its interaction with SREBP1a only. Lamin A 389-664 did not interact with Nek2, but did with Narf and SREBP1a; lamin C failed to interact with SREBP1a.

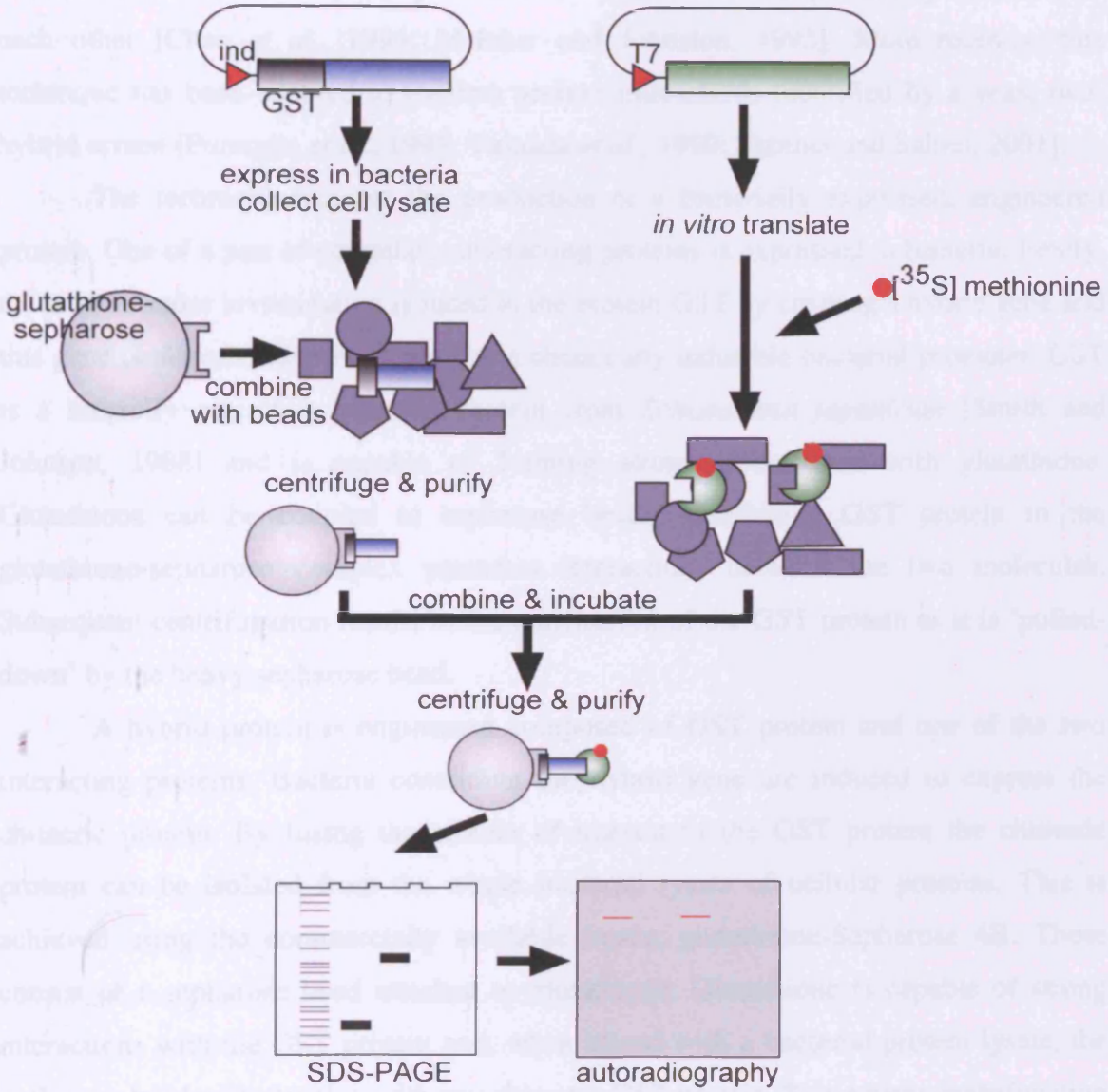

Figure 27. Overview of the GST pull-down. Two plasmids are created, one containing a GST tagged cDNA, the other, a cDNA downstream of a T7 promoter. The GST-tagged gene is expressed in *E. coli* and the proteins harvested. Glutathione-Sepharose is used to purify the GST protein by combining with the total cellular lysate followed by centrifugation. The second protein is *in vitro* translated with [^{35}S] methione (red circle) and combined with the glutathione-Sepharose purified GST protein. Further purification steps result in the co-purification of the radiolabelled protein with the GST protein if an interaction exists. GST only protein is used as a negative control, to demonstrate that the GST tag is not responsible for the 'pull-down'. The protein samples are resolved using SDS-PAGE and subjected to autoradiography to detect the presence of radiolabelled protein.

1994]. Eukaryotic gene transcription is initiated by the interaction of many different transcription factors and RNA polymerase. Use of the GST pull-down technique enabled the further validation of proteins that were believed to specifically interact with each other [Chen *et al.*, 1994; Melcher and Johnston, 1995]. More recently, this technique has been adapted to confirm protein interactions identified by a yeast two-hybrid screen [Pumiglia *et al.*, 1995; Yamada *et al.*, 1999; Skinner and Saltiel, 2001].

The technique requires the production of a bacterially expressed, engineered protein. One of a pair of potentially interacting proteins is expressed in bacteria. Firstly, the protein under investigation is fused to the protein GST by creating a hybrid gene and this gene is placed under the control of a chemically inducible bacterial promoter. GST is a naturally occurring bacterial protein from *Schistosoma japonicum* [Smith and Johnson, 1988] and is capable of forming strong interactions with glutathione. Glutathione can be coupled to sepharose beads. Combining GST protein to the glutathione-sepharose complex promotes interactions between the two molecules. Subsequent centrifugation results in the purification of the GST protein as it is 'pulled-down' by the heavy sepharose bead.

A hybrid protein is engineered composed of GST protein and one of the two interacting proteins. Bacteria containing the hybrid gene are induced to express the chimeric protein. By fusing the protein of interest to the GST protein the chimeric protein can be isolated from the whole bacterial lysate of cellular proteins. This is achieved using the commercially available beads, glutathione-Sepharose 4B. These consist of a sepharose bead attached to glutathione. Glutathione is capable of strong interactions with the GST protein and, when mixed with a bacterial protein lysate, the sepharose bead will complex with any chimeric GST protein. Subsequent centrifugation steps isolate the GST fusion protein as a consequence of the sedimentation properties of the dense sepharose bead. After several centrifugation steps and stringency washes the sepharose bead pellet will be complexed with the desired chimeric GST protein and purified from other cellular proteins.

This purified GST protein can be subsequently incubated with a second protein considered as a potential interactor. The second protein is synthesised *in vitro* using the transcription and translation kit (Section 5.4). The radioactive labelling of the protein aids in its detection in subsequent steps. The two proteins (the GST protein is left attached to the sepharose beads) are incubated at conditions promoting protein interaction. If a protein interaction exists between the chimeric GST protein and the

radiolabelled protein then this would result in a three-component complex consisting of the sepharose bead, the GST protein and, finally, the radiolabelled protein. Following incubation the samples are centrifuged and subjected to several stringency washes. The pellet, thus obtained, should only contain the sepharose bead, the GST protein and any other protein capable of interacting with the GST fusion protein. If the radiolabelled protein does not interact with the GST protein then it would be washed away in the supernatant. The protein samples attached to the sepharose beads are then subjected to PAGE and the resulting gels exposed to X-ray film. Any radioactive proteins found in the protein pellet will be detected on an autoradiograph.

This technique was used to investigate the *in vitro* binding of lamin A and SREBP1a. Lamin A residues 389-664 were fused to the GST protein. Both GST alone and GST-lamin A were induced in *E. coli* BL21 (a strain deficient in proteases) [Shin *et al.*, 1997]. The two proteins were subsequently purified using the sepharose beads. To both samples radiolabelled SREBP1a was added. The experiment was also duplicated using radiolabelled lamin A in the place of SREBP1a. All of the samples were incubated to facilitate protein interactions. The samples were washed, centrifuged and the proteins eluted from the sepharose beads. Proteins were electrophoresed on a polyacrylamide gel, then stained using a standard protein detection method (Figure 28a). Figure 28a shows the presence of GST protein and also the GST lamin A fusion protein (accompanied by degradation products). The exposure of this stained gel to X-ray film resulted in the detection of radioactive SREBP1a and lamin A in the 'pulled-down' protein pellets (Figure 28b) confirming the yeast two-hybrid analyses.

As discussed, the SREBPs exist as ER membrane bound proteins which, upon activation, are proteolytically cleaved to form a mature peptide that translocates to the nucleus. Lamin A/C is located primarily in the nuclear lamina at the periphery of the nuclear compartment, although some reports have described its presence in the ER. The site of interaction between lamin A and SREBP1 was considered to be at either the endoplasmic ER or the nuclear lamina. To investigate this, further GST pull-downs were performed using truncated SREBP1 proteins. Firstly, a truncated SREBP1a protein was created which terminated prior to the first transmembrane domain (residues 1-487). SREBP1c, the shorter SREBP1c isoform, was also generated and terminated at the same site as SREBP1a truncated protein (residues 1-463). These two proteins were equivalent to the mature SREBP1 proteins, consisting of the bHLH-Zip domain, previously known to directly translocate to the nucleus [Brown and Goldstein, 1999].

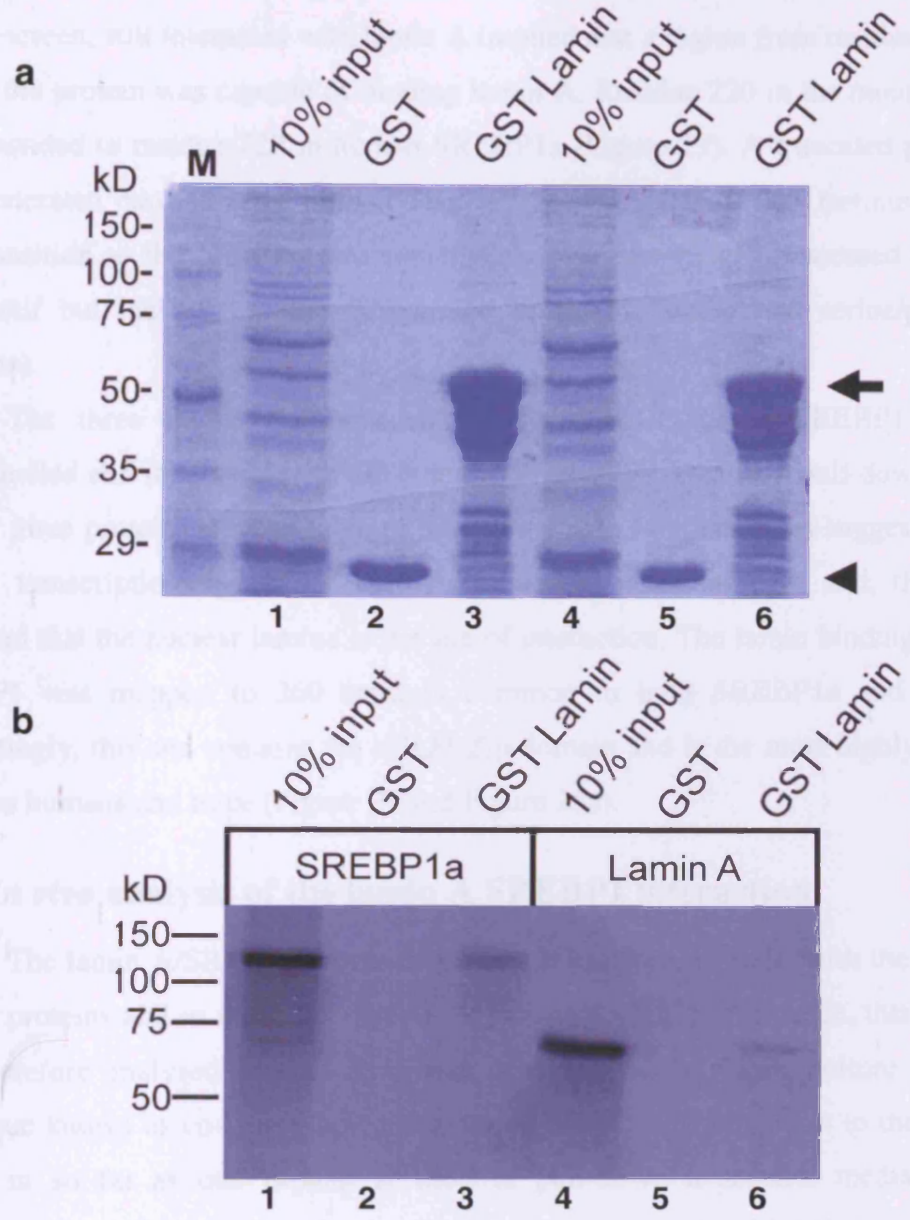

Figure 28. GST pull-down of SREBP1a with GST-lamin. (a) SDS-polyacrylamide gel stained with coomassie blue. Molecular weight marker (M) is shown with corresponding sizes. GST protein of 26 kDa is shown (arrowhead) and GST fused to lamin A (residues 389-664) of predicted Mw ≈54 kDa is shown (arrow). IVT synthesised SREBP1a was 'pulled-down' with GST alone (lane 2) or GST-lamin (lane 3). SREBP1a IVT (10% of that used in the GST pull-down) was loaded directly on the gel (lane 1). This was repeated using IVT lamin A substituted for SREBP1a (lanes 4, 5, 6). (b) X-ray film was overlaid onto to the gel presented in a) and subsequently developed. Radiolabelled SREBP1a (≈125 kDa) is present in lanes 1 and 3, and radiolabelled lamin A (≈70 kDa) is present in lanes 4 and 6.

The finding that the shortest of the SREBP cDNAs, isolated from the yeast two-hybrid screen, still interacted with lamin A implied that a region from residue 220 to the end of the protein was capable of binding lamin A. Residue 220 in the mouse SREBP1 corresponded to residue 227 in human SREBP1a (Figure 23). A truncated protein was also generated consisting of human SREBP1 residues 227 to 487 (terminated at the same position as the previous two constructs). This protein still possessed the bHLH-Zip motif but lacked the first 226 amino acids (the acidic and serine/proline-rich domains).

The three SREBP proteins, SREBP1a, SREBP1c and SREBP1-227, were radiolabelled and incubated with GST-lamin (Figure 29). The GST pull-down indicated that all three proteins were capable of interacting with lamin A. This suggested that the mature transcriptionally active SREBPs interacted with lamin A and, thus, it was proposed that the nuclear lamina is the site of interaction. The lamin binding domain of SREBP1 was mapped to 260 residues common to both SREBP1a and SREBP1c. Interestingly, this site contains the bHLH-Zip domain and is the most highly conserved between humans and mice (Figure 23 and Figure 25a).

5.12 *In vivo* analysis of the lamin A SREBP1 interaction

The lamin A/SREBP1 interaction had been proven in yeast, with the mouse and human proteins and *in vitro*. To explore its true biological significance, this interaction was therefore analysed *in vivo*. This was performed using tissue culture cells and a technique known as co-immunoprecipitation (Co-IP). Co-IP is similar to the GST-pull-down, in so far as one protein is used to pull-down a second, mediated by the centrifugation of sepharose beads. The two proteins considered to interact are transfected into tissue culture cells. Following expression of these proteins and growth of the cells the cellular proteins are harvested. Firstly, an antibody is used which binds the lamin protein. A second antibody (coupled to a sepharose bead) is also added which specifically interacts with the first antibody. Subsequent centrifugation will result in the pull-down of the complex of proteins attached to the sepharose beads. If any proteins interact with lamin A then they will also be purified. The proteins present in the sepharose complex can be detected using western blot analyses.

A Co-IP was performed using protein extracts from cells transfected with SREBP1a and lamin A (Figure 30). SREBP1a co-immunoprecipitated with lamin A, thus, confirming that the interaction occurred *in vivo*.

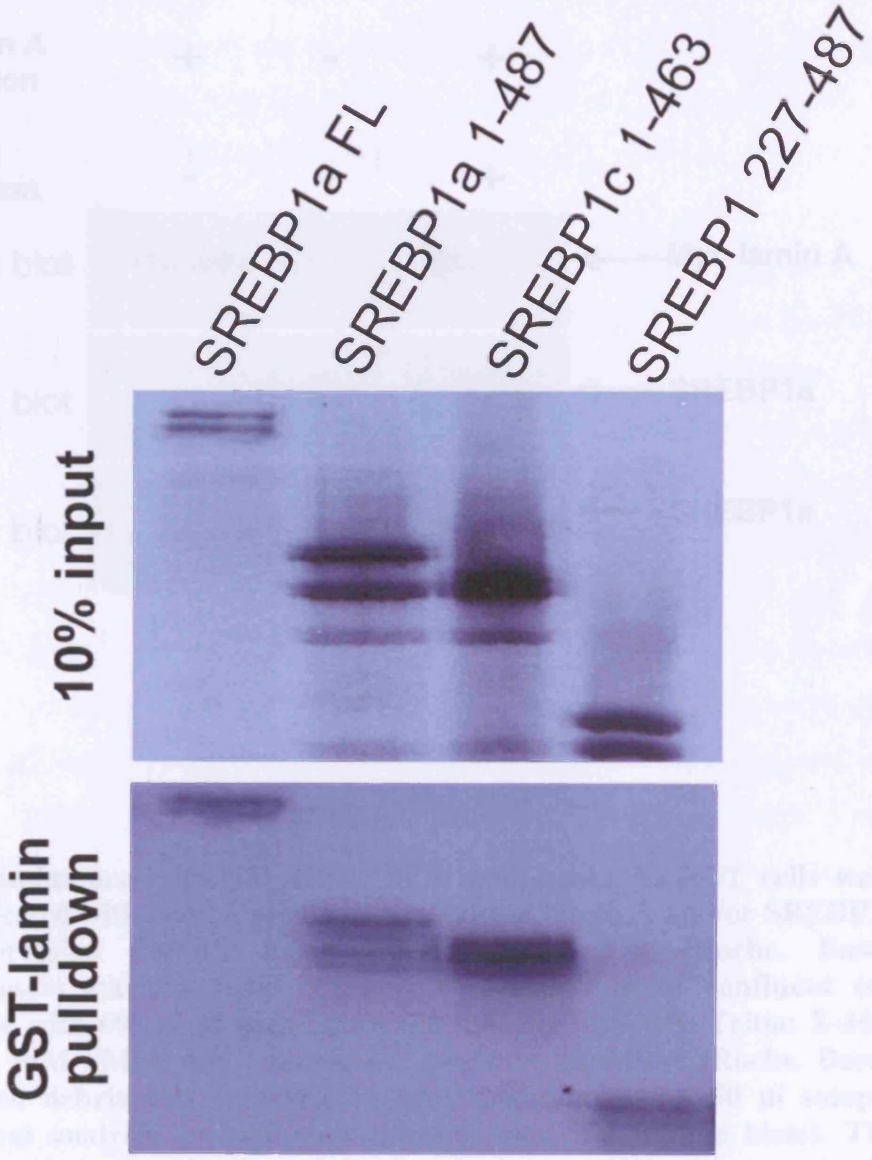

Figure 29. GST lamin pull-down of different SREBP1 truncations. SREBP1a full-length, SREBP1a 1-487, SREBP1c 1-463 and SREBP1 227-487 were *in vitro* translated and 10% of the amount used in the pull-down was subjected to SDS-PAGE and autoradiography. The pull-down with lamin A successfully indicated that all four proteins interacted.

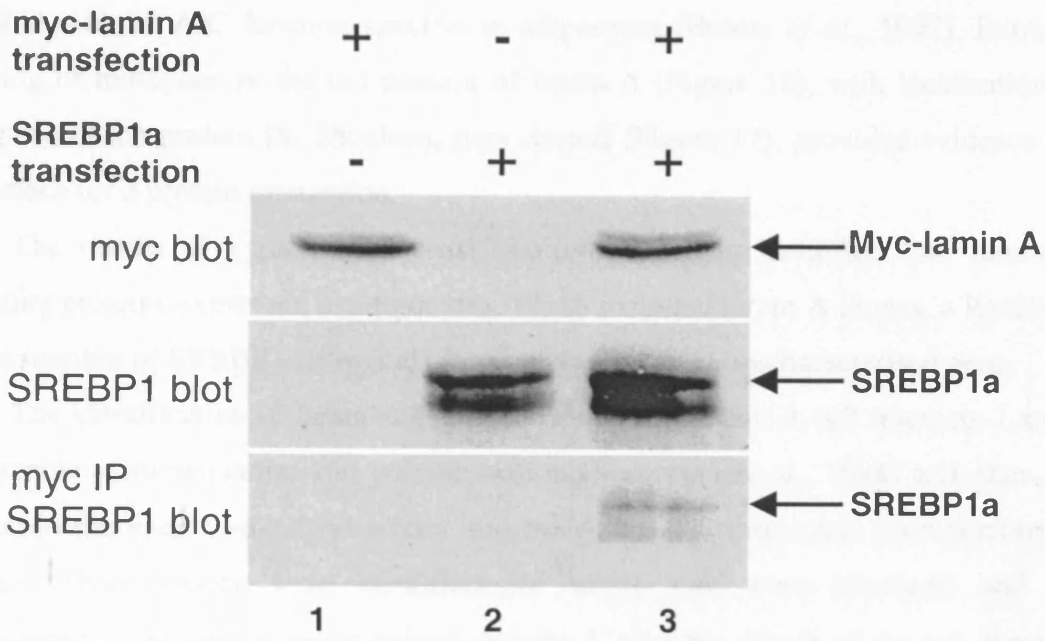

Figure 30. Co-immunoprecipitation of SREBP1a and lamin A. 293T cells were transiently transfected with combinations of myc-tagged lamin A and/or SREBP1a mammalian expression vectors using Fugene 6 reagent (Roche. Basel, Switzerland). Protein extracts were obtained by incubation of confluent cell monolayers on ice with 600 µl of lysis buffer (50 mM HEPES, 1% Triton X-100, 150 mM NaCl, 1 mM PMSF and Complete™ protease inhibitors [Roche. Basel, Switzerland]). Cell debris was removed by centrifugation and a 50 µl sample removed for direct analysis by immunoblotting (upper and middle blots). The remaining supernatant was pre-cleared by incubation at 4°C with protein A-Sepharose beads (Amersham-Pharmacia Biotech. Little Chalfont, UK), followed by centrifugation. The supernatant was incubated at 4°C for 2 hours with 2 µg of 9E10 anti-myc antibody (Zymed. San Francisco, USA). Protein A-sepharose beads were then added and the incubation continued for a further 1 hour. The beads were washed with lysis buffer and solubilised in 2× protein sample buffer. Samples were boiled for 5 min prior to separation on 7.5% acrylamide gel and immunoblotting. The membrane was probed with anti-SREBP1 antibodies (H160; Santa Cruz Biotechnologies), followed by alkaline phosphatase-conjugated anti-rabbit antibodies (Promega. Madison, USA). The myc antibody 9E10 immunoprecipitated myc tagged lamin A and co-immunoprecipitated SREBP1a (lane 3).

5.13 Discussion

The finding of site-specific missense mutations in *LMNA*, responsible for FPLD, highlighted the role of the A-type lamins and nuclear lamina in adipocyte development and function. Given the near-ubiquitous expression of lamin A/C in almost all cell types suggested a lamin A/C function specific to adipocytes [Broers *et al.*, 1997]. Extreme clustering of mutations in the tail domain of lamin A (Figure 16), with localisation to the surface of the protein [S. Shoelson, *pers comm*] (Figure 17), provided evidence for an interface for a protein interaction.

The results of a successful yeast two-hybrid screen identified four lamin A interacting proteins expressed in adipocytes. These included lamin A clones, a RanBPM clone, a number of SREBP clones and clones representing an uncharacterised gene.

The identification of lamin A clones indicated that lamin A self interacts. Lamin A is capable of dimerisation and polymerisation [Stuurman *et al.*, 1998] and, thus, its isolation in the yeast two-hybrid screen suggested that the screen had been performed correctly. Three clones were identified (of which two were identical) and all corresponded to the end of the α-helical domain 2, plus the whole of the tail domain. Several significant conclusions may be extrapolated from this. The identification of two identical clones indicated that the yeast two-hybrid screen was saturated and all interacting proteins from the library had been identified. Furthermore, the lamin A tail domain (residues 389-664) was capable of forming interactions with a second lamin A. It is well established that lamin self-interactions are mediated through the α-helical domain (residues 1-388) [Stuurman *et al.*, 1998] and the tail domains are adjacent to each other. The finding of lamin tail self-interactions provides evidence for the role of the globular tail in dimerisation. Equally, given the head-to-tail interaction of dimers, the tail domain could bind the head domain of an adjacent lamin molecule. However, the absence of lamin head domains in the isolated interacting cDNA clones fails to support this latter hypothesis. Therefore, the lamin A tail domain alone is sufficient to promote lamin A dimerisation. The ability of lamin A and lamin C to heterodimerise is unknown. The three clones identified from the yeast two-hybrid screen were all lamin A. Two explanations can be proposed for this observation. Firstly, it could indicate that dimerisation mediated by the lamin A tail domain only permits homodimerisation. Secondly, it could represent the relative abundance of lamin A and lamin C isoforms in adipocytes. Thus, if lamin A is the only A-type lamin expressed in adipocytes then the

lamin A used as bait would not identify lamin A-lamin C interactions. The ability of lamin A and lamin C to form heterodimers, mediated by the α-helical domain, was not investigated.

The functional significance of lamin A self-interaction in adipocytes, with respect to FPLD, does not provide a basis for the derivation of a putative disease mechanism. The near-ubiquitous expression of lamin A/C suggests that this interaction occurs in all cell types. Thus, it cannot be envisaged how site-specific mutations selectively affect adipocyte dysfunction by perturbation of the lamin A interaction.

The identification of seven SREBP clones which interact with the tail domain of lamin may provide an explanation for the selective adipocyte degeneration in FPLD individuals. SREBP is a transcription factor capable of directing expression of genes involved in adipocyte differentiation and cholesterol biosynthesis (Section 1.1.3.3). Three different isoforms of SREBP exist: SREBP1a, SREBP1c (also known as ADD1) and SREBP2. SREBP1a and SREBP1c/ADD1 are transcribed from a single gene and differ in their extreme amino terminus. SREBP2 is transcribed from a different gene. The SREBP proteins exist as ER membrane bound precursors and upon activation, the bHLH-Zip domain translocates to the nucleus.

Northern blot analyses have shown that SREBP1 is expressed exclusively in the liver and adipose tissue (both brown and white adipocytes) [Tontonoz *et al.*, 1993; Yokoyama *et al.*, 1993]. In contrast, SREBP2 exhibits a ubiquitous expression pattern [Hua *et al.*, 1993]. The different SREBP1 isoforms have different patterns of expression [Shimomura *et al.*, 1997]. SREBP1a possesses a longer acidic activation domain than SREBP1c. In those tissues that express SREBP1, a higher level of SREBP1c was detected in both humans and mice. The difference in SREBP1 and SREBP2 expression indicates their importance. It can be concluded that SREBP2 function is necessary in all cell types, whereas SREBP1 confers a function specific to the liver and adipocytes. The differences between SREBP isoforms at the protein level has been proposed to provide a wider range of transcriptional regulation [Flier and Hollenberg, 1999]. SREBP2 is more associated with cholesterol biosynthesis and metabolism [Shimano *et al.*, 1997b] and SREBP1 is more strongly associated with control of genes involved in fatty acid biosynthesis.

The bHLH-Zip domain of the SREBP proteins is capable of binding two different regulatory elements in gene promoters [Kim *et al.*, 1995; Brown and Goldstein, 1997]. The first is termed the sterol response element (SRE; 5'-

TCACCCCCCAC-3') and is present in the promoters of genes involved in cholesterol biosythesis, including the low density lipoprotein (LDL) receptor and 3-hydroxy-3-methylglutaryl CoA (HMG-CoA) [Smith *et al.*, 1988; Smith *et al.*, 1990]. SREBPs can also bind at an E-box motif (5'-CACGTG-3') present in the promoters of genes involved in fatty acid synthesis, including fatty acid synthase (FAS) and acetyl CoA carboxylase (ACC) [Tontonoz *et al.*, 1993]. The ability of SREBP1c/ADD1 in promoting adipogenesis has been extensively studied [Kim and Spiegelman, 1996] (Section 1.1.3.3). SREBP1c/ADD1 induces genes involved in adipogenesis including PPARγ, FAS and LPL. SREBP1a has not been investigated as an adipogenic transcription factor.

Many different transgenic mice have been generated, as a result of manipulations with the SREBP genes. Transgenic mice were made that expressed the transcriptionally active SREBP proteins in the liver, TgSREBP1a, TgSREBP1c and TgSREBP2. TgSREBP1a mice have massively enlargened livers, engorged with cholesterol and triglyceride [Shimano *et al.*, 1996]. These mice also showed signs of a progressive decrease in adipose tissue, considered to be a consequence of 'triglyceride steal' by the liver. TgSREBP1c mice had no increase in cholesterol levels, but significantly elevated levels of triglyceride [Shimano *et al.*, 1997a]. TgSREBP2 mice possessed enlargened livers, similar to TgSREBP1a mice, but with less triglyceride accumulation [Horton *et al.*, 1998]. As predicted, SREBP2 has a more significant role in cholesterol synthesis than SREBP1 isoforms. Interestingly, these transgenic studies provided a functional difference for the SREBP1 isoforms, as a consequence of the difference in acidic activation domain length.

Mice possessing targeted disruptions of SREBP1 [Shimano *et al.*, 1997b] and SREBP2 [J. Horton *et al.*, unpublished] have been generated. Mice deficient in SREBP1 proteins were phenotypically normal. This was thought to be a consequence of elevated levels of SREBP2 and, as a consequence, cholesterol levels were elevated compared to wild-type mice. SREBP2 deficient mice were embyonic lethal. These data provide evidence for the absolute requirement for SREBP2 and its ability to compensate for reduced SREBP1 levels.

To further the investigation of SREBP1 role in adipocytes, transgenic mice were developed which expressed the transcriptionally active SREBP1c protein specifically in adipocytes. The resultant phenotype in these mice bore a remarkable resemblance to that of lipodystrophy in humans (Section 1.2.4).

Considering the biological role of SREBP1, its interaction with lamin A was considered to be of great biological significance. Identification of six SREBP1 cDNA clones that interact with lamin suggested their 'non-coincidental' isolation. In addition to the two identical lamin A clones identified, two identical SREBP clones were also isolated, confirming the clone saturation of the yeast two-hybrid screen. The co-isolation of a single SREBP2 clone confirmed the validity of the screen and excluded the concept that the SREBP1 interaction may be incorrect. The relative frequency of SREBP1 versus SREBP2 clones could indicate the preferential interaction of lamin A with SREBP1, as both are highly expressed in adipocytes. The reconstitution of this interaction with the human orthologues further validated this interaction. *In vitro* and *in vivo* analyses provided unequivocal evidence for lamin A and SREBP1 interaction and demonstrated that both of the SREBP1 isoforms were capable of this interaction. The use of the GST pull-down technique enabled the mapping of the domain responsible for binding lamin A. This domain is between residues 227 and 487 in human SREBP1a (corresponding to 203 and 463 in SREBP1c) and encompasses the bHLH-Zip domain as well as the region proximal to the first ER transmembrane domain.

Thus, transcriptionally active SREBP1 is capable of interacting with the tail domain of lamin A, known to contain all of the FPLD missense mutations. This, therefore, raises the question of how this interaction is biologically relevant in adipocytes and the effect, if any, of FPLD mutations. Furthermore, the tail domain of lamin C fails to interact with SREBP1a. It is possible that only lamin A interacts with SREBP1a and possesses features at the C-terminus which contribute to SREBP1a binding. Mutations which cause FPLD would therefore be in the common lamin A/C tail and the lamin A specific carboxyl terminus.

As determined by the *in vitro* analyses, SREBP1 potentially interacts with lamin A at the nuclear envelope. It is possible that the interaction occurs during nuclear import, whilst SREBP1 is translocated through the nuclear pores. Nuclear pores consist of a multitude of proteins. Spanning the nuclear membranes are the nucleoporins (Nups) [Vasu and Forbes, 2001], which form a large multimeric structure contributing to the body of the nuclear pore. At the nuclear face, the nucleoporins are attached to the lamina, mediated by Nup153 and lamin B3 [Smythe *et al.*, 2000]. The *in vivo*, orthoganol appearance of the lamina is considered to be responsible for the regular placement of pores in the nuclear envelope [Aebi *et al.*, 1986]. Proteins termed importin α and importin β are situated at the cytoplasmic face of the nuclear pore. Importin α is

known to bind the nuclear localisation signal present in many nuclear targeted proteins (consensus KRKK) [Dingwall and Laskey, 1991]. Upon complex formation, importin α binds importin β and the complex translocates through the nuclear pore. Thus, the nuclear targeting of SREBP1 implicates the nuclear import machinery in lamina binding. Active SREBP proteins do not possess a nuclear localisation signal and their passage to the nucleus was considered uncertain. Nagoshi and colleagues focussed on the nuclear import mechanism of SREBP2 [Nagoshi *et al.*, 1999]. Their investigations revealed that SREBP2 did not bind importin α (the cargo-importin β mediary protein), instead bound directly to importin β. Presumably, the functional significance of this is to permit the operation of the ER retention signal without competition with an importin α NLS. Hence, lamin A and SREBP may interact as a result of complex formation of several proteins in the nuclear pore.

In support the concept of a lamin A complex at the nuclear pore was the identification of the fourth class of interacting clones, RanBPM. As previously stated, RanBPM was localised to the centrosome [Nakamura *et al.*, 1998] and was, thus, considered to be a false-positive isolated in the yeast two-hybrid screen. Concomitant with the writing of this thesis was the publication of a second RanBPM report, written by the same group [Nishitani *et al.*, 2001]. Their new findings disproved the previous localisation of RanBPM at the centrosome, as the protein was found to be predominantly situated at the nuclear periphery. This recent report indicates that the lamin/RanBPM interaction may be correct. RanBPM interacts with Ran, a small GTPase involved in nucleoplasmic trafficking [Vasu and Forbes, 2001]. Ran interacts with importin β at the nuclear face of the nuclear pore and upon binding importin β, releases its cargo which has passed through the nuclear pore. Therefore, a whole set of cellular proteins can be envisaged at the nuclear pore, in association with lamin A and SREBP. SREBP binds importin β, which binds Ran, to which RanBPM binds. In addition, lamin A is capable of interacting with SREBP and RanBPM.

This concept appears valid and SREBP association with the lamina has recently been proposed [Hegele, 2001]. However, given that many proteins translocate through the nuclear pore, the question of why SREBP was specifically identified as a lamin A interactor remains. Explanations for this could be that SREBP is the only protein cargo capable of binding importin β directly. Alternatively, the lamin A and SREBP interaction may not be a result of complex formation at the nuclear pore.

It is equally possible that the lamin A and SREBP interaction occurs within the nucleus. Other transcription factors have been shown to co-localise with the nuclear lamina [Mancini *et al.*, 1994; Ozaki *et al.*, 1994; Rafiq *et al.*, 1998; Cohen *et al.*, 2001]. SREBP1 could be 'shuttled' to the lamina (lamin A), immediately after nuclear entry and the lamina may be involved in the dispersal of SREBP around the nucleus.

The mouse model of lipodystrophy was generated by increasing the nuclear levels of SREBP1c. It is feasible that a transcription factor involved in promoting adipogenesis, when over-expressed, would increase adipogenesis and fat accumulation. Surprisingly, over-expression of SREBP1c in adipose tissue resulted in lipodystrophy, in opposition to the expected phenotype. Shimomura *et al.* proposed mechanisms for the lipodystrophy. The most plausible was the action of the over-expressed SREBP1c in sequestration of SRE and E-box sites in the promoters of adipogenic genes. Thus, the more potent SREBP isoforms, SREBP1a and SREBP2, were not able to exert their transcriptional effects at these promoters. However, although SREBP1c possesses a smaller acidic activation domain, it is still able to direct the synthesis of genes involved in fatty acid biosynthesis and adipogenesis and, hence, fails to explain the complete absence of adipose tissue.

The discovery that these two proteins are associated with lipodystrophy in humans and mice, strongly suggests that the interaction between them may underlie the molecular mechanism of FPLD.

6 CHARACTERISATION OF THE NOVEL LAMIN A BINDING PROTEIN

6.1 Introduction

The identification of lamin A as the defective gene in FPLD and the evidence of interaction with an adipogenic transcription factor, SREBP1, suggested a role for these proteins in the development and maintenance of adipocytes. No functional biological assays are presently available to investigate the effect of *LMNA* mutations on the lamin A/SREBP1 interaction. Hence, the contribution of this pathway to the generation of the FPLD phenotype cannot be fully clarified. Additional studies were also performed to characterise the novel gene identified in the yeast two-hybrid screen. Since the novel gene had not been previously characterised, its function was unknown and the possibility existed that it could offer a second mechanism for adipose tissue degeneration in FPLD patients.

Because of its identification as a lamin interacting protein, obtained from an adipocyte library the term LIPA was used to refer to the protein (mouse cDNA is referred to as *Lipa*).

6.2 Yeast two-hybrid identification of *Lipa*

Of thirteen sequenced lamin A interacting clones, two were identified to be a novel transcript. Both were identical in length and sequence as revealed by DNA sequencing, initially using the ADF and T7 vector primers (Figure 21b), followed by a progressive set of nested primers. A DNA sequence of 4058 bases was identified (Figure 31) and confirmed by sequencing both sense and antisense DNA strands. Sequence translation revealed a single open reading frame (ORF). An initiation ATG codon was located 38 bases downstream of the *Eco*RI cloning site, positioned within a translation initiation consensus sequence. The general consensus sequence is 5'-CACC**ATG**G-3' where ATG is the initiation methionine codon [Kozak, 1984]. The putative translation start site in the *Lipa* cDNA sequence is 5'-GAACATGG-3', where only the underlined bases differ. To confirm that this was the true initiation start site it was necessary to confirm that no other ATG sequences existed upstream of this putative start site. To investigate if this was the correct start site, the *Lipa* cDNA sequence was used to screen EST databases [Altschul *et al.*, 1990]. Several

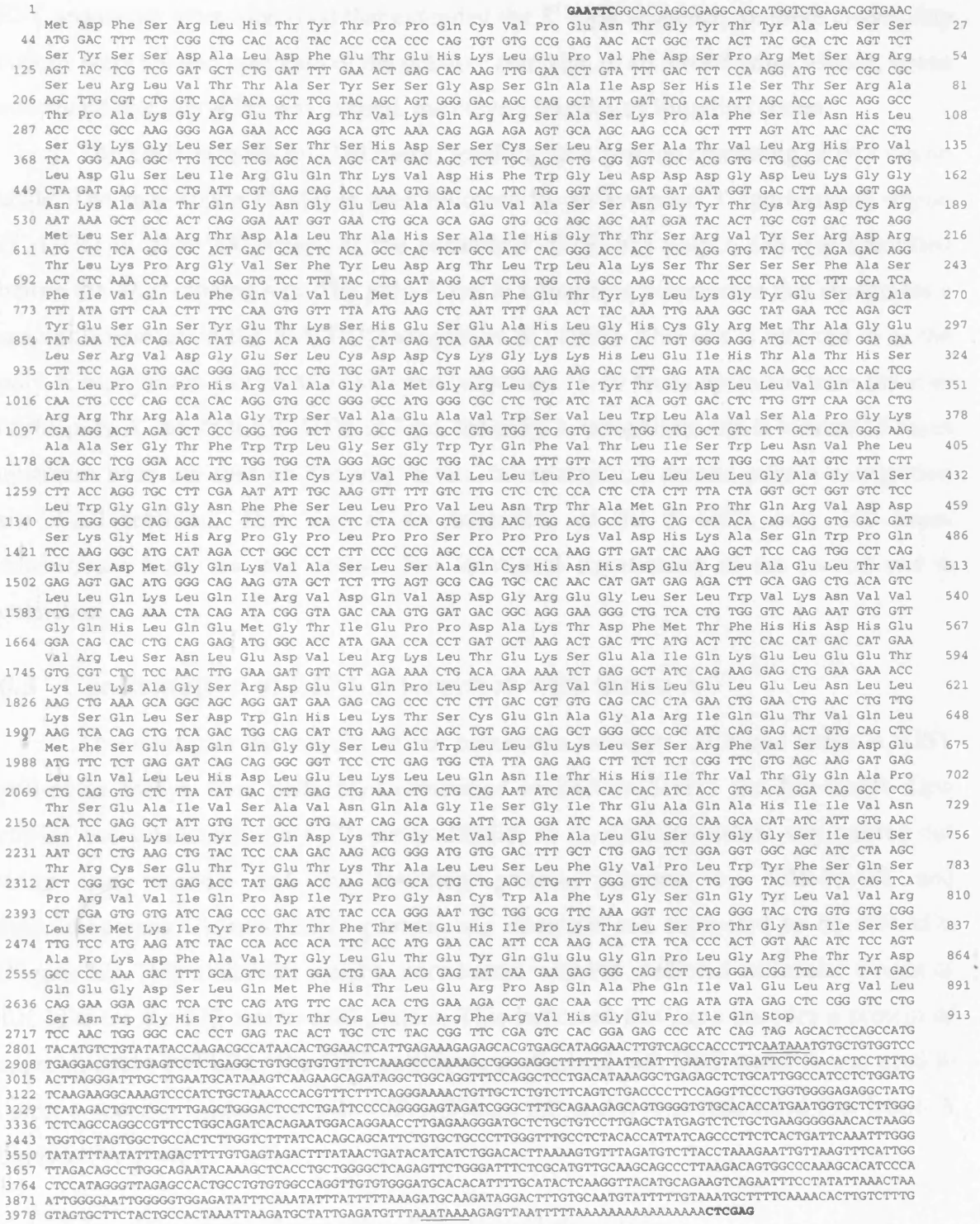

Figure 31. ***Lipa*** **cDNA sequence. The DNA sequence of** ***Lipa*** **was revealed by sequencing the yeast two-hybrid positive clone Y2H67. The cloning sites** ***Eco*****RI and** ***Xho*****I are shown in bold. The putative ORF of 2739 bases is divided into codons, and above each codon is the corresponding amino acid. The 3'-UTR and 5'-UTR is shown by the continuous DNA sequence. Two putative poly-adenylation signals are underlined. The DNA sequence is numbered down the left-hand side and the amino acid sequence is numbered down the right-hand side.**

EST sequences were identified that extended the 5' *Lipa* sequence. In these clones stop codons were located upstream of the putative start site, in all three frames. Hence, it was concluded that this ATG was, indeed, the correct translation initiation codon.

The ORF extends to 2739 bases, resulting in a peptide consisting of 913 amino acids. The stop codon (TAG) is then followed by an extended 3' untranslated region (3'-UTR) of over 900 bases. At the extreme 3'-UTR, the poly-A tail was identified before the *Xho*I cloning site. The poly-A tail is added by a polymerase that recognises a specific sequence in the 3'-UTR [Takagaki *et al.*, 1988]. This site is referred to as the poly-A recognition site (AAUAAA) and is located 11-30 bases upstream from the start of the poly-A tail. In the 3'-UTR of *Lipa,* the poly-A recognition site is located 13 bases upstream from the start on the poly-A tail. Interestingly, a second poly-A recognition site was identified. This was at the beginning of the 3'-UTR, only 100 bases downstream from the stop codon. The functional significance of the second site is unknown.

6.3 Confirmation of LIPA interaction with lamin A

To investigate the validity of the interaction between LIPA and lamin A, GST pull-down assays were performed (described in Section 5.11). The full-length *Lipa* cDNA was subcloned into a T7 vector. Firstly, an *in vitro* translation was carried out using this plasmid and the resulting protein analysed by SDS-PAGE and autoradiography. A radioactive protein was detected and estimated to be 100 kDa (Figure 32). This molecular weight is consistent with the predicted molecular weight of 101 kDa for the 913 amino acid protein. This indicated that *Lipa* encodes a protein of approximately 100 kDa. The GST pull-down performed with GST-lamin A was used to detect a specific interaction with LIPA (Figure 32) and it was concluded that lamin A binds LIPA *in vitro*.

6.4 Identification of putative functional domains

The amino acid sequence was further analysed using a range of bioinformatic programs and databases. Properties of other lamin binding proteins included the presence of a transmembrane domain spanning the inner nuclear membrane (emerin, LAP1, LAP2, LBR). Thus, the presence of transmembrane domains in LIPA was investigated. The 913 amino acids were analysed using SOSUI [Hirokawa *et al.*, 1998]. Two transmembrane domains were identified (Figure 33a), located in the middle

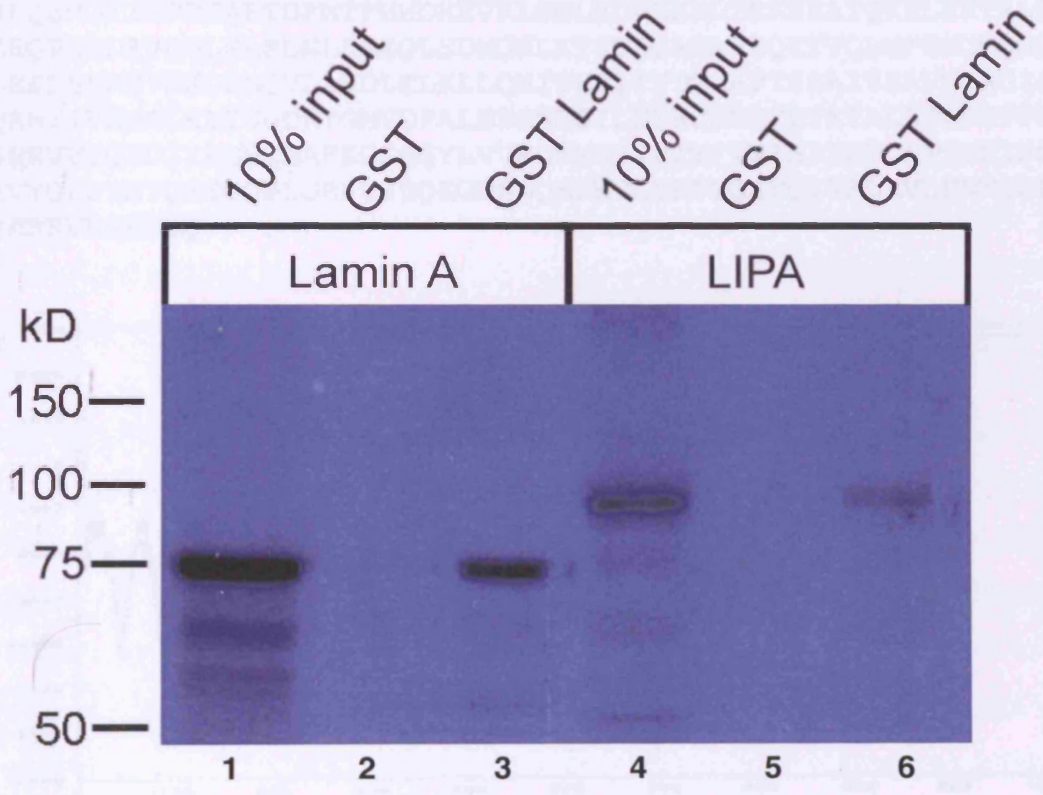

Figure 32. ***In vitro*** **analysis of the lamin A/LIPA interaction. Autoradiograpgh reveals the pull-down of SREBP1a and LIPA by GST tagged lamin A. Radiolabelled lamin A (≈70 kDa) is present in lanes 1 and 3, and radiolabelled LIPA (≈100 kDa) is present in lanes 4 and 6.**

a

MDFSRLHTYTPPQCVPENTGYTYALSSSYSSDALDFETEHKLEPVFDSPRMSRRSLRLVT
TASYSSGDSQAIDSHISTSRATPAKGRETRTVKQRRSASKPAFSINHLSGKGLSSSTSHD
SSCSLRSATVLRHPVLDESLIREQTKVDHFWGLDDDGDLKGGNKAATQGNGELAAEVASS
NGYTCRDCRMLSARTDALTAHSAIHGTTSRVYSRDRTLKPRGVSFYLDRTLWLAKSTSSS
FASFIVQLFQVVLMKLNFETYKLKGYESRAYESQSYETKSHESEAHLGHCGRMTAGELSR
VDGESLCDDCKGKKHLEIHTATHSQLPQPHRVAGAMGRLCIYTGDLLVQALRRTRAAGWS
VAEAVWSVLWLAVSAPGKAASGTFWWLGSGWYQFVTLISWLNVFLLTRCLRNICKVFVLL
LPLLLLLGAGVSLWGQGNFFSLLPVLNWTAMQPTQRVDDSKGMHRPGPLPPSPPPKVDHK
ASQWPQESDMGQKVASLSAQCHNHDERLAELTVLLQKLQIRVDQVDDGREGLSLWVKNVV
GQHLQEMGTIEPPDAKTDFMTFHHDHEVRLSNLEDVLRKLTEKSEAIQKELEETKLKAGS
RDEEQPLLDRVQHLELELNLLKSQLSDWQHLKTSCEQAGARIQETVQLMFSEDQQGGSLE
WLLEKLSSRFVSKDELQVLLHDLELKLLQNITHHITVTGQAPTSEAIVSAVNQAGISGIT
EAQAHIIVNNALKLYSQDKTGMVDFALESGGGSILSTRCSETYETKTALLSLFGVPLWYF
SQSPRVVIQPDIYPGNCWAFKGSQGYLVVRLSMKIYPTTFTMEHIPKTLSPTGNISSAPK
DFAVYGLETEYQEEGQPLGRFTYDQEGDSLQMFHTLERPDQAFQIVELRVLSNWGHPEYT
CLYRFRVHGEPIQ

b

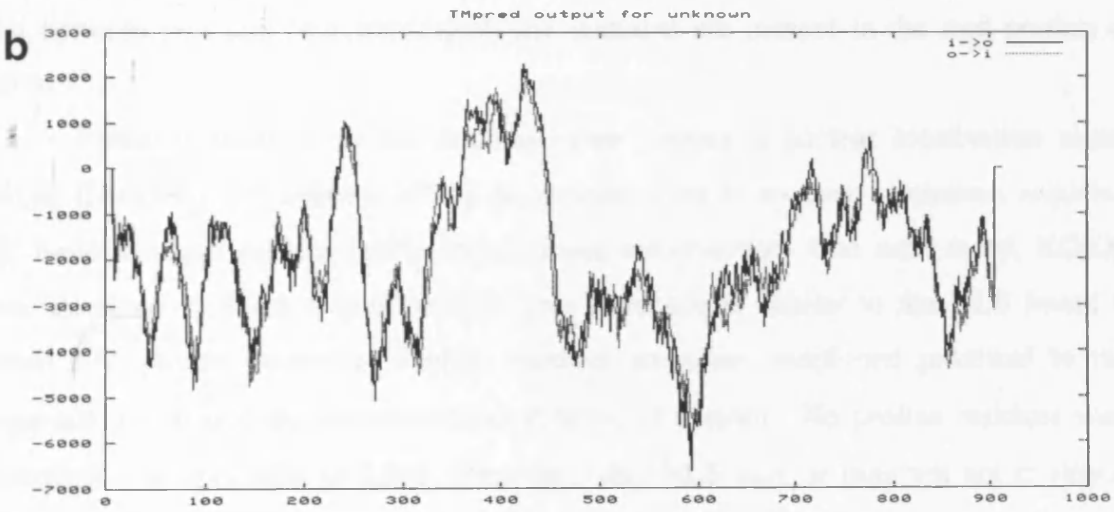

c

```
LIPA        YTCRD--CRMLSARTDALTAHSA-IH
TFIIIA-1    YICSFADCGAAYNKNWKLQAHLC-KH
TFIIIA-4    YVCHFENCGKAFKKHNQLKVHQF-SH
TFIIIA-8    YLCPRDGCDRSYTTAFNLRSHIQSFH
```

Figure 33. LIPA putative domains. (a) Amino acid sequence of LIPA, illustrating the zinc finger and NLS (black shading), the transmembrane domains predicted using SOSUI (outlined) and TMpred (grey shading) are shown. (b) TMpred hydrophobicity plot of LIPA, high peaks suggest the presence of transmembrane domains. (c) Comparison of LIPA zinc finger with zinc fingers 1, 4 and 8 of *Xenopus* TFIIIA, critical residues (black boxes), conserved residues (grey boxes).

portion of the protein, separated by only 24 amino acids. This is reminiscent of the transmembrane domain localisation in SREBP and could imply that *LIPA* also forms a hairpin conformation spanning a membrane. To validate the transmembrane domain prediction using SOSUI a second transmembrane domain program was used, TMpred [Hofmann and Stoffel, 1993]. However, TMpred failed to identify the same domains as SOSUI. The output from TMpred is viewed as a hydrophobicity plot (Figure 33b), representing the degree of hydrophobicity for a 'moving window' of residues (≈ 20 amino acids), over the entire amino acid sequence. High hydrophobicity peaks suggest the location of transmembrane domains. The *LIPA* hydrophobicity plot indicated the presence of four transmembrane domains, of which two are likely to be definite transmembrane domains (suggested by the high peaks). The localisation of these TMpred domains was compared to the position of the SOSUI domains (Figure 33a). There is slight overlap of these domains predicted between programs. It was concluded that between two and four transmembrane domains are present in the mid portion of *LIPA*.

Proteins localised to the nucleus often contain a nuclear localisation signal (NLS) [Dingwall and Laskey, 1991]. In general, there is no clear consensus sequence but basic residues such as lysine and arginine are common. One such motif, KGKK, was identified in *LIPA* at residue 311. This sequence is similar to the NLS found in lamin A/C protein sequence. Proline residues are often positioned proximal to this sequence, to disrupt the structure of an α-helix (if present). No proline residues were identified near this NLS in *LIPA*. Therefore, this NLS may or may not act to import *LIPA* into the nucleus.

Using a number of protein prediction programs available on the Internet [Hofmann *et al.*, 1999; Bateman *et al.*, 2000], a zinc finger binding domain was identified in *LIPA*. Figure 33c illustrates the consensus sequence found in other zinc-finger proteins and compares it to the zinc-finger domain found in *LIPA*. The most common zinc finger motifs are called the C_2H_2 fingers, possessing the general consensus $CX_2CX_{12\text{-}16}HX_3H$ (where X is any amino acid) [Laity *et al.*, 2001]. The zinc-finger motif in *LIPA* exactly matches this consensus sequence. Further amino acids surrounding the cysteine and histidine residues have also been implicated in the function of the zinc finger [Wolfe *et al.*, 2000]. These other consensus sequences consist of $(F/Y)XCX_{2\text{-}5}CX_3(F/Y)X_5¥X_2HX_{3\text{-}5}H$ (where X is any amino acid and ¥ is any

hydrophobic residue). Again, the *LIPA* zinc finger motif exhibits high homology to this sequence (the second F/Y is the only residue not conserved in *LIPA*).

The zinc finger was initially identified in the *Xenopus* transcription factor TFIIIA [Miller *et al.*, 1985b], which contained 9 such zinc fingers. Since then many other zinc finger proteins have been identified and it is predicted that 0.7% of all human genes will contain these motifs [Hoovers *et al.*, 1992]. These sequences fold in the presence of a single zinc ion which is sandwiched between two antiparalled β-sheets and an α-helix (ββα) [Wolfe *et al.*, 2000] The two cysteines and two histidine are tetrahedrally co-ordinated around the zinc atom. Zinc fingers are well known for their ability to bind DNA and act as transcription factors. However DNA recognition usually requires two or more tandemly repeated zinc fingers [Wolfe *et al.*, 2000]. Many other zinc finger proteins have now been identified which do not bind DNA [Laity *et al.*, 2001] Additionally, other functions include RNA packaging, protein interactions, membrane attachment and lipid binding. An example of a zinc finger protein implicated in protein interactions is Ikaros. Ikaros is involved in lymphoid development and has the ability to form homodimers through the association of the zinc finger motifs [Sun *et al.*, 1996].

The presence of the single zinc-finger motif in LIPA appears genuine, as revealed by consensus sequence comparisons. The role of the C_2H_2 finger is unknown but may be involved in DNA or protein interactions.

Several other proteins have been found to localise at the nuclear lamina. Three of these, LAP2, emerin and MAN1 contain a conserved LEM domain found only in these proteins [Lin *et al.*, 2000]. The LEM domain is a unique 43 amino acid motif and is hypothesised to mediate interactions with DNA [Shumaker *et al.*, 2001]. By performing comparative analysis of these proteins with LIPA, it was determined that LIPA is not a LEM domain protein.

In conclusion, three putative domains were recognised in LIPA: a NLS, a zinc finger motif and evidence for several transmembrane domains.

6.5 Comparison to other proteins

Although LIPA appears novel, there were several proteins in the NCBI database exhibiting homology to this protein. BLAST protein searches were performed with the LIPA amino acid sequence. Five proteins with significant homology were identified: three human proteins KIAA0810, SUN1 and SUN2; UNC-84, a protein from the

nematode *Caenorhabditis elegans* and Sad1, a protein from fission yeast *Schizosaccharomyces pombe*. The amino acid sequences were aligned using CLUSTAL W [Thompson *et al.*, 1994] (Figure 34, illustrated in Figure 35a). LIPA was homologous to KIAA0810 over the entire length of the protein, albeit with a low degree of conservation. Of interest, KIAA0810 lacked some residues critical for zinc finger formation. All of the five proteins exhibited homology with LIPA at the extreme C-terminal end of the protein. A small domain of 194 amino acids (residues 727-913) is present in these proteins (SUN A domain); a second domain (SUN B domain) of similar size (residues 487-726) is present in LIPA and the three human proteins only. All of the five proteins are predicted to possess transmembrane domains.

Four of the five proteins have previously been compared based on their homology [Malone *et al.*, 1999]. Malone and co-workers studied UNC-84 in *C. elegans* and determined that UNC-84 is critical for nuclear migration. Nuclear migration occurs in all eukaryotic cells for a variety of interphase functions, including stages of embryogenesis in *Drosophila melanogaster* and to ensure the budding yeast *S. cerevisiae* obtains copies of chromosomes in both mother and daughter cells. It was previously unknown how the nuclei are capable of migrating within the interphase cell [Raff, 1999]. Malone *et al.* demonstrated that UNC-84 was necessary for nuclear migration. A GFP fusion of UNC-84 localised the protein to the nuclear envelope. It was, thus, concluded that UNC-84 was involved in attachment of microtubules which enabled the process of nuclear migration. Homology searches revealed that UNC-84 shared its C-terminal domain with Sad1, a protein from *S. pombe*. This protein was associated with spindle architecture in yeast and located at the nuclear membrane [Hagan and Yanagida, 1995]. Two other human proteins with homology to UNC-84 were identified using BLAST searches and referred to as Sad1-UNC-84 proteins, SUN1 and SUN2.

The fifth protein, KIAA0810, with homology to LIPA had been isolated by a group randomly sequencing cDNA clones [Nagase *et al.*, 2000]. No functional analysis data was available on this protein.

LIPA homology to these proteins would be indicative of a role in nuclear migration and nuclei positioning within the cell.

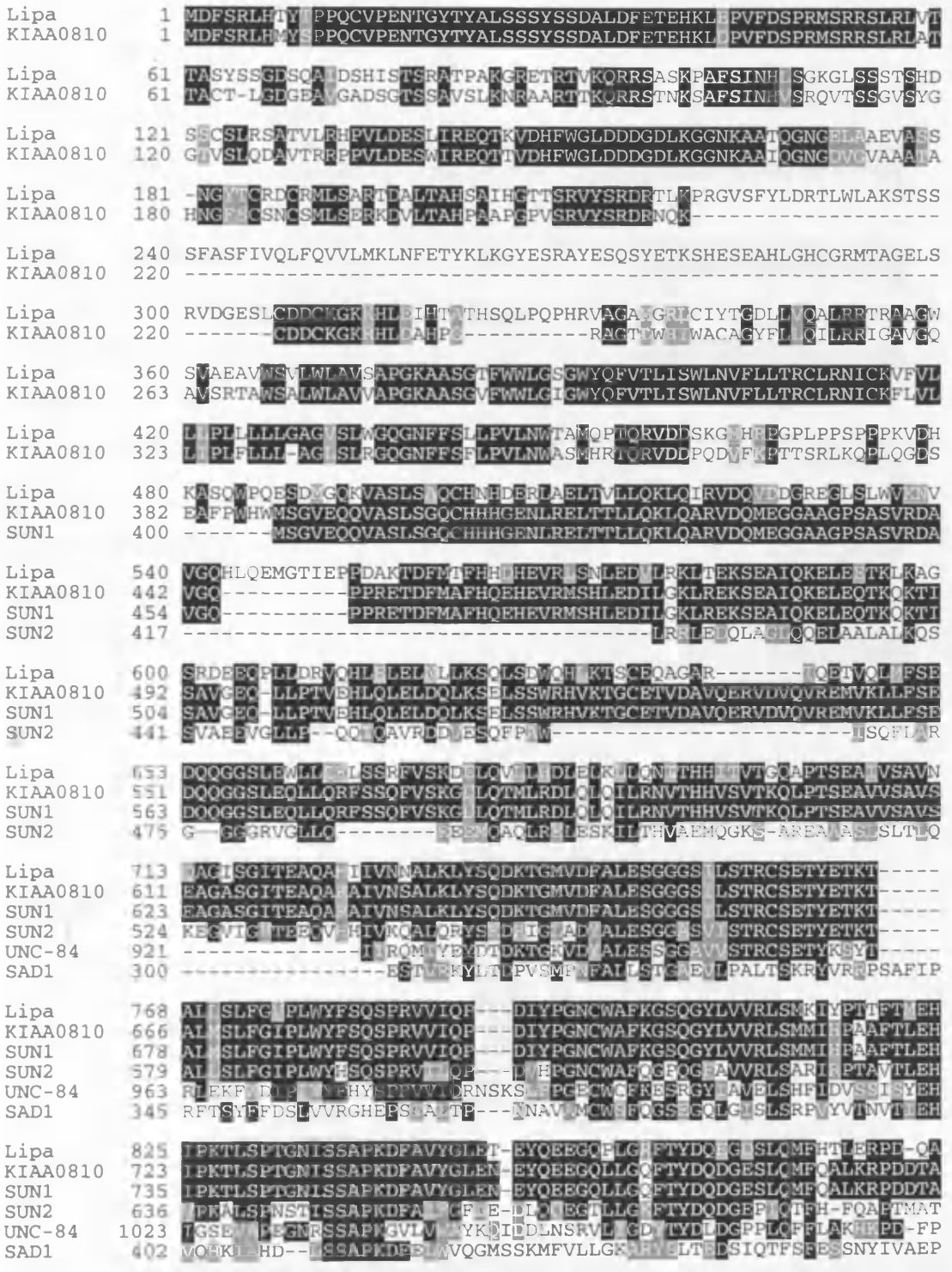

Figure 34. Amino acid comparison of LIPA with other proteins using Clustal W [Thompson *et al.*, 1994]. Amino acids are written in single letter code (Appendix IV), and the relative residue position at the start of each line. Identical amino acids are indicated by black boxes, and amino acids of similar function are indicated by grey boxes.

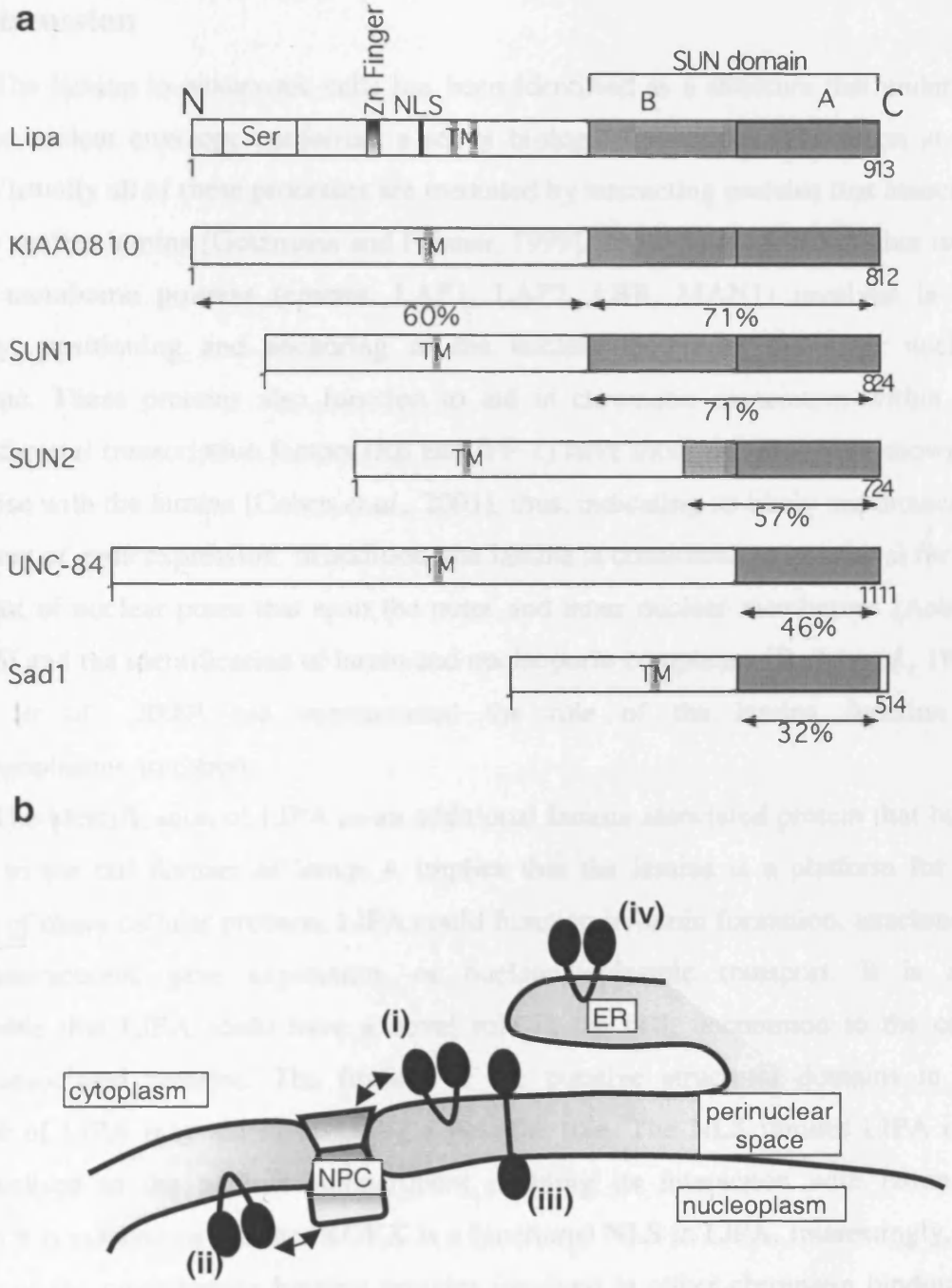

Figure 35. Comparison of LIPA with other proteins. (a) Comparison of LIPA to the SUN, UNC-84 and Sad1 proteins. The SUN-A domain is present in all six proteins (dark grey box), and the SUN-B I is present in the human and mouse proteins only (light grey box). A serine rich domain and a zinc finger was identified in LIPA, but absent from all other proteins. Amino acid identity with LIPA is given under each protein. (b) Four possible locations of LIPA within the cell, (i) outer nuclear membrane with/without association with the nuclear pore (arrow), (ii) inner nuclear membrane, with/without association with the nuclear pores (arrow), (iii) spanning the perinuclear space, (iv) at other cellular membranes.

6.6 Discussion

The lamina in eukaryotic cells has been identified as a structure that underlies the inner nuclear envelope conferring a set of biological functions [Hutchison *et al.*, 2001]. Virtually all of these processes are mediated by interacting proteins that associate with the nuclear lamina [Gotzmann and Foisner, 1999]. These have included other inner nuclear membrane proteins (emerin, LAP1, LAP2, LBR, MAN1) involved in the assembly, positioning and anchoring of the nuclear lamina at the inner nuclear membrane. These proteins also function to aid in chromatin association within the lamina. Several transcription factors (Rb and IPF-1) have more recently been shown to co-localise with the lamina [Cohen *et al.*, 2001], thus, indicating its likely importance in the context of gene expression. In addition, the lamina is considered to be critical for the placement of nuclear pores that span the outer and inner nuclear membranes [Aebi *et al.*, 1986] and the identification of lamin and nucleoporin complexes [Radu *et al.*, 1995; Smythe *et al.*, 2000] has substantiated the role of the lamina function in nucleocytoplasmic transport.

The identification of LIPA as an additional lamina associated protein that binds directly to the tail domain of lamin A implies that the lamina is a platform for the docking of many cellular proteins. LIPA could function in lamin formation, attachment, DNA interactions, gene expression, or nucleocytoplasmic transport. It is also conceivable that LIPA could have a novel role in the cell, uncommon to the other lamina associated proteins. The finding of the putative structural domains in the sequence of LIPA may aid in deducing a possible role. The NLS implies LIPA is at least localised to the nuclear compartment enabling its interaction with lamin A, although it is not known whether KGKK is a functional NLS in LIPA. Interestingly, the majority of the other lamina binding proteins involved in either chromatin binding or the anchoring of the lamina possess transmembrane domains (LAP1, LAP2β, emerin, MAN1, LBR, nurim). Therefore, the presence of two or more transmembrane domains in LIPA is consistent with other lamina proteins and suggests LIPA localisation at the inner nuclear membrane.

The presence of a single zinc finger in LIPA is intriguing as most DNA binding zinc finger proteins contain tandemly repeated fingers [Wolfe *et al.*, 2000]. Therefore, it could have DNA binding and/or gene expression properties. New roles are now being assigned to zinc finger containing proteins, including protein-protein interactions, lipid

binding and membrane attachment [Laity *et al.*, 2001]; LIPA could, potentially, function in any one of these ways. Interestingly, the nuclear pore protein Nup153 interacts with lamin B3 and contains several zinc finger domains [Smythe *et al.*, 2000]. It has been suggested that Nup153 functions to export mRNA from the nucleus to the cytoplasm. The presence of the zinc finger in LIPA could, therefore, be involved in nucleoplasmic transport.

The finding of homology between the C-terminus of LIPA, UNC-84 and the UNC-84-related proteins [Malone *et al.*, 1999] implies a role for LIPA in nuclear migration. Subcellular localisation experiments were performed with UNC-84, positioning the protein at the nuclear envelope. It was assumed that the protein was present at the outer nuclear membrane, in view of its role in the nuclear migration process. Given LIPA exhibits strong homology to the SUN domains present in these nuclear migration proteins, the obvious location for LIPA would also be at the outer nuclear membrane. Thus, it is difficult to envisage how and when LIPA would interact with lamin A. However, it has recently been suggested that UNC-84 is an inner nuclear membrane protein [Cohen *et al.*, 2001] (Figure 6). Several possibilities of LIPA localisation are illustrated in Figure 35b. Theoretically, LIPA could bind at firstly, the inner nuclear membrane (either interacting with just the lamina or the lamina and the nuclear pores); secondly, the outer nuclear membrane (its interaction with lamin A incorrect); third, the inner and outer membranes spanning the perinuclear space (explaining lamin A binding and SUN domain homology); or alternatively, a different membrane within the cell (the binding of lamin A would, thus, be a further function, analogous to lamin A-SREBP1 interaction).

The role of LIPA in the lamin A/C diseases is not known. It is possible that the effects of lamin A/C mutations are mediated through this interaction with LIPA. As nuclear migration is considered to have a role in the development of cells and tissues [Raff, 1999], it cannot be excluded that the UNC-84-like LIPA protein is involved in adipocyte and/or myocyte development and maintenance

7 GENERAL DISCUSSION

7.1 *LMNA* mutation causes partial lipodystrophy and muscle disorders

Several strategies exist for the detection of causative genes for human disorders. Positional cloning is a robust method that uses families suffering from the disorder for recombination-based analyses (Section 1.4.1) to identify a chromosomal region inherited with the disease. Subsequent studies refine the genetic interval, generate a physical map and position genes and ESTs in the disease gene interval. Ultimately, candidate genes are analysed in patients for sequence alterations. FPLD was linked to chromosome 1q21 using whole-genome scans (Section 3.1.2), which specifically localised the gene to a 5.3 cM interval. Haplotype analyses in the UK cohort reduced this further to a genetic distance of 3.8 cM (Section 3.1.6), for which a physical map was constructed (Section 3.2.). Cao and Hegele reported a missense mutation in the *LMNA* gene, that segregated in FPLD families [Cao and Hegele, 2000]. This was surprising, as although *LMNA* had been placed on the UK 1q21 physical map it had been not previously been considered a candidate on account of its mutation in EDMD-AD. However, Cao and Hegele considered the lipodystrophy in FPLD to be analogous to muscular dystrophy in EDMD-AD. The location of the *LMNA* gene at 1q21, close to a highly associated marker, prompted investigation of the gene in all UK FPLD families. Missense mutations were identified in all FPLD patients. The selection of *LMNA* by Cao and Hegele, although obscure with regard to its functional candidacy in FPLD, served to isolate the causative gene. It is of interest that *LMNA* was one of approximately 30 known 1q21 genes, each implicated as the possible disease gene, as a result of a systematic positional cloning approach.

All FPLD mutations are missense and localised to two specific regions in *LMNA*, exon 8 and exon 11 (Section 4.2, 4.4 and 4.7.4). Many different types of mutations, within the *LMNA* gene, had been previously identified in three other muscle and heart disorders. These include missense, frame-shift, splice-site, null and amino acid in-frame deletion mutations located over the entire gene, predominantly identified in EDMD-AD patients. Of particular interest is a null mutation at the extreme 5 prime end of the gene, G6X, which would be predicted to produce no functional protein product. Thus, only 50% the normal levels of the *LMNA* gene product – lamin A/C,

would be present in all cells. Lamin A/C is involved in structural maintenance of the nuclear envelope and functions as a scaffold for other proteins located to the nuclear periphery [Gerace and Burke, 1988; Stuurman *et al.*, 1998; Gotzmann and Foisner, 1999]. Among patients harbouring the G6X mutation it is intriguing to query the effect of this extreme protein truncation. Possible consequences include a reduction in lamina strength and/or a perturbation of the anchoring of other proteins and chromatin within the nucleus. The finding that EDMD-X is caused by emerin dysfunction suggests that the lamin A/C-emerin interaction is defective in all EDMD patients. Emerin is aberrantly targeted in EDMD-X patients and in lamin A/C knockout mice [Fairley *et al.*, 1999; Sullivan *et al.*, 1999]. As a result, the lamin A/C G6X mutation could reduce the level of emerin at the nuclear envelope. However, this would not explain the selective loss of myocytes in these patients, as emerin and lamin A/C are widely expressed [Bione *et al.*, 1994; Broers *et al.*, 1997]. It is of interest that lamin B1 is not expressed in myocytes, whereas it is expressed in most other cell types. Therefore lamin B2 and 50% of normal lamin A/C levels would be the only lamin proteins present in the lamina of myocytes in patients harbouring a G6X mutation. Thus, structural integrity of the lamina could be compromised and, together with the elevated contractile forces within the myocyte, the weakened lamina may not function adequately. In a similar manner the other identified EDMD-AD mutations could potentially disrupt the lamin A/C structure and prevent incorporation into the lamina.

The two other disorders (LGMD1B and CMD1A) caused by *LMNA* mutation are both related at the phenotypic level to EDMD. LGMD1B is similar with regard to muscle degeneration; furthermore, EDMD patients often die as a consequence of cardiac difficulties, which are common in CMD1A. Hence, these three disorders may in fact represent variations of a common phenotype. This was supported by the identification of a frameshift mutation in a family in which four individuals each suffered from distinct muscle and cardiac abnormalities, which collectively resembled EDMD-AD, LGMD1B and CMD1A [Brodsky *et al.*, 2000]. This finding underscores the relatedness of these three disorders at the molecular level.

It is intriguing that FPLD, an apparently unrelated phenotype, also arises through *LMNA* mutation. Specifically adipocyte function is the major cell-type that is perturbed in FPLD, as opposed to myocyte abnormalities in the muscle-related phenotypes.

The two sites of FPLD mutation map to the globular tail domain of lamin A/C. The exon 8 mutations are present in both lamin A and lamin C, whereas the exon 11 mutations only result in amino acid substitution in lamin A. All FPLD mutations are missense and those in exon 8 are located on the protein exterior. The most frequently observed FPLD mutations are located within exon 8 leading to substitutions of amino acids, R482 and K486 (89% of all FPLD mutations) with either uncharged or hydrophobic amino acids. Interestingly, the exon 11 mutations which result in the amino acid substitutions R582H and R584H, are considered to cause a less severe form of lipodystrophy. This is also reflected at the molecular level as, although these two residues are basic, FPLD mutation in these cases results in their alteration to histidine, another basic amino acid. Thus, it would appear that lamin A/C contribution to the lamina is essential in myocytes and cardiomyocytes whereas the FPLD mutated residues potentially possess significant and potentially specific function in adipocytes, which may be dependent on the charge of these amino acids suggesting a protein-protein interaction is involved

7.2 Towards understanding the molecular mechanism of partial lipodystrophy

The use of a yeast two-hybrid screen with lamin A as bait identified four different interacting proteins (Section 5.7). The finding that lamin A self-interacts, specifically mediated by the globular tail domain, raises the possibility that the FPLD mutations could disrupt this association. However, this would not explain why FPLD mutations specifically affect adipocytes.

A more plausible candidate for the mediator of lamin A function/dysfunction in adipocytes is the adipocyte differentiation factor, SREBP1, which was also identified in the yeast two-hybrid interaction screen. This interaction is modulated at the tail domain of lamin A. Interestingly, SREBP1a did not interact with lamin C as revealed by preliminary yeast two-hybrid analysis. This suggests that either the lamin A specific domain (residues 567-664) interacts with SREBP1 or that two SREBP1 binding sites are necessary in the lamin A globular domain, only one of which is present in lamin C. It is tempting to speculate that the latter proposal is correct, due to the identification of two widely spaced sites of mutation in *LMNA* in FPLD individuals, one present in both lamin A and lamin C, the other in lamin A only. However, it is not yet been shown that SREBP1 interacts with lamin A at these sites. The finding that lamin A interacts with

SREBP1 and SREBP2 provides compelling evidence that the interaction is genuine, especially considering that SREBP1a and SREBP2 are only 47% identical at the amino acid level.

The SREBPs have been recognised to mediate different functions within the cell. SREBP1 exists as a longer 1a isoform and a shorter 1c isoform; the latter has strongly been implicated in lipodystrophy, as revealed from transgenic mouse studies (Section 1.2.4). Thus, its interaction with the lamin A tail domain in both humans and mice is a significant biological finding. Although lamin A and SREBP1 involvement has been identified in lipodystrophy and an interaction revealed between these two proteins, a specific molecular mechanism has not been uncovered. Furthermore, the effect of FPLD mutations has not been addressed with regard to the lamin A-SREBP1 interaction. One of three events may occur, each with distinct putative molecular outcomes: 1) no effect; 2) a decrease in interaction; 3) an increase in interaction.

If FPLD mutations do not affect the lamin A-SREBP1 interaction, then it is possible that the lamin A-SREBP1 association is not disrupted in FPLD patients and this interaction is not significant in the aetiology of lipodystrophy.

A decrease in interaction of these proteins could prevent the nuclear targeting of SREBP1. The A-type lamins may be involved in the import of SREBP1 through the nuclear pores and FPLD mutation possibly reduces the nuclear entry of SREBP1; hence SREBP1 would not be able to act as an adipogenic transcription factor and lipodystrophy could result. If the interaction is not involved in the nuclear import of SREBP1, then this interaction must occur at the other sites within the nucleus such as the entire nuclear periphery (not just the peripheral sites associated with NPCs) and intra-nuclear lamin A/C foci. Thus hypothetically, adipogenic genes may be positioned close to these sites; a decrease in SREBP1 concentration as a result of reduced interaction with lamin A/C may result in reduced exposure of specific genes to transcriptionally active SREBP1.

A final, potential consequence of lamin A/C mutation could be the increased interaction of these proteins. If the interaction affected the nuclear import, elevated nuclear SREBP1 levels would result. The scenario of increased SREBP1 in the nucleus mimics the over-expression of SREBP1 in transgenic mice (Section 1.2.4). In this event lipodystrophy may be caused by an elevation of SREBP1 in the nucleus. Conversely, if the interaction does not occur during nuclear import, but at the general nuclear periphery, the increased association of SREBP1 with lamin A would prevent the

accessibility of the transcription factor to adipogenic loci. In this event, lamin A would be predicted to lose its function to release SREBP1 upon demand. This hypothesis is supported by the observation that another transcription factor, the insulin promoter factor-1 (IPF-1), localises to the nuclear periphery [Rafiq *et al.*, 1998]. However, when activated using low concentrations of glucose, IPF-1 is rapidly redistributed from the nuclear periphery to the nucleoplasm, where it can exert its transcriptional effects.

Hence, the lamina could be involved in transcriptional regulation mediated by the binding of transcription factors. Furthermore, FPLD mutations could perturb these interactions and affect the binding of an adipocyte specific factor, of which SREBP1 is a strong potential candidate.

In support of a lamin A-SREBP1 interaction contributing to the FPLD phenotype the report by Caron and colleagues [Caron *et al.*, 2001] appears of interest. The protease inhibitor, indinavir, used to treat patients with HIV has a frequent side effect in the development of lipodystrophy. SREBP1 maturation is dependent on two site-specific proteases (Section 5.9). Caron *et al.* demonstrated that the use of indinavir prevents SREBP1 maturation and as a consequence, its nuclear targeting. These results imply that protease inhibitor-induced lipodystrophy may be associated with a lack of SREBP1 within the nucleus and by analogy, FPLD patients may also exhibit reduced nuclear SREBP1 levels. Whether lamin A mutation affects nuclear import or results in SREBP1 sequestration at the nuclear periphery requires further investigation.

The thiazoladinediones have been recognised as synthetic ligands that can activate the central adipogenic transcription factor, PPARγ (Section 1.1.3.3). Once activated, PPARγ promotes adipogenesis by the cascade activation of other adipogenic genes. Two elaborate experiments demonstrated that SREBP1 directs adipogenesis by providing endogenous ligand for PPARγ [Kim *et al.*, 1998]. Thus if the lamin A/SREBP1 interaction is defective in FPLD individuals, it could be circumvented using the TZD ligands to enable PPARγ activation and adipogenesis. In support of this is a report of several FPLD patients treated with TZDs [Cheng, 2001]. In addition to the improvement in metabolic deviations, body fat was shown to increase by 3%. Interestingly, this adipose tissue accumulation occurred specifically in subcutaneous depots, not in intra-abdominal and visceral sites.

In summary it can be hypothesised that the effect of lamin A mutation in FPLD differs from those effects in the muscle and heart disorders. Lamin A has been

demonstrated to interact with SREBP1 in a yeast two-hybrid screen, *in vitro* and *in vivo*, using both mouse and human genes. Potentially, this interaction reveals the molecular mechanism of lipodystrophy and implicates the A-type lamins in the adipogenic program.

7.3 Future directions

The nuclear lamina and A-type lamins may now be considered as crucial components for the development and maintenance of fat and muscle cells. Specifically, lamin A/C and emerin are two critical proteins at these sites. The structural integrity of the lamina, mediated through the lamins and lamin binding proteins, provides rigidity at the inner nuclear membrane. It is currently hypothesised that the reduced strength of the lamina in EDMD-AD, LGMD1B and CMD1A patients is capable of maintaining most cells, yet makes muscle nuclei susceptible to mechanical stress. Preliminary investigations have shown that the lamina is not securely positioned at the inner nuclear membrane [Fidzianska *et al.*, 1998]. Further experiments are necessary to delineate the contribution of this molecular defect to the development of disease in these patients. Analyses will need to be performed to assess the load-bearing capacity of the nucleus, in nuclei from normals and from cells harbouring lamin A/C or emerin mutations. Such an investigation may entail the use of transfected tissue culture cells and the application of pressure to the cells. The nuclear envelope and lamina could then be analysed for abnormalities in mutated cells compared to wild-type cells. More elaborate experiments would involve the generation of transgenic animals. Transgenic mice with a knock-in EDMD mutation could be generated. Muscle filaments can be isolated from the transgenic animal and subjected to rapid contraction by administering electric shocks, in order to assess rupture of the nuclear envelope compared to wild-type cells.

The unique nature of the FPLD mutations suggested a different disease mechanism and the features of the mutations indicated that a protein-protein interaction was involved. The work performed for this thesis has developed this hypothesis and has identified an intriguing lamin A/C interacting protein, SREBP1, with direct relevance to the aetiology of FPLD. However, the detection of a lamin A-SREBP1 interaction, is not definitive proof of an FPLD disease mechanism. Further studies will be required to confirm direct interaction, localise the site of binding and demonstrate the impact of *LMNA* mutations on SREBP1 function.

Firstly, it is necessary to map the domain of interaction for both proteins. Studies to date suggest SREBP1a binds to the lamin A globular tail domain. However, there is no evidence of interaction with lamin C. It would be important to map those sites in lamin that specifically interact with SREBP1a and to determine whether the full-length tail, present only in lamin A, is necessary for this interaction. Publication of the crystal structure of the lamin A globular domain will enable precise mapping of the exon 11 mutations, and localisation of these residues relative to exon 8 mutation cluster. It would be significant if these residues all map to the same surface of the protein, providing further evidence for a crucial protein interaction. The lamin A binding site in SREBP1a has been mapped to the region 227 to 487, a 260 residue domain. This domain contains the bHLH-Zip domain and has been shown to interact with importin β [Nagoshi *et al.*, 1999]. Nagoshi and colleagues used GST pull-down experiments to prove this interaction and map the importin β binding domain to residues 343 to 403 in SREBP2. This study showed that the bHLH-Zip domain specifically was capable of permitting nuclear import. Thus it is of interest, given the lamin binding domain may also map to this interval, to determine the exact interactions which occur between lamin Á, SREBP and the nucleoplasmic import machinery. One possibility is that the lamin A/SREBP1 interaction is mediated by importin β, or *vice versa*; nonetheless, this interaction is biologically significant with regard to the FPLD phenotype. Equally, a number of different proteins could complex at the nuclear pore, acting synergistically to enable SREBP1 nuclear import. In support of this, the Ran binding protein RanBPM, has also been shown to potentially interact with lamin A (Section 5.13). Attempts to uncover the true cellular interactions in this potential complex could be directed towards utilising co-immunoprecipitation experiments to detect all possible lamin A interacting proteins, especially in adipocytes (such as the 3T3-L1 cells; Section 1.1.1.5). To specifically detect proteins that directly interact, *in vitro* GST pull-downs could be performed using only the two purified proteins. Currently, the whole lysate from the TNT® kit is used in the pull-down, thus accessory proteins potentially involved in mediating the lamin A/SREBP1a may be present. Using chemicals which disrupt functions of the other proteins (e.g. GMP-PNP inhibits importin β interactions [Smythe *et al.*, 2000]) or specifically using the two purified proteins of interest may provide insight as to the precise molecular mechanism of the lamin A and SREBP1 interaction.

Upon activation, SREBP1 adopts a dispersed nucleoplasmic distribution. Given that the 260 residue domain (residues 227-487) interacts with lamin A, it may alone localise to the nuclear periphery. It has already been shown that lamin A harbouring an R482Q mutation is correctly localised to the nuclear periphery in adipocytes [Holt *et al.*, 2001], thus it would be interesting to investigate the precise nuclear positioning of SREBP1 in mutated cells compared to wild-type cells.

Regardless of the plethora of investigations possible to investigate the lamin A/SREBP1 interaction, it is the biological consequences of FPLD mutation that need be addressed. The generation of a transgenic knock-in mouse harbouring an FPLD mutation would confirm lamin A involvement in lipodystrophy. With this resource a range of cell biological-functional assays could be achieved, which would not be possible in human FPLD subjects. In addition to this lengthy investigation, tissue culture experiments could be performed to investigate the downstream effects of lamin A/C mutation. If the lamin A/SREBP1 interaction is relevant in FPLD, then transfection of an FPLD mutant could disrupt SREBP1-directed gene expression and/or the availability of endogenous ligands for PPARγ. Luciferase gene assays can be developed with the use of E-boxes, SRE-1 boxes or PPARγ responsive elements (ARE; Section 1.1.3.2). Using this system, a quantitative approach would be utilised to investigate the effect of FPLD mutations, which may be critical, as lipodystrophy could be a consequence of a subtle defect.

Although the lamin A/SREBP1 interaction is attractive in the pathogenesis of lipodystrophy, it cannot be excluded that other molecular mechanisms are also relevant to the FPLD phenotype. Nonetheless, given the features of the FPLD mutations, it is likely that the defect involves an interacting protein. Bearing this in mind, the interaction of lamin A with the novel protein, LIPA, requires further investigation. Two essential experiments appear obvious. The first is the cellular localisation of LIPA and the second is its expression pattern in various tissues. If LIPA localises to the nuclear periphery, then this would suggest that its interaction with lamin A is *bona fide*. Furthermore, if LIPA exhibits tissue specific expression, then this interaction may have a biological role unique to that tissue. Several transcription factors, including Rb and IPF-1, have been demonstrated to associate with the nuclear lamina. Thus, the role of the zinc finger in LIPA must be determined. Either it is capable of binding DNA and acting as a transcription factor, or possesses a different biological function within the nucleus.

Emerin is a serine-rich, lamin A interacting protein and LIPA possesses both of these two qualities. Thus it may be possible that mutation in LIPA results in other muscular dystrophy phenotypes. The genes for several other muscular dystrophies have evaded identification, thus the mapping of the *LIPA* gene would potentially aid in these studies.

The observed interaction of lamin A and SREBP1 provide little insight in regard of two recognised features of the FPLD phenotype: a) why do FPLD subjects possess normal or elevated adipose tissue levels in the face and neck; and, b) why is FPLD absent at birth, yet develops during puberty? A comparative analysis of neck adipose tissue and other adipose tissue is necessary. The relative expression of lamin A/C, other lamins, lamin binding proteins, all SREBP isoforms and all other adipogenic markers is required, toward understanding the molecular differences, if any, which exist between adipose tissue from these two sites. Secondly, the onset of lipodystrophy during early adolescence implies the involvement of hormones in the initiation of adipocyte degeneration. Interestingly, a retinoic acid responsive element has recently been mapped to the lamin A/C promoter [Okumura *et al.*, 2000], thus lamin A/C expression may correlate with the range of hormonal changes which occur during puberty.

7.4 Conclusion

The positional cloning of the gene responsible for familial partial lipodystrophy has revealed an important role for A-type lamins and the nuclear lamina in adipocyte biology. Furthermore, the finding that lamin A/C and other lamina components, when mutated, cause a range of muscle and heart disorders, emphasises the function of the nuclear lamina. The molecular mechanisms of these diseases, with regard to lamin A/C dysfunction, are beginning to be exposed. Several lamin A binding proteins present in adipocytes have the potential to modulate the effects of the FPLD mutations. A strong candidate involved in this putative mechanism is SREBP1, an adipogenic transcription factor. Further studies are now required to substantiate this interaction and its relevance in FPLD. Ultimately, functional biological assays will determine the role of the lamin A and SREBP1 interaction in contribution to the lipodystrophy phenotype.

The results of these and future studies, through an improved understanding of the molecular mechanisms underlying the FPLD phenotype, are likely to contribute to the development of improved therapies for this distressing and disabling disorder.

REFERENCES

Aaronson, R.P. and G. Blobel. 1975. Isolation of nuclear pore complexes in association with a lamina. *Proc Natl Acad Sci U S A* **72**: 1007-11.

Aebi, U., J. Cohn, L. Buhle, and L. Gerace. 1986. The nuclear lamina is a meshwork of intermediate-type filaments. *Nature* **323**: 560-4.

Agatep, R., R. Kirkpatrick, D. Parchaliuk, R. Woods, and R. Gietz. 1998. Transformation of Saccharomyces cerevisiae by the lithium acetate/single-stranded carrier DNA/polyethylene glycol protocol. *Technical Tips Online* **1**: P01525.

Ailhaud, G. 2001. Development of White adipose Tissue and Adipocyte Differentiation. In *Adipose Tissues* (ed. S. Klaus). Landes Bioscience.

Altschul, S.F., W. Gish, W. Miller, E.W. Myers, and D.J. Lipman. 1990. Basic local alignment search tool. *J Mol Biol* **215**: 403-10.

Anderson, J.L., M. Khan, W.S. David, Z. Mahdavi, F.Q. Nuttall, E. Krech, S.G. West, J.M. Vance, M.A. Pericak-Vance, and M.A. Nance. 1999. Confirmation of linkage of hereditary partial lipodystrophy to chromosome 1q21-22. *Am J Med Genet* **82**: 161-5.

Arner, P. 1997. Regional adipocity in man. *J Endocrinol* **155**: 191-2.

Ashery-Padan, R., A.M. Weiss, N. Feinstein, and Y. Gruenbaum. 1997. Distinct regions specify the targeting of otefin to the nucleoplasmic side of the nuclear envelope. *J Biol Chem* **272**: 2493-9.

Barak, Y., M.C. Nelson, E.S. Ong, Y.Z. Jones, P. Ruiz-Lozano, K.R. Chien, A. Koder, and R.M. Evans. 1999. PPAR gamma is required for placental, cardiac, and adipose tissue development. *Mol Cell* **4**: 585-95.

Barraquer Ferre, L. 1949. Pathogenesis of progressive cephalothoracic lipodystrophy (Barraquers disease). *J Nerv Ment Dis* **109**: 113-121.

Barton, R.M. and H.J. Worman. 1999. Prenylated prelamin A interacts with Narf, a novel nuclear protein. *J Biol Chem* **274**: 30008-18.

Bateman, A., E. Birney, R. Durbin, S.R. Eddy, K.L. Howe, and E.L. Sonnhammer. 2000. The Pfam protein families database. *Nucleic Acids Res* **28**: 263-6.

Becker, P.E. 1986. Dominant autosomal muscular dystrophy with early contractures and cardiomyopathy (Hauptmann-Thannhauser). *Hum Genet* **74**: 184.

Behrens, G.M., D. Lloyd, H.H. Schmidt, R.E. Schmidt, and R.C. Trembath. 2000. Lessons from lipodystrophy: *LMNA*, encoding lamin A/C, in HIV therapy-associated lipodystrophy. *AIDS* **14**: 1854-5.

Berardinelli, W. 1954. An undiagnosed endocrinometabolic syndrome: report of two cases. *J Clin Endocrinol Metab* **14**: 193-204.

Billings, J.K., S.S. Milgraum, A.K. Gupta, J.T. Headington, and J.E. Rasmussen. 1987. Lipoatrophic panniculitis: a possible autoimmune inflammatory disease of fat. Report of three cases. *Arch Dermatol* **123**: 1662-6.

Bione, S., E. Maestrini, S. Rivella, M. Mancini, S. Regis, G. Romeo, and D. Toniolo. 1994. Identification of a novel X-linked gene responsible for Emery-Dreifuss muscular dystrophy. *Nat Genet* **8**: 323-7.

Birnboim, H.C. and J. Doly. 1979. A rapid alkaline extraction procedure for screening recombinant plasmid DNA. *Nucleic Acids Res* **7**: 1513-23.

Bjorntorp, P. 1991. Metabolic implications of body fat distribution. *Diabetes Care* **14**: 1132-43.

Blobel, G. 1985. Gene gating: a hypothesis. *Proc Natl Acad Sci U S A* **82**: 8527-9.

Boeke, J.D., J. Trueheart, G. Natsoulis, and G.R. Fink. 1987. 5-Fluoroorotic acid as a selective agent in yeast molecular genetics. *Methods Enzymol* **154**: 164-75.

Bolinder, J., L. Kager, J. Ostman, and P. Arner. 1983. Differences at the receptor and postreceptor levels between human omental and subcutaneous adipose tissue in the action of insulin on lipolysis. *Diabetes* **32**: 117-23.

Bonne, G., M.R. Di Barletta, S. Varnous, H.M. Becane, E.H. Hammouda, L. Merlini, F. Muntoni, C.R. Greenberg, F. Gary, J.A. Urtizberea, D. Duboc, M. Fardeau, D. Toniolo, and K. Schwartz. 1999. Mutations in the gene encoding lamin A/C cause autosomal dominant Emery-Dreifuss muscular dystrophy. *Nat Genet* **21**: 285-8.

Bonne, G., E. Mercuri, A. Muchir, A. Urtizberea, H.M. Becane, D. Recan, L. Merlini, M. Wehnert, R. Boor, U. Reuner, M. Vorgerd, E.M. Wicklein, B. Eymard, D. Duboc, I. Penisson-Besnier, J.M. Cuisset, X. Ferrer, I. Desguerre, D. Lacombe, K. Bushby, C. Pollitt, D. Toniolo, M. Fardeau, K. Schwartz, and F. Muntoni. 2000. Clinical and molecular genetic spectrum of autosomal dominant Emery-Dreifuss muscular dystrophy due to mutations of the lamin A/C gene. *Ann Neurol* **48**: 170-80.

Boschmann, M. 2001. Heterogeneity of Adipose Tissue Metabolism. In *Adipose Tissues* (ed. S. Klaus). Landes Bioscience.

Brasaemle, D.L., D.M. Levin, D.C. Adler-Wailes, and C. Londos. 2000. The lipolytic stimulation of 3T3-L1 adipocytes promotes the translocation of hormone-sensitive lipase to the surfaces of lipid storage droplets. *Biochim Biophys Acta* **1483**: 251-62.

Brent, R. and M. Ptashne. 1985. A eukaryotic transcriptional activator bearing the DNA specificity of a prokaryotic repressor. *Cell* **43**: 729-36.

Brent, R. and R.L. Finley, Jr. 1997. Understanding gene and allele function with two-hybrid methods. *Annu Rev Genet* **31**: 663-704.

Brodsky, G.L., F. Muntoni, S. Miocic, G. Sinagra, C. Sewry, and L. Mestroni. 2000. Lamin A/C gene mutation associated with dilated cardiomyopathy with variable skeletal muscle involvement. *Circulation* **101**: 473-6.

Broers, J.L., B.M. Machiels, H.J. Kuijpers, F. Smedts, R. van den Kieboom, Y. Raymond, and F.C. Ramaekers. 1997. A- and B-type lamins are differentially expressed in normal human tissues. *Histochem Cell Biol* **107**: 505-17.

Brown, M.S. and J.L. Goldstein. 1997. The SREBP pathway: regulation of cholesterol metabolism by proteolysis of a membrane-bound transcription factor. *Cell* **89**: 331-40.

Brown, M.S. and J.L. Goldstein. 1999. A proteolytic pathway that controls the cholesterol content of membranes, cells, and blood. *Proc Natl Acad Sci U S A* **96**: 11041-8.

Burn, J. and M. Baraitser. 1986. Partial lipoatrophy with insulin resistant diabetes and hyperlipidaemia (Dunnigan syndrome). *J Med Genet* **23**: 128-30.

Cao, H. and R.A. Hegele. 2000. Nuclear lamin A/C R482Q mutation in canadian kindreds with Dunnigan-type familial partial lipodystrophy. *Hum Mol Genet* **9**: 109-12.

Cao, Z., R.M. Umek, and S.L. McKnight. 1991. Regulated expression of three C/EBP isoforms during adipose conversion of 3T3-L1 cells. *Genes Dev* **5**: 1538-52.

Caron, M., M. Auclair, C. Vigouroux, M. Glorian, C. Forest, and J. Capeau. 2001 The HIV protease inhibitor indinavir impairs sterol regulatory element-binding protein-1 intranuclear localization, inhibits preadipocyte differentiation, and induces insulin resistance. *Diabetes* **50**:1378-88.

Carr, A. and D.A. Cooper. 1998. Images in clinical medicine. Lipodystrophy associated with an HIV- protease inhibitor. *N Engl J Med* **339**: 1296.

Chehab, F.F. 2000. Leptin as a regulator of adipose mass and reproduction. *Trends Pharmacol Sci* **21**: 309-14.

Chen, J.L., L.D. Attardi, C.P. Verrijzer, K. Yokomori, and R. Tjian. 1994. Assembly of recombinant TFIID reveals differential coactivator requirements for distinct transcriptional activators. *Cell* **79**: 93-105.

Cheng, J.S. 2001. Treatment of lipodystrophy with troglitazone. *Ann Intern Med* **134**: 1153-4.

Chien, C.T., P.L. Bartel, R. Sternglanz, and S. Fields. 1991. The two-hybrid system: a method to identify and clone genes for proteins that interact with a protein of interest. *Proc Natl Acad Sci U S A* **88**: 9578-82.

Chothia, C. 1984. Principles that determine the structure of proteins. *Ann Rev Biochem* **53**: 537-572.

Christy, R.J., V.W. Yang, J.M. Ntambi, D.E. Geiman, W.H. Landschulz, A.D. Friedman, Y. Nakabeppu, T.J. Kelly, and M.D. Lane. 1989. Differentiation-induced gene expression in 3T3-L1 preadipocytes: CCAAT/enhancer binding protein interacts with and activates the promoters of two adipocyte-specific genes. *Genes Dev* **3**: 1323-35.

Chu, A., R. Rassadi, and U. Stochaj. 1998. Velcro in the nuclear envelope: LBR and LAPs. *FEBS Lett* **441**: 165-9.

Chumakov, I.M., P. Rigault, I. Le Gall, C. Bellanne-Chantelot, A. Billault, S. Guillou, P. Soularue, G. Guasconi, E. Poullier, I. Gros, and *et al.* 1995. A YAC contig map of the human genome. *Nature* **377**: 175-297.

Chung, E. and R. Gardiner. 1996. Mapping Human Disease Genes by Linkage Analysis. In *Methods in Molecular Genetics*.

Church, G.M. and W. Gilbert. 1984. Genomic sequencing. *Proc Natl Acad Sci U S A* **81**: 1991-5.

Cinti, S. 2001. Morphology of the Adipose Organ. In *Adipose Tissues* (ed. S. Klaus). Landes Bioscience.

Clements, L., S. Manilal, D.R. Love, and G.E. Morris. 2000. Direct interaction between emerin and lamin A. *Biochem Biophys Res Commun* **267**: 709-14.

Cohen, D., I. Chumakov, and J. Weissenbach. 1993. A first-generation physical map of the human genome. *Nature* **366**: 698-701.

Cohen, M., K.K. Lee, K.L. Wilson, and Y. Gruenbaum. 2001. Transcriptional repression, apoptosis, human disease and the functional evolution of the nuclear lamina. *Trends Biochem Sci* **26**: 41-7.

Collins, F.S. 1995. Positional cloning moves from perditional to traditional. *Nat Genet* **9**: 347-50.

Cornelius, P., O.A. MacDougald, and M.D. Lane. 1994. Regulation of adipocyte development. *Annu Rev Nutr* **14**: 99-129.

Cowherd, R.M., R.E. Lyle, and R.E. McGehee, Jr. 1999. Molecular regulation of adipocyte differentiation. *Semin Cell Dev Biol* **10**: 3-10.

Cryer, A. and R. Van. 1985. New perspectives in adipose tissue: Structure, Function and development. Butterworths.

Czech, C., G. Tremp, and L. Pradier. 2000. Presenilins and Alzheimer's disease: biological functions and pathogenic mechanisms. *Prog Neurobiol* **60**: 363-84.

Darlington, G.J., S.E. Ross, and O.A. MacDougald. 1998. The role of C/EBP genes in adipocyte differentiation. *J Biol Chem* **273**: 30057-60.

Dechat, T., B. Korbei, O.A. Vaughan, S. Vlcek, C.J. Hutchison, and R. Foisner. 2000. Lamina-associated polypeptide 2α binds intranuclear A-type lamins. *J Cell Sci* **113 Pt 19**: 3473-84.

Deloukas, P., G.D. Schuler, G. Gyapay, E.M. Beasley, C. Soderlund, P. Rodriguez-Tome, L. Hui, T.C. Matise, K.B. McKusick, J.S. Beckmann, S. Bentolila, M. Bihoreau, B.B. Birren, J. Browne, A. Butler, A.B. Castle, N. Chiannilkulchai, C. Clee, P.J. Day, A. Dehejia, T. Dibling, N. Drouot, S. Duprat, C. Fizames, D.R. Bentley, and *et al.* 1998. A physical map of 30,000 human genes. *Science* **282**: 744-6.

Devine, J.H., D.W. Eubank, D.E. Clouthier, P. Tontonoz, B.M. Spiegelman, R.E. Hammer, and E.G. Beale. 1999. Adipose expression of the phosphoenolpyruvate carboxykinase promoter requires peroxisome proliferator-activated receptor gamma and 9-cis- retinoic acid receptor binding to an adipocyte-specific enhancer *in vivo*. *J Biol Chem* **274**: 13604-12.

Dib, C., S. Faure, C. Fizames, D. Samson, N. Drouot, A. Vignal, P. Millasseau, S. Marc, J. Hazan, E. Seboun, M. Lathrop, G. Gyapay, J. Morissette, and J. Weissenbach. 1996. A comprehensive genetic map of the human genome based on 5,264 microsatellites. *Nature* **380**: 152-4.

Dietz, H.C., G.R. Cutting, R.E. Pyeritz, C.L. Maslen, L.Y. Sakai, G.M. Corson, E.G. Puffenberger, A. Hamosh, E.J. Nanthakumar, S.M. Curristin, and *et al.* 1991. Marfan syndrome caused by a recurrent *de novo* missense mutation in the fibrillin gene. *Nature* **352**: 337-9.

Dingwall, C. and R.A. Laskey. 1991. Nuclear targeting sequences-a consensus? *Trends Biochem Sci* **16**: 478-81.

Donis-Keller, H., P. Green, C. Helms, S. Cartinhour, B. Weiffenbach, K. Stephens, T.P. Keith, D.W. Bowden, D.R. Smith, E.S. Lander, and *et al.* 1987. A genetic linkage map of the human genome. *Cell* **51**: 319-37.

Dryja, T.P., T.L. McGee, E. Reichel, L.B. Hahn, G.S. Cowley, D.W. Yandell, M.A. Sandberg, and E.L. Berson. 1990. A point mutation of the rhodopsin gene in one form of retinitis pigmentosa. *Nature* **343**: 364-6.

Duncan, E.A., M.S. Brown, J.L. Goldstein, and J. Sakai. 1997. Cleavage site for sterol-regulated protease localized to a leu-ser bond in the lumenal loop of sterol regulatory element-binding protein-2. *J Biol Chem* **272**: 12778-85.

Dunnigan, M.G., M.A. Cochrane, A. Kelly, and J.W. Scott. 1974. Familial lipoatrophic diabetes with dominant transmission. A new syndrome. *Q J Med* **43**: 33-48.

Edelson, G. 1997. Case reports and a review of lipodystrophy. *Endocrinology and Metabolism* **4**: 69-74.

Ellis, D.J., H. Jenkins, W.G. Whitfield, and C.J. Hutchison. 1997. GST-lamin fusion proteins act as dominant negative mutants in Xenopus egg extract and reveal the function of the lamina in DNA replication. *J Cell Sci* **110**: 2507-18.

Emery, A. and F. Dreifuss. 1966. Unusual type of benign X-linked muscular dystrophy. *J Neurol Neurosurg Psychiatry* **29**: 338-342.

Emery, A.E. 1989. Emery-Dreifuss syndrome. *J Med Genet* **26**: 637-41.

Fairley, E.A., J. Kendrick-Jones, and J.A. Ellis. 1999. The Emery-Dreifuss muscular dystrophy phenotype arises from aberrant targeting and binding of emerin at the inner nuclear membrane. *J Cell Sci* **112**: 2571-82..

Fajas, L., K. Schoonjans, L. Gelman, J.B. Kim, J. Najib, G. Martin, J.C. Fruchart, M. Briggs, B.M. Spiegelman, and J. Auwerx. 1999. Regulation of peroxisome proliferator-activated receptor gamma expression by adipocyte differentiation and determination factor 1/sterol regulatory element binding protein 1:

implications for adipocyte differentiation and metabolism. *Mol Cell Biol* **19**: 5495-503.

Fatkin, D., C. MacRae, T. Sasaki, M.R. Wolff, M. Porcu, M. Frenneaux, J. Atherton, H.J. Vidaillet, Jr., S. Spudich, U. De Girolami, J.G. Seidman, C. Seidman, F. Muntoni, G. Muehle, W. Johnson, and B. McDonough. 1999. Missense mutations in the rod domain of the lamin A/C gene as causes of dilated cardiomyopathy and conduction-system disease. *N Engl J Med* **341**: 1715-24.

Fidzianska, A., D. Toniolo, I. and Hausmanowa-Petrusewicz. 1998. Ultrastructural abnormality of sarcolemmal nuclei in Emery-Dreifuss muscular dystrophy (EDMD). *J Neurol Sci* **159**: 88-93.

Fields, S. and O. Song. 1989. A novel genetic system to detect protein-protein interactions. *Nature* **340**: 245-6.

Fisher, D.Z., N. Chaudhary, and G. Blobel. 1986. cDNA sequencing of nuclear lamins A and C reveals primary and secondary structural homology to intermediate filament proteins. *Proc Natl Acad Sci U S A* **83**: 6450-4.

Flagiello, D., F. Apiou, A. Gibaud, M.F. Poupon, B. Dutrillaux, and B. Malfoy. 1997. Assignment of the genes for cellular retinoic acid binding protein 1 (CRABP1) and 2 (CRABP2) to human chromosome band 15q24 and 1q21.3, respectively, by *in situ* hybridization. *Cytogenet Cell Genet* **76**: 17-8.

Flier, J.S. 1995. The adipocyte: storage depot or node on the energy information superhighway? *Cell* **80**: 15-8.

Flier, J.S. and A.N. Hollenberg. 1999. ADD-1 provides major new insight into the mechanism of insulin action. *Proc Natl Acad Sci U S A* **96**: 14191-2.

Foisner, R. and L. Gerace. 1993. Integral membrane proteins of the nuclear envelope interact with lamins and chromosomes, and binding is modulated by mitotic phosphorylation. *Cell* **73**: 1267-79.

Forman, B.M., P. Tontonoz, J. Chen, R.P. Brun, B.M. Spiegelman, and R.M. Evans. 1995. 15-Deoxy-delta 12, 14-prostaglandin J2 is a ligand for the adipocyte determination factor PPAR gamma. *Cell* **83**: 803-12.

Franke, W.W. 1974. Structure, biochemistry, and functions of the nuclear envelope. *Int Rev Cytol* **Suppl**: 71-236.

Frayn, K.N. and S.W. Coppack. 1992. Insulin resistance, adipose tissue and coronary heart disease. *Clin Sci (Colch)* **82**: 1-8.

Freytag, S.O., D.L. Paielli, and J.D. Gilbert. 1994. Ectopic expression of the CCAAT/enhancer-binding protein alpha promotes the adipogenic program in a variety of mouse fibroblastic cells. *Genes Dev* **8**: 1654-63.

Fried, S.K., C.D. Russell, N.L. Grauso, and R.E. Brolin. 1993. Lipoprotein lipase regulation by insulin and glucocorticoid in subcutaneous and omental adipose tissues of obese women and men. *J Clin Invest* **92**: 2191-8.

Fruhbeck, G., J. Gomez-Ambrosi, F.J. Muruzabal, and M.A. Burrell. 2001. The adipocyte: a model for integration of endocrine and metabolic signaling in energy metabolism regulation. *Am J Physiol Endocrinol Metab* **280**: E827-47.

Fry, A.M., and E.A. Nigg. 1995. Cell cycle. The NIMA kinase joins forces with Cdc2. *Curr Biol* **5**:1122-5.

Fukumoto, H., T. Kayano, J.B. Buse, Y. Edwards, P.F. Pilch, G.I. Bell, and S. Seino. 1989. Cloning and characterization of the major insulin-responsive glucose transporter expressed in human skeletal muscle and other insulin-responsive tissues. *J Biol Chem* **264**: 7776-9.

Furukawa, K. and T. Kondo. 1998. Identification of the lamina-associated-polypeptide-2-binding domain of B-type lamin. *Eur J Biochem* **251**: 729-33.

Furukawa, K., C.E. Fritze, and L. Gerace. 1998. The major nuclear envelope targeting domain of LAP2 coincides with its lamin binding region but is distinct from its chromatin interaction domain. *J Biol Chem* **273**: 4213-9.

Gallagher, A.R., A. Cedzich, N. Gretz, S. Somlo, and R. Witzgall. 2000. The polycystic kidney disease protein PKD2 interacts with Hax-1, a protein associated with the actin cytoskeleton. *Proc Natl Acad Sci U S A* **97**: 4017-22.

Garg, A. 2000. Lipodystrophies. *Am J Med* **108**: 143-52.

Garg, A., J.L. Fleckenstein, R.M. Peshock, and S.M. Grundy. 1992. Peculiar distribution of adipose tissue in patients with congenital generalized lipodystrophy. *J Clin Endocrinol Metab* **75**: 358-61.

Garg, A., R. Wilson, R. Barnes, E. Arioglu, Z. Zaidi, F. Gurakan, N. Kocak, S. O'Rahilly, S.I. Taylor, S.B. Patel, and A.M. Bowcock. 1999a. A gene for congenital generalized lipodystrophy maps to human chromosome 9q34. *J Clin Endocrinol Metab* **84**: 3390-4.

Garg, A., R.M. Peshock, and J.L. Fleckenstein. 1999b. Adipose tissue distribution pattern in patients with familial partial lipodystrophy (Dunnigan variety). *J Clin Endocrinol Metab* **84**: 170-4.

Garg, A., J. Stray-Gundersen, D. Parsons, and L.A. Bertocci. 2000. Skeletal muscle morphology and exercise response in congenital generalized lipodystrophy. *Diabetes Care* **23**: 1545-50.

Garg, A., M. Vinaitheerthan, P.T. Weatherall, and A.M. Bowcock. 2001. Phenotypic heterogeneity in patients with familial partial lipodystrophy (Dunnigan variety) related to the site of missense mutations in lamin A/C gene. *J Clin Endocrinol Metab* **86**: 59-65.

Gedde-Dahl, T., Jr., O. Trygstad, L. Van Maldergem, J. Magre, C.B. van der Hagen, B. Olaisen, M. Stenersen, and B. Mevag. 1996. Genetics of the Berardinelli-Seip syndrome (congenital generalized lipodystrophy) in Norway: epidemiology and gene mapping. Berardinelli- Seip Study Group. *Acta Paediatr Suppl* **413**: 52-8.

Gerace, L. and G. Blobel. 1980. The nuclear envelope lamina is reversibly depolymerized during mitosis. *Cell* **19**: 277-87.

Gerace, L. and B. Burke. 1988. Functional organization of the nuclear envelope. *Annu Rev Cell Biol* **4**: 335-74.

Gitschier, J., W.I. Wood, T.M. Goralka, K.L. Wion, E.Y. Chen, D.H. Eaton, G.A. Vehar, D.J. Capon, and R.M. Lawn. 1984. Characterization of the human factor VIII gene. *Nature* **312**: 326-30.

Glass, C.A., J.R. Glass, H. Taniura, K.W. Hasel, J.M. Blevitt, and L. Gerace. 1993. The alpha-helical rod domain of human lamins A and C contains a chromatin binding site. *EMBO J* **12**: 4413-24.

Goldberg, M., A. Harel, M. Brandeis, T. Rechsteiner, T.J. Richmond, A.M. Weiss, and Y. Gruenbaum. 1999. The tail domain of lamin Dm0 binds histones H2A and H2B. *Proc Natl Acad Sci U S A* **96**: 2852-7.

Golden, M.P., M.A. Charles, E.R. Arquilla, G.L. Myers, B.M. Lippe, W.C. Duckworth, O.F. Zuniga, S.M. Tanner, A.M. Palmer, M. Spell, and *et al.* 1985. Insulin resistance in total lipodystrophy: evidence for a pre-receptor defect in insulin action. *Metabolism* **34**: 330-5.

Gotzmann, J. and R. Foisner. 1999. Lamins and lamin-binding proteins in functional chromatin organization. *Crit Rev Eukaryot Gene Expr* **9**: 257-65.

Green, H. and M. Meuth. 1974. An established pre-adipose cell line and its differentiation in culture. *Cell* **3**: 127-133.

Green, E.D., H.C. Riethman, J.E. Dutchik, and M.V. Olson. 1991. Detection and characterization of chimeric yeast artificial-chromosome clones. *Genomics* **11**: 658-69.

Greenberg, A.S., J.J. Egan, S.A. Wek, N.B. Garty, E.J. Blanchette-Mackie, and C. Londos. 1991. Perilipin, a major hormonally regulated adipocyte-specific phosphoprotein associated with the periphery of lipid storage droplets. *J Biol Chem* **266**: 11341-6.

Gregoire, F.M., C.M. Smas, and H.S. Sul. 1998. Understanding adipocyte differentiation. *Physiol Rev* **78**: 783-809.

Gregory, S.G., G.R. Howell, and D.R. Bentley. 1997. Genome mapping by fluorescent fingerprinting. *Genome Res* **7**: 1162-8.

Guilly, M.N., A. Bensussan, J.F. Bourge, M. Bornens, and J.C. Courvalin. 1987. A human T lymphoblastic cell line lacks lamins A and C. *EMBO J* **6**: 3795-9.

Hagan, I. and M. Yanagida. 1995. The product of the spindle formation gene sad1+ associates with the fission yeast spindle pole body and is essential for viability. *J Cell Biol* **129**: 1033-47.

Hamilton, J.A. 1998. Fatty acid transport: difficult or easy? *J Lipid Res* **39**: 467-81.

Harris, C.A., P.J. Andryuk, S.W. Cline, S. Mathew, J.J. Siekierka, and G. Goldstein. 1995. Structure and mapping of the human thymopoietin (TMPO) gene and relationship of human TMPO beta to rat lamin-associated polypeptide 2. *Genomics* **28**: 198-205.

Heald, R. and F. McKeon. 1990. Mutations of phosphorylation sites in lamin A that prevent nuclear lamina disassembly in mitosis. *Cell* **61**: 579-89.

Hegele, R.A., H. Cao, C.M. Anderson, and I.M. Hramiak. 2000. Heterogeneity of nuclear lamin A mutations in Dunnigan-type familial partial lipodystrophy. *J Clin Endocrinol Metab* **85**: 3431-5.

Hegele, R.A. 2001. Molecular basis of partial lipodystrophy and prospects for therapy. *Trends Mol Med* **7**: 121-6.

Heitlinger, E., M. Peter, M. Haner, A. Lustig, U. Aebi, and E.A. Nigg. 1991. Expression of chicken lamin B2 in *Escherichia coli*: characterization of its structure, assembly, and molecular interactions. *J Cell Biol* **113**: 485-95.

Heitlinger, E., M. Peter, A. Lustig, W. Villiger, E.A. Nigg, and U. Aebi. 1992. The role of the head and tail domain in lamin structure and assembly: analysis of

bacterially expressed chicken lamin A and truncated B2 lamins. *J Struct Biol* **108**: 74-89.

Hertzel, A.V. and D.A. Bernlohr. 2000. The mammalian fatty acid-binding protein multigene family: molecular and genetic insights into function. *Trends Endocrinol Metab* **11**: 175-80.

Hirokawa, T., S. Boon-Chieng, and S. Mitaku. 1998. SOSUI: classification and secondary structure prediction system for membrane proteins. *Bioinformatics* **14**: 378-9.

Hofmann, K. and W. Stoffel. 1993. TMbase-A database of membrane spanning proteins segments. *Biol. Chem.* **374**: 166.

Hofmann, K., P. Bucher, L. Falquet, and A. Bairoch. 1999. The PROSITE database, its status in 1999. *Nucleic Acids Res* **27**: 215-9.

Hoger, T.H., K. Zatloukal, I. Waizenegger, and G. Krohne. 1990. Characterization of a second highly conserved B-type lamin present in cells previously thought to contain only a single B-type lamin. *Chromosoma* **100**: 67-9.

Holm, C., T.G. Kirchgessner, K.L. Svenson, G. Fredrikson, S. Nilsson, C.G. Miller, J.E. Shively, C. Heinzmann, R.S. Sparkes, T. Mohandas, and *et al.* 1988. Hormone-sensitive lipase: sequence, expression, and chromosomal localization to 19 cent-q13.3. *Science* **241**: 1503-6.

Holm, C., D. Langin, V. Manganiello, P. Belfrage, and E. Degerman. 1997. Regulation of hormone-sensitive lipase activity in adipose tissue. *Methods Enzymol* **286**: 45-67.

Holt, I., L. Clements, S. Manilal, S.C. Brown, and G.E. Morris. 2001. The R482Q lamin A/C mutation that causes lipodystrophy does not prevent nuclear targeting of lamin A in adipocytes or its interaction with emerin. *Eur J Hum Genet* **9**: 204-8.

Hoovers, J.M., M. Mannens, R. John, J. Bliek, V. van Heyningen, D.J. Porteous, N.J. Leschot, A. Westerveld, and P.F. Little. 1992. High-resolution localization of 69 potential human zinc finger protein genes: a number are clustered. *Genomics* **12**: 254-63.

Horton, J.D., I. Shimomura, M.S. Brown, R.E. Hammer, J.L. Goldstein, and H. Shimano. 1998. Activation of cholesterol synthesis in preference to fatty acid synthesis in liver and adipose tissue of transgenic mice overproducing sterol regulatory element-binding protein-2. *J Clin Invest* **101**: 2331-9.

Hotamisligil, G.S., P. Arner, J.F. Caro, R.L. Atkinson, and B.M. Spiegelman. 1995. Increased adipose tissue expression of tumor necrosis factor-alpha in human obesity and insulin resistance. *J Clin Invest* **95**: 2409-15.

Hu, E., P. Tontonoz, and B.M. Spiegelman. 1995. Transdifferentiation of myoblasts by the adipogenic transcription factors PPAR gamma and C/EBP alpha. *Proc Natl Acad Sci U S A* **92**: 9856-60.

Hua, X., C. Yokoyama, J. Wu, M.R. Briggs, M.S. Brown, J.L. Goldstein, and X. Wang. 1993. SREBP-2, a second basic-helix-loop-helix-leucine zipper protein that stimulates transcription by binding to a sterol regulatory element. *Proc Natl Acad Sci U S A* **90**: 11603-7.

Hua, X., J. Sakai, M.S. Brown, and J.L. Goldstein. 1996. Regulated cleavage of sterol regulatory element binding proteins requires sequences on both sides of the endoplasmic reticulum membrane. *J Biol Chem* **271**: 10379-84.

Hudson, T.J., L.D. Stein, S.S. Gerety, J. Ma, A.B. Castle, J. Silva, D.K. Slonim, R. Baptista, L. Kruglyak, S.H. Xu, and *et al.* 1995. An STS-based map of the human genome. *Science* **270**: 1945-54.

The Huntington's Disease Collaborative Research Group. 1993. A novel gene containing a trinucleotide repeat that is expanded and unstable on Huntington's disease chromosomes. The Huntington's Disease Collaborative Research Group. *Cell* **72**: 971-83.

Hutchison, C.J., J.M. Bridger, L.S. Cox, and I.R. Kill. 1994. Weaving a pattern from disparate threads: lamin function in nuclear assembly and DNA replication. *J Cell Sci* **107**: 3259-69.

Hutchison, C.J., M. Alvarez-Reyes, and O.A. Vaughan. 2001. Lamins in disease: why do ubiquitously expressed nuclear envelope proteins give rise to tissue-specific disease phenotypes? *J Cell Sci* **114**: 9-19.

Inoue, H., H. Nojima, and H. Okayama. 1990. High efficiency transformation of *Escherichia coli* with plasmids. *Gene* **96**: 23-8.

Ioannou, P.A., C.T. Amemiya, J. Garnes, P.M. Kroisel, H. Shizuya, C. Chen, M.A. Batzer, and P.J. de Jong. 1994. A new bacteriophage P1-derived vector for the propagation of large human DNA fragments. *Nat Genet* **6**: 84-9.

Iwahana, H., K. Yoshimoto, and M. Itakara. 1992. Detection of point mutations by SSCP of PCR-amplified DNA after endonuclease digestion. *Biotechniques* **12**: 64, 66.

Jackson, S.N., T.A. Howlett, P.G. McNally, S. O'Rahilly, and R.C. Trembath. 1997. Dunnigan-Köbberling syndrome: an autosomal dominant form of partial lipodystrophy. *QJM* **90**: 27-36.

Jackson, S.N., J. Pinkney, A. Bargiotta, C.D. Veal, T.A. Howlett, P.G. McNally, R. Corral, A. Johnson, and R.C. Trembath. 1998. A defect in the regional deposition of adipose tissue (partial lipodystrophy) is encoded by a gene at chromosome 1q. *Am J Hum Genet* **63**: 534-40.

Jagatheesan, G., S. Thanumalayan, B. Muralikrishna, N. Rangaraj, A.A. Karande, and V.K. Parnaik. 1999. Colocalization of intranuclear lamin foci with RNA splicing factors. *J Cell Sci* **112**: 4651-61.

James, P., J. Halladay, and E.A. Craig. 1996. Genomic libraries and a host strain designed for highly efficient two- hybrid selection in yeast. *Genetics* **144**: 1425-36.

Kahn, C.R. 2000. Triglycerides and toggling the tummy. *Nat Genet* **25**: 6-7.

Kainulainen, K., L. Pulkkinen, A. Savolainen, I. Kaitila, and L. Peltonen. 1990. Location on chromosome 15 of the gene defect causing Marfan syndrome. *N Engl J Med* **323**: 935-9.

Kass, S., C. MacRae, H.L. Graber, E.A. Sparks, D. McNamara, H. Boudoulas, C.T. Basson, P.B. Baker 3rd, R.J. Cody, M.C. Fishman, and et al. 1994. A gene defect that causes conduction system disease and dilated cardiomyopathy maps to chromosome 1p1-1q1. *Nat Genet* **7**: 546-51.

Kawamata, H., P.J. McLean, N. Sharma, and B.T. Hyman. 2001. Interaction of alpha-synuclein and synphilin-1: effect of Parkinson's disease-associated mutations. *J Neurochem* **77**: 929-34.

Kazlauskaite, R., A.T. Santomauro, J. Goldman, K. Silver, S. Snitker, B.A. Beamer, C.J. Yen, A.R. Shuldiner, and B.L. Wajchenberg. 2001. A case of congenital generalized lipodystrophy: metabolic effects of four dietary regimens. Lack of association of CGL with polymorphism in the lamin A/C Gene. *Clin Endocrinol (Oxf)* **54**: 412-4.

Kelley, J.M., C.E. Field, M.B. Craven, D. Bocskai, U.J. Kim, S.D. Rounsley, and M.D. Adams. 1999. High throughput direct end sequencing of BAC clones. *Nucleic Acids Res* **27**: 1539-46.

Kilic, F., D.A. Johnson, and M. Sinensky. 1999. Subcellular localization and partial purification of prelamin A endoprotease: an enzyme which catalyzes the conversion of farnesylated prelamin A to mature lamin A. *FEBS Lett* **450**: 61-5.

Kim, J.B., G.D. Spotts, Y.D. Halvorsen, H.M. Shih, T. Ellenberger, H.C. Towle, and B.M. Spiegelman. 1995. Dual DNA binding specificity of ADD1/SREBP1 controlled by a single amino acid in the basic helix-loop-helix domain. *Mol Cell Biol* **15**: 2582-8.

Kim, J.B. and B.M. Spiegelman. 1996. ADD1/SREBP1 promotes adipocyte differentiation and gene expression linked to fatty acid metabolism. *Genes Dev* **10**: 1096-107.

Kim, J.B., H.M. Wright, M. Wright, and B.M. Spiegelman. 1998. ADD1/SREBP1 activates PPARgamma through the production of endogenous ligand. *Proc Natl Acad Sci U S A* **95**: 4333-7.

Kitten, G.T. and E.A. Nigg. 1991. The CaaX motif is required for isoprenylation, carboxyl methylation, and nuclear membrane association of lamin B2. *J Cell Biol* **113**: 13-23.

Klaus, S. 2001. Biological Significance of Fat and Adipose Tissues. In *Adipose Tissues* (ed. S. Klaus). Landes Bioscience.

Klein, S., F. Jahoor, R.R. Wolfe, and C.A. Stuart. 1992. Generalized lipodystrophy: *in vivo* evidence for hypermetabolism and insulin-resistant lipid, glucose, and amino acid kinetics. *Metabolism* **41**: 893-6.

Köbberling, J., B. Willms, R. Kattermann, and W. Creutzfeldt. 1975. Lipodystrophy of the extremities. A dominantly inherited syndrome associated with lipatrophic diabetes. *Humangenetik* **29**: 111-20.

Köbberling, J. and M.G. Dunnigan. 1986. Familial partial lipodystrophy: two types of an X-linked dominant syndrome, lethal in the hemizygous state. *J Med Genet* **23**: 120-7.

Kozak, M. 1984. Compilation and analysis of sequences upstream from the translational start site in eukaryotic mRNAs. *Nucleic Acids Res* **12**: 857-72.

Laity, J.H., B.M. Lee, and P.E. Wright. 2001. Zinc finger proteins: new insights into structural and functional diversity. *Curr Opin Struct Biol* **11**: 39-46.

Lawrence, R. 1946. Lipodystrophy and hepatomegaly with diabetes, lipaemia, and other metabolic disturbances. A case throwing new light on the action of insulin. *Lancet* **1**: 724.

Lehmann, J.M., L.B. Moore, T.A. Smith-Oliver, W.O. Wilkison, T.M. Willson, and S.A. Kliewer. 1995. An antidiabetic thiazolidinedione is a high affinity ligand for peroxisome proliferator-activated receptor gamma (PPAR gamma). *J Biol Chem* **270**: 12953-6.

Lennon, G., C. Auffray, M. Polymeropoulos, and M.B. Soares. 1996. The I.M.A.G.E. Consortium: an integrated molecular analysis of genomes and their expression. *Genomics* **33**:151-2.

Letovsky, S.I., R.W. Cottingham, C.J. Porter, and P.W. Li. 1998. GDB: the Human Genome Database. *Nucleic Acids Res* **26**: 94-9.

Lewin, B. 1997. Genes VI. Oxford University Press.

Li, X.J., S.H. Li, A.H. Sharp, F.C. Nucifora, Jr., G. Schilling, A. Lanahan, P. Worley, S.H. Snyder, and C.A. Ross. 1995. A huntingtin-associated protein enriched in brain with implications for pathology. *Nature* **378**: 398-402.

Lin, F.T. and M.D. Lane. 1992. Antisense CCAAT/enhancer-binding protein RNA suppresses coordinate gene expression and triglyceride accumulation during differentiation of 3T3- L1 preadipocytes. *Genes Dev* **6**: 533-44.

Lin, F. and H.J. Worman. 1993. Structural organization of the human gene encoding nuclear lamin A and nuclear lamin C. *J Biol Chem* **268**: 16321-6.

Lin, F. and H.J. Worman. 1997. Expression of nuclear lamins in human tissues and cancer cell lines and transcription from the promoters of the lamin A/C and B1 genes. *Exp Cell Res* **236**: 378-84.

Lin, F., D.L. Blake, I. Callebaut, I.S. Skerjanc, L. Holmer, M.W. McBurney, M. Paulin-Levasseur, and H.J. Worman. 2000. MAN1, an inner nuclear membrane protein that shares the LEM domain with lamina-associated polypeptide 2 and emerin. *J Biol Chem* **275**: 4840-7.

MacDougald, O.A. and M.D. Lane. 1995. Transcriptional regulation of gene expression during adipocyte differentiation. *Annu Rev Biochem* **64**: 345-73.

Magenis, R.E., C.L. Maslen, L. Smith, L. Allen, and L.Y. Sakai. 1991. Localization of the fibrillin (FBN) gene to chromosome 15, band q21.1. *Genomics* **11**: 346-51.

Magré, J., M. Delépine, E. Khallouf, T. Gedde-Dahl, L. Van Maldergem, E. Sobel, J. Papp, M. Meier, A. Mégarbané, BSCL Working Group, M. Lathrop, and J. Capeau. 2001. Identification of the gene altered in Berardinelli-Seip congenital lipodystrophy on chromosome 11q13. *Nat Genet* **28**: 365-370

Malone, C.J., W.D. Fixsen, H.R. Horvitz, and M. Han. 1999. UNC-84 localizes to the nuclear envelope and is required for nuclear migration and anchoring during *C. elegans* development. *Development* **126**: 3171-81.

Mancini, M.A., B. Shan, J.A. Nickerson, S. Penman, and W.H. Lee. 1994. The retinoblastoma gene product is a cell cycle-dependent, nuclear matrix-associated protein. *Proc Natl Acad Sci U S A* **91**: 418-22.

Manilal, S., T.M. Nguyen, and G.E. Morris. 1998. Colocalization of emerin and lamins in interphase nuclei and changes during mitosis. *Biochem Biophys Res Commun* **249**: 643-7.

Martin, L., C. Crimaudo, and L. Gerace. 1995. cDNA cloning and characterization of lamina-associated polypeptide 1C (LAP1C), an integral protein of the inner nuclear membrane. *J Biol Chem* **270**: 8822-8.

Mathieson, P.W., R. Wurzner, D.B. Oliveria, P.J. Lachmann, and D.K. Peters. 1993. Complement-mediated adipocyte lysis by nephritic factor sera. *J Exp Med* **177**: 1827-31.

Maxam, A.M. and W. Gilbert. 1977. A new method for sequencing DNA. *Proc Natl Acad Sci U S A* **74**: 560-4.

McKeon, F. 1991. Nuclear lamin proteins: domains required for nuclear targeting, assembly, and cell-cycle-regulated dynamics. *Curr Opin Cell Biol* **3**: 82-6.

McKnight, G.S., D.E. Cummings, P.S. Amieux, M.A. Sikorski, E.P. Brandon, J.V. Planas, K. Motamed, and R.L. Idzerda. 1998. Cyclic AMP, PKA, and the physiological regulation of adiposity. *Recent Prog Horm Res* **53**: 139-59.

Melcher, K. and S.A. Johnston. 1995. GAL4 interacts with TATA-binding protein and coactivators. *Mol Cell Biol* **15**: 2839-48.

Michels, V.V., P.P. Moll, F.A. Miller, A.J. Tajik, J.S. Chu, D.J. Driscoll, J.C. Burnett, R.J. Rodeheffer, J.H. Chesebro, and H.D. Tazelaar. 1992. The frequency of familial dilated cardiomyopathy in a series of patients with idiopathic dilated cardiomyopathy. *N Engl J Med* **326**: 77-82.

Miller, R., R. Layzer, M. Mellenthin, M. Golabi, R. Francoz, and J. Mall. 1985a. Emery-Dreifuss muscular dystrophy with autosomal dominant transmission. *Neurology* **35**: 1230-1233.

Miller, J., A.D. McLachlan, and A. Klug. 1985b. Repetitive zinc-binding domains in the protein transcription factor IIIA from Xenopus oocytes. *EMBO J* **4**: 1609-14.

Min, H.Y. and B.M. Spiegelman. 1986. Adipsin, the adipocyte serine protease: gene structure and control of expression by tumor necrosis factor. *Nucleic Acids Res* **14**: 8879-92.

Mitchell, S. 1885. Singular case of absence of adipose matter in the upper half of the body. *Am J Med Sci* **90**: 105-106.

Moir, R.D., A.D. Donaldson, and M. Stewart. 1991. Expression in *Escherichia coli* of human lamins A and C: influence of head and tail domains on assembly properties and paracrystal formation. *J Cell Sci* **99**: 363-72.

Moir, R.D., T.P. Spann, H. Herrmann, and R.D. Goldman. 2000. Disruption of nuclear lamin organization blocks the elongation phase of DNA replication. *J Cell Biol* **149**: 1179-92.

Moitra, J., M.M. Mason, M. Olive, D. Krylov, O. Gavrilova, B. Marcus-Samuels, L. Feigenbaum, E. Lee, T. Aoyama, M. Eckhaus, M.L. Reitman, and C. Vinson. 1998. Life without white fat: a transgenic mouse. *Genes Dev* **12**: 3168-81.

Morris, G.E. and S. Manilal. 1999. Heart to heart: from nuclear proteins to Emery-Dreifuss muscular dystrophy. *Hum Mol Genet* **8**: 1847-51.

Muchir, A., G. Bonne, A.J. van der Kooi, M. van Meegen, F. Baas, P.A. Bolhuis, M. de Visser, and K. Schwartz. 2000. Identification of mutations in the gene encoding lamins A/C in autosomal dominant limb girdle muscular dystrophy with atrioventricular conduction disturbances (LGMD1B). *Hum Mol Genet* **9**: 1453-9.

Murray, J.C., K.H. Buetow, J.L. Weber, S. Ludwigsen, T. Scherpbier-Heddema, F. Manion, J. Quillen, V.C. Sheffield, S. Sunden, G.M. Duyk, and *et al.* 1994. A comprehensive human linkage map with centimorgan density. Cooperative Human Linkage Center (CHLC). *Science* **265**: 2049-54.

Nagano, A., R. Koga, M. Ogawa, Y. Kurano, J. Kawada, R. Okada, Y.K. Hayashi, T. Tsukahara, and K. Arahata. 1996. Emerin deficiency at the nuclear membrane in patients with Emery-Dreifuss muscular dystrophy. *Nat Genet* **12**: 254-9.

Nagase, T., R. Kikuno, K. Ishikawa, M. Hirosawa, and O. Ohara. 2000. Prediction of the coding sequences of unidentified human genes. XVII. The complete sequences of 100 new cDNA clones from brain which code for large proteins *in vitro*. *DNA Res* **7**: 143-50.

Nagoshi, E., N. Imamoto, R. Sato, and Y. Yoneda. 1999. Nuclear import of sterol regulatory element-binding protein-2, a basic helix-loop-helix-leucine zipper (bHLH-Zip)-containing transcription factor, occurs through the direct interaction of importin beta with HLH- Zip. *Mol Biol Cell* **10**: 2221-33.

Nakajima, N. and T. Sado. 1993. Nucleotide sequence of a mouse lamin A cDNA and its deduced amino acid sequence. *Biochim Biophys Acta* **1171**: 311-4.

Nakamura, M., H. Masuda, J. Horii, K. Kuma, N. Yokoyama, T. Ohba, H. Nishitani, T. Miyata, M. Tanaka, and T. Nishimoto. 1998. When overexpressed, a novel centrosomal protein, RanBPM, causes ectopic microtubule nucleation similar to gamma-tubulin. *J Cell Biol* **143**: 1041-52.

Nigg, E.A. 1992. Assembly-disassembly of the nuclear lamina. *Curr Opin Cell Biol* **4**: 105-9.

Nishitani, H., E. Hirose, Y. Uchimura, M. Nakamura, M. Umeda, K. Nishii, N. Mori, and T. Nishimoto. 2001. Full-sized RanBPM cDNA encodes a protein possessing a long stretch of proline and glutamine within the N-terminal region, comprising a large protein complex. *Gene* **272**: 25-33.

Ntambi, J.M. and K. Young-Cheul. 2000. Adipocyte differentiation and gene expression. *J Nutr* **130**: 3122S-3126S.

Oefner, P.J. and P.A. Underhill. 1995. *Am J Hum Genet* **57**: A266.

Okumura, K., K. Nakamachi, Y. Hosoe, and N. Nakajima. 2000. Identification of a novel retinoic acid-responsive element within the lamin A/C promoter. *Biochem Biophys Res Commun* **269**: 197-202.

Olivecrona, G. and U. Beisiegel. 1997. Lipid binding of apolipoprotein CII is required for stimulation of lipoprotein lipase activity against apolipoprotein CII-deficient chylomicrons. *Arterioscler Thromb Vasc Biol* **17**: 1545-9.

Ophoff, R.A., G.M. Terwindt, M.N. Vergouwe, R. van Eijk, P.J. Oefner, S.M. Hoffman, J.E. Lamerdin, H.W. Mohrenweiser, D.E. Bulman, M. Ferrari, J. Haan, D. Lindhout, G.J. van Ommen, M.H. Hofker, M.D. Ferrari, and R.R. Frants. 1996. Familial hemiplegic migraine and episodic ataxia type-2 are caused by mutations in the Ca^{2+} channel gene CACNL1A4. *Cell* **87**: 543-52.

Orita, M., H. Iwahana, H. Kanazawa, K. Hayashi, and T. Sekiya. 1989. Detection of polymorphisms of human DNA by gel electrophoresis as single-strand conformation polymorphisms. *Proc Natl Acad Sci U S A* **86**: 2766-70.

Osoegawa, K., A.G. Mammoser, C. Wu, E. Frengen, C. Zeng, J.J. Catanese, and P.J. de Jong. 2001. A bacterial artificial chromosome library for sequencing the complete human genome. *Genome Res* **11**: 483-96.

Osterlund, T. 2001. Structure-function relationships of hormone-sensitive lipase. *Eur J Biochem* **268**: 1899-907.

Osuga, J., S. Ishibashi, T. Oka, H. Yagyu, R. Tozawa, A. Fujimoto, F. Shionoiri, N. Yahagi, F.B. Kraemer, O. Tsutsumi, and N. Yamada. 2000. Targeted disruption of hormone-sensitive lipase results in male sterility and adipocyte hypertrophy, but not in obesity. *Proc Natl Acad Sci U S A* **97**: 787-92.

Ozaki, T., M. Saijo, K. Murakami, H. Enomoto, Y. Taya, and S. Sakiyama. 1994. Complex formation between lamin A and the retinoblastoma gene product: identification of the domain on lamin A required for its interaction. *Oncogene* **9**: 2649-53.

Ozer, F., J. Lichtenstein, P. Kwiterovich, and V. McKusick. 1973. A 'new' genetic variety of lipodystrophy. *Clinical Research* **21**: 533.

Pajukanta, P., I. Nuotio, J.D. Terwilliger, K.V. Porkka, K. Ylitalo, J. Pihlajamaki, A.J. Suomalainen, A.C. Syvanen, T. Lehtimaki, J.S. Viikari, M. Laakso, M.R. Taskinen, C. Ehnholm, and L. Peltonen. 1998. Linkage of familial combined hyperlipidaemia to chromosome 1q21-q23. *Nat Genet* **18**: 369-73.

Panse, I., E. Vasseur, M.L. Raffin-Sanson, F. Staroz, E. Rouveix, and P. Saiag. 2000. Lipodystrophy associated with protease inhibitors. *Br J Dermatol* **142**: 496-500.

Parchaliuk, D., R. Kirkpatrick, S. Simon, R. Agatep, and R. Gietz. 1999. Yeast two-hybrid system. *Technical Tips Online* **1**: P01616.

Peter, M., G.T. Kitten, C.F. Lehner, K. Vorburger, S.M. Bailer, G. Maridor, and E.A. Nigg. 1989. Cloning and sequencing of cDNA clones encoding chicken lamins A and B1 and comparison of the primary structures of vertebrate A- and B-type lamins. *J Mol Biol* **208**: 393-404.

Peter, M., J. Nakagawa, M. Doree, J.C. Labbe, and E.A. Nigg. 1990. *In vitro* disassembly of the nuclear lamina and M phase-specific phosphorylation of lamins by cdc2 kinase. *Cell* **61**: 591-602.

Peter, M., J.S. Sanghera, S.L. Pelech, and E.A. Nigg. 1992. Mitogen-activated protein kinases phosphorylate nuclear lamins and display sequence specificity overlapping that of mitotic protein kinase p34cdc2. *Eur J Biochem* **205**: 287-94.

Peters, D.K., J.A. Charlesworth, J.G. Sissons, D.G. Williams, J.M. Boulton-Jones, D.J. Evans, O. Kourilsky, and L. Morel-Maroger. 1973. Mesangiocapillary nephritis, partial lipodystrophy, and hypocomplementaemia. *Lancet* **2**: 535-8.

Peters, J.M., R. Barnes, L. Bennett, W.M. Gitomer, A.M. Bowcock, and A. Garg. 1998. Localization of the gene for familial partial lipodystrophy (Dunnigan variety) to chromosome 1q21-22. *Nat Genet* **18**: 292-5.

Pickup, J. and G. Williams. 1997. Textbook of Diabetes: Volume 1. Blackwell Science.

Porter, W.M., O. O'Gorman-Lalor, R.J. Lane, N. Francis, and C.B. Bunker. 2000. Barraquer-Simons lipodystrophy, Raynaud's phenomenon and cutaneous vasculitis. *Clin Exp Dermatol* **25**: 277-80.

Prins, J.B., C.U. Niesler, C.M. Winterford, N.A. Bright, K. Siddle, S. O'Rahilly, N.I. Walker, and D.P. Cameron. 1997. Tumor necrosis factor-alpha induces apoptosis of human adipose cells. *Diabetes* **46**: 1939-44.

Printen, J.A., M.J. Brady, and A.R. Saltiel. 1997. PTG, a protein phosphatase 1-binding protein with a role in glycogen metabolism. *Science* **275**: 1475-8.

Pumiglia, K.M., H. LeVine, T. Haske, T. Habib, R. Jove, and S.J. Decker. 1995. A direct interaction between G-protein beta gamma subunits and the Raf-1 protein kinase. *J Biol Chem* **270**: 14251-4.

Radu, A., G. Blobel, and M.S. Moore. 1995. Identification of a protein complex that is required for nuclear protein import and mediates docking of import substrate to distinct nucleoporins. *Proc Natl Acad Sci U S A* **92**: 1769-73.

Raff, J.W. 1999. The missing (L) UNC? *Curr Biol* **9**: R708-10.

Rafiq, I., H.J. Kennedy, and G.A. Rutter. 1998. Glucose-dependent translocation of insulin promoter factor-1 (IPF-1) between the nuclear periphery and the nucleoplasm of single MIN6 beta-cells. *J Biol Chem* **273**: 23241-7.

Raffaele Di Barletta, M., E. Ricci, G. Galluzzi, P. Tonali, M. Mora, L. Morandi, A. Romorini, T. Voit, K.H. Orstavik, L. Merlini, C. Trevisan, V. Biancalana, I. Housmanowa-Petrusewicz, S. Bione, R. Ricotti, K. Schwartz, G. Bonne, and D. Toniolo. 2000. Different mutations in the *LMNA* gene cause autosomal dominant and autosomal recessive Emery-Dreifuss muscular dystrophy. *Am J Hum Genet* **66**: 1407-12.

Rangwala, S.M. and M.A. Lazar. 2000. Transcriptional control of adipogenesis. *Annu Rev Nutr* **20**: 535-59.

Reddy, P.H., M. Williams, and D.A. Tagle. 1999. Recent advances in understanding the pathogenesis of Huntington's disease. *Trends Neurosci* **22**: 248-55.

Rober, R.A., K. Weber, and M. Osborn. 1989. Differential timing of nuclear lamin A/C expression in the various organs of the mouse embryo and the young animal: a developmental study. *Development* **105**: 365-78.

Rolls, M.M., P.A. Stein, S.S. Taylor, E. Ha, F. McKeon, and T.A. Rapoport. 1999. A visual screen of a GFP-fusion library identifies a new type of nuclear envelope membrane protein. *J Cell Biol* **146**: 29-44.

Ron, D. and J.F. Habener. 1992. CHOP, a novel developmentally regulated nuclear protein that dimerizes with transcription factors C/EBP and LAP and functions as a dominant-negative inhibitor of gene transcription. *Genes Dev* **6**: 439-53.

Rosen, E.D., P. Sarraf, A.E. Troy, G. Bradwin, K. Moore, D.S. Milstone, B.M. Spiegelman, and R.M. Mortensen. 1999. PPAR gamma is required for the differentiation of adipose tissue *in vivo* and *in vitro*. *Mol Cell* **4**: 611-7.

Rosen, E.D. and B.M. Spiegelman. 2000. Molecular regulation of adipogenesis. *Annu Rev Cell Dev Biol* **16**: 145-71.

Rosen, E.D., C.J. Walkey, P. Puigserver, and B.M. Spiegelman. 2000. Transcriptional regulation of adipogenesis. *Genes Dev* **14**: 1293-307.

Ross, S.R., R.A. Graves, A. Greenstein, K.A. Platt, H.L. Shyu, B. Mellovitz, and B.M. Spiegelman. 1990. A fat-specific enhancer is the primary determinant of gene expression for adipocyte P2 *in vivo*. *Proc Natl Acad Sci U S A* **87**: 9590-4.

Ross, M., L. Romrell, and G. Kaye. 1995. Histology - A text and atlas. Williams and Wilkins.

Saiki R.K., S. Scharf, F. Faloona, K.B. Mullis, G.T. Horn, H.A. Erlich, and N. Arnheim. 1988. Enzymatic amplification of beta-globin genomic sequences and restriction site analysis for diagnosis of sickle cell anemia.. *Science* **230**: 1350-4.

Sakaki, M., H. Koike, N. Takahashi, N. Sasagawa, S. Tomioka, K. Arahata, and S. Ishiura. 2001. Interaction between emerin and nuclear lamins. *J Biochem (Tokyo)* **129**: 321-7.

Saltiel, A.R. 2000. Another hormone-sensitive triglyceride lipase in fat cells? *Proc Natl Acad Sci U S A* **97**: 535-7.

Sanger, F., S. Nicklen, and A.R. Coulson. 1977. DNA sequencing with chain-terminating inhibitors. *Proc Natl Acad Sci U S A* **74**: 5463-7.

Sato, R., J. Yang, X. Wang, M.J. Evans, Y.K. Ho, J.L. Goldstein, and M.S. Brown. 1994. Assignment of the membrane attachment, DNA binding, and transcriptional activation domains of sterol regulatory element-binding protein-1 (SREBP-1). *J Biol Chem* **269**: 17267-73.

Schaffler, A., E. Orso, K.D. Palitzsch, C. Buchler, W. Drobnik, A. Furst, J. Scholmerich, and G. Schmitz. 1999. The human apM-1, an adipocyte-specific gene linked to the family of TNFs and to genes expressed in activated T cells, is mapped to chromosome 1q21.3-q23, a susceptibility locus identified for familial combined hyperlipidaemia (FCH). *Biochem Biophys Res Commun* **260**: 416-25.

Schirmer, E.C., T. Guan, and L. Gerace. 2001. Involvement of the lamin rod domain in heterotypic lamin interactions important for nuclear organization. *J Cell Biol* **153**: 479-89.

Seip, M. 1959. Lipodystrophy and gigantism with associated endocrine manifestations: a new diencephalic syndrome? *Acta Paediat* **48**.

Seip, M. and O. Trygstad. 1996. Generalized lipodystrophy, congenital and acquired (lipoatrophy). *Acta Paediatr Suppl* **413**: 2-28.

Senior, A. and L. Gerace. 1988. Integral membrane proteins specific to the inner nuclear membrane and associated with the nuclear lamina. *J Cell Biol* **107**: 2029-36.

Shackleton, S., D.J. Lloyd, S.N. Jackson, R. Evans, M.F. Niermeijer, B.M. Singh, H. Schmidt, G. Brabant, S. Kumar, P.N. Durrington, S. Gregory, S. O'Rahilly, and R.C. Trembath. 2000. *LMNA*, encoding lamin A/C, is mutated in partial lipodystrophy. *Nat Genet* **24**: 153-6.

Shen, W.J., S. Patel, V. Natu, and F.B. Kraemer. 1998. Mutational analysis of structural features of rat hormone-sensitive lipase. *Biochemistry* **37**: 8973-9.

Shen, W.J., K. Sridhar, D.A. Bernlohr, and F.B. Kraemer. 1999. Interaction of rat hormone-sensitive lipase with adipocyte lipid-binding protein. *Proc Natl Acad Sci U S A* **96**: 5528-32.

Shen, W.J., S. Patel, R. Hong, and F.B. Kraemer. 2000. Hormone-sensitive lipase functions as an oligomer. *Biochemistry* **39**: 2392-8.

Shimano, H., J.D. Horton, R.E. Hammer, I. Shimomura, M.S. Brown, and J.L. Goldstein. 1996. Overproduction of cholesterol and fatty acids causes massive liver enlargement in transgenic mice expressing truncated SREBP-1a. *J Clin Invest* **98**: 1575-84.

Shimano, H., J.D. Horton, I. Shimomura, R.E. Hammer, M.S. Brown, and J.L. Goldstein. 1997a. Isoform 1c of sterol regulatory element binding protein is less active than isoform 1a in livers of transgenic mice and in cultured cells. *J Clin Invest* **99**: 846-54.

Shimano, H., I. Shimomura, R.E. Hammer, J. Herz, J.L. Goldstein, M.S. Brown, and J.D. Horton. 1997b. Elevated levels of SREBP-2 and cholesterol synthesis in livers of mice homozygous for a targeted disruption of the SREBP-1 gene. *J Clin Invest* **100**: 2115-24.

Shimomura, I., H. Shimano, J.D. Horton, J.L. Goldstein, and M.S. Brown. 1997. Differential expression of exons 1a and 1c in mRNAs for sterol regulatory element binding protein-1 in human and mouse organs and cultured cells. *J Clin Invest* **99**: 838-45.

Shimomura, I., R.E. Hammer, J.A. Richardson, S. Ikemoto, Y. Bashmakov, J.L. Goldstein, and M.S. Brown. 1998. Insulin resistance and diabetes mellitus in transgenic mice expressing nuclear SREBP-1c in adipose tissue: model for congenital generalized lipodystrophy. *Genes Dev* **12**: 3182-94.

Shin, C.S., M.S. Hong, C.S. Bae, and J. Lee. 1997. Enhanced production of human mini-proinsulin in fed-batch cultures at high cell density of *Escherichia coli* BL21(DE3)[pET-3aT2M2]. *Biotechnol Prog* **13**: 249-57.

Shizuya, H., B. Birren, U.J. Kim, V. Mancino, T. Slepak, Y. Tachiiri, and M. Simon. 1992. Cloning and stable maintenance of 300-kilobase-pair fragments of human DNA in *Escherichia coli* using an F-factor-based vector. *Proc Natl Acad Sci U S A* **89**: 8794-7.

Shumaker, D.K., K.K. Lee, Y.C. Tanhehco, R. Craigie, and K.L. Wilson. 2001. LAP2 binds to BAF.DNA complexes: requirement for the LEM domain and modulation by variable regions. *EMBO J* **20**: 1754-64.

Skinner, J.A. and A.R. Saltiel. 2001. Cloning and identification of MYPT3: a prenylatable myosin targetting subunit of protein phosphatase 1. *Biochem J* **356**: 257-67.

Smas, C.M. and H.S. Sul. 1993. Pref-1, a protein containing EGF-like repeats, inhibits adipocyte differentiation. *Cell* **73**: 725-34.

Smas, C.M., L. Chen, L. Zhao, M.J. Latasa, and H.S. Sul. 1999. Transcriptional repression of Pref-1 by glucocorticoids promotes 3T3-L1 adipocyte differentiation. *J Biol Chem* **274**: 12632-41.

Smith, D.B. and K.S. Johnson. 1988. Single-step purification of polypeptides expressed in *Escherichia coli* as fusions with glutathione S-transferase. *Gene* **67**: 31-40.

Smith, L.M., J.Z. Sanders, R.J. Kaiser, P. Hughes, C. Dodd, C.R. Connell, C. Heiner, S.B. Kent, and L.E. Hood. 1986. Fluorescence detection in automated DNA sequence analysis. *Nature* **321**: 674-9.

Smith, J.R., T.F. Osborne, M.S. Brown, J.L. Goldstein, and G. Gil. 1988. Multiple sterol regulatory elements in promoter for hamster 3-hydroxy-3- methylglutaryl-coenzyme A synthase. *J Biol Chem* **263**: 18480-7.

Smith, J.R., T.F. Osborne, J.L. Goldstein, and M.S. Brown. 1990. Identification of nucleotides responsible for enhancer activity of sterol regulatory element in low density lipoprotein receptor gene. *J Biol Chem* **265**: 2306-10.

Smith, S.J., S. Cases, D.R. Jensen, H.C. Chen, E. Sande, B. Tow, D.A. Sanan, J. Raber, R.H. Eckel, and R.V. Farese Jr. 2000. Obesity resistance and multiple mechanisms of triglyceride synthesis in mice lacking *Dgat*. *Nat Genet* **25**: 87-90.

Smythe, C., H.E. Jenkins, and C.J. Hutchison. 2000. Incorporation of the nuclear pore basket protein nup153 into nuclear pore structures is dependent upon lamina assembly: evidence from cell- free extracts of Xenopus eggs. *EMBO J* **19**: 3918-31.

Sniderman, A.D. and K. Cianflone. 1994. The adipsin-ASP pathway and regulation of adipocyte function. *Ann Med* **26**: 388-93.

Soderlund C., S. Humphrey, A. Dunhum, and L. French. 2000. Contigs built with fingerprints, markers and FPC v4.7. *Genome Research* **10**:1772-1787.

South, A.P., A. Cabral, J.H. Ives, C.H. James, G. Mirza, I. Marenholz, D. Mischke, C. Backendorf, J. Ragoussis, and D. Nizetic. 1999. Human epidermal differentiation complex in a single 2.5 Mbp long continuum of overlapping DNA cloned in bacteria integrating physical and transcript maps. *J Invest Dermatol* **112**: 910-8.

Speckman, R.A., A. Garg, F. Du, L. Bennett, R. Veile, E. Arioglu, S.I. Taylor, M. Lovett, and A.M. Bowcock. 2000. Mutational and haplotype analyses of families with familial partial lipodystrophy (Dunnigan variety) reveal recurrent missense mutations in the globular C-terminal domain of lamin A/C. *Am J Hum Genet* **66**: 1192-8.

Stabler, S.M., L.L. Ostrowski, S.M. Janicki, and M.J. Monteiro. 1999. A myristoylated calcium-binding protein that preferentially interacts with the Alzheimer's disease presenilin 2 protein. *J Cell Biol* **145**: 1277-92.

Steffan, J.S., A. Kazantsev, O. Spasic-Boskovic, M. Greenwald, Y.Z. Zhu, H. Gohler, E.E. Wanker, G.P. Bates, D.E. Housman, and L.M. Thompson. 2000. The Huntington's disease protein interacts with p53 and CREB-binding protein and represses transcription. *Proc Natl Acad Sci U S A* **97**: 6763-8.

Stevens, A. and J. Lowe. 1997. Human Histology. Mosby.

Strachan, T. and A.P. Read. 1996. Human Molecular Genetics. BIOS Scientific Publishers Ltd.

Stuurman, N., S. Heins, and U. Aebi. 1998. Nuclear lamins: their structure, assembly, and interactions. *J Struct Biol* **122**: 42-66.

Sullivan, T., D. Escalante-Alcalde, H. Bhatt, M. Anver, N. Bhat, K. Nagashima, C.L. Stewart, and B. Burke. 1999. Loss of A-type lamin expression compromises nuclear envelope integrity leading to muscular dystrophy. *J Cell Biol* **147**: 913-20.

Sun, L., A. Liu, and K. Georgopoulos. 1996. Zinc finger-mediated protein interactions modulate Ikaros activity, a molecular control of lymphocyte development. *EMBO J* **15**: 5358-69.

Takagaki, Y., L.C. Ryner, and J.L. Manley. 1988. Separation and characterization of a poly(A) polymerase and a cleavage/specificity factor required for pre-mRNA polyadenylation. *Cell* **52**: 731-42.

Tanaka, T., N. Yoshida, T. Kishimoto, and S. Akira. 1997. Defective adipocyte differentiation in mice lacking the C/EBPbeta and/or C/EBPdelta gene. *EMBO J* **16**: 7432-43.

Tang, Q.Q., M.S. Jiang, and M.D. Lane. 1997. Repression of transcription mediated by dual elements in the CCAAT/enhancer binding protein alpha gene. *Proc Natl Acad Sci U S A* **94**: 13571-5.

Taniura, H., C. Glass, and L. Gerace. 1995. A chromatin binding site in the tail domain of nuclear lamins that interacts with core histones. *J Cell Biol* **131**: 33-44.

Tatusova, T.A. and T.L. Madden. 1999. BLAST 2 Sequences, a new tool for comparing protein and nucleotide sequences. *FEMS Microbiol Lett* **174**: 247-50.

Taylor, S. and P. Jones. 1979. Multiple new phenotypes induced in 10T1/2 and 3T3 cells treated with 5-azacytidine. *Cell* **17**: 771-779.

Taylor, J., C.A. Sewry, V. Dubowitz, and F. Muntoni. 1998. Early onset, autosomal recessive muscular dystrophy with Emery-Dreifuss phenotype and normal emerin expression. *Neurology* **51**: 1116-20.

Terwilliger, J.D. and J. Ott. 1994. Handbook of Human Genetic Linkage. John Hopkins University Press.

Thabrew, I. and R. Ayling. 2001. Biochemistry for Clinical Medicine. Greenwich Medical Media Ltd.

Thompson, J.D., D.G. Higgins, and T.J. Gibson. 1994. CLUSTAL W: improving the sensitivity of progressive multiple sequence alignment through sequence weighting, position-specific gap penalties and weight matrix choice. *Nucleic Acids Res* **22**: 4673-80.

Tontonoz, P., J.B. Kim, R.A. Graves, and B.M. Spiegelman. 1993. ADD1: a novel helix-loop-helix transcription factor associated with adipocyte determination and differentiation. *Mol Cell Biol* **13**: 4753-9.

Tontonoz, P., R.A. Graves, A.I. Budavari, H. Erdjument-Bromage, M. Lui, E. Hu, P. Tempst, and B.M. Spiegelman. 1994a. Adipocyte-specific transcription factor ARF6 is a heterodimeric complex of two nuclear hormone receptors, PPAR gamma and RXR alpha. *Nucleic Acids Res* **22**: 5628-34.

Tontonoz, P., E. Hu, and B.M. Spiegelman. 1994b. Stimulation of adipogenesis in fibroblasts by PPAR gamma 2, a lipid-activated transcription factor. *Cell* **79**: 1147-56.

Tontonoz, P., E. Hu, J. Devine, E.G. Beale, and B.M. Spiegelman. 1995. PPAR gamma 2 regulates adipose expression of the phosphoenolpyruvate carboxykinase gene. *Mol Cell Biol* **15**: 351-7.

Trayhurn, P., N. Hoggard, and D.V. Rayner. 2001. White adipose tissue as a secretory and endocrine organ: Leptin and other secreted proteins. In *Adipose Tissues* (ed. S. Klaus). Landes Bioscience.

Unger, R.H., Y.T. Zhou, and L. Orci. 1999. Regulation of fatty acid homeostasis in cells: novel role of leptin. *Proc Natl Acad Sci U S A* **96**: 2327-32.

Ursich, M.J., R.T. Fukui, M.S. Galvao, J.A. Marcondes, A.T. Santomauro, M.E. Silva, D.M. Rocha, and B.L. Wajchenberg. 1997. Insulin resistance in limb

and trunk partial lipodystrophy (type 2 Köbberling-Dunnigan syndrome). *Metabolism* **46**: 159-63.

Vague, J. 1956. The degree of masculine differentiation of obesities, a factor determining predisposition to diabetes, atherosclerosis, gout and uric calculous disease. *Am J Clin Nutr* **4**: 20-34.

van Criekinge, W. and R. Beyaert. 1999. Yeast two-hybrid: State of the art. *Biological Procedures Online* **2**.

van der Kooi, A.J., T.M. Ledderhof, W.G. de Voogt, C.J. Res, G. Bouwsma, D. Troost, H.F. Busch, A.E. Becker, and M. de Visser. 1996. A newly recognized autosomal dominant limb girdle muscular dystrophy with cardiac involvement. *Ann Neurol* **39**: 636-42.

van der Kooi, A.J., M. van Meegen, T.M. Ledderhof, E.M. McNally, M. de Visser, and P.A. Bolhuis. 1997. Genetic localization of a newly recognized autosomal dominant limb- girdle muscular dystrophy with cardiac involvement (LGMD1B) to chromosome 1q11-21. *Am J Hum Genet* **60**: 891-5.

Vasu, S.K. and D.J. Forbes. 2001. Nuclear pores and nuclear assembly. *Curr Opin Cell Biol* **13**: 363-75.

Vigouroux, C., L. Fajas, E. Khallouf, M. Meier, G. Gyapay, O. Lascols, J. Auwerx, J. Weissenbach, J. Capeau, and J. Magre. 1998. Human peroxisome proliferator-activated receptor-gamma2: genetic mapping, identification of a variant in the coding sequence, and exclusion as the gene responsible for lipoatrophic diabetes. *Diabetes* **47**: 490-2.

Vigouroux, C., J. Magre, M.C. Vantyghem, C. Bourut, O. Lascols, S. Shackleton, D.J. Lloyd, B. Guerci, G. Padova, P. Valensi, A. Grimaldi, R. Piquemal, P. Touraine, R.C. Trembath, and J. Capeau. 2000. Lamin A/C gene: sex-determined expression of mutations in Dunnigan-type familial partial lipodystrophy and absence of coding mutations in congenital and acquired generalized lipoatrophy. *Diabetes* **49**: 1958-62.

Vojtek, A.B., S.M. Hollenberg, and J.A. Cooper. 1993. Mammalian Ras interacts directly with the serine/threonine kinase Raf. *Cell* **74**: 205-14.

Wahrenberg, H., F. Lonnqvist, and P. Arner. 1989. Mechanisms underlying regional differences in lipolysis in human adipose tissue. *J Clin Invest* **84**: 458-67.

Walter, M.A. and P.N. Goodfellow. 1993. Radiation hybrids: irradiation and fusion gene transfer. *Trends Genet* **9**: 352-6.

Walter, M.A., D.J. Spillett, P. Thomas, J. Weissenbach, and P.N. Goodfellow. 1994. A method for constructing radiation hybrid maps of whole genomes. *Nat Genet* **7**: 22-8.

Wang, N.D., M.J. Finegold, A. Bradley, C.N. Ou, S.V. Abdelsayed, M.D. Wilde, L.R. Taylor, D.R. Wilson, and G.J. Darlington. 1995. Impaired energy homeostasis in C/EBP alpha knockout mice. *Science* **269**: 1108-12.

Wang, D.G., J.B. Fan, C.J. Siao, A. Berno, P. Young, R. Sapolsky, G. Ghandour, N. Perkins, E. Winchester, J. Spencer, L. Kruglyak, L. Stein, L. Hsie, T. Topaloglou, E. Hubbell, E. Robinson, M. Mittmann, M.S. Morris, N. Shen, D. Kilburn, J. Rioux, C. Nusbaum, S. Rozen, T.J. Hudson, E.S. Lander, and *et al.* 1998. Large-scale identification, mapping, and genotyping of single-nucleotide polymorphisms in the human genome. *Science* **280**: 1077-82.

Wanker, E.E., C. Rovira, E. Scherzinger, R. Hasenbank, S. Walter, D. Tait, J. Colicelli, and H. Lehrach. 1997. HIP-I: a huntingtin interacting protein isolated by the yeast two- hybrid system. *Hum Mol Genet* **6**: 487-95.

Ward, G.E. and M.W. Kirschner. 1990. Identification of cell cycle-regulated phosphorylation sites on nuclear lamin C. *Cell* **61**: 561-77.

Watson, J.D. and F.H.C. Crick. 1953. A structure for DNA. *Nature* **171**: 737-738.

Weber, J.L. and P.E. May. 1989. Abundant class of human DNA polymorphisms which can be typed using the polymerase chain reaction. *Am J Hum Genet* **44**: 388-96.

Weinstein, L.S., A. Shenker, P.V. Gejman, M.J. Merino, E. Friedman, and A.M. Spiegel. 1991. Activating mutations of the stimulatory G protein in the McCune-Albright syndrome. *N Engl J Med* **325**: 1688-95.

Weissenbach, J., G. Gyapay, C. Dib, A. Vignal, J. Morissette, P. Millasseau, G. Vaysseix, and M. Lathrop. 1992. A second-generation linkage map of the human genome. *Nature* **359**: 794-801.

Wheeler, D.L., D.M. Church, A.E. Lash, D.D. Leipe, T.L. Madden, J.U. Pontius, G.D. Schuler, L.M. Schriml, T.A. Tatusova, L. Wagner, and B.A. Rapp. 2001. Database resources of the National Center for Biotechnology Information. *Nucleic Acids Res* **29**: 11-6.

White, P.S., A. Forus, T.C. Matise, B.C. Schutte, N. Spieker, P. Stanier, J.M. Vance, and S.G. Gregory. 1999. Report of the fifth international workshop on human chromosome 1 mapping 1999. *Cytogenet Cell Genet* **87**: 143-71.

Wilson, K.L. 2000. The nuclear envelope, muscular dystrophy and gene expression. *Trends Cell Biol* **10**: 125-9.

Wiltshire, S., A.T. Hattersley, G.A. Hitman, M. Walker, J.C. Levy, M. Sampson, S. O'Rahilly, T.M. Frayling, J.I. Bell, G.M. Lathrop, A. Bennett, R. Dhillon, C. Fletcher, C.J. Groves, E. Jones, P. Prestwich, N. Simecek, P.V. Rao, M. Wishart, R. Foxon, S. Howell, D. Smedley, L.R. Cardon, S. Menzel, and M.I. McCarthy. 2001. A genomewide scan for loci predisposing to type 2 diabetes in a U.K. population (the diabetes UK warren 2 repository): analysis of 573 pedigrees provides independent replication of a susceptibility locus on chromosome 1q. *Am J Hum Genet* **69**: 553-69.

Wion, K.L., T.G. Kirchgessner, A.J. Lusis, M.C. Schotz, and R.M. Lawn. 1987. Human lipoprotein lipase complementary DNA sequence. *Science* **235**: 1638-41.

Wolfe, S.A., L. Nekludova, and C.O. Pabo. 2000. DNA recognition by Cys2His2 zinc finger proteins. *Annu Rev Biophys Biomol Struct* **29**: 183-212.

Wood, J.D., J.C. MacMillan, P.S. Harper, P.R. Lowenstein, and A.L. Jones. 1996. Partial characterisation of murine huntingtin and apparent variations in the subcellular localisation of huntingtin in human, mouse and rat brain. *Hum Mol Genet* **5**: 481-7.

Worman, H.J., J. Yuan, G. Blobel, and S.D. Georgatos. 1988. A lamin B receptor in the nuclear envelope. *Proc Natl Acad Sci U S A* **85**: 8531-4.

Wu, Z., Y. Xie, N.L. Bucher, and S.R. Farmer. 1995. Conditional ectopic expression of C/EBP beta in NIH-3T3 cells induces PPAR gamma and stimulates adipogenesis. *Genes Dev* **9**: 2350-63.

Wu, Z., P. Puigserver, and B.M. Spiegelman. 1999. Transcriptional activation of adipogenesis. *Curr Opin Cell Biol* **11**: 689-94.

Wydner, K.L., J.A. McNeil, F. Lin, H.J. Worman, and J.B. Lawrence. 1996. Chromosomal assignment of human nuclear envelope protein genes *LMNA*, *LMNB1*, and *LBR* by fluorescence in situ hybridization. *Genomics* **32**: 474-8.

Yamada, K., H. Osawa, and D.K. Granner. 1999. Identification of proteins that interact with NF-YA. *FEBS Lett* **460**: 41-5.

Ye, Q. and H.J. Worman. 1994. Primary structure analysis and lamin B and DNA binding of human LBR, an integral protein of the nuclear envelope inner membrane. *J Biol Chem* **269**: 11306-11.

Ye, Q., I. Callebaut, A. Pezhman, J.C. Courvalin, and H.J. Worman. 1997. Domain-specific interactions of human HP1-type chromodomain proteins and inner nuclear membrane protein LBR. *J Biol Chem* **272**: 14983-9.

Ye, J., U.P. Dave, N.V. Grishin, J.L. Goldstein, and M.S. Brown. 2000. Asparagine-proline sequence within membrane-spanning segment of SREBP triggers intramembrane cleavage by site-2 protease. *Proc Natl Acad Sci U S A* **97**: 5123-8.

Yeh, W.C., Z. Cao, M. Classon, and S.L. McKnight. 1995. Cascade regulation of terminal adipocyte differentiation by three members of the C/EBP family of leucine zipper proteins. *Genes Dev* **9**: 168-81.

Yokoyama, C., X. Wang, M.R. Briggs, A. Admon, J. Wu, X. Hua, J.L. Goldstein, and M.S. Brown. 1993. SREBP-1, a basic-helix-loop-helix-leucine zipper protein that controls transcription of the low density lipoprotein receptor gene. *Cell* **75**: 187-97.

Yuh, W.T., J.S. Collison, W.J. Sickels, T.J. Barloon, D.C. Brennan, and M.J. Flanigan. 1988. Partial lipodystrophy. Magnetic resonance findings in one case. *J Comput Tomogr* **12**: 287-91.

Zhang, Y., R. Proenca, M. Maffei, M. Barone, L. Leopold, and J. Friedman. 1994. Positional cloning of the mouse obese gene and its human homologue. *Nature* **372**: 425-432.

Zhao, K., A. Harel, N. Stuurman, D. Guedalia, and Y. Gruenbaum. 1996. Binding of matrix attachment regions to nuclear lamin is mediated by the rod domain and depends on the lamin polymerization state. *FEBS Lett* **380**: 161-4.

Appendix I
STSs used for primary physical map screen

Pool1	Other name
stSG24	stSG24
stSG449	stSG449
stSG824	stD1S305
stSG1211	stD1S506
stSG1526	stSG1526
stSG1725R	stSG1725R
stSG1815R	stSG1815R
stSG2578	stSG2578
stSG2587	stSG2587
stSG2606	stSG2606
stSG3119	stSG3119
stSG3266	stSG3266
stSG3515	stSG3515
stSG3698	stSG3698
stSG3869	stSG3869
stSG4048	stSG4048
stSG4066	stSG4066
stSG4094	stSG4094
stSG4749	stSG4749
stSG4977	stSG4977
stSG4979	stSG4979
stSG8006	stSG8006
stSG8620	stSG8620
stSG8645	stSG8645
stSG8670	stSG8670

Pool2	Other name
stSG9965	stSG9965
stSG10251	stSG10251
stSG10313	stSG10313
stSG10425	stCHLC.GATA43A04
stSG10457	stSG10457
stSG12743	stSG12743
stSG13548	stA002N39
stSG13640	stD1S2118
stSG13720	stD1S2463
stSG13812	stD1S3443
stSG13819	stD1S3312
stSG13844	stD1S3359
stSG13908	stD1S3249
stSG13929	stWI-11851
stSG13965	stWI-12606
stSG13981	stIB1737
stSG14035	stD1S2405
stSG14226	stA002G08
stSG14328	stD1S2624
stSG14338	stD1S2635
stSG14530	stAFMa082wc1
stSG16134	stSG16134
stSG16412	stSG16412
stSG16430	stSG16430
stSG21768	stSG21768

Pool3	Other name
stSG22819	stSGC34568
stSG22855	stWI-14846
stSG22901	stWI-15073
stSG22919	stWI-17762
stSG23021	stWI-15733
stSG23070	stSHGC-34121
stSG23210	stGDB:181583
stSG23225	stD1S176
stSG23245	stD1S262E
stSG23298	stGDB:193110
stSG23379	stD1S362E
stSG23502	stGDB:375812
stSG23517	stGDB:437124
stSG23518	stGDB:437910
stSG23600	stD1S1908E
stSG23632	stD1S1945E
stSG23701	stD1S2025E
stSG24021	stD1S3139
stSG24106	stD1S3272
stSG24168	stD1S3503
stSG24185	stD1S3522
stSG27661	stSG27661
stSG27664	stSG27664
stSG28025	stSG28025
stSG28128	stSG28128
stSG28237	stSG28237

Pool4	Other name
stSG28956	stSG28956
stSG29147	stSG29147
stSG32504FS	stSG32504FS
stSG32631FS	stSG32631FS
stSG32669FS	stSG32669FS
stSG32775FS	stSG32775FS
stSG33220FS	stSG33220FS
stSG33635FS	stSG33635FS
stSG34236	stSG34236
stSG34524	stSG34524
stSG39079	stSG39079
stSG41436	stSG41436
stSG42997	stSG42997
stSG44607	stSG44607
stSG44780	stSG44780
stSG44996	stSG44996
stSG45134	stSG45134
stSG46135	stSG46135
stSG47418	stSG47418
stSG47972	stSG47972
stSG48828	stSHGC-11135
stSG49739	stSG49739
stSG50247	stSG50247
stSG50477	stSG50477
stSG50849	stSG50849
stSG52115	stSG52115

Appendix II
BAC end derived STSs

	Sense 5' - 3'	Antisense 5' - 3'
157A11T7	CACCTGTTCAATCCATCCTA	GTTGTTCTTGAATCTTCATGGGC
157A11SP6	GCCGCCACTGAGCACACACC	AGTCCAAGGAGAAGCTAGCC
73C10T7	GGAATGGCTGGAAGTACAAA	CACAAGTGTGGCTGCCATCTAAG
73C10SP6	CTCATGTTTCCCATGCTGG	AAGGCGCATGACTGTAATCCC
16P22T7	CAGCCAGACACATGGCAGAC	GCCTGGCTGCATATTAGTGCC
244C8T7F	GTCGCCCAGGCTGGAGTGCAA	GTTCCCTTGGGTCAGGGGTTT
244C8SP6	GCAGAGTACCAATAAACTGA	ATTTGGTATGTGGGGTTTGCC
415L1SP6	GTCAAGCCTGTTATTGTTTGC	GAGACAAGTGGACGTCAGCAC
138H22T7	GCTCAGGCTGGAGTGCAGTG	GAGTTCGAGACTAGCCTGG
140A22T7	AGAAGTTCAAGACCAGCTTG	GTGGCATTGCTCATTGTAGC
121L15SP6	TCAGATGCAGCCTTCGTATC	TGGGACTAGAATCCTGCTC
144B19T7	GGCCACAGGTACTGATGAC	AGCGAATGAGTTAACACATG
16P22SP6	CTGATGGACTAGAGGCTATCG	ATAAGGGATCCGACTTACC
98G7T7	CCCTTGTGAGGAGGTATG	TTGTCCTGTTAGGCCTCACG
10M7T7	TAGCTGCCACATACTGACTGC	CCACACAGAGGCGTGGGCAC
10M7SP6	GCTGCCAGTACCTCAGCTGG	CCTAGAGTAGGTCTGGCAC
54H19T7	GCGGTGAGGTCTAGGACAGG	CATGCTGTTCACAGTGCCTCAG
54H19SP6	TCAGAAGCAGAGCACCTGTG	GCTAGGCTGGACTCAAACTC
114H16T7	GACAGTTCCTCTAAGCTCC	CAGAGTAGGAGCAGTGGATG
114H16SP6	AGCATCCCTGACACAGTAAG	AAACACTAGGCAAATCTAAC
21N7T7	GGAGCTCCAGAGCCCGAGCTG	TACAGATAGATGAGGCCCC
21N7SP6	TTCAGAGTCATGAGAAGGAG	TAAACCAGGTTCACATCCACC
101J8T7	CTGGCGGACATTAGTTAGGAG	AGCACCTGCCTGGAGTCAAGC
101J8SP6	GTCTTATGTGAGTTCTGAG	CTTCCTTGCCTCTATTCCTTGC
157D17T7	CACTAGAGCACTGGGTACATC	CCATTGGAAGCATGTGCTGG
157D17SP6	AATGTGAGTGGCTGGAGCAG	GATGGAAGCTGCCTGAGTCAT
196D4T7	CATATTGCACCCCTTGTTAGC	TGCATACCTGGAAGATCGGC
196D4SP6	TATTTGAAGCAGTAAGGCCAA	GTGCAGCTAGGAGGGTGGAC
35P22T7	CATCTGTGCTCCGGGAGT	AATCCAACCCCAAACTCTTC
35P22SP6	GGGCAGAATTAATGCCTGACT	GTTTCAGTGAGGGGAGAGGA
69N22T7	GCCAAGTCATTCCCACCTCT	CCCTGCTGTATTTGTCTGTG
69N22SP6	GTTCCCACTTATTCTCTACCCA	GGTTCTTGCCCTGTGTGT
262A11T7	TGTTATCAGGCCATCAG	ACGTTGCTTTGCACAGTC
262A11SP	GGCACTTGATAATAATGCACAG	GTATGTCCATGGTTAAGGGAAC
21G11T7	CAGTAAGAATTTACAGGTG	ACTCACAGCACTCACAAG
177O6T7	TGTTGTGTGAGCTGGAATCTC	ACCAGTCCAGTTTTTCTCACTG
317L8T7	CACTACATAGGTTTCTTTC	AAGATGGTAATTTTACCAC
317L8SP6	ATGGTGAATTGGTAAGCTAC	GTTGAGCCATTGTAAGTTGG
263K19T7	CACAACGGATAGTGCATTACC	GCGTCTGTAGGGTTTGGAG
263K19SP6	CCCATAGATAATTAAGTAG	ACATTTGGGCTTACAGATG
101O6T7	GACCACATTGAGATCATCCCT	TTAGAACAGCCATCAGGGAC
101O6SP6	TTCTCTTCTTCAGACTCACC	CTCAGGACAGCTGTAGTGG

Appendix III
Calculation to determine the quantity of 3T3-L1 adipocyte library DNA required to obtain 6×10^6 yeast transformants

Transformation efficiency (Figure 19)

A 1× scale transformation using:

0.1 μg of DNA	results in	2.5×10^5 transformants/ μg
0.2 μg of DNA	results in	2.1×10^5 transformants/ μg
0.5 μg of DNA	results in	1.8×10^5 transformants/ μg
1.0 μg of DNA	results in	1.3×10^5 transformants/ μg

∴ The highest transformation efficiency is achieved using 0.1 μg in a 1× scale transformation.
If the total desired number of transformants is to be 6×10^6, then 24 μg of 3T3-L1 library DNA must be used.

$$24\ \mu g \times 2.5 \times 10^5 \text{ transformants/ } \mu g = 6 \times 10^6 \text{ total transformants}$$

However,
to use 24 μg of library DNA the reaction must be scaled up 240× as only 0.1 μg was used in the 1× reaction, thus,

$$0.1\ \mu g \text{ (DNA used in 1× transformation)} \times 240 = 24 \mu g \text{ total library DNA}$$

To scale the 1× transformation up 240× this would require the prior growth of a liquid culture too large to conveniently handle (approximately 1.2 litres).

Transformation using 1 μg in a 1× transformation

Using 1 μg of library DNA in a 1× transformation still results in comparatively high transformation efficiency. Using the transformation conditions of 1 μg in a 1× transformation then 60 μg of DNA would be necessary in a 60× scale up reaction.

$$60\ \mu g \times >1.0 \times 10^5 \text{ transformants/ } \mu g = >6 \times 10^6 \text{ total transformants}$$

Although this method is less efficient and uses 2.5× more DNA it was considered preferable as the culture volume could be kept to a minimum

Appendix IV.
Universal genetic code

1st base	2nd base: T	2nd base: C	2nd base: A	2nd base: G	3rd base
T	TTT Phe (F)	TCT Ser (S)	TAT Tyr (Y)	TGT Cys (C)	T
	TTC Phe (F)	TCC Ser (S)	TAC Tyr (Y)	TGC Cys (C)	C
	TTA Leu (L)	TCA Ser (S)	TAA STOP	TGA STOP	A
	TTG Leu (L)	TCG Ser (S)	TAG STOP	TGG Trp (W)	G
C	CTT Leu (L)	CCT Pro (P)	CAT His (H)	CGT Arg (R)	T
	CTC Leu (L)	CCC Pro (P)	CAC His (H)	CGC Arg (R)	C
	CTA Leu (L)	CCA Pro (P)	CAA Gln (Q)	CGA Arg (R)	A
	CTG Leu (L)	CCG Pro (P)	CAG Gln (Q)	CGG Arg (R)	G
A	ATT Ile (I)	ACT Thr (T)	AAT Asn (N)	AGT Ser (S)	T
	ATC Ile (I)	ACC Thr (T)	AAC Asn (N)	AGC Ser (S)	C
	ATA Ile (I)	ACA Thr (T)	AAA Lys (K)	AGA Arg (R)	A
	ATG Met (M)	ACG Thr (T)	AAG Lys (K)	AGG Arg (R)	G
G	GTT Val (V)	GCT Ala (A)	GAT Asp (D)	GGT Gly (G)	T
	GTC Val (V)	GCC Ala (A)	GAC Asp (D)	GGC Gly (G)	C
	GTA Val (V)	GCA Ala (A)	GAA Glu (E)	GGA Gly (G)	A
	GTG Val (V)	GCG Ala (A)	GAG Glu (E)	GGG Gly (G)	G

Nucleotides are indicated in the grey boxes. The first , second and third bases of the codon are positioned on the left, top and right, respectively. Each of the 64 codons are presented in the centre, accompanied by the relevant amino acid in three letter code and single letter code (in brackets).

Appendix V.
Amino acid characteristics

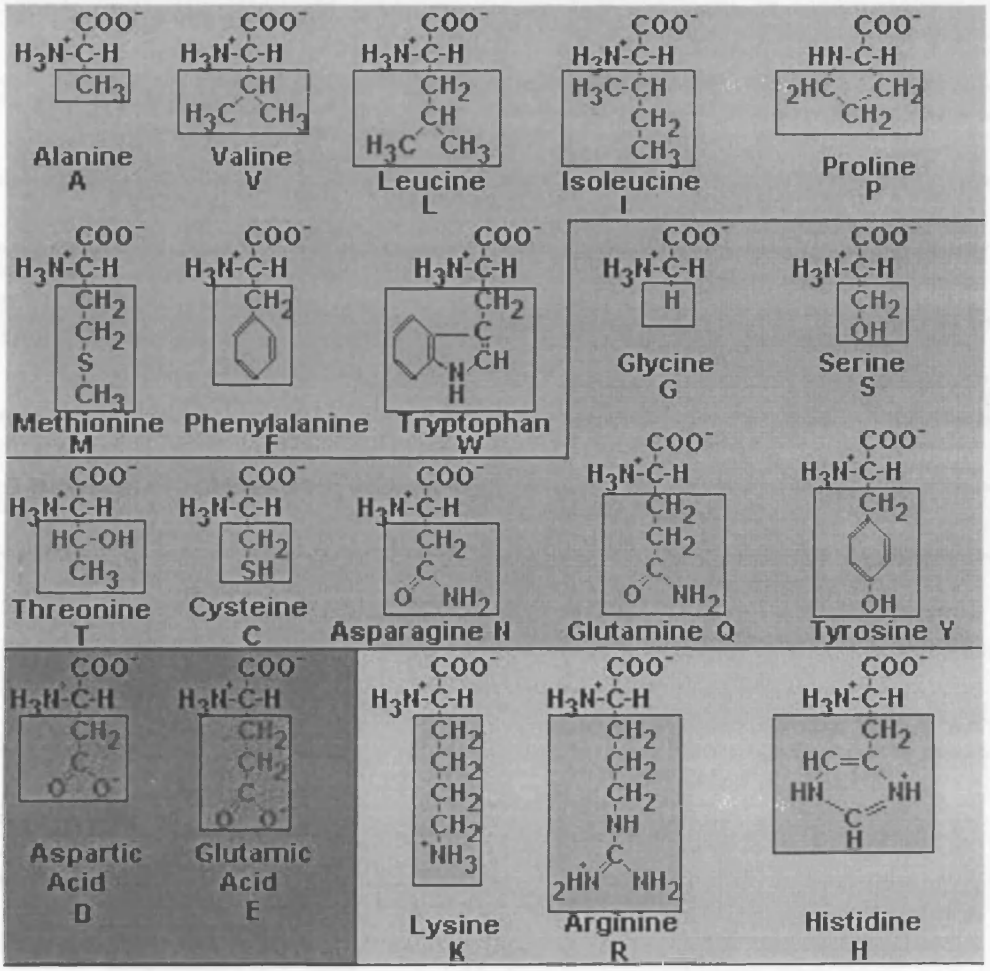

The amino acids all vary in their side chains (inner boxes). The eight amino acids in the upper area are nonpolar and hydrophobic. The other amino acids are polar and hydrophilic ("water loving"). The two amino acids in the bottom-left box are acidic ("carboxy" group in the side chain).The three amino acids in the bottom-right box are basic ("amine" group in the side chain). Reproduced with permission from www.people.virginia.edu/~rjh9u/humbiol.html

Appendix VI
Internet addresses used as bioinformatic databases and for computational analyses

Name	Function	HTTP://
BLAST	Comparison of DNA and protein sequence against the NCBI database	www.ncbi.nlm.nih.gov/BLAST
BLAST2	Comparison of two sequences (DNA or protein) with each other	www.ncbi.nlm.nih.gov/blast/bl2seq/bl2
Box Shade	Utilises CLUSTAL W output of a protein sequence to shade the identical residues	www.ch.embnet.org/software/BOX_form.html
CHLC	Database of tetranucleotide microsatellite markers	www.chlc.org
Chromosome 1 webace	Database of all chromosome 1 mapping data	www.sanger.ac.uk
CLUSTAL W	Comparative alignment of two protein sequences against each other	www.ebi.ac.uk/clustalw
GDB	General database of genes and markers	www.gdb.org
Généthon	Database of $(CA)_n$ microsatellite markers	www.genethon.fr
HGMP	General database of genome resources available in the UK, including IMAGE clones	www.hgmp.mrc.ac.uk
ISREC pfscan server	Home to four protein databases, which can be scanned for domain and motif homology	www.isrec.isb-sib.ch/software/PFSCAN_form.html
NCBI	Comprehensive database containing all known information associated with genes and genomes	www.ncbi.nlm.nih.gov
OMIM	Factual database, reviewing all known genes and inherited diseases	www.ncbi.nlm.nih.gov/OMIM
Primer 3	Internet program that generates primer sequences to a target sequence	www-genome.wi.mit.edu/cgi-bin/primer/primer3_www.cgi
SOSUI	Program developed to predict transmembrane domains in a protein sequence	sosui.proteome.bio.tuat.ac.jp/cgi-bin/sosui.cgi?/sosui_submit.html
TIGR	Database of BAC end sequence from several genomic libraries	www.tigr.org/tdb/humgen/bac_end_search/bac_end_search.html
TMpred	Program developed to predict transmembrane domains in a protein sequence	www.ch.embnet.org/software/TMPRED_form.html

Appendix VII
Publications
(* denotes joint authorship)

Shackleton, S.*, D.J. Lloyd*, S.N. Jackson, R. Evans, M.F. Niermeijer, B.M. Singh, H. Schmidt, G. Brabant, S. Kumar, P.N. Durrington, S. Gregory, S. O'Rahilly, and R.C. Trembath. 2000. *LMNA*, encoding lamin A/C, is mutated in partial lipodystrophy. *Nat Genet* **24**: 153-6.

Behrens, G.M., D. Lloyd, H.H. Schmidt, R.E. Schmidt, and R.C. Trembath. 2000. Lessons from lipodystrophy: *LMNA*, encoding lamin A/C, in HIV therapy-associated lipodystrophy. *AIDS* **14**: 1854-5.

Vigouroux, C., J. Magre, M.C. Vantyghem, C. Bourut, O. Lascols, S. Shackleton, D.J. Lloyd, B. Guerci, G. Padova, P. Valensi, A. Grimaldi, R. Piquemal, P. Touraine, R.C. Trembath, and J. Capeau. 2000. Lamin A/C gene: sex-determined expression of mutations in Dunnigan-type familial partial lipodystrophy and absence of coding mutations in congenital and acquired generalized lipoatrophy. *Diabetes* **49**: 1958-62.

Lloyd, D.J., R.C. Trembath, and S. Shackleton. 2001. A novel interaction between lamin A and SREBP1: Implications for the laminopathies. *Submitted for publication*

LMNA, encoding lamin A/C, is mutated in partial lipodystrophy

Sue Shackleton[1]*, David J. Lloyd[1]*, Stephen N.J. Jackson[1], Richard Evans[2], Martinus F. Niermeijer[3], Baldev M. Singh[4], Hartmut Schmidt[5], Georg Brabant[6], Sudesh Kumar[7], Paul N. Durrington[8], Simon Gregory[2], Stephen O'Rahilly[9] & Richard C. Trembath[1]

*These authors contributed equally to this work.

The lipodystrophies are a group of disorders characterized by the absence or reduction of subcutaneous adipose tissue. Partial lipodystrophy (PLD; MIM 151660) is an inherited condition in which a regional (trunk and limbs) loss of fat occurs during the peri-pubertal phase[1,2]. Additionally, variable degrees of resistance to insulin action, together with a hyperlipidaemic state, may occur and simulate the metabolic features commonly associated with predisposition to atherosclerotic disease[3]. The PLD locus has been mapped to chromosome 1q with no evidence of genetic heterogeneity[4]. We, and others, have refined the location to a 5.3-cM interval between markers *D1S305* and *D1S1600* (refs 5,6). Through a positional cloning approach we have identified five different missense mutations in *LMNA* among ten kindreds and three individuals with PLD. The protein product of *LMNA* is lamin A/C, which is a component of the nuclear envelope. Heterozygous mutations in *LMNA* have recently been identified in kindreds with the variant form of muscular dystrophy (MD) known as autosomal dominant Emery-Dreifuss MD (EDMD–AD; ref. 7) and dilated cardiomyopathy and conduction-system disease[8] (CMD1A). As *LMNA* is ubiquitously expressed, the finding of site-specific amino acid substitutions in PLD, EDMD–AD and CMD1A reveals distinct functional domains of the lamin A/C protein required for the maintenance and integrity of different cell types.

We have recently described the clinical and genetic features of autosomal dominant PLD (Dunnigan-Köbberling type) in two PLD families ascertained in the United Kingdom[2]. Nuclear magnetic resonance imaging confirmed the absence of subcutaneous adipose tissue in a site-specific manner affecting the trunk and limbs, but with retention of intra-cavity fat deposits. A relative increase in adiposity was observed in the head and neck[2,9]. In a genetic linkage study, we located the PLD gene at 1q11–q23 with evidence of a common founder haplotype[5]. Regional fine-mapping, using a panel of 10 markers typed in an additional seven independently ascertained kindreds with PLD, detected several disease-specific haplotypes (Fig. 1). We saw two chromosome recombination events in two affected individuals in PLD family 7 and PLD family 8 (Fig. 1), suggesting that the disease gene is located in a 3.9-cM interval between markers *D1S2346* (centromeric boundary) and *D1S2624* (telomeric boundary). Using radiation-hybrid-mapping data (http://www.sanger.ac.uk), we selected 102 STSs from this interval to construct a bacterial artificial chromosome (BAC) contig covering approximately 90% of the estimated 3 Mb that include the PLD interval (Fig. 2). We identified 36 ESTs, clustered as 26 potential transcriptional units, including the following characterized human genes: *NPR1*, *S100A13*, *DAP3*, *SCAMP3*, *INSRR* and *LMNA*.

	markers	recombinants fam 7	recombinants fam 8	fam 1 UK	fam 2 UK	fam 4 UK	fam 8 D	fam 7 NL	fam 9 NL	fam 3 UK	fam 5 UK	fam 6 UK
	D1S2346	□	■	99	99	93	99	89	99	93	93	99
	D1S305	■	■	162	162	160	170	162	162	170	166	170
	D1S2715	■	■	162	162	162	162	160	160	162	150	162
	D1S303	■	■	183	183	179	179	179	179	177	183	177
	D1S2777	■	■	269	269	269	267	265	265	267	265	267
3.9 cM	*D1S2714*	■	■	183	183	183	183	191	191	183/7	187	183
	D1S2140	■	■	254	254	254	254	246	246	262	250	250
	D1S3757	■	■	241	241	265	N/D	265	265	251	265	245
	D1S2721	■	■	242	242	234	234	244	244	242	234	244
	D1S2624	■	□	203	203	205	205	205	205	209	207	207

Fig. 1 Sites of recombination and PLD family haplotypes for 1q21. Open boxes identify recombinant markers for disease haplotypes in individuals from PLD families 7 and 8, which reduce the PLD critical interval at both the proximal and distal ends of the region. Segregating PLD disease haplotypes for each family are shown on the right, together with the country of origin of the grandparents (NL, Netherlands; D, Germany). Shading illustrates the distinct PLD haplotypes associated with the recurrent R482W mutation.

[1]*Division of Medical Genetics, Departments of Medicine and Genetics, University of Leicester, Leicester, UK.* [2]*Sanger Centre, Wellcome Trust Genome Campus, Hinxton, Cambridge, UK.* [3]*Department of Clinical Genetics, Erasmus University and Academic Hospital Dijkzigt, Rotterdam, The Netherlands.* [4]*Diabetes Centre, New Cross Hospital, Wolverhampton, UK.* [5]*IV. Med. Klinik m.S. Gastroenterologie, Hepatologie und Endokrinologie, Charite Campus Mitte, Berlin, Germany.* [6]*Abt. Klinische Endokrinologie, Medizinische Hochschule Hannover, Hannover, Germany.* [7]*Division of Medical Sciences, Birmingham Heartlands Hospital, University of Birmingham, UK.* [8]*University of Manchester, Department of Medicine, Manchester Royal Infirmary, Manchester, UK.* [9]*Departments of Medicine and Clinical Biochemistry, Addenbrooke's Hospital, University of Cambridge, Cambridge, UK. Correspondence should be addressed to R.C.T. (e-mail: rtrembat@hgmp.mrc.ac.uk).*

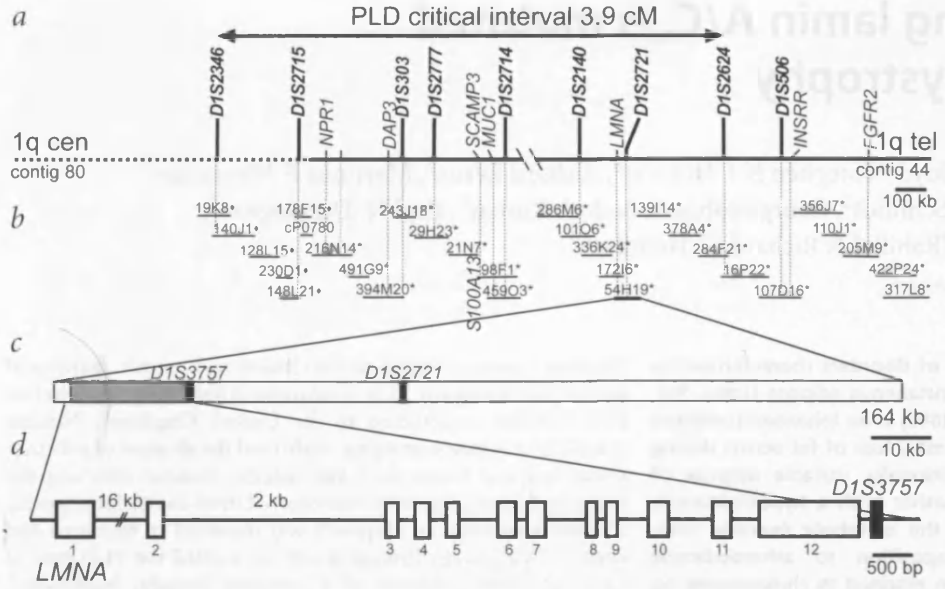

Fig. 2 Physical map of the PLD interval at 1q21 and genomic organization of *LMNA*. **a**, Position of microsatellite markers (bold) and known genes on two contigs, 80 and 44, spanning the interval. Contig 80 also contains clones from a published map denoted by the horizontal dotted line[20]. The size of the gap between the contigs is currently unknown. **b**, Minimum tiling path of PACs (◆), BACs (*) and one cosmid (cP0780), with each clone identifier given above. **c**, Sequenced BAC clone 54H19, illustrating position of *LMNA* (shaded box) alongside the markers (black lines) *D1S2721* and novel microsatellite *D1S3757*, 45 kb and 100 bp 3′ to exon 12, respectively. **d**, Genomic structure of *LMNA* showing exons (open boxes) and approximate sizes of the introns (horizontal lines).

We focused on *LMNA* following the description of a single, large, multigenerational family in which a missense mutation (R482Q) was identified and seen to co-segregate with the PLD phenotype (R. Hegele, pers. comm.). The A-type lamins (lamins A and C) are two alternatively transcribed products of *LMNA* and are members of the intermediate filament (IF) family of proteins, which form components of the nuclear lamina, a fibrous, proteinaceous meshwork underlying the inner nuclear membrane[10,11]. Heterozygous mutation of *LMNA* has recently been reported in EDMD–AD (ref. 7) and CMDIA (ref. 8). The EDMD–AD phenotype, although variable both within and between families, is characterized by a myopathic process associated with muscle contractures and cardiac conduction defects. CMD1A is characterized by age-related onset of cardiac ventricular dilatation leading to impaired cardiac function, and is frequently associated with abnormal cardiac conduction. The molecular basis of the relative tissue specificity of EDMD–AD and CMD1A is poorly understood[7,8,12].

LMNA had been localized to 1q21.2 in an interval containing the markers *D1S2624* and *D1S2125* by radiation-hybrid mapping[7]. We positioned *LMNA* on the BAC physical map of the PLD disease interval, flanked by markers *D1S2140* and *D1S2721*, and identified a novel dinucleotide repeat marker, *D1S3757*, 100 bp downstream of *LMNA* (Fig. 2). We searched for mutation of *LMNA* in a cohort of ten families and three singletons with the PLD phenotype. We designed intronic primers to PCR amplify the 12 exons of *LMNA*, and analysed them by automated sequencing in both affected and unaffected members of each PLD family. Affected individuals of all families were found to carry heterozygous mutations in exon 8 of *LMNA* (Fig. 3). Six families (PLD families 1, 2, 4, 7, 8 and 9) as well as the three singletons carried a C→T transition in codon 482, resulting in an arginine (CGG)-to-tryptophan (TGG) substitution (R482W). In PLD family 3, a G→A transition in codon 482 resulted in substitution of arginine for glutamine (CAG; R482Q). In PLD family 5, a G→T transversion led to a third mutation in codon 482, substituting arginine for leucine (CTG; R482L). Sequencing of PLD family 6 revealed a G→C transition in codon 486, resulting in substitution of lysine (AAG) for asparagine (AAC; K486N). PLD family 10 carried a G→T transversion in codon 486, again substituting lysine for asparagine (AAT).

Restriction endonuclease digestion or sequence analysis of affected and unaffected first-degree relatives confirmed co-segregation of the observed mutation with the disease phenotype in each of the ten families studied (Fig. 4, and data not shown).

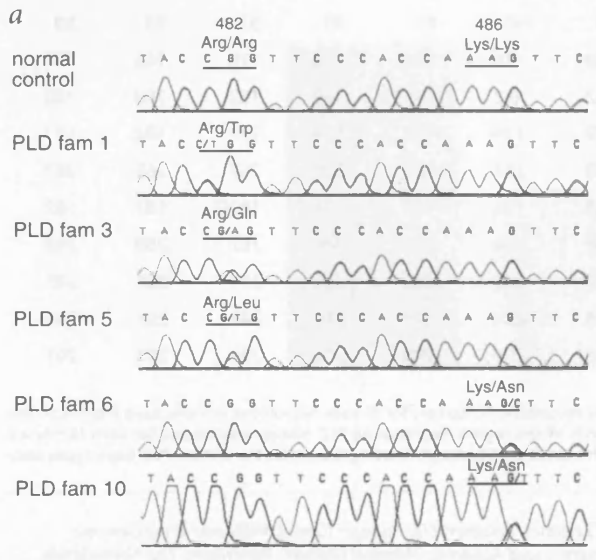

b

			482				486				
	Thr	Tyr	Arg	Phe	Pro	Pro	Lys	Phe	Thr	Leu	Number
WT	ACT	TAC	CGG	TTC	CCA	CCA	AAG	TTC	ACC	CTG	observed
R482W	...	...	T..	...	...	...	...	...	...	...	9
R482Q	...	...	.A.	...	...	...	...	...	...	...	1
R482L	...	...	.T.	...	...	...	...	...	...	...	1
K486N	...	...	...	...	...	...	..C	...	...	...	2
K486N	...	...	...	...	...	...	..T	...	...	...	1

Fig. 3 Mutations identified in exon 8 of *LMNA* in PLD patients. **a**, DNA sequence analysis extending from codon 481 to 487, showing one normal individual (top chromatogram) and PLD patients carrying the five independent heterozygous *LMNA* mutations. Underlined sequences highlight the wild-type codon in the normal control and the heterozygous mutation in each family. The corresponding amino acid change is shown above the codon. **b**, Range of mutations observed in PLD patients. The far left column indicates the amino acid changes. The far right column shows the number of independently ascertained kindreds possessing each mutation.

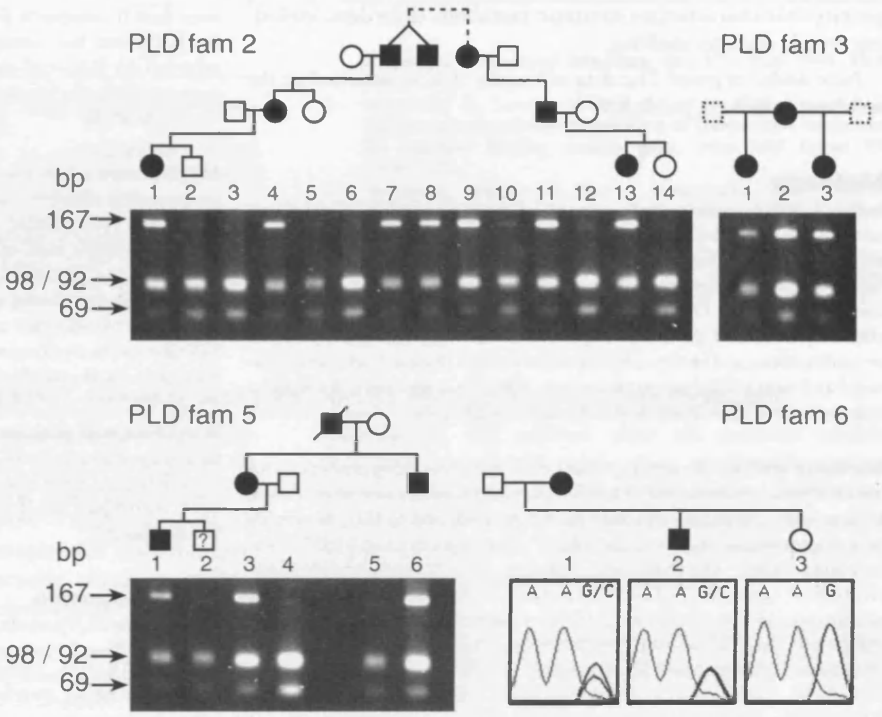

Fig. 4 Co-segregation of *LMNA* mutations with the PLD phenotype. Restriction-digest analysis of PLD families 2, 3 and 5. Arrows indicate the sizes of the observed *Hpa*II fragments (167-bp band represents heterozygous presence of the mutations in codon 482, each of which results in the loss of a *Hpa*II site). Dotted lines in PLD family 2 indicate a common ancestor three generations previously. The diagnosis of PLD in individual 2 (age 10) of PLD family 5 was considered equivocal at the time of ascertainment. Sequence analysis of PLD family 6 was performed as the K486N mutation did not create or destroy a restriction site.

Each of these missense mutations substitutes a highly conserved, positively charged amino acid, arginine at position 482 and lysine at position 486 (Fig. 5). Together with the absence of the mutations from healthy, unrelated individuals (100 normal chromosomes, data not shown), these observations provide evidence that the mutations cause disease. Detailed analysis of the 1q21 haplotypes, including the novel polymorphic microsatellite marker *D1S3757*, was used to further investigate the origin of the common R482W mutation observed in nine PLD families (Fig. 3*b*). We saw the C→T transition at codon 482 on three distinct haplotypes (PLD families 1 and 2, PLD families 7 and 9, and PLD families 4 and 8; Fig. 1), suggesting that this is a site of recurrent mutation. We have so far been unable to ascertain any geneological links between the families in either group. The molecular basis for recurrent mutation at this location of *LMNA* is likely to reflect the deamination of C→T at a CpG site. The mutations observed in EDMD–AD include three missense mutations in exons 7 and 9 and one nonsense mutation, predicting a truncated lamin A/C of only five amino acids[7]. In CMD1A, five missense mutations in exons 1, 3 and 10 have been reported[8]. In contrast, all five independent PLD mutations observed here were missense and restricted to a 15-bp region of exon 8.

Available evidence indicates a role for lamins in DNA replication, chromatin organization, spatial arrangements of nuclear pore complexes, nuclear growth and anchorage of nuclear envelope proteins (for review, see ref. 13). Lamin A, and the splice-variant lamin C, are expressed late in embryonic development and are found in all somatic tissues with the exception of erythrocytes[14]. Lamins, similar to other IF proteins, consist of a central α-helical rod domain flanked by a non-α-helical head and a globular carboxy-terminal tail domain. It remains unclear whether the PLD mutations, which affect the C-terminal domain, alter any of these functions of lamin. In a targeted disruption of mouse *Lmna*, homozygous null mice have a phenotype similar to both EDMD and CMD1A (ref. 15). Tissue-specific changes in nuclear structure and number in skeletal and cardiac muscle were observed, in addition to a redistribution of a further component of the nuclear envelope, emerin[15]. The mutations in PLD identified here are site-specific. In contrast, *LMNA* mutations in EDMD and CMD1A are distributed across several exons. These data suggest that the region encompassing codons 482 and 486, within the globular domain of lamin A/C, determines specific functions in the adipocyte. Confirmation will require detailed investigation of the expression and distribution of lamin A/C in the different tissue types and, in particular, analysis of their interactions with other nuclear components.

Identification of multiple independent, but tightly clustered, mutations in *LMNA* provides evidence that this gene is associated with a range of disease phenotypes and is the first gene known to be altered in the inherited lipodystrophies. Our data broaden the range of disorders for which components of the nuclear envelope may be considered as putative candidates. The known functions of lamin A/C provide little insight into the molecular mechanisms of tissue specificity or into the metabolic disturbances, including insulin resistance and hyperlipaemia, which occur in PLD. *LMNA*, however, now represents a candidate gene in studies aimed at disentangling the genetic hetero-

```
                                        482  486
human    lamin A/C   465   GNWQIKRQNGDDPLLTYRFPPKFTLKAGQVVTIWAA
500
mouse    lamin A/C   465   GNWQIRRQNGDDPLMTYRFPPKFTLKAGQVVTIWAS
500
rat      lamin A/C   465   GNWQIRRQNGDDPLMTYRFPPKFTLKAGQVVTIWAS
```

Fig. 5 Alignment of the amino acid sequence of lamin A/C from human and other species, illustrating the high degree of conservation across this region. The amino acids Arg482 and Lys486, which are mutated in PLD patients, are shown in bold. Shaded boxes show conservative substitution of these amino acids in *Xenopus laevis*.

geneity that characterizes common metabolic disorders, including type II diabetes mellitus.

Note added in proof: The data of Hegele *et al.* mentioned in the text have now been published[21].

Methods

Patients. Following informed consent (Leicestershire Health Ethics Committee), we performed clinical assessment on 55 PLD patients and their unaffected first-degree relatives as described[2,5]. Families were ascertained from the UK, Germany and Holland. The PLD phenotype was considered distinct from both EDMD and dilated cardiomyopathy. Specifically, no affected patient had clinical evidence of skeletal or cardiac muscle disease or contractures, and in two subjects serum creatine kinase levels were measured and were within the normal range. Affection status was considered as unknown in all individuals under the age of eight years.

Haplotype analysis. We genotyped all family members using genomic DNA isolated from peripheral blood lymphocytes and used fluorescently labelled PCR primers (sequences obtained from Genethon and CHLC) to amplify each microsatellite marker as described[16]. The novel marker *D1S3757* was amplified using the following primers: 5′–AATGAGCAGGAGGATGCAGT–3′ and 5′–GGTTTTGGCAAACGCTAAAG–3′. We separated products on an ABI 377 fluorescent DNA sequencer and analysed the results using Genotyper 2.0 software (Perkin Elmer). This allowed haplotypes to be constructed and compared across families.

Construction of a BAC contig. On the basis of Sanger Centre radiation hybrid mapping data, we used 102 STSs positioned within the PLD critical interval to screen the RPCI 11 male genomic BAC library[17]. We generated radioactive probes for each STS by PCR and pooled them before screening. Positive clones were identified and used in subsequent screens using each STS individually. Positives clones for each STS were recorded onto the Sanger Centre Chromosome 1 database (http://www.sanger.ac.uk). BACs were then fluorescently fingerprinted[18] and these data were used to order the BACs into two contigs. Gap closure between these contigs has been achieved by BAC-end-clone walking by creating STSs from end-clone sequence (http://www.tigr.org). Maps of contigs are available on the Sanger Centre database.

Mutation detection. We designed PCR primers for all exons of *LMNA* (sequences available on request; ref. 19) and used them to amplify genomic DNA from both affected and unaffected members of each family. Primers used for amplification of exon 8 (together with exon 9) were as follows: 5′–TCAATTGCAGGCAGGCAGAG–3′ and 5′–CCTCCGATGTTGGCCATCAG–3′. We carried out automated sequencing analysis using the ABI Big Dye terminator mix and with both forward and reverse PCR primers. Reactions were run on an ABI 377 sequencer and analysed with Sequence Analysis 3.2 software (Perkin Elmer).

Restriction endonuclease digestion. Exon 8 was PCR amplified using the following primers: 5′–TCAATTGCAGGCAGGCAGAG–3′ and 5′–GCTCCCATCGACACCCAAGG–3′. We digested an aliquot (10 µl) overnight at 37 °C with *Hpa*II (10 U; Gibco) and separated the digested fragments on a 4% agarose gel.

Acknowledgements

We thank the PLD patients and their relatives for support and encouragement, and R. Gwilliam for technical support. The following physicians provided clinical details and are responsible for the medical care of many of the patients described: P. Heyburn, R. Temple, R. Greenwood, P. McNally, T. Howlett, R. Corral, A. Johnson, J. Pinkney, J. Reckless and M. Dunnigan. This work had financial support from the British Diabetic Association (Ph.D. Studentship, D.J.L.) and the British Heart Foundation (project grant RCT).

Received 1 November; accepted 7 December 1999.

1. Köbberling, J. & Dunnigan, M. Familial partial lipodystrophy: two types of an X linked dominant syndrome, lethal in the hemizygous state. *J. Med. Genet.* **23**, 120–127 (1986).
2. Jackson, S., Howlett, T., McNally, P., O'Rahilly, S. & Trembath, R. Dunnigan-Köbberling syndrome: an autosomal dominant form of partial lipodystrophy. *Q. J. Med.* **90**, 27–36 (1997).
3. Reaven, G. Role of insulin resistance in human disease. *Diabetes* **37**, 1595–1607 (1988).
4. Peters, J. *et al.* Localisation of the gene for familial partial lipodystrophy (Dunnigan variety) to chromosome 1q21–22. *Nature Genet.* **18**, 292–295 (1998).
5. Jackson, S. *et al.* A defect in the regional deposition of adipose tissue (partial lipodystrophy) is encoded by a gene at chromosome 1q. *Am. J. Hum. Genet.* **63**, 534–540 (1998).
6. Anderson, J. *et al.* Confirmation of linkage of hereditary partial lipodystrophy to chromosome 1q21–22. *Am. J. Med. Genet.* **82**, 161–165 (1999).
7. Bonne, G. *et al.* Mutations in the gene encoding lamin A/C cause autosomal dominant Emery-Dreifuss muscular dystrophy. *Nature Genet.* **21**, 285–288 (1999).
8. Fatkin, D. *et al.* Missense mutations in the rod domain of the lamin A/C gene as causes of dilated cardiomyopathy and conduction-system disease. *N. Engl. J. Med.* **341**, 1715–1724 (1999).
9. Garg, A., Peshock, R. & Fleckenstein, J. Adipose tissue distribution pattern in patients with familial partial lipodystrophy. *J. Clin. Endocrinol. Metab.* **84**, 170–174 (1999).
10. Fisher, D.Z., Chaundhary, N. & Blobel, G. cDNA sequencing of nuclear lamins A and C reveals primary and secondary structural homology to intermediate filament proteins. *Proc. Natl Acad. Sci. USA* **83**, 6450–6454 (1986).
11. McKeon, F.D., Kirschner, M.W. & Caput, D. Homologies in both primary and secondary structure between nuclear envelope and intermediate filament proteins. *Nature* **319**, 463–468 (1986).
12. Morris, G. & Manilal, S. Heart to heart: from nuclear proteins to Emery-Dreifuss muscular dystrophy. *Hum. Mol. Genet.* **8**, 1847–1851 (1999).
13. Stuurman, N., Heins, S. & Aebi, U. Nuclear lamins: their structure, assembly and interactions. *J. Struct. Biol.* **122**, 42–66 (1998).
14. Wolin, S., Krohne, G. & Kirschner, M. A new lamin in *Xenopus* somatic tissues displays strong homology to human lamin A. *EMBO J.* **6**, 3809–3818 (1987).
15. Sullivan, T. *et al.* Loss of A-type lamin expression compromises nuclear envelope integrity leading to muscular dystrophy. *J. Cell Biol.* **147**, 913–919 (1999).
16. Coyle, B. *et al.* Pendred syndrome (goitre and sensorineural hearing loss) maps to chromosome 7 in the region containing the nonsyndromic deafness gene *DFNB4*. *Nature Genet.* **12**, 421–423 (1996).
17. Shizuya, H. *et al.* Cloning and stable maintenance of 300-kilobase-pair fragments of human DNA in Escherichia coli using an F-factor-based vector. *Proc. Natl Acad. Sci. USA* **89**, 8794–8797 (1992).
18. Gregory, S., Howell, G.R. & Bentley, D.R. Genome mapping by fluorescent fingerprinting. *Genome Res.* **7**, 1162–1168 (1997).
19. Lin, F. & Worman, H. Structural organisation of the human gene encoding nuclear lamin A and nuclear lamin C. *J. Biol. Chem.* **268**, 16321–16326 (1993).
20. South, A. *et al.* Human epidermal differentiation complex in a single 2.5 Mbp long continuum of overlapping DNA cloned in bacteria integrating physical transcript maps. *J. Invest. Dermatol.* **112**, 910–918 (1999).
21. Cao, H. & Hegele, R. Nuclear lamin A/C R482Q mutation in Canadian kindreds with Dunnigan-type familial partail lipodystrophy. *Hum. Mol. Genet.* **9**, 109–112 (2000).

References

1. Turner MW. **Mannose-binding lectin (MBL) in health and disease.** *Immunobiology* 1998, **199**:327–339.
2. Garred P, Madsen HO, Balslev U, *et al.* **Susceptibility to HIV infection and progression of AIDS in relation to variant alleles of mannose-binding lectin.** *Lancet* 1997, **349**:236–240.
3. Maas J, de Roda Husman AM, Brouwer M, *et al.* **Presence of the variant mannose-binding lectin alleles associated with slower progression to AIDS.** *AIDS* 1998, **12**:2275–2280.
4. McBride MO, Fischer PB, Sumiya M, *et al.* **Mannose-binding protein in HIV-seropositive patients does not contribute to disease progression or bacterial infections.** *Int J STD AIDS* 1998, **9**:683–688.
5. Lipscombe RJ, Sumiya M, Hill AV, *et al.* **High frequencies in African and non-African populations of independent mutations in the mannose binding protein gene.** *Hum Mol Genet* 1992, **1**:709–715.
6. Nielsen SL, Andersen PL, Koch C, Jensenius JC, Thiel S. **The level of the serum opsonin, mannan-binding protein in HIV-1 antibody-positive patients.** *Clin Exp Immunol* 1995, **100**:219–222.
7. Garred P, Pressler T, Madsen HO, *et al.* **Association of mannose-binding lectin gene heterogeneity with severity of lung disease and survival in cystic fibrosis.** *J Clin Invest* 1999, **104**:431–437.

Lessons from lipodystrophy: *LMNA*, encoding lamin A/C, in HIV therapy-associated lipodystrophy

The treatment of HIV-1 infection is frequently associated with the development of acquired regional fat loss (lipodystrophy) and metabolic disturbances. In this study, we characterized 16 HIV-1-infected patients with therapy-associated lipodystrophy for missense mutations in the *LMNA* gene recently found in individuals with inherited partial lipodystrophy.

A wide range of body habitus abnormalities and complex metabolic alterations have been observed in patients receiving highly active antiretroviral therapy (HAART) [1,2]. The most obvious clinical feature developing in HIV-1-infected individuals receiving HAART consists of lipodystrophy, which denotes a regional or generalized lack or loss of subcutaneous fat. The pathogenetic reasons for these therapy-related abnormalities remain unknown. The inhibition by protease inhibitors of several host-cell proteins involved in lipid and carbohydrate metabolism and mitochondrial toxicity of nucleoside-analogue reverse transcriptase inhibitors has been proposed. In non-HIV-infected individuals, the lipodystrophy syndrome is rare. The various syndromes that have been reported can be either familial or acquired, and are classified as localized, partial or generalized. Inherited lipodystrophy includes (familial) partial lipodystrophy (PLD) with the regional loss of trunk and limbs, variable degrees of insulin resistance and hyperlipidaemia leading to the predisposition to atherosclerotic disease. PLD, frequently combined with alterations of glucose and lipid metabolism, shows a close similarity to HAART-related lipodystrophy syndrome. PLD has been mapped to chromosome 1q with no evidence of genetic heterogeneity. Recently, five different missense mutations in *LMNA*, encoding lamin A/C, have been identified in patients with PLD and their families [2].

We analysed 16 HIV-1-infected patients (two women, 14 men, aged 32–72 years) with HAART-related lipodystrophy syndrome for possible mutations of the *LMNA* gene. Body shape alterations after the initiation of HAART had variable severity and presented mainly as peripheral subcutaneous fat loss (mean body mass index 23.3 kg/m^2). Clinical assessments were performed by patients' reports and were confirmed by physical examination. All patients were on protease inhibitor treatment combined with two nucleoside-analogue reverse transcriptase inhibitors. Metabolic variables were determined after 12 h fasting. Genotyping and analysis of the *LMNA* gene were performed using primers and conditions as previously described [3].

Patients with lipodystrophy presented with insulin resistance indicated by significant increased fasting insulin [mean 115.13 pmol/l (7.0–26.0), $P = 0.01$], proinsulin [mean 27.7 pmol/l (8–106), $P = 0.003$], and C-peptide [mean 3.36 μg/l (1.55–6.77), $P = 0.002$] in comparison with 17 protease inhibitor-naive HIV-1-infected individuals (two women, 15 men, aged 23–60 years) without peripheral fat loss. Basal glucose was in the same range in both groups [mean 6.0 mmol/l (4.0–13.4) versus control group 4.8 mmol/l (3.3–5.5), $P = 0.51$]. Seven (54%) out of 13 lipodystrophy-positive HIV-1 patients evaluated in an oral glucose tolerance test were defined as having impaired glucose tolerance; in two patients diabetes was diagnosed. HAART-related peripheral fat wasting was accompanied by significant hyperlipidaemia compared with the control group with an increased serum concentration for LDL-lipoprotein cholesterol [mean 5.5 mmol/l (3.7–7.14), $P = 0.00001$; normal < 4.2 mmol/l], VLDL-cholesterol [mean 2.12 (0.43–4.54), $P = 0.0003$; normal < 1.0 mmol/l], apolipoprotein B [mean 1.49 g/l (1.11–1.93), $P = 0.0002$; normal 0.55–1.35 g/l], and apolipoprotein E [mean 0.83 g/l (0.4–1.7), $P = 0.002$; normal 0.2–0.6 g/l].

Lamin A and the splice variant lamin C is ubiquitously expressed. Lamins have a dynamic role in DNA replication, chromatin organization, and nuclear growth. However, its exact functional role has yet to be determined. Heterozygous mutations in *LMNA* have recently been identified as cause of a variant form of muscular dystrophy known as autosomal dominant Emery–Dreifuss muscular dystrophy [4] and dilated cardiomyopathy and conduction system disease [5]. The mechanism by which lamin A/C mutations induce these different diseases is unknown. Although we excluded germline mutations of *LMNA* in exon 8, we now suggest that lamin A/C and its related proteins

represent important candidate pathways for involvment in HAART-induced lipodystrophy. For example, nuclear lamins contribute to the maintenance and integrity of the nuclear envelope in various cell types. The alteration of lamin-dependent nuclear functions because of genetically determined or pharmacologically induced inhibition in dividing cells may result in cell death. However, we found no homology of the amino acid sequences between lamin A/C and HIV-1 protease, providing no evidence for the direct inhibition of lamins by HIV-1 protease inhibitors. Extending our knowledge on the interaction of intermediate filaments such as lamins and other nuclear factors in the pathogenesis of complex metabolic and tissue-related disorders will provide new strategies to elucidate HAART-associated lipodystrophy and drug-related adverse events.

Georg M.N. Behrens[a], David Lloyd[b], Hartmut H.-J. Schmidt[c], Reinhold E. Schmidt[a] and Richard C. Trembath[b], *[a]Division of Clinical Immunology, Department for Internal Medicine, Hannover Medical School, Germany; [b]Division of Medical Genetics, Departments of Medicine and Genetics, University of Leicester, UK; and [c]IV. Medische Klinik, Charite Campus Mitte, Berlin, Germany.*

Received: 7 March 2000; accepted: 16 March 2000.

References

1. Carr A, Samaras K, Thorisdottir A, Kaufmann GR, Chisholm DJ, Cooper DA. **Diagnosis, prediction, and natural course of HIV-1 protease-inhibitor-associated lipodystrophy, hyperlipidaemia, and diabetes mellitus: a cohort study.** *Lancet* 1999, **353**:2093–2099.
2. Behrens G, Dejam A, Schmidt H, *et al.* **Impaired glucose tolerance, beta cell function and lipid metabolism in HIV-patients under treatment with protease inhibitors.** *AIDS* 1999, **13**: F63–F70.
3. Shackelton S, Lloyd DJ, Jackson SN, *et al.* **LMNA, encoding lamin A/C, is mutated in partial lipodystrophy.** *Nat Genet* 2000, **24**:153–156.
4. Bonne G, Di Barletta MR, Varnous S, *et al.* **Mutations in the gene encoding lamin A/C cause autosomal dominant Emery–Dreifuss muscular dystrophy.** *Nat Genet* 1999, **21**:285–288.
5. Fatkin D, MacRae C, Sasaki T, *et al.* **Missense mutations in the rod domain of the lamin A/C gene as causes of dilated cardiomyopathy and conduction system disease.** *N Engl J Med* 1999, **341**:1715–1724.

Respiratory chain dysfunction associated with multiple mitochondrial DNA deletions in antiretroviral therapy-related lipodystrophy

Highly-active antiretroviral therapy (HAART) can induce a characteristic lipodystrophy syndrome characterized by peripheral fat wasting and central adiposity, usually associated with hyperlipidaemia and insulin resistance [1,2]. Indirect data have led some authors to propose that mitochondrial dysfunction could play a role in this syndrome [3,4]. To date, as recently outlined by Kakuda *et al.* [5]in this journal, HIV-infected patients developing lipodystrophy have not been studied for mitochondrial changes or respiratory chain capacity.

We studied a 67-year-old woman with an unremarkable past history except for HIV infection diagnosed 5 years earlier, without previous opportunistic infections. During the 4 months before the current evaluation, she developed central and peripheral lipodystrophy associated with raised serum triglyceride levels (from 130 to 543 mg/dl) and no changes in cholesterolaemia or glycaemia. The total CD4 lymphocyte count was 401/mm^3, and viral load was 790 copies/mm^3. She had previously received zidovudine (total cumulative dose;

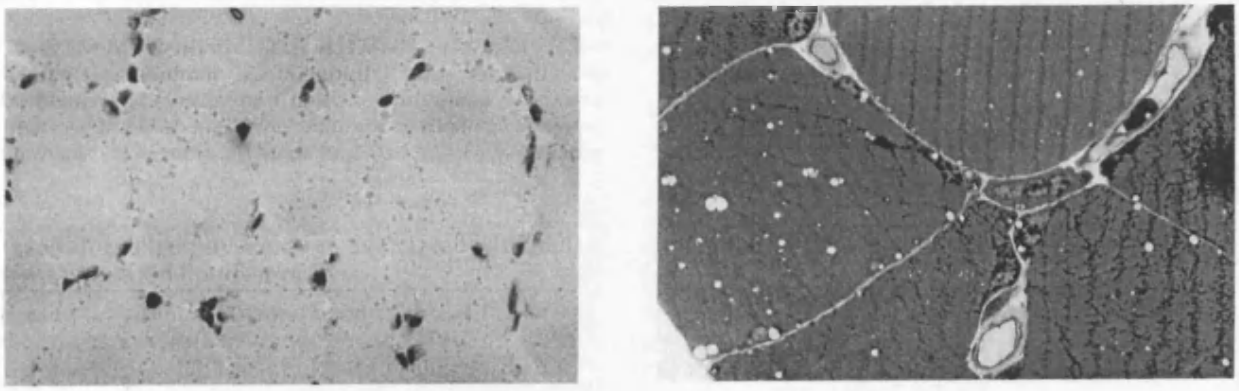

Fig. 1. Skeletal muscle from HIV patient with highly-active antiretroviral therapy-related lipodystrophy. Oil-red 0 staining shows abundant neutral lipids (up; original magnification: 200×). Lipid droplets are also evident in semithin sections (down, original magnification: 800×).

Brief Genetics Report

Lamin A/C Gene

Sex-Determined Expression of Mutations in Dunnigan-Type Familial Partial Lipodystrophy and Absence of Coding Mutations in Congenital and Acquired Generalized Lipoatrophy

Corinne Vigouroux, Jocelyne Magré, Marie-Christine Vantyghem, Charlotte Bourut, Olivier Lascols, Sue Shackleton, David J. Lloyd, Bruno Guerci, Giuseppina Padova, Paul Valensi, André Grimaldi, Régis Piquemal, Philippe Touraine, Richard C. Trembath, and Jacqueline Capeau

Missense mutations of the lamin A/C gene, *LMNA*, have been recently identified in Dunnigan-type familial partial lipodystrophy (FPLD), which belongs to a heterogeneous group of rare disorders affecting adipose tissue distribution and metabolism. In this study, we sequenced the *LMNA* coding region from patients presenting with FPLD or other forms of lipodystrophy. We identified two heterozygous mutations in exon 8, R482W and R482Q, in FPLD patients (six families and one individual) with various clinical presentations. In addition, we found a novel heterozygous mutation (R584H) in exon 11, encoding specifically the lamin A isoform, in a patient with typical FPLD. Clinical and biochemical investigations in FPLD patients revealed that the expression and the severity of the phenotype were markedly dependent on sex, with female patients being more markedly affected. In subjects with generalized lipoatrophy, either congenital (13 case subjects) or acquired (14 case subjects), or Barraquer-Simon syndrome (2 case subjects), the entire *LMNA* coding sequence was normal. Although FPLD mutations are predominantly localized in exon 8 of *LMNA*, the finding of a novel mutation at codon 584, together with the R582H heterozygous substitution recently described, confirms that the C-terminal region specific to the lamin A isoform is a second susceptibility region for mutations in FPLD. *Diabetes* 49:1958–1962, 2000

From INSERM U.402, Faculté de Médecine Saint-Antoine (C.V., J.M., C.B., J.C.), and Laboratoire de Biologie Moléculaire (O.L.), Fédération de Biochimie, Hôpital Saint-Antoine; Service de Diabétologie (A.G.), Hôpital de la Pitié-Salpêtriere; Service d'Endocrinologie (P.T.), Hôpital Necker, Paris; Service d'Endocrinolgie (M.-C.V.), Clinique Marc Linquette, Lille; Service de Diabétologie (B.G.), Centre Hospitalier Universitaire, Nancy; Service d'Endocrinologie (P.V.), Hôpital Jean Verdier, Bondy; Service de Médicine Interne (R.P.), Centre Hospitalier, Blois, France; Division of Medical Genetics (S.S., D.J.L., R.C.T.), University of Leicester, Leicester, United Kingdom; and the Divisione di Endocrinologia (G.P.), Ospedale Garibaldi, Catania, Italy.

Address correspondence and reprint requests to Jacqueline Capeau, INSERM U.402, Faculté de Médecine Saint-Antoine, 27 rue Chaligny, 75571 Paris Cedex 12, France. E-mail: capeau@st-antoine.inserm.fr.

Received for publication 30 March 2000 and accepted in revised form 17 July 2000.

CMD1A, dilated cardiomyopathy and conduction-system disease; EDMD, Emery-Dreifuss muscular dystrophy; FPLD, familial partial lipodystrophy of the Dunnigan type; PCR, polymerase chain reaction.

Lipodystrophies represent a heterogeneous group of diseases characterized by alterations in body fat distribution and, in most cases, insulin resistance. The other cardinal signs are acanthosis nigricans, hyperandrogenism in females, muscular hypertrophy, hepatomegaly, altered glucose tolerance, and hypertriglyceridemia (1). Among them, the familial partial lipodystrophy of the Dunnigan type (FPLD), dominantly inherited, is characterized by a lack of adipose tissue in the limbs, buttocks, and trunk with fat accumulation in the neck and face, and results from heterozygous missense mutations of *LMNA* (2–5). Lamin A and C, encoded by this gene, are ubiquitous structural proteins that polymerize in the nuclear lamina, a meshwork underlying the inner nuclear membrane, in which they interact with integral proteins and chromatin (6).

In the present study, we searched for mutations in *LMNA* in patients affected with FPLD or other lipodystrophies and analyzed the different clinical presentations.

Concerning FPLD, we sequenced the coding region of *LMNA* in the probands from six families and two individuals. Previous haplotype analysis at the FPLD locus (chromosome 1q) confirmed that these Caucasian families were not related (data not shown). A heterozygous CGG→TGG transition at codon 482 (exon 8), leading to an arginine to tryptophane substitution (R482W) was found in probands from families DE, DR, G, K, H, and P. At the same codon, patient J.M. displayed a heterozygous CGG→CAG transition, which predicts an arginine to glutamine substitution (R482Q). These mutations have been previously reported in FPLD (2–5).

In patient PI, we found a heterozygous CGC→CAC transition at codon 584 (exon 11), leading to an arginine to histidine substitution (R584H). This DNA variation, which has not been previously reported, was absent in 100 unrelated control subjects screened using a *Dra* III restriction polymor-

phism (see RESEARCH DESIGN AND METHODS), therefore representing a new *LMNA* mutation.

The dominant transmission of FPLD was evident in each of the families (Fig. 1) and was considered likely in individuals J.M. and P.I., because lipodystrophy was observed in their mothers, one of whom presented with acute pancreatitis.

All the other *LMNA* nucleotide variations that we detected in these patients were silent polymorphisms either exonic (S17 [AGC→AGT], A287 [GCT→GCC], D446 [GAT→GAC] and H566 [CAC→CAT]), or intronic (intron 4: nt+13 [G→T]; intron 8: nt-41 [C→T] and intron 9: nt-5 [A→G]).

We also sequenced the 12 exons of *LMNA* in patients presenting with other forms of lipodystrophy as follows: 13 patients affected by a congenital and 14 by an acquired form of generalized lipoatrophy, and 2 patients by a Barraquer-Simon syndrome characterized by cephalothoracic lipoatro-

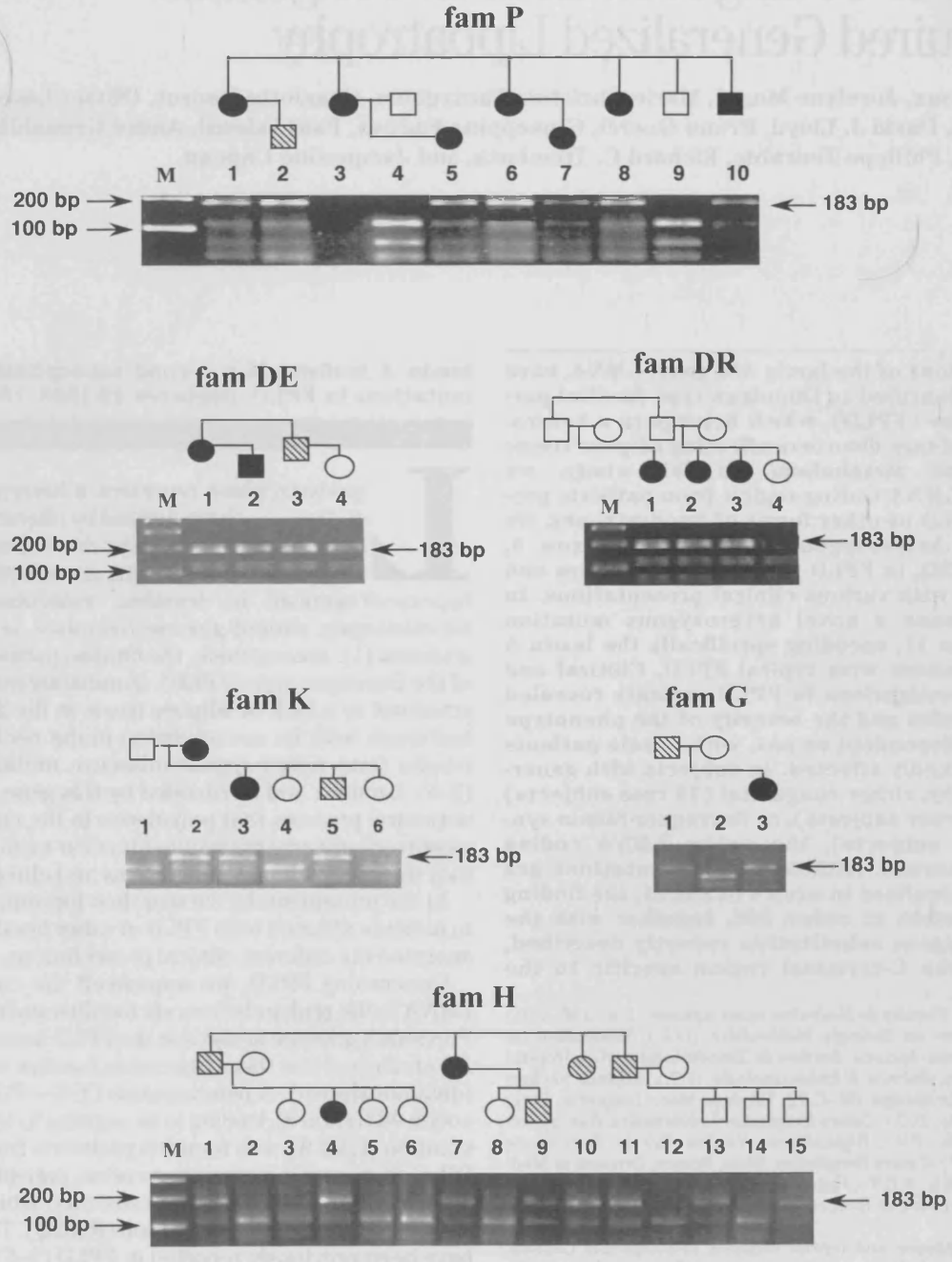

FIG. 1. Dominant inheritance of an R482W heterozygous mutation in FPLD families. C→T transition at codon 482 abolishes an *Msp*I restriction site in the exon 8-PCR fragment of 229 bp. *Msp*I digestion of the wild-type allele generates three fragments (of 114, 69, and 46 bp), whereas digestion of the R482W allele reveals a 183-bp band (→). Phenotypes of patients are symbolized as follows: (●, ■) patients affected by FPLD, (⦸, ▨) patients probably affected by FPLD, and (○, □) nonclinically affected individuals. M, molecular-weight marker.

phy and accumulation of fat in the lower part of the body. We did not find any alteration in *LMNA* coding sequence in any of these patients. Furthermore, 5 of 10 congenital lipoatrophic patients born from consanguineous unions were heterozygous for several intragenic polymorphisms, suggesting that defects at the *LMNA* locus are not responsible for this rare autosomal recessive disease (7).

The evaluation of the main clinical and biological characteristics of individuals bearing *LMNA* mutations revealed that the disease expressivity was variable, especially between men and women (Table 1). In women, limb and trunk lipoatrophy with muscular hypertrophy was generally present and associated with fat accumulation in face and neck, giving a cushingoid appearance. However, this classical phenotype was not universally evident, especially in lean patients, in whom lipoatrophic signs could be predominant. Signs of hyperandrogenism were generally present in affected women, albeit of varying severity. In men, the clinical diagnosis of FPLD was more problematic because of the absence of the characteristic lipodystrophy in most cases, as reported previously (8). Insulin resistance and hypertriglyceridemia were also generally more severe in women. Three individuals, all lean women (DE1, K3, JM), presented with severe diabetes poorly controlled despite high dose insulin therapy (>100 U per day), whereas their affected male relatives had either a normal glucose tolerance (K5) or milder forms of diabetes, easily controlled by oral hypoglycemic agents (DE2 and 3). In the same way, six patients (all women) had striking hypertriglyceridemia that led to acute pancreatitis in two of them (G3 and K3).

In most cases, the lipodystrophy appeared progressively after puberty and was secondary to the first biological signs, either hyperinsulinemia or hypertriglyceridemia, when evaluated. Two prepubertal children, H13 and H15, were bearing the mutation without any phenotypic features of FPLD. At 22 years of age, subject DE4 still has a normal clinical and biological phenotype, suggesting either incomplete penetrance or a delayed form of the disease.

Because mutations in *LMNA* are also responsible for Emery-Dreifuss muscular dystrophy (EDMD) (9,10) and dilated cardiomyopathy and conduction-system disease (CMD1A) (11,12), we searched for clinical features of skele-

TABLE 1
Clinical and biological characteristics of the patients with mutations in the lamin A/C gene

Patient	Age at investigation (years)	BMI (kg/m^2)	Clinical lipodystrophy	Diabetes (D) or severe insulin resistance (IR)*	Plasma triglycerides >2.5 mmol/l	Antecedent of acute pancreatitis or plasma triglycerides >10 mmol/l
Women						
DE1	53	23	FPLD	D	+	+
DE4	22	18.4	NO	–	–	–
DR1	20	27.3	FPLD	IR	+	–
DR2	23	20.7	LA	IR	+	+
DR3	21	20.8	LA	IR	+	–
G3	18	23.5	FPLD	D	+	+
H4	17	23.9	FPLD	IR	+	–
H7	32	24	FPLD	IR	+	–
H10	42		NA	IR	–	–
K2	50	22.5	FPLD	D	–	–
K3	19	19.9	LA	D	+	+
P1	52	24.6	FPLD	D	NA	–
P5	19	22.2	FPLD	NA	NA	–
P6	47	24.5	FPLD	D	+	–
P7	27	22.7	FPLD	D	–	–
P8	39	27.3	FPLD	D	+	+
JM	34	21.2	LA	D	+	+
PI	21	36.7	FPLD	IR	–	–
Men						
DE2	22	19	LA	D	+	–
DE3	54		NO	D	–	–
G1	46		NO	D	+	–
H1	45		NO	IR	–	–
H9	15	25	NO	–	–	–
H11	38		NO	–	–	–
H13	12		NO	–	–	–
H15	7		NO	–	–	–
K5	24	22	NO	–	+	–
P2	27	26.7	NO	–	–	–
P10	36	30	FPLD	NA	NA	–

All patients bear an R482W heterozygous mutation in LMNA, except JM and PI, who carry an R482Q and an R584H heterozygous mutation, respectively. *Severe insulin resistance is defined by severe hyperinsulinemia (>140 pmol/l in the fasting state and/or >700 pmol/l 2 h after a 75-g oral glucose tolerance test) in the absence of diabetes. FPLD, lipoatrophy of limbs and trunk with fat accumulation in neck and face; LA, predominant lipoatrophy; NO, not obvious; NA, not available; +, present; –, absent.

tal or cardiac muscular dysfunction in our patients. With only one exception, FPLD patients had no history of muscular weakness and/or contractions. Most of them displayed a characteristic muscular hypertrophy with athletic appearance, whereas muscular atrophy is a typical feature of EDMD. In patient H10, a proximal myopathy that did not fit the diagnostic criteria for EDMD (13) was noted. The level of serum creatine-kinase was found within the normal range in all the patients tested. Electrocardiography performed in eight patients did not reveal any rhythm or conduction abnormality. No history of cardiac rhythm disturbance or cases of sudden death in patients' relatives were reported.

In FPLD, all of the previously reported mutations except one were clustered within exon 8, coding for a proximal C-terminal domain of lamin A/C, and concerned only three codons (465, 482, and 486) (2–5). In our patients, the *LMNA* mutation affected codon 482 in all of the cases but one, confirming that exon 8, and in particular codon 482, is indeed a mutational hot spot for FPLD. This is in contrast with what is seen in EDMD and CMD1A, in which most alterations reported to date are located either in the central rod dimerization or in the tail domain of lamin A/C, with only one reported mutation localized to exon 8 of the gene (I469T) (9–12).

Interestingly, we found in a typical FPLD patient a novel mutation located at codon 584, in the distal part of the coding sequence, within a highly conserved region of the C-terminal domain specific for the lamin A isoform. Recently, a R582H heterozygous substitution has been reported in FPLD, although in a less clinically pronounced form (4). It has been observed in vitro that the lamin A–specific C-terminal domain acts as a binding site for nuclear actin, with these two components being implicated in the organization of nuclear chromatin domains. Therefore, it is possible that these lamin A–specific mutations, through alterations in the nuclear lamina-chromatin relations, could modify the expression of adipose tissue–specific genes (5,14).

Molecular screening for *LMNA* mutations in FPLD may not be limited to the exon 8 of the gene. It is important to distinguish FPLD from other forms of lipodystrophies, especially acquired generalized lipoatrophy, in which clinical presentation could be very similar and to ensure the diagnosis in men, in whom the clinical and biochemical features may be less marked.

RESEARCH DESIGN AND METHODS

Patients. All patients and their families gave their informed consent for genetic studies, which were approved by an institutional review committee.

The biological and clinical characteristics of patients DE1 and K3 have been previously reported (15,16). Patients DE1 and 2 were also affected by familial benign hypercalcemia caused by a heterozygous mutation in the calcium-sensing receptor gene (17). Most patients with congenital and acquired generalized lipoatrophy have been previously presented (18,19).

Genetic studies. Genomic DNA was obtained from peripheral white blood cells by standard procedures (20). *LMNA* exons 1 to 12 and the surrounding intronic sequences were amplified by polymerase chain reaction (PCR) using primers and conditions previously described (3,9). After purification on Qiagen columns, the PCR products were directly sequenced using the ABI Dye terminator mix. Reactions were run on an ABI 377 sequencer and analyzed with Sequence Analysis 3.2 software (Perkin Elmer).

A rapid genotyping assay was used to screen for the mutations in exons 8 and 11 of *LMNA*. After amplification with specific primers (8F: 5′-CCAAGAG CCTGGGTGAGCCTC-3′, 8R: 5′-GACACTTACCCCAGCGCTCC-3′ or 11F: 5′-TG GTCAGTCCCAGACTCGCC-3′, 11R: 5′-GCCTGCAGGATTTGGAAGA-3′), PCR products (15 µl) were digested with 10 U of the specific restriction enzymes (New England BioLabs, Beverly, MA). After a 3-h incubation at 37°C, the fragments were separated on a 3% agarose gel and visualized after staining with ethidium bromide. The C to T transition at codon 482 abolishes an *Msp*I restriction site in the exon 8-PCR fragment of 229 bp, leading to a 183 bp additional DNA fragment (Fig. 1). The G to A transition at codon 584 creates a unique *Dra* III restriction site in the exon 11-PCR product (360 bp), which generates two DNA fragments of 259 and 101 bp.

ACKNOWLEDGMENTS

This work was supported by grants from INSERM, Aide aux Jeunes Diabétiques, the British Diabetic Association (PhD studentship, D.J.L.), the British Heart Foundation (R.C.T.), and Programme Hospitalier de Recherche Clinique and Direction de la Recherche Clinique-Assistance Publique-Hôpitaux de Paris at the Clinical Investigation Center of Saint-Antoine University Hospital.

We thank the patients and their families for their collaboration; the physicians that have previously referred to us lipodystrophic patients; Drs. Pascale Benlian, Antoine Gancel, Caroline Lapouille, and Laurent Meyer for providing us with clinical and biological informations about their FPLD patients; Dr. Gisèle Bonne for the helpful advice about molecular analysis of *LMNA*; Drs Jon-Andoni Urtizberea and Henri-Marc Bécane for medical information about EDMD patients; Dr. Dominique Récan and her colleagues for immortalization of lymphocytes; the Molecular Biology Laboratory of St. Antoine Hospital, Paris (directed by Prof E. Clauser) for *LMNA* sequencing; and Muriel Meier for her technical expertise and Betty Jacquin for her expert secretarial assistance.

REFERENCES

1. Moller DE, O'Rahilly S: Syndromes of severe insulin resistance: clinical and patho-physiological features. In *Insulin resistance*. Moller DE, Ed. New York, Wiley and Sons, 1993, p. 49–81
2. Cao H, Hegele RA: Nuclear lamin A/C R482Q mutation in canadian kindreds with Dunnigan-type familial partial lipodystrophy. *Hum Mol Genet* 9:109–112, 2000
3. Shackleton S, Lloyd DJ, Jackson SNJ, Evans R, Niermeijer MF, Singh BM, Schmidt H, Brabant G, Kuma S, Durrington PN, Gregory S, O'Rahilly S, Trembath RC: *LMNA*, encoding lamin A/C, is mutated in partial lipodystrophy. *Nat Genet* 24:153–156, 2000
4. Speckman RA, Garg A, Du F, Bennett L, Veile R, Arioglu E, Taylor SI, Lovett M, Bowcock AM: Mutational and haplotype analyses of families with familial partial lipodystrophy (Dunnigan variety) reveal recurrent missense mutations in the globular C-terminal domain of lamin A/C. *Am J Hum Genet* 66:1192–1198, 2000
5. Hegele RA, Anderson CM, Wang J, Jones DC, Cao H: Association between nuclear lamin A/C R482Q mutation and partial lipodystrophy with hyperinsulinemia, dyslipidemia, hypertension, and diabetes. *Genome Res* 10:652–658, 2000
6. Stuurman N, Heins S, Aebi U: Nuclear lamins: their structure, assembly, and interactions. *J Struct Biol* 122:42–66, 1998
7. Lander ES, Botstein D: Homozygosity mapping: a way to map human recessive traits with the DNA of inbred children. *Science* 236:1567–1570, 1987
8. Burn J, Baraitser M: Partial lipoatrophy with insulin resistant diabetes and hyperlipidaemia (Dunnigan syndrome). *J Med Genet* 23:128–130, 1986
9. Bonne G, Raffaele Di Barletta M, Varnous S, Becane HM, Hammouda EH, Merlini L, Muntoni F, Greenberg CR, Gary F, Urtizberea JA, Duboc D, Fardeau M, Toniolo D, Schwartz K: Mutations in the gene encoding lamin A/C cause autosomal dominant Emery-Dreifuss muscular dystrophy. *Nat Genet* 21:285–288, 1999
10. Raffaele Di Barletta M, Ricci E, Galluzzi G, Tonali P, Mora M, Morandi L, Romorini A, Voit T, Orstavik KH, Merlini L, Trevisan C, Biancalana V, Housmanowa-Petrusewicz I, Bione S, Ricotti R, Schwartz K, Bonne G, Toniolo D: Different mutations in the LMNA gene cause autosomal dominant and autosomal recessive Emery-Dreifuss muscular dystrophy. *Am J Hum Genet* 66:1407–1412, 2000
11. Fatkin D, MacRae C, Sasaki T, Wolff MR, Porcu M, Frenneaux M, Atherton J, Vidaillet HJ Jr, Spudich S, De Girolami U, Seidmann JG, Seidman C, Muntoni F, Muehle G, Johnson W, McDonough B: Missense mutations in the rod

domain of the lamin A/C gene as causes of dilated cardiomyopathy and conduction-system disease. *N Engl J Med* 341:1715–1724, 1999
12. Brodsky GL, Muntoni F, Miocic S, Sinagra G, Sewry C, Mestroni L: Lamin A/C gene mutation associated with dilated cardiomyopathy with variable skeletal muscle involvement. *Circulation* 101:473–476, 2000
13. Emery AE: Emery-Dreifuss syndrome. *J Med Genet* 26:637–641, 1989
14. Sasseville AMJ, Langelier Y: In vitro interaction of the carboxy-terminal domain of lamin A with actin. *FEBS Lett* 425:485–489, 1998
15. Meyer L, Hadjadj S, Guerci B, Delbachian I, Ziegler O, Drouin P: Lipoatrophic diabetes mellitus treated by continuous subcutaneous insulin infusion. *Diabetes Metab* 23:544–546, 1998
16. Vantyghem MC, Vigouroux C, Magré J, Desbois-Mouthon C, Pattou F, Fontaine P, Lefebvre J, Capeau J: Late-onset lipoatrophic diabetes: phenotypic and genotypic familial studies and effect of treatment with metformin and lispro insulin analog. *Diabetes Care* 22:1374–1376, 1999
17. Vigouroux C, Bourut C, Guerci B, Ziegler O, Magré J, Capeau J, Meyer L: A new missense mutation in the calcium-sensing receptor in familial benign hypercalcemia associated with partial lipoatrophy and insulin resistant diabetes. *Clin Endocrinol*, 53:393–398, 2000
18. Desbois-Mouthon C, Magré J, Amselem S, Reynet C, Blivet MJ, Goossens M, Capeau J, Besmond C: Lipoatrophic diabetes: genetic exclusion of the insulin-receptor gene. *J Clin Endocrinol Metab* 80:314–319, 1995
19. Vigouroux C, Khallouf E, Bourut C, Robert JJ, De Kerdanet M, Tubiana-Rufi N, Fauré S, Weissenbach J, Capeau J, Magré J: Genetic exclusion of 14 candidate genes in lipoatropic diabetes using linkage analysis in 10 consanguineous families. *J Clin Endocrinol Metab* 82:3438–3444, 1997
20. Sambrook J, Fritsch EF, Maniatis T: In *Molecular Cloning: a Laboratory Manual*, 2nd ed. New York, Cold Spring Harbor Laboratory Press, 1989, p. 9.17–9.19